ADDIS ABABA UNIVERSITY

ADDIS ABABA INSTITUTE OF TECHNOLOGY SCHOOL OF CIVIL AND ENVIRONMENTAL ENGINEERING

Static and Dynamic Lateral Response of Single Piles Using Kerr-Equivalent Pasternak Subgrade Model

A Thesis in Geotechnical Engineering

By Abey Lulseged

September 2021

Addis Ababa

Advisor: Dr.-Ing. Asrat Worku

A Thesis

Submitted in Partial Fulfillment of the Requirements for the Degree of Master of Science

UNDERTAKING

I, the undersigned, declare that the research work entitled "**Static and dynamic lateral response of Single Piles Using Kerr-Equivalent Pasternak Subgrade Model**" is my original work. The work has not been presented as a thesis elsewhere. Furthermore, all sources of materials used have been appropriately acknowledged.

Abey Lulseged	_____	_____
Researcher	Signature	Date

This is to certify that the above declaration made by the candidate is correct to the best of my knowledge.

Asrat Worku (Dr.-Ing)	_____	_____
Advisor	Signature	Date

ABSTRACT

The most widely used model to perform piles analysis under static and dynamic lateral loads consists of modeling the pile as beam elements and representing the soil as a group of unconnected, concentrated springs perpendicular to the pile (Discrete Winkler Model). The absence of interaction between the individual springs in the Discrete Winkler Model produces an unrealistic response.

This study aims to perform an analytical and numerical study of the static and dynamic response of the pile-soil system under lateral loads (considering homogeneous soil profile) using a two-parameter subgrade model. In order to develop a rational method that includes shear interaction between the concentrated springs, a two-parameter model proposed by Worku (2014) was used.

A simplified expression for the adopted model parameters was obtained by performing a series of numerical and parametric investigation. The proposed model was calibrated using outputs from PLAXIS 3D, and from the result, it was observed that the proposed model could predict pile-head stiffness within a maximum error of 3% when compared to FE output. A new approach for determining the critical pile length is also introduced. Using this new approach, critical pile lengths for different boundary conditions are introduced. Based on the variation of pile-head stiffness, a new classification, other than "short" and "long" piles, was introduced, namely "transitional" piles. Simplified expressions for pile head stiffness for piles in a "transitional" state are provided.

The dynamic stiffness (or impedance) and the kinematic response are investigated. Equivalent spring and dashpot coefficients at the pile-head are computed to provide a simplified procedure to replace the entire soil-pile system with a spring and a dashpot at the top that will produce the same effect on the overlying structure.

Equivalent spring coefficients at the top of the pile are obtained from the beam on elastic foundation techniques. Equivalent damping coefficients are obtained following a simplified approach that uses the concept of conservation of energy. Results are compared with those given by a dynamic finite element (DFE) analysis over a range of frequencies for piles in a homogeneous soil layer, and from the result, it is evident that the model is in good agreement with the DFE results.

ACKNOWLEDGEMENT

I am very grateful to my advisor, Asrat Worku (Ph.D.), for his endless enthusiasm throughout my studies and the countless hours he devoted to this research.

Furthermore, I am also grateful to my family and friends for their consistent moral and unfailing support. The success is theirs just as much as it is mine.

TABLE OF CONTENT

LIST OF TABLES

LIST OF FIGURES

LIST OF SYMBOLS AND ABBREVIATIONS

a_o	dimensionless cyclic frequency
C_1, C_2, C_3 and C_4	Integration constants depending on boundary conditions and type of loading.
d	pile diameter
E_s	Young's modulus of soil
E_P	Young's modulus of pile
FEM	finite element method
FxHFBP	fixed-head floating base pile
FxHFxBP	fixed-head fixed base pile
FHFBP	free-head floating base pile
FHFxBP	free-head fixed base pile
G_s and G_S^*	real- and complex-valued shear modulus of soil
G_P	parameter representing shear interaction
H	thickness of soil layer
I_P	moment of inertia of the pile in bending
I_u	translational response factor
I_φ	rotational response factor
k_P	soil's reaction modulus
L	Pile length
$\hat{m}$	is the pile mass per unit length
q	wave number
r_P	Radius of pile
t	time variable
V_s and V_S^*	real-valued and complex-valued soil shear wave propagation velocity
u_g	time and depth dependent displacement of bedrock.
u_{ff}	time and depth dependent displacement of bedrock.
w	lateral pile displacement

Greek Symbols

β_S	soil material damping
β_r	radiation damping
Φ and Φ^*	variation factor for static and dynamic case
ν_s	soil Poisson's ratio
ρ_s	soil mass density
ρ_P	pile mass density
ω	cyclic excitation frequency
Γ	kinematic response coefficient

CHAPTER 1
INTRODUCTION

1.1 Background

Predicting and modeling piles' behavior and pile groups for lateral loads remains a puzzling task to geotechnical engineers. Following the destruction caused by recent earthquakes, many have raised concerns about current codes and the approaches used to design structures and foundations. Since then, many researchers have proposed different approaches for modeling the lateral response of piles.

Researchers and designers currently use two approaches to analyze both static and dynamic pile response. They are the Beam on Winkler Foundation (BWF) method and the Finite Element (FE) method. Concerning the Beam on Winkler Foundation (BWF) method, they are widely accepted by engineers, used for both axially and laterally-loaded piles under static or dynamic conditions (Nogami and Novak 1977, Scott 1981, Yin 2000, Guo and Lee 2001). Their popularity stems primarily from their ability to yield pile response predictions with substantially smaller computational effort than the more rigorous alternatives.

The fundamental problem in the implementation of Winkler models lies in assessing the modulus of the Winkler springs, which is mainly due to lack of interaction between the springs. Current methods for determining this parameter can be classified into three main groups (Mylonakis 2001): (A) experimental methods, (B) calibration with rigorous numerical solutions, (C) simplified theoretical models. Despite the significance of the above methods, they can all be criticized for the lack of interaction between the individual springs.

In this study, an approximate yet realistic analytical solution is presented for a laterally-loaded pile in a homogeneous soil stratum in the linear elastodynamic theory framework. While maintaining conceptual and analytical simplicity, the proposed model has distinct advantages over other models, in a way that it includes interaction between springs by using a shear membrane between the spring and the pile, which will give realistic deformation of the pile.

The two parameters are fully established in advance, leaving only room for adjustment or fine-tuning.

1.2 Statement of The Problem

Foundation systems composed of isolated piles or pile groups are extensively used to support different structures placed over soft soil layers, where shallow foundations are not appropriate because they do not provide the required capacity or may experience too large settlements.

These pile foundations have to be designed to support lateral loads due to earthquakes, wind, and vehicle impact loads, among others. The most widely used model to perform the analysis of piles under lateral loads consists of modeling the pile as a series of beam elements and considering the pile-soil interaction by representing the soil as a group of unconnected, concentrated springs perpendicular to the pile (Discrete Winkler Model). The non-linear soil behavior can be modeled through variation of the springs based non-linear load-deflection relationship that depends on the type of soil and type of pile.

To adequately address pile response under earthquake actions or analyze heavy vibratory machine foundations, it is often required to perform dynamic analysis of the pile for transverse (lateral) vibrations. For dynamic analysis, it is critical to have an adequate representation of the system stiffness (force-deflection relationships) and adequate representation of the system mass involved in the vibration phenomena. The Winkler model only uses individual springs to calculate and estimate pile deformation due to lateral loading and does not consider the spring interaction contribution to the inertia characteristics of the system.

The study aims to perform an analytical and numerical investigation of the static and dynamic response of the pile-soil system under lateral loads by using a two-parameter subgrade model to develop a rational method that will give us reasonable deformation and stress distribution throughout the pile length.

1.3 Objectives

1.3.1 General Objective

This study's main objective is to assess the static and dynamic response of a soil-pile system using a two-parameter mechanical model and develop a rational method that will realistically approximate the response of a pile-soil system under static and dynamic lateral loads.

1.3.2 Specific Objectives

The specific objectives of the study are to:

I. use a FE model to study pile lateral response in elastic soils.
II. propose critical pile length under both static and dynamic loading cases.
III. develop impedance functions due to inertial interaction,
IV. study the influence of pile diameter, length and end conditions, and intensity of the ground motions on the static and dynamic lateral response of single piles.

1.4 Scope of the study

In this paper, only the lateral response of single piles in a homogeneous soil profile is studied. This work only considers flexible circular piles. Rectangular piles or piles with other shapes and also rigid piles are not studied. The soil is considered as an isotropic elastic medium with no variation of its parameter with depth.

1.5 Methodology

It is evident from the objective that this study focuses on both the static and dynamic lateral response of single piles. So, the methodology is presented as such.

A detailed study and literature review of relevant topics (such as piles under static and dynamic lateral loads, seismic-soil-pile interaction, soil-structure interaction) is primarily performed.

1.5.1 Methodology overview for the static case

First, the governing differential equations (DE) of a pile on Kerr-equivalent Pasternak type subgrade model is formulated and solved using an analytical approach.

Second, the calibration process is started by performing a 3D finite element parametric study using FEM based software PLAXIS 3D. Using curve fitting between the result from FEM and the analytical result obtained from the two-parameter model, the calibration factors, χ , of the two-parameter model used in the study are determined. Before calculating a pile deflection using an analytical approach, to simplify the curve fitting and the analysis process, an excel spreadsheet program is developed.

Finally, to assess the proposed model's performance against other models from literature, a detailed parametric investigation was performed to compare the model used in this study with other discrete models.

1.5.2 Methodology overview for the dynamic case

After completing the static case, the dynamic analysis started by developing a damping model for both the kinematic and inertial responses; after this, the generalized DE of motion is solved using an analytical procedure. Finally, the results of both kinematic and inertial responses obtained from the proposed model are compared with the results from dynamic finite element analysis and literature results. For this purpose, programs are developed in Mathematica 12.

1.6 Organization

In Chapter 1, a brief background to the static and dynamic lateral response of piles is presented. The statement of the problem, the objective, scope, and methodology of the study are concisely presented.

In Chapter 2, a summary of a literature review of relevant topics (piles under static and dynamic lateral loads, seismic-soil-pile interaction, soil-structure interaction) is provided.

In Chapter 3, detailed descriptions of the pile and soil properties and materials used for the development of the propsed model with a discription of PLAXIS 3D, the FE software used, are presented.

In Chapter 4, simple analytical solutions are developed for computing the static response of single piles embedded in homogenous soils. Pile-soil interaction is realistically represented through a Kerr-equivalent Pasternak-type model. The values of a calibration

factor associated with the model parameters are derived from finite-element analysis output.

In Chapter 5, expressions for all piles head stiffnesses (swaying, cross swaying-rocking, and rocking stiffness) are derived.

In Chapter 6, expressions for radiation damping using a simplified approach is developed, and a simplified radiation damping coefficient is presented.

In Chapter 7 and Chapter 8, the simple analytical methods of Chapter 4 and Chapter 6 are extended to dynamic lateral pile response. Simple analytical solutions for kinematic pile response (Chapter 7) and inertial response (Chapter 8) are presented.

Chapter 9 contains conclusions drawn and recommendations made for future research

CHAPTER 2
MODELS FOR LATERALLY LOADED PILES

A review of soil-pile behavior under lateral loads is presented in the following sections. The purpose of this chapter is to present state of the art and past practice in the analysis of piles under static and dynamic lateral loads, pointing out some milestones in this development, rather than giving a comprehensive review of all the papers and reports related to these topics. The chapter has two major sections relevant to the proposed research topic and will serve as theoretical background and reference: modeling piles under static lateral loads and the analysis of piles under dynamic loads.

2.1 Models for piles under static lateral load

According to Poulos and Davis (1980), there are three major approaches for the load-deflection prediction of laterally loaded piles: the beam on elastic foundation approach, the elastic continuum approach, and the Finite-element approach, which are briefly presented below.

2.1.1 Beam on Elastic Foundation Approach

2.1.1.1 Beam on one parameter elastic model.

Winkler (1867) proposed this model. The model, also known as *Beam on Winkler Foundation* (BWF), proposes that the deflection (w) at any point of the soil in contact with the pile is linearly related to the contact pressure (p) at that point and independent of the contact stresses at other points. In other words, the model represents the soil as a series of unconnected uniformly distributed springs, as shown in Figure 2.1.

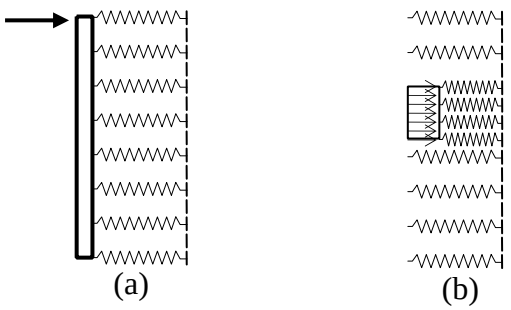

Figure 2-1: Beam on one parameter elastic model: (a) Vertical section, (b) Plan view

The load-deformation behavior portrayed in Figure 2-1 can be expressed as

$$P = k_w w \tag{2.1}$$

The spring modulus of the model is the soil modulus of lateral (Horizontal) subgrade reaction k_w [force/length^3], which represents the horizontal pressure (or horizontal force acting on a unit vertical area; or the distributed force along the pile length, acting on a unit length) required to produce a unit horizontal displacement. It depends on the soil type, depth of embedment, and pile diameter.

The differential equation of equilibrium of a beam (pile) subjected to a static lateral force at the head and resting on Winkler foundation is given by:

$$(EI)_P \frac{d^4 w}{dz^4} + Bk_w = 0 \tag{2.2}$$

where;

E_p: elastic modulus of the pile (N / m^2)

I_p: the moment of inertia of the pile in bending (m^4)

$w(z)$: horizontal displacement of the pile (m)

z: depth (m)

k_w: Winkler subgrade modulus for horizontal loading (N / m^3)

B: diameter of the pile (m)

Closed-form solutions have been obtained for this equation for the case of k_w constant with depth and specific boundary conditions (e.g. Hetenyi (1946), Scott (1981)). Although limited in practical applications, these solutions provide significant insight into the pile response and the factors that affect the soil-pile interaction.

Vesic (1961) presented a rigorous analysis of beams resting on an elastic, isotropic half-space medium, obtaining analytical solutions (deflection, slope, bending moment, shear force, and contact pressure) for infinite beams acted upon by a concentrated load and by a couple. He compared these solutions with the Winkler model solutions and recommended values for the subgrade reaction modulus by matching the deflections. He also

demonstrated that the Winkler model gives reasonably accurate results for long and medium beams (Poulos and Davis 1980). Numerous attempts to use this model for laterally loaded piles have been made in the past.

2.1.1.2 Beam on two-parameter elastic model.

The Winkler model is straightforward. However, interactions between springs are not considered; so, it does not accurately represent many practical foundations' characteristics. A continuous medium model is more accurate for some problems, but it is difficult to obtain an exact solution with this model and is expensive to obtain a numerical result by finite element methods.

The inherent deficiency of the Winkler Model in its lack of portraying the ground's continuous behavior and the mathematical complexities of the elastic continuum approach led to the development of many other simple ground response models. These models possess some of the characteristic features of continuous elastic solids (Hetenyi 1950, Kerr 1964).

The term ‘two-parameter’ signifies the fact that two types of mechanical elements define the mechanical model. The development of these two-parameter models has been approached along two distinct lines. The first type proceeds from the Winkler model and eliminates its discontinuous behavior by providing a mechanical interaction between the individual spring elements. Such physical models of ground behavior have been proposed by Filonenko-Borodich (1950), Hetenyi (1946), and Pasternak (1954), where interaction between adjacent spring elements is provided by either elastic membranes, elastic beams, or elastic layers capable of purely shearing deformation. The second approach used to develop and also improve the two-parameter model is the elastic continuum method. Both approaches are discussed in the following sections.

2.1.1.2.1 Filonenko-Borodich Model (1950)

The model proposed by Filonenko-Borodich (1950), achieves continuity between individual Winkler springs by connecting them to a smooth thin elastic membrane subjected to uniform tension, T. Two elastic constants characterize the Filonenko-Borodich model, k_s and T as shown in Figure 2-2. In the case of beams and two-dimensional plane strain problems such as strip foundations, the relationship between the contact pressure and the deflection is given by

$$p(z) = k_s w(z) - T\frac{d^2 w(z)}{dz^2} \tag{2.3}$$

2.1.1.2.2 Hetenyi Model (1946)

In the model proposed by Hetenyi (1946), the interaction between the independent spring elements is accomplished by incorporating an elastic plate in three-dimensional problems or an elastic beam in the case of two-dimensional problems (Figure 2-2). The response function of this model is given by

$$p(z) = k_s w(z) - EI\frac{d^4 w}{dz^4} \tag{2.4}$$

where EI is the flexural rigidity of the beam that is replaced by D, the plate rigidity, in the case of plates.

2.1.1.2.3 Pasternak Model (1954)

The model of ground behavior proposed by Pasternak (1954) assumes the existence of shear interaction between the spring elements. This is achieved by connecting the spring elements to a layer of incompressible vertical elements that deform in transverse shear (Figure 2.2). For an isotropic linear shear layer in the x–y plane with shear moduli $G_x = G_y = G$, the expressions for the shear stresses in the vertical direction are

$$p(z) = k_p w(z) - G_p H\frac{d^2 w(z)}{dz^2} \tag{2.5}$$

The Pasternak model is the most reasonable, generalized two-parameter model and is easily conceivable for geotechnical applications as the ground exhibits both compressibility and deformation in shear.

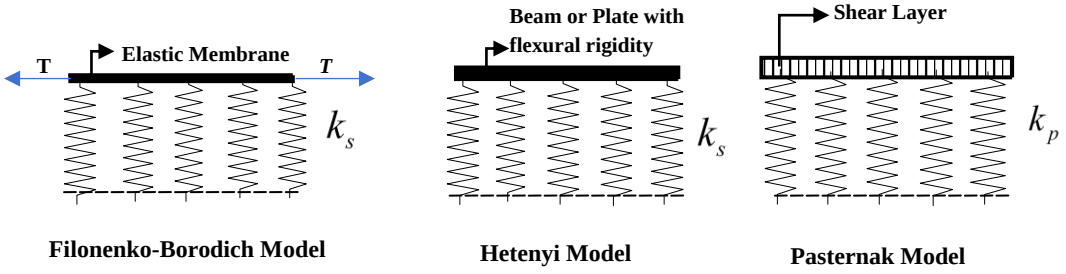

Figure 2-2: Two parameter models.

2.1.1.2.4 Kerr-equivalent Pasternak model

Worku (2014) introduced a new two-parameter model in which he replaced a three-parameter Kerr model, which he found as a match for his rigorous continuum model (see Section 2.1.2.2), with a two-parameter Pasternak model resulting in the same response. In the process, he established Pasternak parameters that give results in agreement with the Kerr model, which has been calibrated in his previous work (Worku 2013). The parameters proposed in the model are given below, and the representation of the model is portrayed in Figure 2-3.

$$k_p = \frac{\left(0.4v_s + 0.67\right) \times E_s}{\chi \times B} \text{ and}$$

$$G_P = \left(1.36v_S + 2.28\right) G_S \times \chi \times B$$

where,

G_P : is Pasternak's coefficient of the shear layer (N/m)

k_p : is Pasternak's spring stiffness (force/lenght^3)

χ : calibration factor

v_S : Poisson's ratio

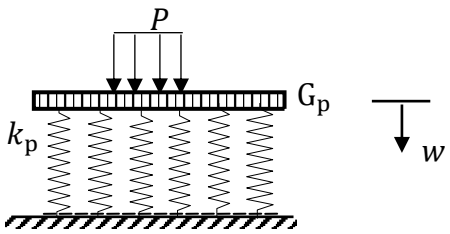

Figure 2-3: Kerr-equivalent Pasternak model after Worku (2014)

The determination of χ for various boundary conditions of piles is part of the task of this work.

2.1.1.3 The p-y Method

The original Beam on Elastic Foundation (BEF) model does not account for the soil's nonlinear response. The most widely-employed approach to consider the nonlinear nature of soil response is the *p-y Method*, where the spring stiffness is variable, allowing consideration of a non-proportional relationship between the soil resistance per unit pile length (p) and the lateral displacement (y). (Note that y replaces w in this approach)

The *p-y* approach was developed by Reese and Matlock. In a series of papers, they described how to construct the p-y curves for different soils and depths based on experimental results, how to develop a solution by the finite deference method (FDM), and how to develop a computer program (Reese and Matlock 1960, Matlock 1970, Reese 1977). Their study was motivated by the need for the design and construction of off-shore platforms subjected to large lateral loads due to ocean currents and waves. Figure 2-4 shows a schematic of the soi ding p-y curve for each non-linear spring.

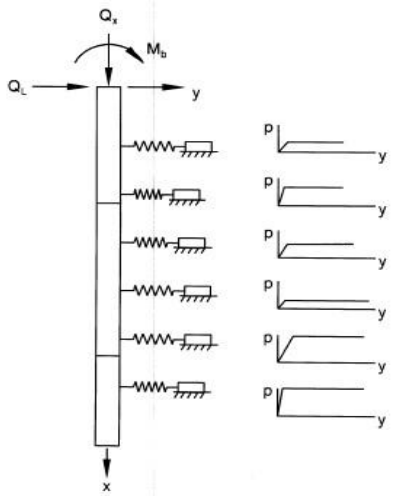

Figure 2-4: Schematic of Pile-Soil Model for the p-y Approach (FHWA, 1997).

It is important to point out that p is not the contact stress (as in the original Winkler model), but the resultant of the contact stresses (with complex distribution) and the friction (adhesion) along the pile perimeter for a given depth, resulting in a contact (interaction) load per unit length of the pile. Figure 2-5 shows a distribution of contact stresses before and after lateral pile deflection. The value of *p* depends on soil type, pile type and shape, depth, and value of the deflection *y* (since the response is non-linear).

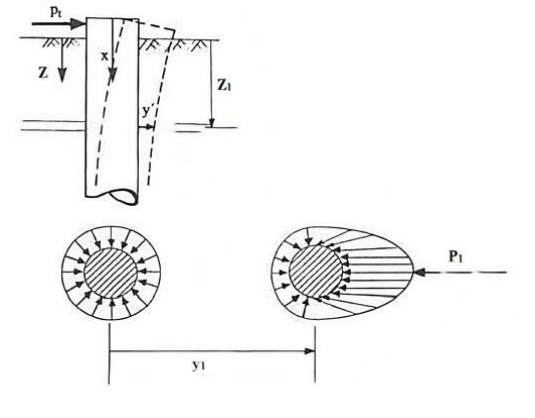

Figure 2-5: Distribution of contact stresses against a pile before and after lateral deflection (Reese and Impe 2011).

2.1.2 Elastic Continuum Approach

The representation of the soil as a homogeneous elastic continuum has also been proposed to analyze the soil-pile interaction.

Some authors developed *Plane Strain Models* (e.g. Davis and Booker, 1971) to analyze limit pile capacity. These solutions are relevant for the case of shallowly embedded sheet piling and may also be accurate for a group of piles closely spaced in a single long row (i.e., wall footing). Plane strain models are also used for modeling the 3D system as a series of parallel horizontal planes in plane strain.

Poulos and Davis (1980) presented the implementation of the model proposed by Poulos (1971, 1972). In their model the pile is assumed to be a thin rectangular vertical strip divided into elements, and it is considered that each element is acted upon by uniform horizontal stresses (see Figure 2-6), which are related to the element displacements. Finally, they solved the differential equation of equilibrium of a beam element on a continuous soil with the finite difference method (FDM), in which the soil pressures over each element are unknown variables.

The model has the advantage that it can take into account the continuous nature of the soil, the semi-infinite dimension of the half-space, and the boundary conditions along the unloaded ground surface.

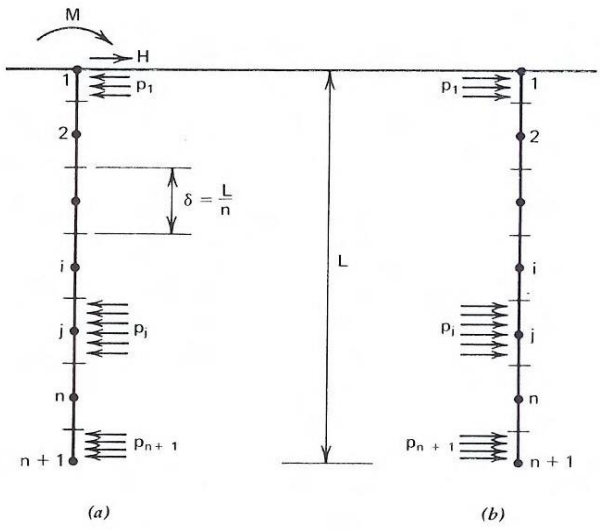

Figure 2-6: General Pile Discretization for the Analysis of Soil as a Continuous. Stresses acting on (a) pile, (b) soil adjacent to pile (Poulos and Davis, 1980)

It was noted that two of the drawbacks of the discretization by means of the FDM is the difficulty to introduce general boundary conditions at pile top and bottom and the required uniform size of the elements. Basile and House (2002) reported that this soil model was also used for the boundary element method (BEM) analysis of piled foundations.

The methods mentioned above for the analysis of piles using the elastic continuum approach mostly originated from the pioneering works of Reissner (1958) and Vlasov (1966), who made significant simplifying assumptions. The model used in this study is originated from a much recent, more rigorous elastic continuum approach proposed by Worku (2010).

2.1.2.1 Reissner's Model

Reissner (1958) proposed a continuum subgrade model for beams and plates idealized as shown in Figure 2-7. It is based on an isotropic elastic layer of thickness H. To simplify the ensuing mathematical complication in the proposed model, he neglected the in-plane stresses ($\sigma_x = \sigma_y = \tau_{xy} = 0$). The governing differential equation (DE) for beams and plates on Reissner's model is given as

$$p - \frac{G_s H^2}{12 E_s} \nabla^2 p = \frac{E_S}{H} w - \frac{G_s H^2}{12 E_s} \nabla^2 w \tag{2.6}$$

where H is the subgrade thickness, p is the contact pressure at the interface and ∇ is the Laplace operator. Note that the second derivatives of both the deflection and the contact pressure are involved in contrast to those of the single and two-parameter mechanical models presented above.

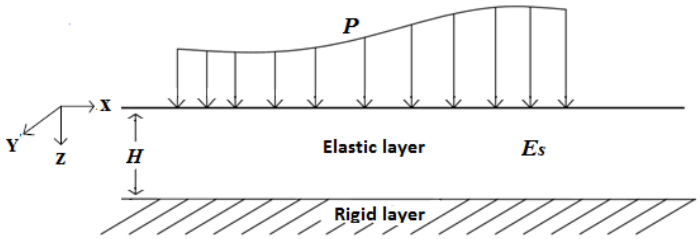

Figure 2-7: Simplified elastic continuum model (Worku 2010)

Different researchers have proposed modifications in order to extend Reissner's model. Out of these models, the one proposed by Horvath (1983) is worth mentioning. He extended the concept of Reissner to produce two simplified models (Winkler-Type

Simplified Continuum and Pasternak- Type Simplified Continuum models). With constant, linear, and parabolic Young's modulus variation with depth (Horvath ,1983) as referred by Meron (2018). Equation (2.7) and Equation (2.8) are expressions for the Winkler-Type and Pasternak- Type simplified continuum models of constant Young's modulus, respectively.

$$p = \frac{E_S}{H} w \tag{2.7}$$

$$p = \frac{E_S}{H} w - \frac{G_s H^2}{2} \nabla^2 w \tag{2.8}$$

However, since both models are based on further simplifying assumptions, they result in responses that significantly deviate from reality (Worku; 2010, 2013, 2014).

2.1.2.2 Worku's Generalized Model

Worku (2010) has introduced a more generalized continuum subgrade model based on a physical model the same as Reissner (1958) but without neglecting any stress, deformation, or strain components (Figure 2-8). Even if the result is of the same order of differential equation as Ressner, significant improvements were observed (Worku 2010). He also incorporated the variation of Young's modulus with depth in the model. The relation between the vertical deflection and the contact stress at the surface is given by Equation (2.9):

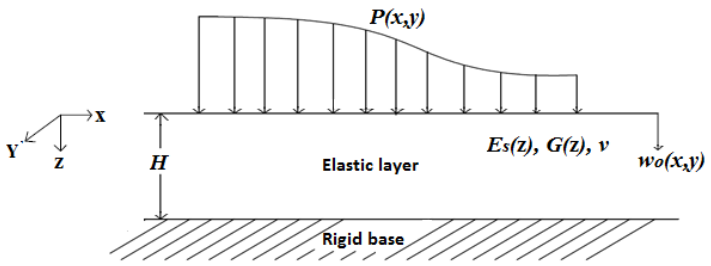

Figure 2-8: Elastic continuum model used in Worku's generalized model (Worku 2010)

$$p(x,y) - \frac{G_s}{E_s}\frac{1}{K_I}\left(L_{gI} - \frac{K_{gI}L_g}{K_g}\right)\nabla^2 p(x,y) = \frac{E_S}{K_g} w_o(x,y) - \frac{G_s L_{gI}}{K_g K_I}\nabla^2 w_0(x,y) \tag{2.9}$$

where E_s and G_s are the elastic and shear modulus of the soil. The coefficients involve the definite integrals given below:

$$K_g = \int_0^H g dz \; ; \; K_{gI} = \int_0^H g\tilde{I}_z dz \; ; \; K_I = \int_0^H I_z dz$$

$$L_g = \int_0^H \left[\int g dz - \left(\int g dz \right)_{z=H} \right] dz \; ; L_{gI} = \int_0^H \left[\int g\tilde{I}_z dz - \left(\int g\tilde{I}_z dz \right)_{z=H} \right] dz$$

$$g(z) = 1 - \nu_s \left[g_x(z) + g_y[z] \right] ; \; \tilde{I}_z(z) = \left(\int I_z dz \right)_{z=0} - \int I_z dz$$

The coefficients I_z, g_x and g_y are depth functions of z. The functions g_x and g_y are introduced to express the lateral normal stress components σ_x and σ_y, in terms of the normal vertical stress σ_z. On the other hand, I_z is introduced to express the vertical shear stresses, τ_{xz} and τ_{yz}, as a function of x and y as given below

$$\sigma_x(x,y,z) = g_x(z)\sigma_z(x,y,z); \; \sigma_y(x,y,z) = g_y(z)\sigma_z(x,y,z)$$

$$\tau_{xz}(x,y,z) = I_{zx}(z)\bar{\tau}_{zx}(x,y); \; \tau_{zy}(x,y,z) = I_{zy}(z)\bar{\tau}_{zy}(x,y)$$

The differential equation (DE) obtained is of a second-order and similar in form and order to Kerr's mechanical model (Kerr 1964). However, the coefficients are generally different.

2.1.3 The Finite Element Approach

Finite Element Method (FEM) has been used to obtain the solution of laterally loaded flexible piles in an elastoplastic soil mass.

As reported by Poulos and Davis (1980), the first attempts included two-dimensional finite element models in the horizontal plane (Baguelin and Frank, 1979), axi-symmetric geometries (Banerjee and Davies, 1978), and general three-dimensional finite element analysis (Desai and Appel, 1976).

Some recent publications include the work by Yang and Jeremić (2002), who used 3D FE models of a laterally loaded pile embedded in uniform and layered soil profiles to numerically obtain p-y curves and compare them to experimental ones.

The FE method can account for soil nonlinearity by applying appropriate constitutive models, such as the Drucker-Prager formulation (Ben Jamaa and Shiojiri (2000); Yang and

Jeremić (2002)), and to use gap-elements to model possible pile-soil separation. These modeling capabilities are usually available in robust general-purpose FEM programs (such as ABAQUS and ANSYS) or special geotechnical engineering-oriented codes (e.g., PLAXIS, Midas GTS nx).

There is a general agreement among many researchers that the FEM analysis is impractical for design except for expensive structures due to the cost of the specialized software, the time-consuming model generation, the time required for the non-linear analysis, the difficulty in the interpretation of the result in terms of typical pile (beam) variables, and the uncertainties associated with non-linear soil modeling in 3D (Mostafa and El Naggar 2002).

Finally, it is appropriate to mention that, recently, a powerful 3D Finite Difference Method program called Flac3D (Itasca Consulting Group, Inc, 1996) has been used to solve complex geotechnical engineering problems. However, the program has rarely been used for pile analysis. An example is the work by Ng and Zhang (2001), who used a 3D FDM model to analyze the behavior of piles placed on a cut slope. In particular, they investigated the effect of the sleeving (annulus of a compressible material that is usually constructed between the piles and the adjacent soil to minimize the transfer of lateral load from the buildings to the shallow depths of the slope) on the pile performance (Ng and Zhang 2001).

2.2 Analysis of Piles under Dynamic Lateral Loads

The equations of motion of a complete soil-foundation-structure system can be expressed in the form (Kramer 1996):

$$[M]\{\ddot{u}\} + K^*\{u\} = -[M]\{\ddot{u}_b(t)\} \tag{2.10}$$

where $[M]$ is the mass matrix, K^* ($=[K]+i\omega[C]$) is the complex stiffness matrix, and $\ddot{u}_b(t)$ is the vector containing motion at the nodal points of the base. Figure 2-9 portrays the simplest soil-structure interaction expressed by Equation (2.10). Two more degrees of freedom are included at the foundation due to the interaction.

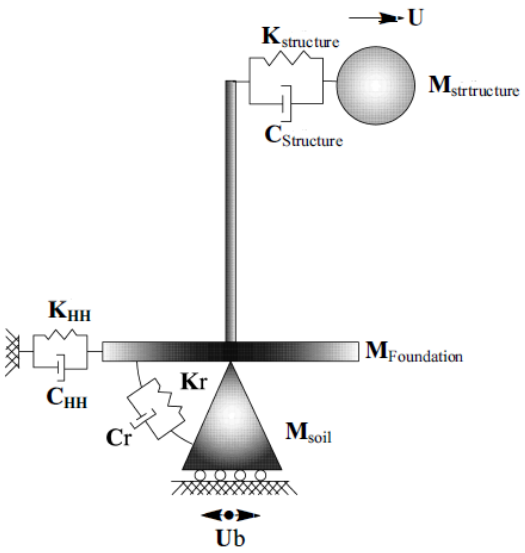

Figure 2-9: Dynamic soil-foundation-structure interaction (Moghaddasi et al. 2011)

Two types of soil-structure instruction (kinematic and inertial) are identified that are briefly explained in the following two sections.

2.2.1 Kinematic Interaction

In kinematic interaction, it is assumed that only soil has mass, while the foundation and the superstructure have stiffness but no mass. Under these assumptions, the equations of motion become:

$$\left[M_{Soil}\right]\left\{\ddot{u}_{K1}\right\}+\left[K^{*}\right]\left\{u_{K1}\right\}=-\left[M\right]\left\{\ddot{u}_{b}(t)\right\} \tag{2.11}$$

where $\left[M_{Soil}\right]$ is the soil mass matrix (the structure being massless) and $\left\{\ddot{u}_{K1}\right\}$ is the foundation input motion. Once Equation (2.11) is solved, the foundation's motion in the absence of a structural mass is available. Such motion represents the kinematic interaction between different elements. It must be noted that the term $\left[K^{*}\right]$ is the complex stiffness of the whole system (soil and structure); it follows that the structure influences the kinematic interaction by its stiffness. Concerning the kinematic interaction, many efforts have been made in the past. A brief review of the main contributions is presented below.

In one-dimensional free-field conditions, a vertically incident S-wave induces only horizontal displacements. A cylindrical pile diffracts the incident and reflected vertical waves, thereby modifying the free wave field. Consequently, the horizontal displacement

of the pile cap is different from the surface free-field motion, and the pile top experiences a rotation (Gazetas 1984).

Gazetas (1984) introduced the *displacement* and *rotation kinematic interaction factors* and defined them as:

$$I_u = \frac{|u_p|}{u_{ff}} \tag{2.12}$$

$$I_\phi = \frac{|\phi_p| r_p}{u_{ff}} \tag{2.13}$$

where u_p and ϕ_p are the displacement and the rotation of the pile head, while u_{ff} is the free-field displacement and r_p is the radius of the pile. Moreover, he defined the *displacement* and *rotation kinematic amplification factors* as:

$$A_u = \frac{|u_p|}{u_g} \tag{2.14}$$

$$A_\phi = \frac{|\phi_p| r_p}{u_g} \tag{2.15}$$

where u_g is the displacement of the rigid bedrock. All these displacements and rotations are amplitudes of harmonic motions. In the absence of kinematic interaction, $I_u = 1, I_\emptyset = A_\emptyset = 0$. Because of damping, the displacements and rotations are not in-phase with the excitation; the four factors are complex functions of frequency (completely defined by amplitude and phase), even though this study is carried out only with reference to amplitudes.

2.2.2 Inertial Interaction

In the case of inertial interaction, both the structure (superstructure and foundation) and the soil have mass and stiffness. If the superstructure is excited by a foundation input motion, inertial forces due to its mass are triggered (inertial interaction). Such inertial forces could vary if the soil-foundation system, as it is, is not rigid. In other terms, the superstructure's deformation is different from the case in which it has a fixed base. Assuming that the soil has no mass, the equations of motion become (Kramer 1996):

$$[M]\{\ddot{u}_{II}\}+[K^{*}]\{u_{II}\}=-[M_{Structure}]\{\ddot{u}_{b}(t)-\ddot{u}_{K1}\} \tag{2.16}$$

where $[M_{Structure}]$ is the mass matrix (superstructure and foundation). The above equation's right side represents the inertial loading only on the structure-foundation system; it follows that inertial loading also depends on the kinematic interaction through $\ddot{u}_{K1}$.

By assuming linear elastic behavior for all the components (soil, foundation, superstructure), it is possible to consider a superposition method. This means to add Equation (2.11) and Equation (2.16), which result in the original equation (Equation (2.10).

From the above discussion, it can be concluded that it is possible to separate kinematic interaction from inertial interaction only if the components' hypotheses of linear elastic behavior are valid. This means that the effects of kinematic and inertial interaction coming from separate analyses carried out under different hypotheses cannot be added.

Inertial interaction analysis is also conveniently performed in two steps: first computing the foundation dynamic impedance (“springs” and “dashpots”) associated with each mode of vibration, and then calculating the seismic response of the structure and foundation supported on these springs and dashpots, subjected to the kinematic accelerations $\ddot{u}_{b}(t)$ of the base.

As a result, an essential step is to estimate, using analytical or numerical methods, the (dynamic) impedance functions associated with a rigid foundation. Several techniques have been developed in the past for computing and using foundation impedances, including analytical solutions based on integral transform techniques, semi-analytical and boundary-element formulations requiring discretization of only the top surface; dynamic finite-element methods using special “wave-transmitting” lateral boundaries; and hybrid methods combining analytical and finite-element approaches.

Gazetas (1991a), collecting several previous authors' works, presented a complete set of simple formulas and graphs covering both surface and embedded foundations in a homogeneous half-space. This choice has been made because such a soil model is the only idealization for which a complete set of results could be found or easily obtained, and that

keeps the number of problem parameters to a minimum. However, the deposit need not be very deep for the half-space idealization to be applicable (Gazetas 1991a).

There are six modes of vibration for the usual case of a rigid foundation: three translational (dynamic displacements along the axes x, y, and z) and three rotational (dynamic rotations around the same axes). For each vibration mode, the soil is replaced by a dynamic spring and by a dashpot arranged in parallel. Figure 2-10 illustrates the vertical spring and dashpot of an embedded foundation. Subjected to harmonic vertical force $P_z(t) = P_z \cos(\omega t + a)$ with amplitude P_z and frequency ω. This foundation experiences a harmonic steady-state displacement $u_z(t)$ which has the same frequency but is out-of-phase with $P_z(t)$. Expressing the above quantities as complex numbers, the dynamic vertical impedance (force-displacement ratio) becomes (Mylonakis et al. 2006):

$$k^*_z = \frac{P_z}{u_z} = K^*_z + i\omega C_z \tag{2.17}$$

In which both K^*_z and C_z are, in general, functions of frequency. The spring coefficient, K^*_z, termed dynamic stiffness, reflects the stiffness and inertia of the supporting soil. Its frequency dependence relates solely to the influence that frequency exerts on inertia since soil material properties are frequency independent. The dashpot coefficient, C_z, reflects the two types of damping (radiation and material) generated in the system; the former due to energy carried by the waves spreading away from the foundation, and the latter due to energy dissipated in the soil through hysteretic action (Mylonakis et al. 2006).

Similarly, Equation (2.17) is also applicable to each of the other five modes of vibration, including the horizontal impedance, k^*_x.

For the three lateral impedances (“springs” and “dashpots”) defined in Figure 2-11 for a pile, Velez et al. (1983) presented formulas. However, they are valid only for piles with length greater than the critical (active) pile length. These piles are described as "flexible" piles in the literature. Indeed, a good majority of piles, even some with large diameters, falls into this category.

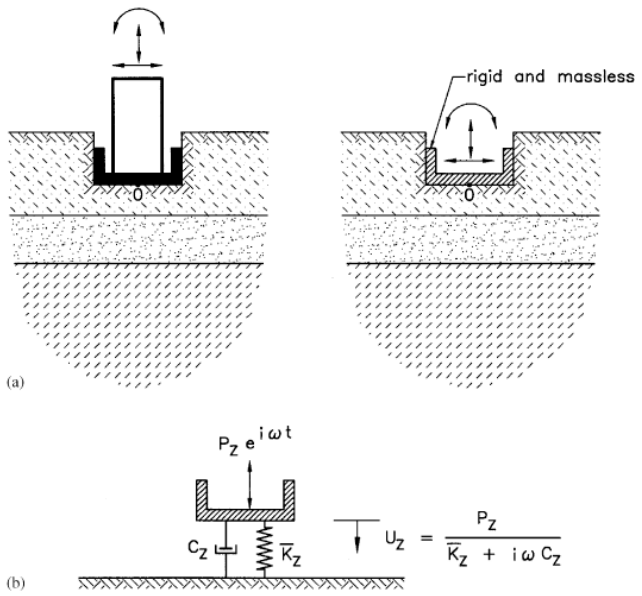

Figure 2-10: Physical interpretation of dynamic impedance in vertical mode of vibration (Mylonakis et al. 2006)

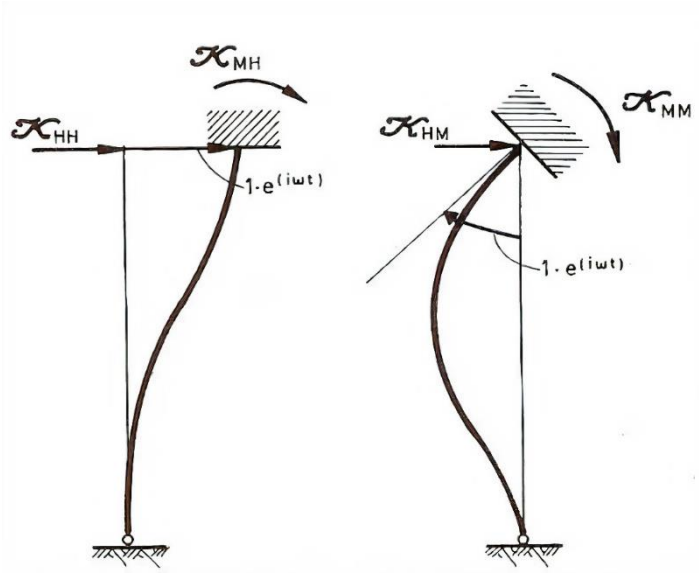

Figure 2-11: Dynamic impedance of a single pile (Velez et al. 1983).

In the past 40 years, different approaches described in Section 2.1 were also proposed to calculate the dynamic response of single piles under horizontal dynamic loads. There are the Finite Element Method (FEM) and the Boundary Element Method (BEM) that treat the soil as an unbounded continuum and are used extensively in research. Also, there are

the simplified methods, most of which use the beam on dynamic Winkler foundation (BDWF) approach.

The BDWF methods can be classified into two based on whether the spring stiffness is frequency-dependent or not.

2.2.3 Beam on dynamic Winkler foundation (BDWF)

The difference between the dynamic and static beam on Winkler foundation models is that in the dynamic case, the excitation frequency is involved in addition to the force and displacement. To implement the beam on elastic foundation model for the dynamic loads, the soil stiffness and damping contributions are represented by a series of unconnected individual springs and dashpots distributed along the pile length (Pacheco et al. 2008). Depending on the model (Frequency dependent or independent) the representation of the models differs (Figure 2-12).

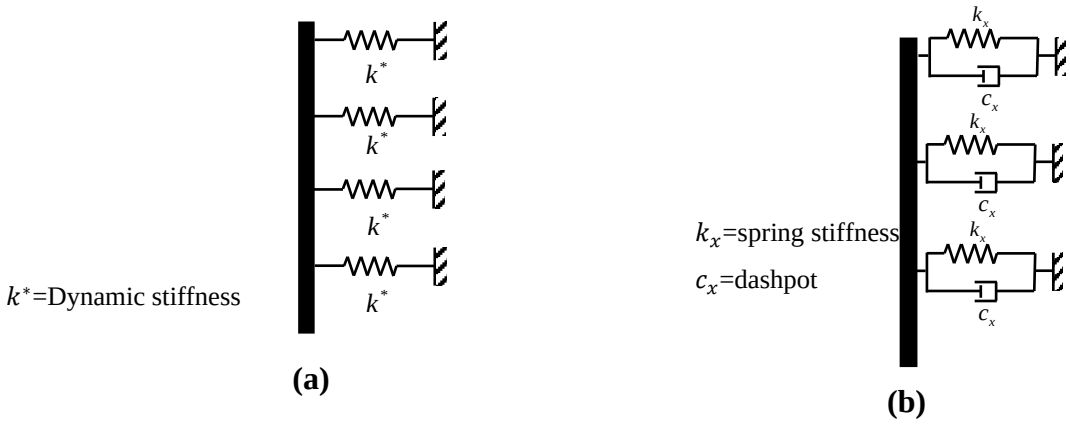

Figure 2-12: Two dynamic pile models: (a) frequency-dependent model (b) frequency-independent model

Frequency dependent dynamic pile stiffness

It was proposed to use a dynamic stiffness in the earlier work of Novak (1974). He assumed that the soil is composed of a set of independent, infinitesimally thin horizontal layers in plane strain state that extend laterally to infinity and experience small displacements. The soil layers are considered homogeneous, isotropic, and linear-elastic. The pile is assumed to be vertical, cylindrical and moving as a rigid body. The massless rigid circular disc that represents the pile cross section is considered to experience a

harmonic vibration. No separation is allowed between the rigid cylinder and the soil medium (Novak, 1974).

This approach was later extended by Novak and his coworkers (Novak et al. 1978) to viscoelastic materials with frequency independent material damping (also called hysteretic damping). The damping is considered by means of the complex shear modulus $G_s^* = G_s(1+i2\beta_s)$, where β_s is the material damping ratio. The expression for dynamic stiffness proposed by Novak et al. (1978) is given by Equation (2.18)

$$k^* = \pi G^*_s s^2 \frac{4K_1(q)K_1(s)+sK_1(q)K_0(s)+qK_0(q)K_1(s)}{qK_0(q)K_1(s)+sK_1(q)K_0(s)+qsK_0(q)K_0(s)} \tag{2.18}$$

where

$$s = \frac{ia_o}{2\sqrt{1+2i\beta_s}}, \quad q = \frac{s}{\eta_s} \ \ and \ \ \eta_s = \sqrt{\frac{2(1-\nu_s)}{1-2\nu_s}}$$

in which ν_s is Poisson's ratio, K_n is the modified Bessel function of the second kind of order n, a_0 is a dimensionless frequency, defined as $a_o = \omega d / V_s$ (Novak et al. 1978).

Most recently Anoyatis and Lemnitzer (2017) improved the dynamic stiffness. Even if the expression looks the same (Equation (2.19)), the presence of a_{cutoff} in the expression of s, makes it capable of capturing the resonant effects.

$$k^* = \pi G^*_s s\left(s + \frac{K_1(s)}{K_0(s)}\right) \tag{2.19}$$

where

$$s = \frac{1}{2\eta^{\chi_\eta}_s}\sqrt{a^2_{cutoff} - \frac{a^2_o}{1+2i\beta_s}}, \ \ \eta_s = \sqrt{\frac{2-\nu_s}{1-\nu_s}} \ and \ a_{cutoff} = \frac{\pi}{2}\frac{d}{H}$$

The value of χ_η is an empirical parameter (varying from 1 to 5), incorporated to capture the effect of Poisson's ratio (Anoyatis et al. 2016).

According to Pacheco et al. (2008), the frequency-dependent dynamic stiffness approach can only be implemented in the frequency domain analysis, and it is hard to calculate the dynamic stiffness using a pocket calculator. So, it was important for researchers to introduce frequency-independent spring stiffness.

Frequency-independent approach

Frequency independent expression of Winkler springs can be seen in the early works of (Dobry et al. (1982), Gazetas and Dobry (1984), Makris and Gazetas (1992), Kavvadas et al. (1993)).

Dobry et al. (1982), using an FE code, developed expression for both the Winkler spring and damping ratio as given in Equation (2.20) and Equation (2.21), respectively.

$$k_x = 1.67\left(\frac{E_p}{E_s}\right)^{-0.053} \tag{2.20}$$

$$c_x = \frac{2k_x\beta_s}{\omega} + 1.55(1+\nu_s)\left(\frac{E_p}{E_S}\right)^{0.124} d\rho_s V_s \tag{2.21}$$

Gazetas and Dobry (1984) extended the work of Dobry et al. (1982) by providing expressions for the Winkler spring for two pile head conditions (fixed head and free head). Unlike Dobry et al. (1982), instead of using a unique expression, they used range for expressing the Winkler spring modulus. Equation (2.22) and Equation (2.23) represent the Winkler spring modulus provided by Gazetas and Dobry (1984) for free-head and fixed-head piles, respectively.

$$k_x = E_s \; to \; 1.2E_s \tag{2.22}$$

$$k_x = 1.5E_s \; to \; 2.5E_s \tag{2.23}$$

The dashpot coefficient provide by Gazetas and Dobry (1984), considers the effect pile embedment depth has on the radiation damping. So, they provided expressions for shallow and deep depth pile foundations separately.

$$c_x = \frac{2k_x\beta_s}{\omega} + 4\left(\frac{\pi}{4}\right)^{\frac{3}{4}}\left(a_o\right)^{-\frac{1}{4}}\left(1+\left(\frac{3.4}{\pi\left(1-\nu_s\right)}\right)^{\frac{5}{4}}\right)d\rho_s V_s;\ z > 2.5d \tag{2.24}$$

$$c_x = \frac{2k_x\beta_s}{\omega} + 8\left(\frac{\pi}{4}\right)^{\frac{3}{4}}\left(a_o\right)^{-\frac{1}{4}}d\rho_s V_s;\ \ z \le 2.5d \tag{2.25}$$

Kavvadas et al. (1993) improved the expression for the Winkler modulus by considering the effect of slenderness ratio (L/d).

$$k_x = \frac{3E_s}{1-\nu_s^2}\sqrt[8]{\frac{E_P}{E_S}\cdot\frac{L}{d}} \tag{2.26}$$

Kavvadas et al. (1993), like Gazetas and Dobry (1984), have provided two dashpot coefficient for two ranges of embedment depth.

$$c_x = \frac{2k_x\beta_s}{\omega} + 2\left(\frac{\pi}{4}\right)^{\frac{3}{4}}\left(a_o\right)^{-\frac{1}{4}}\left(1+\left(\frac{3.4}{\pi\left(1-\nu_s\right)}\right)^{\frac{5}{4}}\right)d\rho_s V_s;\ z > 2.5d \tag{2.27}$$

$$c_x = \frac{2k_x\beta_s}{\omega} + 4\left(\frac{\pi}{4}\right)^{\frac{3}{4}}\left(a_o\right)^{-\frac{1}{4}}d\rho_s V_s;\ \ z \le 2.5d \tag{2.28}$$

CHAPTER 3
MATERIALS AND GEOMETRIC PARAMETERS USED IN THE STUDY

This chapter aims to describe the basic input parameters and briefly describe the finite element software PLAXIS 3D, employed for the calibration of the static and dynamic pile head stiffnesses to be derived subsequently.

3.1 Parameters used

To obtain a pile head stiffness that represents a wide range of practical problems for the case of both static and dynamic loading, different soil and pile properties are involved.

3.1.1 Soil parameters

In order to perform the analysis, a wide range of soil properties are used. These values are extracted mainly from Obrzud and Truty (2012) and Bowles (1997).

Young's modulus (E_s)

Soil Young's modulus (E), commonly referred to as soil elastic modulus, is an elastic soil parameter and a measure of soil stiffness. It is defined as the ratio of the stress along an axis over the strain along that axis within the elastic strain range.

Table 3-1: Soil Young's modulus for different types of soils (Bowles 1997)

Soil	$E_s\ (MPa)$
Clay	
Soft	5-25
Medium	15-25
Hard	50-100
Sandy	25-250
Sand	
Silty	5-20
Loose	10-25
Dense	50-81
Sand and gravel	
Loose	50-150
Dense	100-500

Based on the ranges in Table 3-1, soil Young's modulus within a range of 5-300 MPa are used in this study.

Poisson's ratio (v_s)

Poisson's ratio is the ratio of transverse contraction to a longitudinal extension. According to Bowles (1997), the value of Poisson's ratio of a soil lies between 0.2-0.5. The detailed values are given in Table 3-2. In this study, the values of Poisson's ratio used are 0.2, 0.25, 0.35, 0.4 and 0.45.

Table 3-2: Soil Poisson's ratio for different soil types (Bowles (1997)).

Soil	v_s
Most clay soils	0.4-0.5
Saturated clay soil	0.45-0.5
Cohesionless-medium and dense	0.3-0.4
Cohesionless-loose to medium	0.2-0.35

Density of soil (ρ_s)

The density of soil varies from soil to soil. In order to capture a wide range of soils, in this study, the value of soil density is varied from 16 kN/m^3 to 21 kN/m^3.

3.1.2 Pile parameters

To understand the effect of pile properties on the lateral response of single piles, an effort is made to include a wide range of piles. The parameters described in the following sections are considered based on their use in practice.

Most of the time, reinforced concrete is used in the construction of pile foundations. Due to this reason, more emphasis is given to reinforced concrete piles. So, the material properties listed below are only for reinforced concrete. However, this does not imply that the model is not calibrated for piles made of other materials.

Pile Young's modulus (E_p)

According to ES EN 1992:2015 (Part 1.1, Table 3.1), the modulus of elasticity varies depending on the compressive strength of concrete and is given by Equation (3.1)

$$E_{cm} = 22\left(\frac{f_{cm}}{10}\right)^{0.3} \tag{3.1}$$

where $f_{cm} = f_{ck} + 8MPa$ and f_{ck} is the characteristic compressive strength.

Based on the above expression, we can plot the modulus of elasticity against the characteristic compressive strength of concrete, as shown in Figure 3-1.

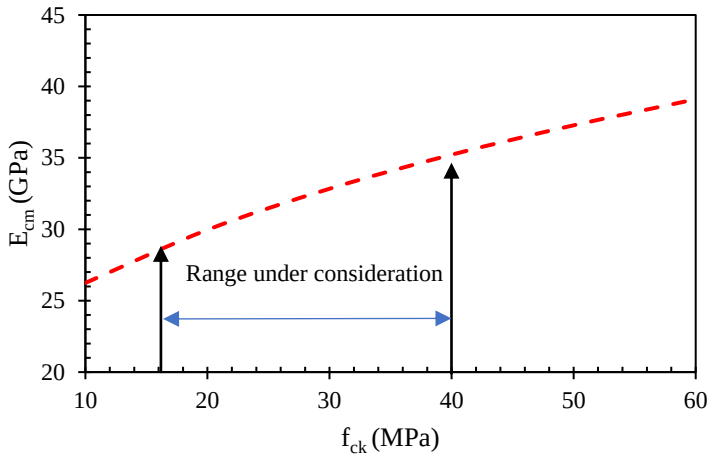

Figure 3-1: Variation of modulus of elasticity of concrete versus characteristic compressive strength

The range of modulus of elasticity under consideration is between 28-35 GPa. This range is selected based on the characteristic compressive strength of concrete commonly used to construct piles. In most pile foundation construction projects, the value of f_{ck} varies between 16 to 40 MPa (C 20 – C 50).

Pile slenderness ratio (L/d)

The effect of length and diameter of the pile is included in the analysis in terms of slenderness ratio (L/d). The slenderness ratio used in this paper varies from 5-50. For L/d less than 5, the pile acts as a perfectly rigid pile, which is not within the scope of this research; and for $L/d > 50$, pile head stiffness remains constant. This implies that increasing the pile length beyond $L/d = 50$, does not affect the overall pile response under horizontal loading. A detailed explanation regarding the effect of L/d is given in Chapter 4.

Diameter of pile (d)

For the calibration of the model using PLAXIS 3D, the following diameters are used: 0.4m, 0.6m, 0.8m, 1m, 1.5m and 2m.

3.1.3 Dynamic soil properties

Shear wave velocity (V_s)

Shear wave velocity is an essential dynamic property of soil that significantly influences pile foundations' lateral stability. In this paper, rather than using shear wave velocities proposed in literature, the well-known analytical relationship between shear wave velocity, soil shear modulus, and soil unit weight is used to make realistic estimates; i.e.

$$V_s = \sqrt{\frac{G_s}{\rho_s}} = \sqrt{\frac{E_s}{2(1+\nu_s)\rho_s}} \tag{3.2}$$

where ρ_s is density of soil.

Material or hysteretic damping ratio (β_s)

Three different material or hysteretic damping values are used: 5%, 10%, and 15%. According to Whitman and Richart (1967), the value of material damping for low strain dynamic loads (e.g., Machine foundation) is about 5%. However, in this study, because the proposed model is to be calibrated not only for machine foundations but also for seismic and other applications, a more comprehensive range of damping is allowed that includes radiation damping.

Dimensionless frequency ratio (a_o)

In this study, rather than using cyclic frequency $\omega(=2\pi f)$, to reduce the number of parameters used in the analysis, dimensionless frequency ratio (similar to the one used by Novak et al. (1978)) is used.

$$a_o = \frac{\omega d}{V_s} = 2\pi f \frac{d}{V_s} \tag{3.3}$$

According to Gazetas (1991b), very high frequencies are always within the range of (a_o <1). Based on this, the value of f/f_n varies between 1-5 (Figure 3-2), where f is frequency under consideration and f_n is the fundamental frequency of the soil layer . The fundamental frequency of a uniform soil deposit on a rigid rock is expressed with the well-known analytical relationship between shear wave velocity and layer thickness H as;

$$f_n = \frac{V_s}{4H} \tag{3.4}$$

In order to determine the range of dimensionless frequency ratio, the following steps are followed. First, the value of f/f_n is assumed to be y. So, based on this, the value of f is rewritten as yf_n or Equation (3.4) takes the form;

$$f = \left(\frac{V_s}{4H}\right) y \tag{3.5}$$

Substituting this into Equation (3.3) and simplifying, the expression given in Equation (3.6) is found.

$$a_o = \frac{\pi}{2}\frac{d}{H} y \tag{3.6}$$

When the value of y is set to one (i.e., $f = f_n$ or resonance), Equation (3.6) and a_{cutoff}, in Equation (2.19), become identical. For different values of H/d and y, the value of a_o is portrayed in Figure 3-2.

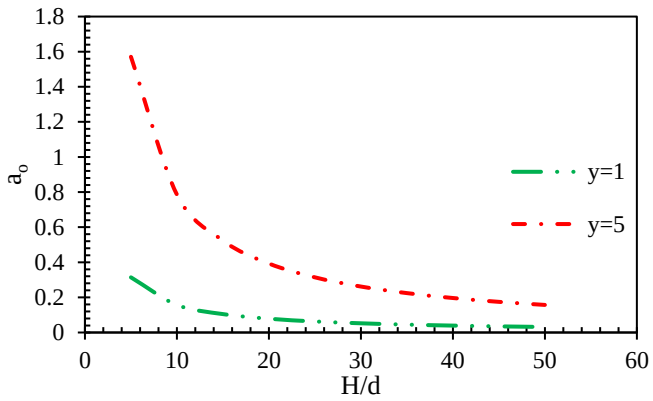

Figure 3-2: Variation of dimensionless frequency ratio

For most engineering problems, the value of H/d is seldom less than 10. Using the maximum excitation frequency of $5f_n$, as sown in Figure 3-2, the dimensionless frequency ratio varies between 1 and 0. For this reason, the range of $0 \le a_o \le 1$ is considered in this study.

3.2 Finite Element analysis using PLAXIS 3D.

For three-dimensional numerical modeling the software PLAXIS 3D is used. It is a commercial finite element tool developed by PLAXIS bv for the analysis of geotechnical problems. All simulations were made using PLAXIS 3D version 2013.

3.2.1 Soil model used

One of PLAXIS 3D's essential features is the wide range of soil models that this software offers to solve particular geotechnical problems. Since beam on an elastic subgrade model was used, and the theory assumes the soil as a linear elastic material, it makes sense to use linear elasticity to model the soil-pile system in the finite element program for compatible results.

3.2.2 Adopted geometry

Adopted model geometry presented in Figure 3-3 is mainly based on the works of (Gupta and Basu 2019), Helwany (2007) and Syngros (2004).

According to Gupta and Basu (2019), the response of laterally loaded piles depends on the location of the boundaries. In their work, they assessed the variation of "normalized radial soil displacement, u_r / r_p" as can be seen in Figure 3-4. It is evident from Figure 3-4 that, beyond $20r_p$, the effect of the applied lateral load almost vanishes. In the figure, r_p is the radius of the pile, r is the radial distance from the center of the pile, and u_r is soil deformation at r distance from the center of the pile. Based on this observation, the adopted geometry uses boundaries located at a distance of $20r_p$ in the x and y directions away from the center of the pile.

Regarding the total thickness of the soil deposit used in the analysis, Helwany (2007) and Syngros (2004) proposed, for the sake of better mesh output, to use $H > 2L$. However, for piles with $L/d > 80$, using $H > 2L$ results in excessive numbers of elements. Hence, Syngros (2004) suggested using $H = 1.25L$ for piles with $L/d > 60$ and $H = 2.5L$ for piles with $60 > L/d > 20$.

3.2.3 Structural model

After defining the soil model and its geometry, defining the structural model in detail is necessary. The pile is modeled using an embedded pile element in PLAXIS 3D. An embedded pile is considered a beam that connects to the surrounding soil through special skin and foot interfaces. As illustrated in Figure 3-5, these interfaces are modeled as a series of springs located on each pile node and pile tip. K_s denotes the elastic shear stiffness while K_n and K_t are the normal elastic stiffness, in the n and t direction, respectively, of the embedded interface elements (Figure 3-5).

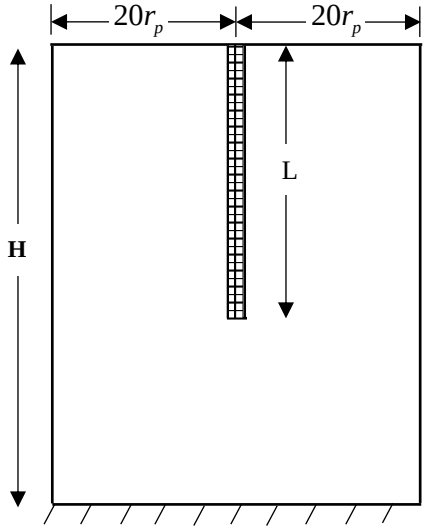

Figure 3-3: Adopted geometry in PLAXIS 3D

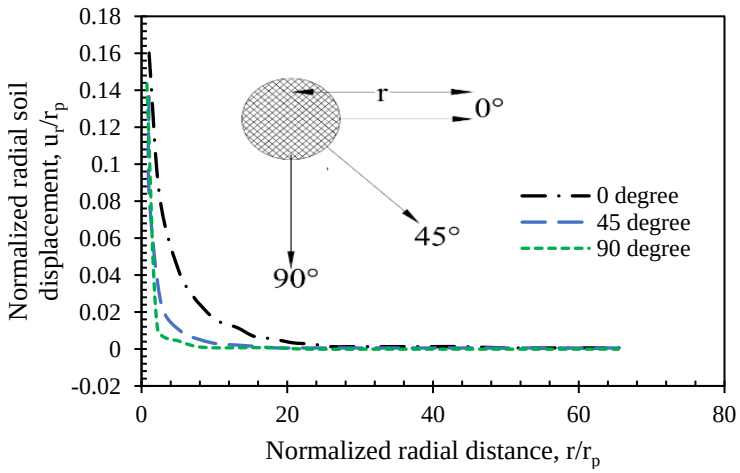

Figure 3-4: Pile and soil responses obtained from 3D FE analysis (Gupta and Basu 2019)

It is necessary to describe the reason behind not using a volume element. In comparison with volume elements, embedded pile elements have their benefits in that the total number of elements in the mesh is lower, which reduces the calculation time. Also, these structural elements allow evaluating the forces using PLAXIS 3D output processor directly.

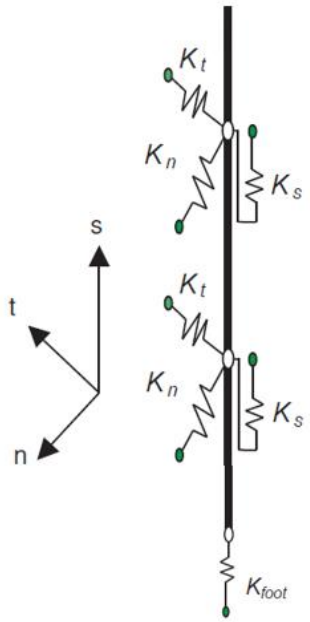

Figure 3-5: Embedded pile model, adapted from Brinkgreve et al. (2013)

3.2.4 Mesh

The finite element mesh should be chosen with special care since choices affect the accuracy of results and calculation time. In PLAXIS 3D, there are five meshing options (very coarse, coarse, medium, fine, and very fine). As the degree of fineness increases, the result's accuracy also increases, but calculation time also increases. A fine mesh is used in this study to achieve better accuracy and minimize the calculation time.

3.2.5 Element type

The soil elements in PLAXIS 3D are 10-node tetrahedral elements. Tetrahedral elements are volume elements with four vertices, six edges, and is bounded by four triangular faces (Figure 3-6). The three nodes per edge in the tetrahedral element shown in Figure 3-6 allows a second-degree approximation of the displacement field.

In PLAXIS, the average element size (l_e) is defined according to Equation (3.7), where the calculation of l_e is based on total size of the model and the relative element size factor (r_e) which varies from very fine ($r_e = 0.5$) to very coarse($r_e = 2$).

$$l_e = \frac{r_e}{20}\sqrt{\left(x_{\max} - x_{\min}\right)^2 + \left(y_{\max} - y_{\min}\right)^2 + \left(z_{\max} - z_{\min}\right)^2} \tag{3.7}$$

where $x_{\min}$, $x_{\max}$, $y_{\min}$, $y_{\max}$, $z_{\min}$ and $z_{\max}$ are coordinates of the pile-soil system under consideration.

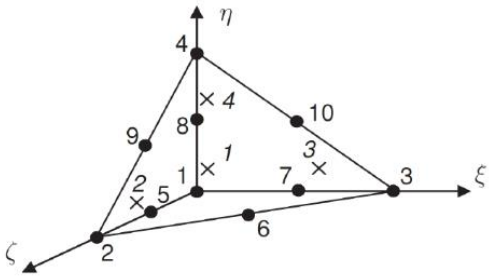

Figure 3-6: 10-node tetrahedral element used in PLAXIS 3D

It is considered good practice to refine the finite element mesh in areas where large deformation gradients are expected. This allows us to have more accurate results with minimum calculation time. Based on this principle, the mesh around the pile was refined, as shown in Figure 3-7.

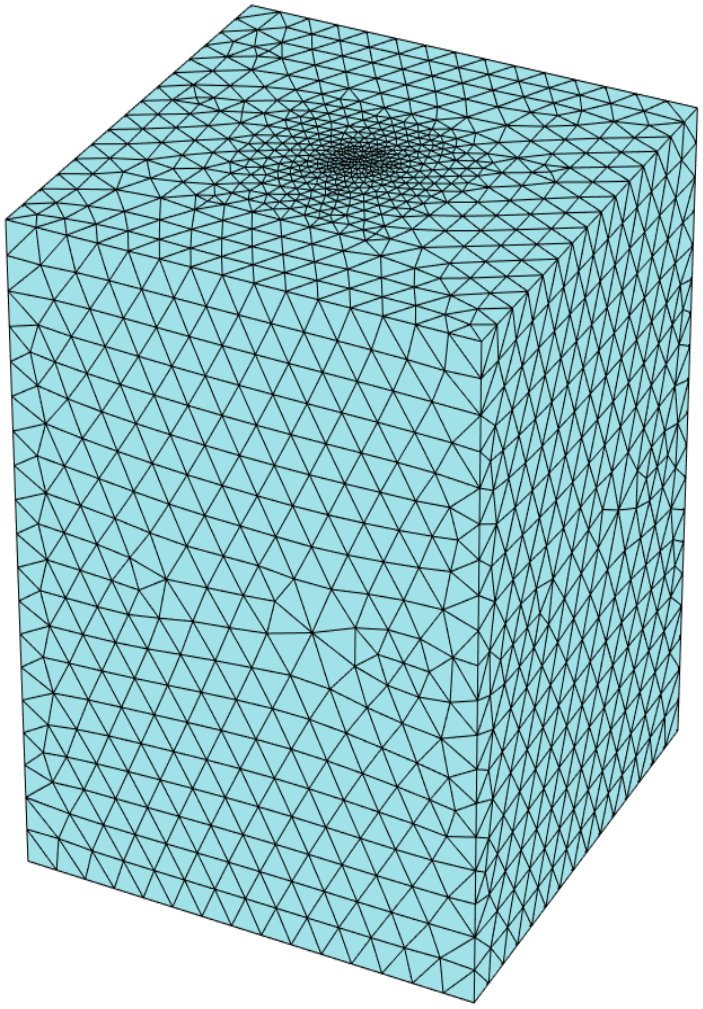

Figure 3-7: Adopted mesh for

CHAPTER 4
STATIC LATERAL RESPONSE

4.1 Introduction

The analysis of piles under lateral loading has been one of the big research areas in geotechnical engineering for the past 40 years or so. According to Sun (1994), the problem is complicated because the soil reaction is dependent on the pile movement, and on the other hand, the pile movement is dependent on soil response. Because of this interdependence, the problem of piles' lateral response can be classified as a problem of soil-structure interaction.

The problem of pile subjected to horizontal loads can be studied as a beam resting on an elastic foundation. Winkler (1867) hypothesized that the deflection at any point of the foundation is proportional to the pressure applied at that point and is independent of the pressures acting at nearby points. Consequently, the foundation acts as if it consisted of infinitely many closely spaced linear springs. The model is simple, but it lacks the fundamental principle that the soil shear resistance must be included. Obviously, it does not accurately represent the characteristics of many practical foundations. Due to this, different models with additional mechanical elements were proposed in the past, as discussed in Chapter 2 in detail.

The purpose of this study is to present an analytical model for laterally loaded piles based on a two-parameter subgrade model that idealizes the subgrade as an elastic continuum. This model is also presented in Chapter 2. A numerical approach based on the model proposed by Worku (2014) for analyzing beams and plates on elastic foundations is adopted for the analysis of a laterally loaded pile.

This chapter focuses on the static elastic response of laterally loaded piles, and more specifically, it aims to:

- derive the deflection equation for different pile-head and base boundary conditions.
- Provide formulas to estimate the pile head static stiffness for different pile-head and base conditions.
- Provide an expression for the critical (active) pile length for laterally loaded piles for different pile-head and base boundary conditions.

- Compare the proposed formulas for pile-head, deflection, stiffness and active pile length with existing relationships in the literature.

4.2 Pile deflection under various boundary conditions

The deflection equations for different boundary conditions are derived and presented in the following sections.

4.2.1 Model description

The system considered is depicted in Figure 4-1: a solid cylindrical pile with a length, L, and diameter, d, is embedded in a linear elastic, homogeneous and isotropic medium, subjected to a horizontal load, P, at the pile head. There are four different boundary conditions: two at the pile head and two at the pile base (Figure 4-2).

Concerning pile-head boundary conditions: the first case is when the pile-head is restrained against rotation; this happens when a thick cap is used in a pile group, and in the case of the second boundary condition, the pile head is not restrained, being able to rotate as it displaces horizontally.

Regarding pile-base boundary conditions: the first case is when the pile-base is restrained against rotation and translation; this happens when the pile is socketed into rigid bedrock, and in the second case, the pile-base is not fixed (floating base), and hence it can rotate and translate at the same time.

4.2.2 Differential equation for pile supported by a two-parameter elastic subgrade

The differential equation (DE) for both the static and dynamic response of laterally loaded piles is derived based on Figure 4.1. The problem is identical to the problem proposed by Hetenyi (1946) for a straight bar under the simultaneous action of axial and transverse loading.

A pile in elastic soil will now be assumed to be subjected to a horizontal load at the pile head. We cut out of this pile an infinitely small unloaded element with length dz (Figure 4-1b).

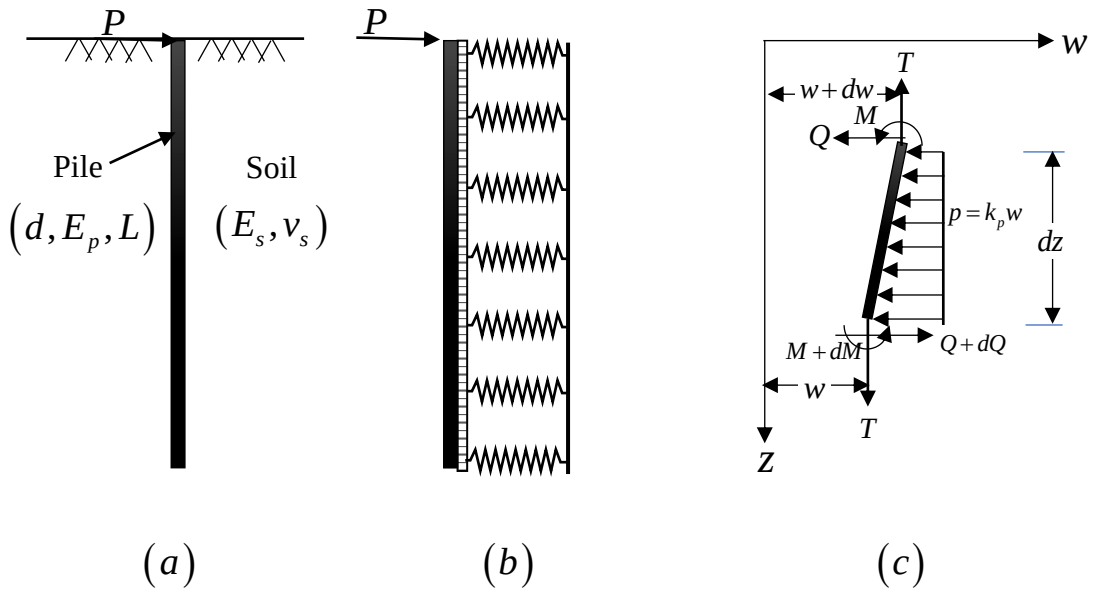

Figure 4-1: Schematic of (a) single pile (b) laterally loaded pile supported by two-parameter subgrade (c) a pile element

For moment equilibrium:

$$(M + dM) - M + Tdw - Qdz = 0$$

$$dM + Tdw - Qdz = 0$$

dividing the whole equation by dz,

$$\frac{dM}{dz} + T\frac{dw}{dz} - Q = 0 \tag{4.1}$$

For horizontal force equilibrium

$$Q - (Q + dQ) + k_p w dz$$

$$-dQ + k_p w dz = 0$$

dividing the whole equation by dz

$$\frac{dQ}{dz} = k_p w \tag{4.2}$$

from mechanics of an Euler-Bernoulli beam we know that

$$\text{Moment } (M) = -EI\frac{d^2 w}{dz^2} \tag{4.3}$$

Substituting Equation (4.3) back into Equation (4.1) and differentiating with respect to z, one obtains

$$-(EI)_P \frac{d^4w(z)}{dz^4} + T\frac{d^2w(z)}{dz^2} - \frac{dQ}{dz} = 0 \tag{4.4}$$

From Equation (4.2), we have $\frac{dQ}{dz} = k_p w$. So, substituting this back into Equation (4.4), we have the well-known differential equation of a beam on a two-parameter subgrade model, which serves as the governing differential equation for the horizontally loaded pile

$$(EI)_P \frac{d^4w(z)}{dz^4} - T\frac{d^2w(z)}{dz^2} + k_p w(z) = 0 \tag{4.5}$$

where;

E_P: elastic modulus of the pile (N/m^2)

I_P: the moment of inertia of the pile in bending (m^4)

$w(z)$: horizontal displacement of the pile (m)

z: depth (m)

k_p : soil's modulus of reaction for horizontal loading (N/m)

T : the soil shear parameter (N/m)

4.2.3 Solution of the differential equation

The governing defferential equation given in Equation (4.5) is solved using method of variation of parameter. Taking a trial solution of $w(z) = e^{mz}$, the characterisic equation shown below is obtained.

$$m^4 - \frac{T}{(EI)_P}m^2 + \frac{k_s}{(EI)_P} = 0$$

The above characterisic equation have four distnict roots ($m_{1,2,3 \text{ and } 4}$); where

$$m_{1,2} = \pm\sqrt{\frac{T}{2(EI)_p} + i\sqrt{\frac{k_s}{EI} - \left(\frac{\tilde{T}}{2(EI)_p}\right)^2}} \text{ and } m_{3,4} = \pm\sqrt{\frac{T}{2(EI)_p} - i\sqrt{\frac{k_s}{EI} - \left(\frac{\tilde{T}}{2(EI)_p}\right)^2}}$$

The value of the expression under the internal square root can be posetive, zero and negative. The three cases can also be represented by $\bar{T} < 1$, $\bar{T} = 1$ and $\bar{T} > 1$; where

$\bar{T} = \tilde{T} / \left(2\sqrt{k_s \left(EI \right)_p} \right)$. The detailed mathematical formulation of all three cases is given in Appendix A.1.

In normal conditions, the pile is stronger than surrounding soil, so only the case of $\bar{T} < 1$ is of practical interest (Scott 1981, Yin 2000), and as shown in Appendix A.1, for this case, the four distnict roots exist as two pairs of conjugate complex numbers ($m_{1,2} = \pm(\alpha + i\beta)$ and $m_{3,4} = \pm(\alpha - i\beta)$).

Substituting back these distnict roots back into the characterstic equation, the deflection equation in the direction of the applied horizontal load is obtained in the form of four unknown coefficients, as shown in Equation (4.6).

$$w(z) = \left(C_1 e^{\alpha z} + C_2 e^{-\alpha z} \right) \cos(\beta z) + \left(C_3 e^{\alpha z} + C_4 e^{-\alpha z} \right) \sin(\beta z) \tag{4.6}$$

where;

$$\alpha = \sqrt{\lambda^2 + \frac{\tilde{T}}{4(EI)_P}},\ \beta = \sqrt{\lambda^2 - \frac{\tilde{T}}{4(EI)_P}} \text{ and } \lambda = \sqrt[4]{\frac{k_s}{4(EI)_P}} \tag{4.7}$$

$$\tilde{T} = Td \text{ and } k_s = k_p d \tag{4.8}$$

The solutions, which are presented in the next sections, are dependent on the two subgrade model parameters T and k_p. Different researchers have tried to use different approaches in order to determine these parameters. In this work, the relations proposed by Worku (2014) are used.

Worku (2014) noting the fact that a two-parameter models is more suitable for practical applications, he established Pasternak parameters by equating the surface deformation of the Pasternak model with his Kerr-type model, which was already devised in his previous work (Worku 2013) in accordance with the continuum approach of subgrade development.

The parameter entailed a calibration factor χ (Equation (4.9) and Equation (4.10)), which makes the modelel proposed by Worku (2013) unique from other models in the literature. If the calibration factor is evaluated with care, the model yields excellent results for the deformation of beams and plates, as demonstrated in the work of Worku (2014).

In this paper, the model is calibrated for piles under lateral static and dynamic force. The detailed study is presented in section 4.3. The parameters proposed by Worku (2014) are given in Equation (4.9) and Equation (4.10) with the open calibration factor, χ.

$$k_p = \frac{(0.4\nu_s + 0.67) \times E_s}{\chi \times B} \tag{4.9}$$

$$T = (1.36\nu_S + 2.28) G_S \chi B \tag{4.10}$$

4.2.4 Boundary conditions studied

Four different soil-pile boundary conditions have been studied as shown in Figure 4-2 for deriving the defection equation of a single pile in a homogenous soil profile subjected to an applied lateral force and moment at the pile head.

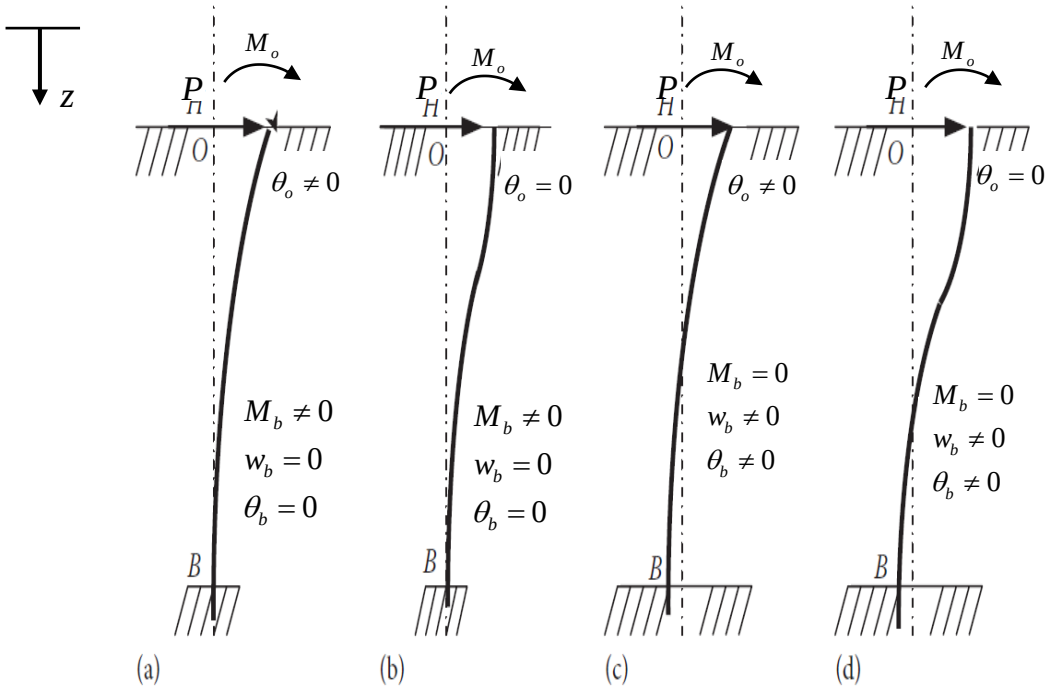

Figure 4-2: Schematic of a) free head, fixed base pile b) fixed head, fixed base pile c) free head, floating base pile d) fixed head, floating base pile (after Guo and Lee (2001)).

4.2.4.1 The boundary conditions

a) **Free-head piles**: - for free head piles, as discussed before, the pile head is free to rotate and translate simultaneously. This implies, the moment induced due to applied lateral load is zero. So, moment at the pile head equals the applied moment.

$$\left(EI\right)_p\left(\frac{d^2}{dz^2}w(z)\right)_{z=0} = -M \tag{4.11}$$

Moreover, the shear force at the pile head is a combination of the applied horizontal force and the contribution of the soil shear resistance. The expression for the shear force at the pile head is derived based on Figure 4-3, where Q is the horizontal shear force, Q_n is the tangential shear acting in the plane of section, expressed in the form of

$$Q_n = Q\cos(\theta) - T\sin(\theta)$$

where θ is a small angle expressed using the tangent function ($\tan\theta = \frac{dw}{dz}$). For small values, $\cos\theta \simeq 1$ and $\sin\theta \simeq \tan\theta = \frac{dw}{dz}$. Substituting back this approximation, we obtain (Hetenyi 1946).

$$Q_n = Q - T\frac{dw}{dz}$$

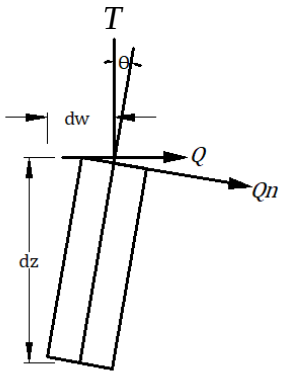

Figure 4-3: Schematic of shear at the pile head

Using the above expression, the second boundary condition (concerning shear force) is derived and presented as

$$(EI)_p\left(\frac{d^3}{dz^3}w(z)\right)_{z=0} - T\left(\frac{d}{dz}w(z)\right)_{z=0} = P \tag{4.12}$$

where $T = G_p$ and are interchangeable.

b) **Fixed-head pile**

For fixed-head piles, because of head fixity, rotation is not allowed. The slope at the pile head is zero, and also the shear force at the pile head is equal to the applied horizontal force. The above statement is expressed in mathematical form as

$$\left(\frac{d}{dz}w(z)\right)_{z=0} = 0 \;\; and \;\; (EI)_p\left(\frac{d^3}{dz^3}w(z)\right)_{z=0} = P$$

c) **Fixed-base piles**:

For fixed base piles, because of the pile-base fixity, rotation and translation at pile base are zero.

$$\left(\frac{d}{dz}w(z)\right)_{z=L} = 0 \;\; and \;\; w(L) = 0$$

d) Floating-base pile:

Guo (2001) has provided simple boundary conditions for floating base pile at pile base. The expressions are given below

$$-T\left(\frac{d}{dz}w(z)\right)_{z=L} - \sqrt{Tk_s}\,w(L) = 0$$

$$(EI)_p\left(\frac{d^2}{dz^2}w(z)\right)_{z=L} = 0$$

4.2.5 Deflection equation

Using the above boundary conditions, the displacement equations for all soil-pile boundary conditions are determined using the commercial software Mathematica 12, and the results are presented below. The workflow used in Mathematica 12 is presented in Appendix A.2 for one of the cases.

Free head floating pile (FHFBP)

$$w(z)=\begin{pmatrix}\dfrac{P}{(EI)_P\,\eta_1}\left(A_1(z)+\dfrac{\sqrt{\tilde{T}k_s}}{(EI)_P}B_1(z)\right)\\ +\dfrac{M_o}{(EI)_P\,\eta_1}\left(C_1(z)+\dfrac{\sqrt{\tilde{T}k_s}}{(EI)_P}D_1(z)\right)\end{pmatrix} \tag{4.13}$$

where;

$$A_1(z)=2\lambda^2\begin{pmatrix}2\alpha^2\beta\left(\alpha^2-3\beta^2\right)\cos\left((L-z)\beta\right)\cosh\left(z\alpha\right)\sin\left(z\alpha\right)\\ +\alpha\left(\alpha^4-4\alpha^2\beta^2+3\beta^4\right)\sin\left(L\beta\right)\sin\left((L-z)\beta\right)\sinh\left(z\alpha\right)\\ +\beta\left(-3\alpha^2+\beta^2\right)\begin{pmatrix}-2\alpha\beta\cos\left(z\beta\right)\cosh\left((L-z)\alpha\right)\\ +\left(-\alpha^2+\beta^2\right)\sin\left(z\beta\right)\sinh\left((L-z)\alpha\right)\end{pmatrix}\sinh\left(L\beta\right)\end{pmatrix}$$

$$B_1(z)=2\alpha\beta\begin{pmatrix}\sinh\left(L\alpha\right)\begin{pmatrix}\left(\alpha^2-\beta^2\right)\cosh\left((L-z)\alpha\right)\sin\left(z\beta\right)\\ +2\alpha\beta\cos\left(z\beta\right)\sinh\left(L-z\right)\alpha\end{pmatrix}\\ -\sin\left(L\beta\right)\begin{pmatrix}-2\alpha\beta\cosh\left(z\alpha\right)\sin\left((L-z)\alpha\right)+\\ \left(\alpha^2-\beta^2\right)\cos\left((L-z)\beta\right)\sinh\left(z\alpha\right)\end{pmatrix}\end{pmatrix}$$

$$C_1(z)=4\lambda^4\begin{pmatrix}\alpha\left(\alpha^2-3\beta^2\right)\sin\left(\beta L\right)\begin{pmatrix}\alpha\cosh\left(\alpha z\right)\sin\left((L-z)\beta\right)\\ -\beta\sinh\left(\alpha z\right)\cos\left((L-z)\beta\right)\end{pmatrix}\\ +\beta\left(3\alpha^2-\beta^2\right)\sinh\left(\alpha L\right)\begin{pmatrix}\alpha\cosh\left((L-z)\alpha\right)\sin\left(\beta z\right)\\ -\beta\sinh\left((L-z)\alpha\right)\cos\left(\beta z\right)\end{pmatrix}\end{pmatrix}$$

$$D_1(z)=4\alpha\beta\lambda^2\begin{pmatrix}\sinh\left(\alpha L\right)\begin{pmatrix}\alpha\sinh\left((L-z)\alpha\right)\sin\left(\beta z\right)\\ -\beta\cosh\left((L-z)\alpha\right)\cos\left(\beta z\right)\end{pmatrix}\\ +\cos\left(\beta L\right)\begin{pmatrix}\beta\sinh\left(\alpha z\right)\cos\left((L-z)\beta\right)\\ -\alpha\cosh\left(\alpha z\right)\sin\left((L-z)\beta\right)\end{pmatrix}\end{pmatrix}$$

$$\eta_1 = \lambda^2 \begin{pmatrix} 2\lambda^2\left(-\left(\alpha^2+\beta^2\right)^3\right)+\left(\alpha^3-3\alpha\beta^2\right)^2\cos\left(2L\beta\right)+\left(-3\alpha^2\beta+\beta^3\right)^2\cosh\left(2L\beta\right) \\ +2\dfrac{\sqrt{\tilde{T}k_s}}{\left(EI\right)_P}\alpha\beta\left(\alpha\left(\alpha^2-3\beta^2\right)\sin\left(2L\beta\right)-\beta\left(-3\alpha^2+\beta^2\right)\sinh 2L\alpha\right) \end{pmatrix}$$

Free-head fixed base (FHFxBP)

$$w(z) = \frac{P}{\left(EI\right)_P \eta_2}\left(A_2(z)\right) + \frac{M_o}{\left(EI\right)_P \eta_2}\left(C_2(z)\right) \tag{4.14}$$

where;

$$A_2(z) = 2\alpha\beta \begin{pmatrix} -\alpha\cos\left(L\beta\right)\cosh\left(z\alpha\right)\sin\left(\left(L-z\right)\beta\right)+\beta\cos\left(z\beta\right)\cosh\left(L\alpha\right)\sinh\left(\left(L-z\right)\alpha\right) \\ -\left(\alpha^2-\beta^2\right)\begin{pmatrix}\left(-\beta\sin\left(z\beta\right)\sinh\left(L\alpha\right)\sinh\left(\left(L-z\right)\alpha\right)\right) \\ +\alpha\sin\left(L\beta\right)\sin\left(\left(L-z\right)\beta\right)\sinh\left(z\alpha\right)\end{pmatrix} \end{pmatrix}$$

$$C_2\left(z\right) = 2\lambda^2 \begin{pmatrix} \beta\sinh\left(\left(L-z\right)\alpha\right)\begin{pmatrix}\alpha\cosh\left(\alpha L\right)\sin\left(\beta z\right) \\ -\beta\sinh\left(\alpha L\right)\cos\left(\beta z\right)\end{pmatrix} \\ +\alpha\sin\left(\left(L-z\right)\beta\right)\begin{pmatrix}\beta\sinh\left(\alpha z\right)\cos\left(\beta L\right) \\ -\alpha\cosh\left(\alpha z\right)\sin\left(\beta L\right)\end{pmatrix} \end{pmatrix}$$

$$\eta_2 = \lambda^2\left(4\lambda^4-\alpha^2(\alpha^2-3\beta^2)\cos\left(2L\beta\right)-\beta^2(-3\alpha^2+\beta^2)\cosh\left(2L\alpha\right)\right)$$

Fixed-head floating base (FxHFBP)

$$w(z) = \frac{P}{\left(EI\right)_P \eta_3}\left(A_3(z)+\frac{\sqrt{\tilde{T}k_s}}{\left(EI\right)_P}B_3(z)\right) \tag{4.15}$$

$$A_3(z) = 2\lambda^2 \begin{pmatrix} 2\alpha\lambda^2\left(\alpha\cos\left(z\beta\right)\cosh\left(z\alpha\right)-\beta\sin\left(z\beta\right)\sinh\left(z\alpha\right)\right) \\ -\beta\left(-3\alpha^2+\beta^2\right)\sinh\left(L\alpha\right)\begin{pmatrix}\alpha\cosh\left(\left(L-z\right)\alpha\right)\sin\left(z\beta\right) \\ +\beta\cos\left(z\beta\right)\sinh\left(L-z\right)\alpha\end{pmatrix} \\ -\alpha\left(\alpha^2-3\beta^2\right)\cos L\beta\begin{pmatrix}\alpha\cos\left(\left(L-z\right)\beta\right)\cosh z\alpha \\ -\beta\sin\left(L-z\right)\beta\sinh\left(z\alpha\right)\end{pmatrix} \end{pmatrix}$$

$$B_3(z) = 2\alpha\beta\begin{pmatrix} -\alpha\cos(L\beta)\cosh(z\alpha)\sin((L-z)\beta) \\ +\beta\cos(z\beta)\cosh((L-z)\alpha)\sinh(L\alpha) \\ \alpha\sin(z\beta)\sinh(L\alpha)\sinh((L-z)\alpha) \\ -\beta\cos((L-z)\beta)\cos(L\beta)\sinh(z\alpha) \end{pmatrix}$$

$$\eta_3 = 2\lambda\alpha\beta\begin{pmatrix} (\alpha^2+\beta^2)(\beta(3\alpha^2-\beta^2)\sinh(2L\alpha)-\alpha(\alpha^2-3\beta^2)\sin(2L\beta)) \\ 2\alpha\beta\dfrac{\sqrt{\tilde{T}k_s}}{(EI)_P}(\mathrm{Cos}(2L\beta)+\cosh(2L\alpha)) \end{pmatrix}$$

Fixed-head Fixed-Base Pile (FxHFxBP)

$$w(z) = \frac{P}{(EI)_P\,\eta_4}A_4(z) \tag{4.16}$$

$$A_4 = \beta\begin{pmatrix} \alpha\cosh(L\alpha)\sin(z\beta)\sinh(L-z)\alpha \\ +\beta\cos(z\beta)\sinh L\alpha\sinh((L-z)\alpha) \\ -\alpha\cos(L\beta)\sin((L-z)\beta)\sinh z\alpha \end{pmatrix} - \alpha^2\cosh(z\alpha)\sin(L\beta)\sin(L-z)\beta$$

$$\eta_4 = 2\alpha\beta\lambda^2(\alpha\sin(2L\beta)+\beta\sinh(2L\alpha))$$

4.3 Calibration factor

Since the model proposed by Worku (2014) is used to analyze the pile response, the value of the calibration factor must be determined for each set of soil-pile boundary conditions. The determination of the calibration factor χ is based on the results obtained from PLAXIS 3D. For the sake of checking the agreement of the proposed model with other previous works, results in literature are compared in the process.

As could be seen from the foregoing results, the problem of the static lateral response of a single pile in a homogeneous soil profile is governed by four dimension-bound parameters (E_s, E_p, d and L) and one dimensionless parameter (v_s). Using the principle of Buckingham (1914), given that three dimensions of basic physical quantities are involved (time, mass and length), the system can be represented by three dimensionless ratios (E_p/E_s, L/d and v_s,).

The calibration is performed by using the above dimensionless ratios. So, in order to capture the effect of each parameter, the following steps are followed.

Step 1: The pile's slenderness is kept constant, and all the soil and pile parameters are varied.

Step 1.1: Poisson's ratio is kept constant, and the dimensionless stiffness ratio, E_p/E_s is varied.

Step 1.2: The dimensionless stiffness ratio, E_p/E_s, is kept constant, and Poisson's is ratio varied.

Step 2: The effect of slenderness is studied by varying the pile's diameter and length while keeping the soil and pile properties constant.

4.3.1 Parameters used for calibration

A detailed explanation for selecting parameters is given in Chapter 3. Because in this chapter, dimensionless ratios are used, it is found important to list the parameters used in the calibration process. They are

- Pile-soil stiffness ratio (E_p/E_s) = 100 to 100,000
- Poisson's ratio (v_s) = 0.25, 0.3, 0.35, 0.4, 0.45 and 0.5
- Pile slenderness (L/d) = 5 to 50

4.3.2 Calibration factor determination

As discussed in Chapter 2, the analytical model parameters used in this work involve a calibration factor yet to be determined for different applications. In this section, the model is calibrated specifically for laterally loaded piles.

In general, the calibration process focuses on fitting the deflection profile found using the analytical model with the deflection profile from PLAXIS 3D by adjusting the value of the calibration factor, χ. Then each discrete calibration factor is curve fitted to give simple expressions. The detailed calibration process is given in Appendix B.

During the calibration process, it was noticed that the calibration factor is only dependent on the pile head boundary conditions. This implies that the value calculated for fixed-head floating pile can also work for fixed-head fixed base pile, and also the value calculated for free-head floating base pile can also work for free-head fixed base piles. So, the results below are presented as the calibration factor for fixed-head pile and free-head pile regardless of the base condition.

The calibration factor for fixed-head piles is given by Equation (4.17) and the one obtained for free-head piles is given by Equation (4.18).

$$\chi = \left(0.2536 v_s + 0.2727\right) * \left(\frac{E_p}{E_s}\right)^{0.0936} \tag{4.17}$$

$$\chi = \left(0.478 v_s + 0.514\right) * \left(\frac{E_p}{E_s}\right)^{-0.002} \tag{4.18}$$

The calibration factor, χ, is plotted for the fixed-head (Figure 4-4) and free-head piles (Figure 4-5) for selected values of the soil Poisson's ratio.

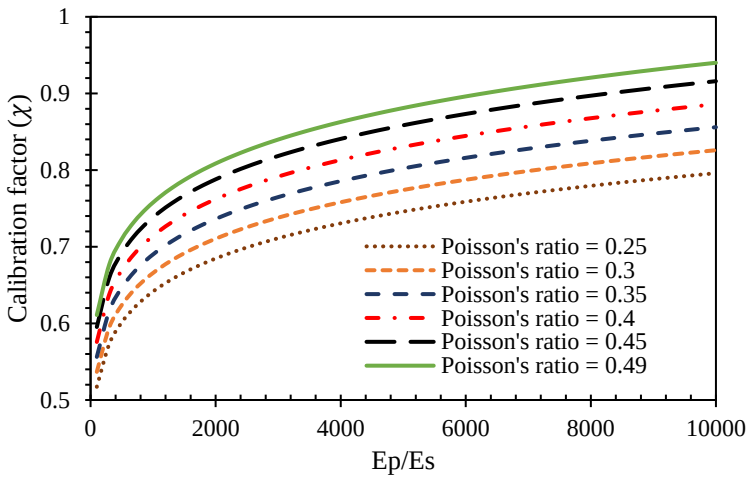

Figure 4-4: Calibration factor for fixed-head piles in a homogeneous soil profile subjected to an applied lateral force at the head.

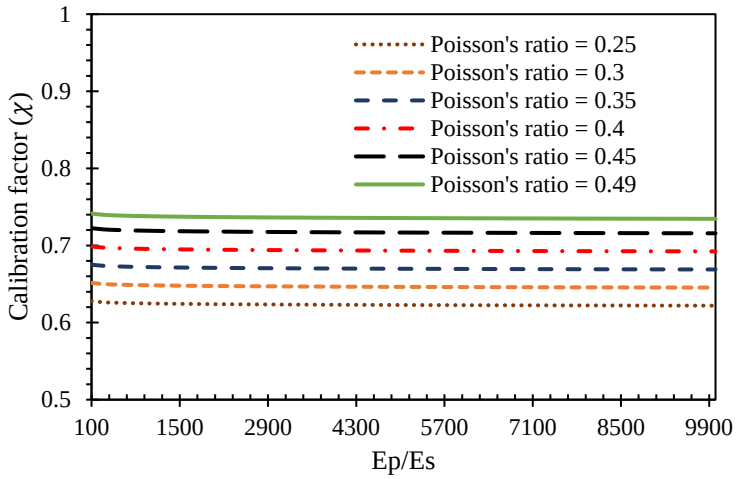

Figure 4-5: Calibration factor for free-head piles in a homogeneous soil profile subjected to an applied lateral force at the head.

The calibration factor, χ , is plotted for both fixed-head and free-head piles against v_s for selected values of the pile-soil stiffness ratio.

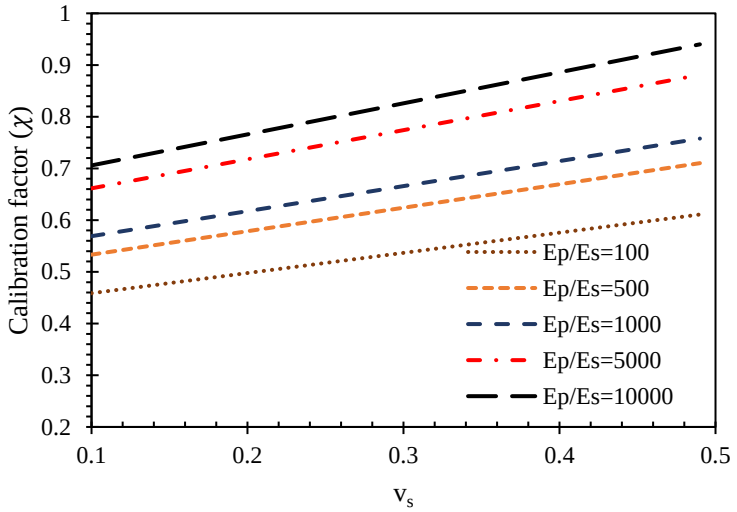

Figure 4-6: Calibration factor for fixed-head piles in a homogeneous soil profile subjected to an applied lateral force at the head: effect of pile-soil stiffness ratio.

The following points are worth mentioning concerning the variation of the calibration factor χ for both free-head and fixed-head piles.

- The calibration factor varies within a narrow range in all cases; indicating that proper consideration of the subgrade model's soil shear effect is important.
- The proposed calibration factor χ in the case of fixed-head piles (Figure 4-4) is more dependent on the pile-soil stiffness ratio than free head piles. Because of the pile head fixity, the pile response depends on the pile stiffness rather than the soil's property.

- In the case of a free-head pile (Figure 4-5 and Figure 4-7), the calibration factor is much dependent on the Poisson's ratio rather than the pile-soil stiffness ratio. In other words, the pile's response under horizontal loading in the case of free-head condition is much dependent on the response of the soil surrounding the pile.
- Figure 4-7 portrays that the calibration factor of free-head piles is practically independent of the pile-soil stiffness ratio. So, the contribution of E_p/E_s in Equation (4.18) can be neglected, and a simplified equation is obtained (Equation (4.19)).

$$\chi = 0.478v_s + 0.514 \tag{4.19}$$

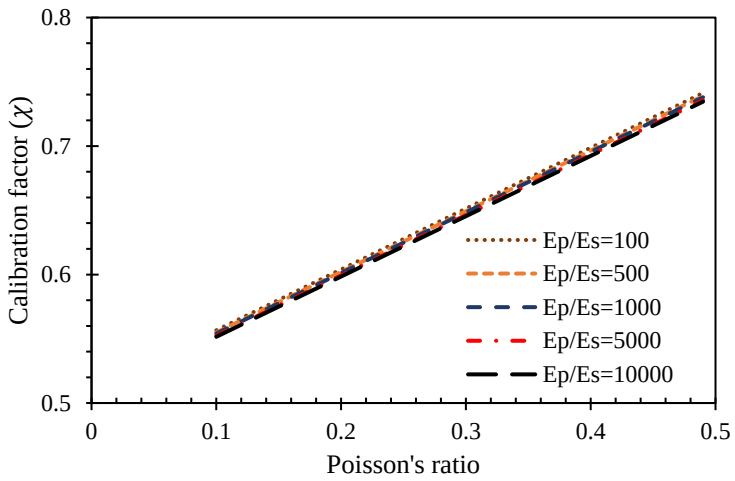

Figure 4-7: Calibration factor for free-head piles in a homogeneous soil profile subjected to an applied lateral force at the head: effect of pile-soil stiffness ratio.

The subgrade model parameters used in this study given in Equation (4.9) and (4.10) can now be simplified by substituting back the calibration factors thus obtained.

Fixed-head

After substituting the calibration factor given in Equation (4.17) back into Equation (4.9) and (4.10), k_p and T take the form

$$k_p = \left(\frac{0.4v_s + 0.67}{0.2536v_s + 0.2727}\right) E_s \left(\frac{E_p}{E_s}\right)^{-0.0936} / d$$

$$T = \left(\frac{(1.36v_s + 2.28)(0.2536v_s + 0.2727)}{2(1+v_s)}\right) E_s \left(\frac{E_p}{E_s}\right)^{0.0936} d$$

Both expressions can be further simplified by fitting the values in the first bracket. Using linear regression analysis, both functions (for $0.1 \le v_s \le 0.5$) can be fitted with a minimum R-square of 99%. Therefore, the expression of k_p and T after curve fitting become

$$k_p = \left(2.41 - 0.47 v_s \right) E_s \left(\frac{E_p}{E_s} \right)^{-0.0936} / d$$

$$T = \left(0.17 v_s + 0.31 \right) E_s \left(\frac{E_p}{E_s} \right)^{0.0936} d$$

Free-head

Following a similar approach like the fixed-head case, the simplified expressions of k_p and T are found for free-head piles as

$$k_p = \left(1.28 - 0.25 v_s \right) E_s / d$$

$$T = \left(0.32 v_s + 0.58 \right) E_s d$$

4.3.3 Comparison of pile head response under lateral loading

The calibration process was mainly dependent on PLAXIS 3D software output, and as it can be seen from Figure 4.8 and Figure 4-9, it gives a head deformation with a maximum error of $\pm 3\%$ for $v_s = 0.25$ and $L/d = 25$. With the aim of comparing the proposed model with recent recommendations, head deformations computed by Higgins et al. (2013) for fixed-head (Equation (4.20)) and free head (Equation (4.21)) piles are used. A formula suggested for free-head piles by Randolph (1981) (Equation (4.22)) is also provided.

$$w_{top} = 0.24 \frac{P}{G_s \left(1 + 0.75 v_s \right) r_p} \left(\frac{E_P}{G_s \left(1 + 0.75 v_s \right)} \right)^{-0.20} \quad (4.20)$$

$$w_{top} = 0.34 \frac{P}{G_s \left(1 + 0.75 v_s \right) r_p} \left(\frac{E_P}{G_s \left(1 + 0.75 v_s \right)} \right)^{-0.18} \quad (4.21)$$

$$w_{top} = 0.25 \frac{P}{G_s \left(1 + 0.75 v_s \right) r_p} \left(\frac{E_P}{G_s \left(1 + 0.75 v_s \right)} \right)^{-\frac{1}{7}} \quad (4.22)$$

Figures 4-8 and 4-9 portray the variation of pile head deformation under a lateral load of 1000 kN. From the figures, it is evident that the proposed model can predict piles' response with a maximum error of $\pm 5\%$.

A more generalized comparison is given in Figure 4-10 and Figure 4-11, which display dimensionless plots of the pile head deformation for fixed-head and free-head piles, respectively.

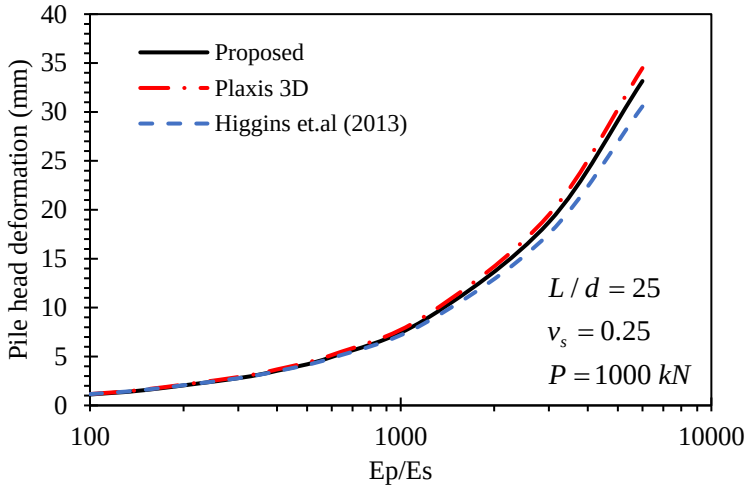

Figure 4-8: Pile-head displacement for fixed-head piles in a homogeneous soil profile subjected to an applied 1000kN lateral force at the head.

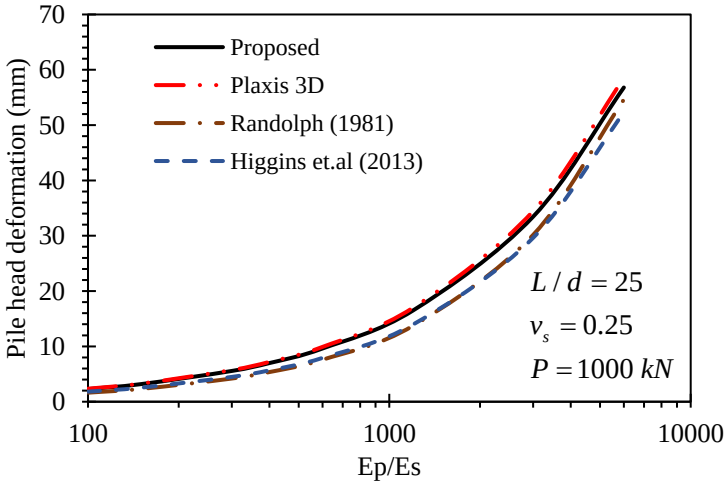

Figure 4-9: Pile-head displacement for free-head piles in a homogeneous soil profile subjected to an applied 1000kN lateral force at the head.

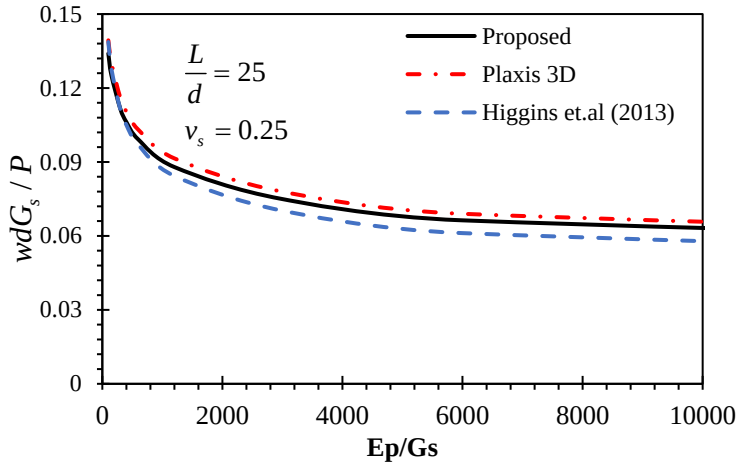

Figure 4-10: Dimensionless pile head displacement for fixed-head piles in homogeneous soil profiles subjected to applied lateral force at the head

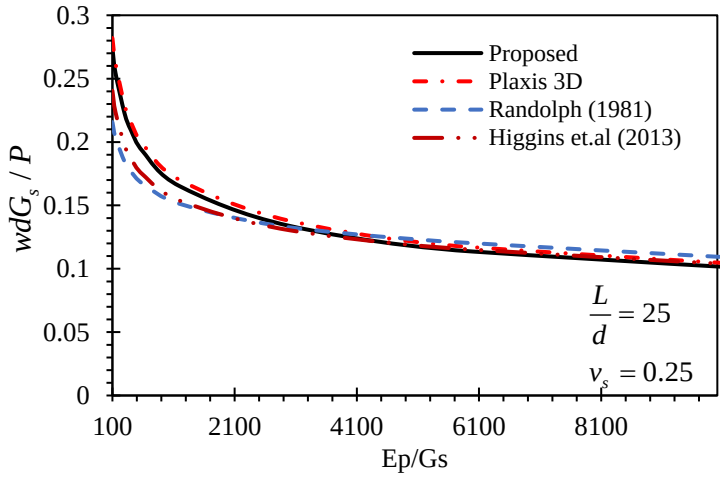

Figure 4-11: Dimensionless pile head displacement for free-head piles in a homogeneous soil profile subjected to an applied lateral force at the head

The following points are worth mentioning based on the results plotted, Figure 4-8 through Figure 4-11.

- The proposed calibration factor for both fixed-head and free-head piles gives excellent results for all ranges of soil-pile stiffness ratios compared to FE results.
- The values proposed by Higgins et al. (2013) and Randolph (1981) for free-head piles gives good results for pile-soil stiffness ratio greater than 2000.
- For fixed-head piles, both Higgins et al. (2013) and Randolph (1981) give a very close solution for a pile-soil stiffness ratio less than 2000, representing most pile foundation problems.

Expressions for the pile head deformation of both free-head and fixed-head long flexible piles in a homogeneous soil are obtained by curve fitting to the plots in Figure 4-10 and Figure 4-11. The equations for the free-head and fixed-head piles are obtained as Equation (4.23) and Equation (4.24), respectively.

$$w_{top} = 0.465 \frac{P}{G_s \left(0.98 + v_s\right) r_p} \left(\frac{E_P}{E_s}\right)^{-0.214} \tag{4.23}$$

$$w_{top} = 0.21 \frac{P}{G_s \left(1.15 + v_s\right) r_p} \left(\frac{E_P}{E_s}\right)^{-0.171} \tag{4.24}$$

The proposed pile head deformations described in Equation (4.23) and Equation (4.24) are employed in the analyses; and the results are compared to the respective deflection equation proposed by Higgins et al. (2013). From the comparison, it was observed that the maximum difference in dimensionless pile head deformation for practical significance cases (concrete pile) was less than $\pm 4\%$.

4.3.3.1 Comparison between the proposed model and one-parameter (Winkler) models

For the past 30 years, different researchers have proposed Winkler subgrade modulus for the analysis of lateral pile response in a homogenous soil. In this work, five different sources for the Winkler modulus from the literature are used for comparison with the proposed model (Table 4-1).

The solutions obtained above for a two-parameter support can still be used for the single parameter Winkler models by setting T=0. Accordingly, the various expressions in Table 4.5 can be used to evaluate the pile response. Solving Equation (4.13) through Equation (4.16) at z=0 for various boundary conditions, one obtains the results shown in Figures 4-12 and 4-13

As we can see from Figure 4-12 and Figure 4-13, the model proposed by Dobry and O'Rourke (1983) and Syngros (2004) give more close results to the current model (and hence PLAXIS 3D), while those proposed by both Vesic (1961) and Biot (1937) are far from the proposed relationship.

Table 4-1: Static expressions for subgrade modulus found in literature

Studies	Subgrade modulus k_s
Francis (1964)	$k_s = 1.3\frac{E_s}{\left(1-\nu_s^2\right)}\left(\frac{\left(EI\right)_p}{E_s d^4}\right)^{-\frac{1}{12}}$
Dobry and O'Rourke (1983)	$k_s = 3G_s$
Syngros (2004) Fixed-head pile Free-head pile	 $k_s = 2E_s\left(E_p / E_s\right)^{-0.075}$ $k_s = 3.5E_s\left(E_p / E_s\right)^{-0.11}$
Biot (1937)	$k_s = 0.95\frac{E_s}{\left(1-\nu_s^2\right)}\left(\frac{\left(1-\nu_s^2\right)\left(EI\right)_p}{E_s d^4}\right)^{-0.108}$
Vesic (1961)	$k_s = 0.65\frac{E_s}{\left(1-\nu_s^2\right)}\left(\frac{\left(EI\right)_p}{E_s d^4}\right)^{-\frac{1}{12}}$

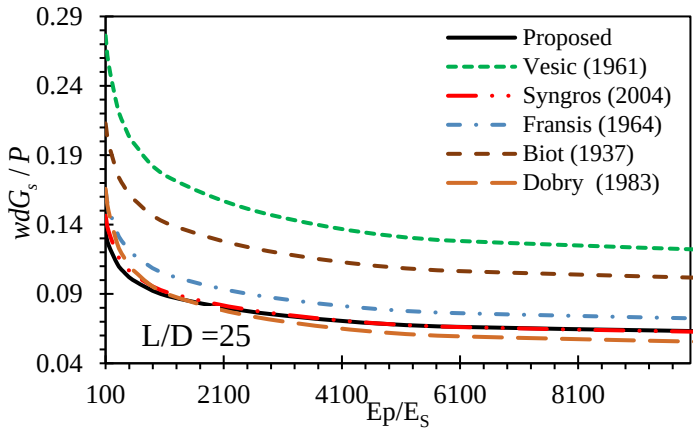

Figure 4-12: Dimensionless pile head displacement for fixed-head piles

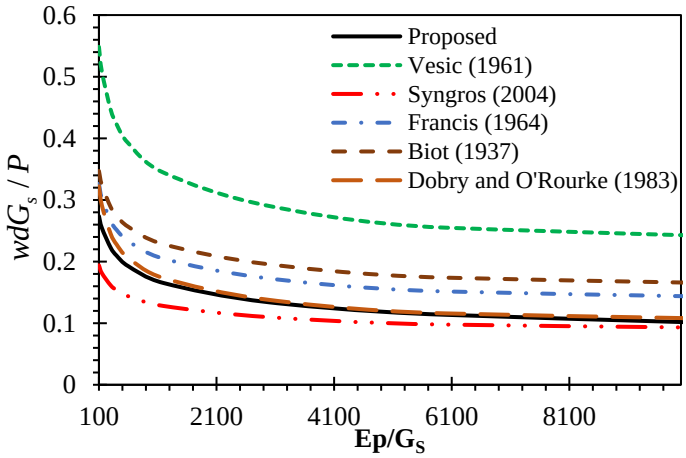

Figure 4-13: Dimensionless pile head displacement for free-head piles

Francis (1964) considered that the pile condition differs from beams; that is, piles are entirely surrounded by foundation material, and therefore the subgrade modulus k_s, for pile, should be twice as much as the value given by Vesic (1961). Because of this adjustment, the value proposed by Francis (1964) is much closer to the proposed value than that of Vesic (1961).

In order to get closer values of pile head deflection using subgrade modulus of both Vesic (1961) and Biot (1937), an adjustment factor, δ, was introduced ($k_{s(new)} = \delta k_s$). In order to obtain the adjustment factors, a trial and error approach was used (for given pile-soil properties, different adjustment factors are tried until close enough values are obtained). The results for fixed-head piles are presented in Table 4-2 for selected Poisson's ratio values.

Table 4-2: Subgrade modulus adjustment factors for fixed-head piles

Model	Adjustment factor (δ)					
	Poisson's ratio (v_s)					
	0.25	0.3	0.35	0.4	0.45	0.49
Vesic (1961)	2.5	2.4	2.3	2.1	2.0	1.9
Biot (1937)	1.9	1.8	1.7	1.6	1.5	1.4

For general use, the adjustment factors of fixed-head piles in Table 4-2 are given as linear functions for Biot (1937) and Vesic (1961) in Equation (4.25) and Equation (4.26), respectively. It is important to note that these factors are relatively sensitive to v_s.

$$\delta_B = 2.41 - 2.03 v_s \tag{4.25}$$

$$\delta_V = 3.2 - 2.65 v_s \tag{4.26}$$

Using the subgrade adjustment factors for fixed-head piles, Equation (4.25) and Equation (4.26), the expressions of subgrade modulus of Vesic (1961) and Biot (1937), after some simplification, are rewritten as Equation (4.27) and Equation (4.28), respectively.

$$k_s = 0.65 \frac{E_s}{\left(-0.282 v_s^{\,2} + 0.336 v_s + 0.3044\right)} \left(\frac{(EI)_p}{E_s d^4} \right)^{-\frac{1}{12}} \tag{4.27}$$

$$k_s = 0.95 \frac{E_s}{\left(-0.378 v_s^{\,2} + 0.465 v_s + 0.4\right)} \left(\frac{\left(1 - v_s^{\,2}\right)(EI)_p}{E_s d^4} \right)^{-0.108} \tag{4.28}$$

The plot of normalized pile head deflection using the new subgrade modulus is given in Figure 4-14. The match is almost perfect over the entire range of pile-to-soil relative stiffness ratio.

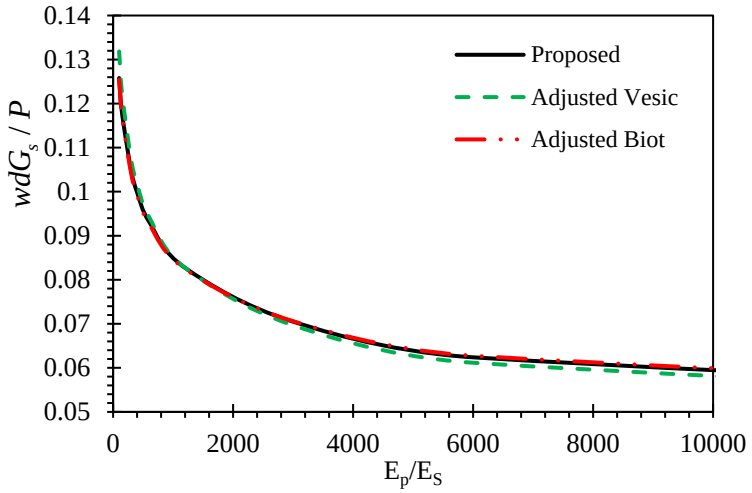

Figure 4-14: Dimensionless pile head displacement for fixed-head piles in a homogeneous soil profile subjected to an applied lateral force at the head: adjusted subgrade models

Using the same procedure as the fixed-head pile, the adjustment factors for free head piles are obtained. The results are given in Table 4-3.

Table 4-3: Subgrade modulus adjustment factors for free-head piles

Model	Adjustment factor (δ)					
	Poisson's ratio (v_s)					
	0.25	0.3	0.35	0.4	0.45	0.49
Vesic (1961)	3.41	3.18	2.94	2.71	2.47	2.28
Biot (1937)	1.97	1.83	1.68	1.54	1.40	1.28

The adjustment factors like the fixed-head are relatively sensitive to Poisson's ratio, v_s. The expressions for the adjustment factor for the subgrade model of Biot (1937) and Vesic (1961) are given in Equation (4.29) and Equation (4.30), respectively.

$$\delta_B = 2.695 - 2.887 v_s \tag{4.29}$$

$$\delta_V = 4.592 - 4.71 v_s \tag{4.30}$$

The new subgrade modulus of Biot (1937) and Vesic (1961), which incorporate the adjustment factor, are given in Equation (4.31) and Equation (4.32), respectively. Also, their plot is given in Figure 4-15.

$$k_s = 0.95\frac{E_s}{\left(0.2714v_s^{\,2}+0.29v_s+0.385\right)}\left(\frac{\left(1-v_s^{\,2}\right)\left(EI\right)_p}{E_s d^4}\right)^{-0.108} \tag{4.31}$$

$$k_s = 0.65\frac{E_s}{\left(0.0485v_s^{\,2}+0.2054v_s+0.2202\right)}\left(\frac{\left(EI\right)_p}{E_s d^4}\right)^{-\frac{1}{12}} \tag{4.32}$$

In Figure 4-14 and Figure 4-15, results from the present study are compared against adjusted subgrade models of Biot (1937) and Vesic (1961). From the results, it is evident that the adjustment factors introduced produced a very close solution. So, it is proposed that the adjustment factors provided be used whenever a single-parameter model is used for the analysis of pile head deformation. The corresponding expressions may thus be referred to as the modified/improved Vesic and Biot subgrade moduli, respectively

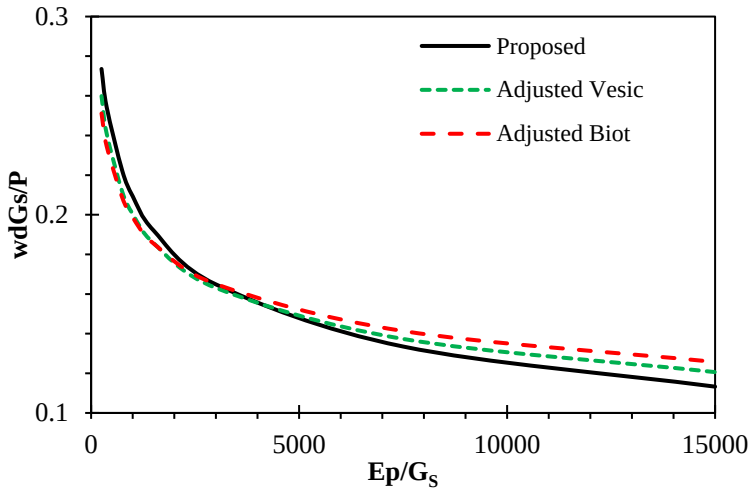

Figure 4-15: Dimensionless pile head displacement for free-head piles in a homogeneous soil profile subjected to an applied lateral force at the head from literature: adjusted subgrade models

4.3.3.2 Deflection profiles

Even if this study's primary concern is to assess the static and dynamic response of piles at the pile head, with the aim of investigating the response throughout the pile length, deflection profiles for selected soil-pile properties are presented in Figure 4-16 and Figure 4-17. The following observations can be made in comparison with the studies mentioned above

- From Figure 4-16, it is evident that for free-head piles, the Plaxis 3D output is in good agreement with the FE results obtained by Syngros (2004) and Dobry and O'Rourke (1983). So, the FE model used in this work to model free-head piles is adequate for the job. Also, from Figure 4-17, we can see that the FE model used for modeling fixed-head piles is in good agreement with the results obtained by Syngros (2004) and Dobry and O'Rourke (1983).
- Figure 4-18 and Figure 4-19 portray the agreement between the proposed model and FE result for both free-head and fixed head piles over the entire pile length.
- The adjusted Biot (1937) and Vesic (1961) subgrade moduli give very close results to the FE result for both free-head (Figure 4-20) and fixed-head piles (Figure 4-21). To appreciate the effect of the adjustment factor, the subgrade moduli before and after adjustment are used.

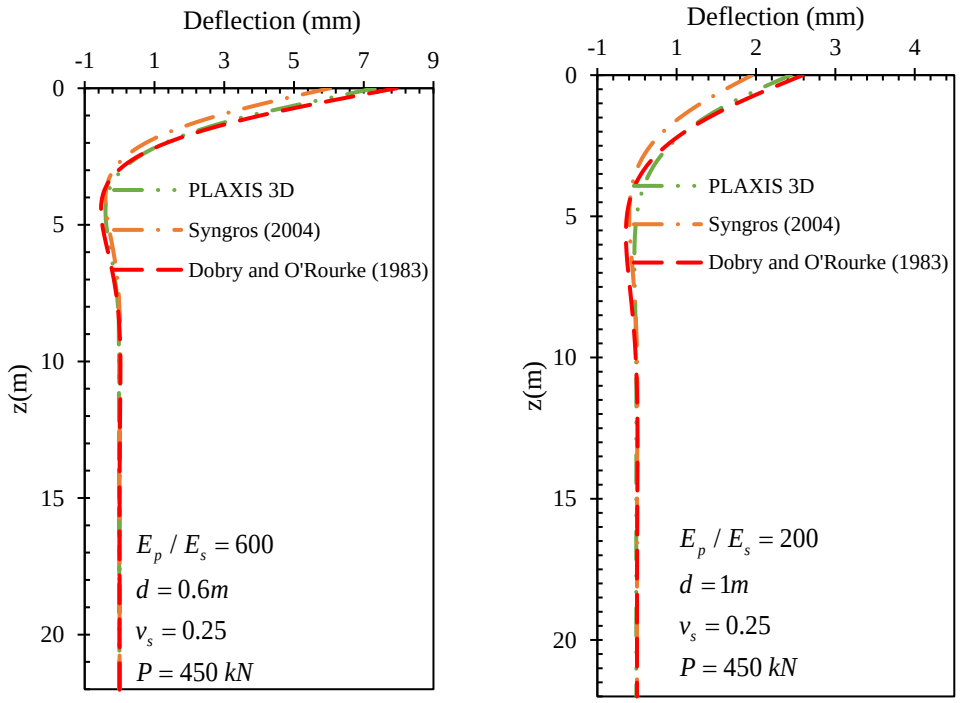

Figure 4-16: Comparison of the deflection profile for free-head piles: between FE models

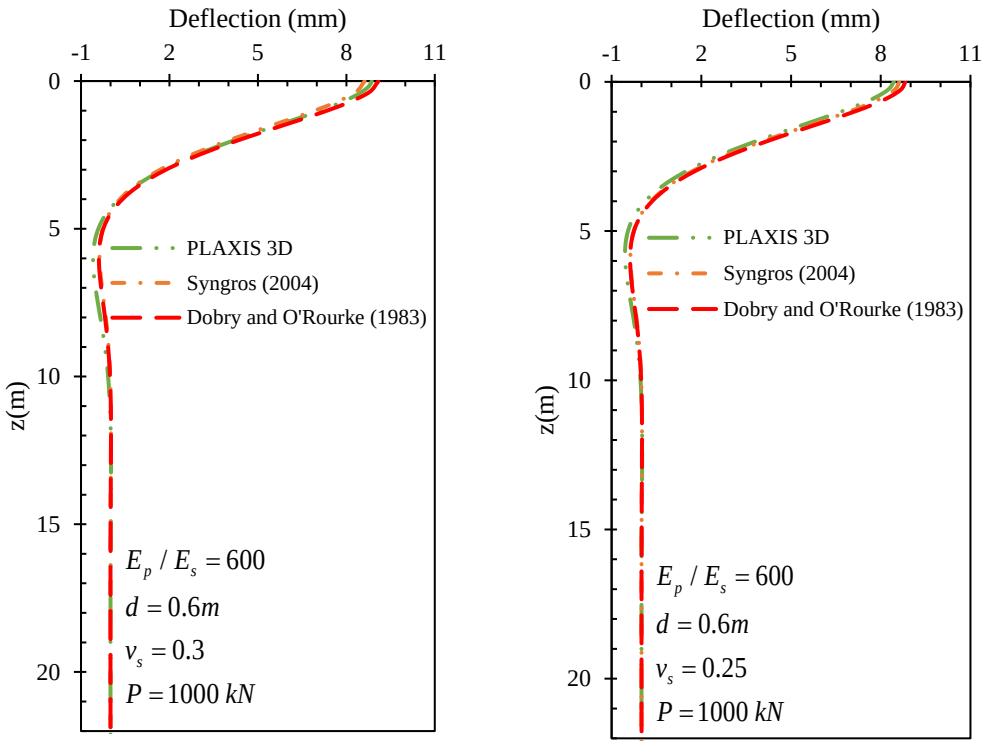

Figure 4-17: Comparison of the deflection profile for fixed-head piles: between FE models

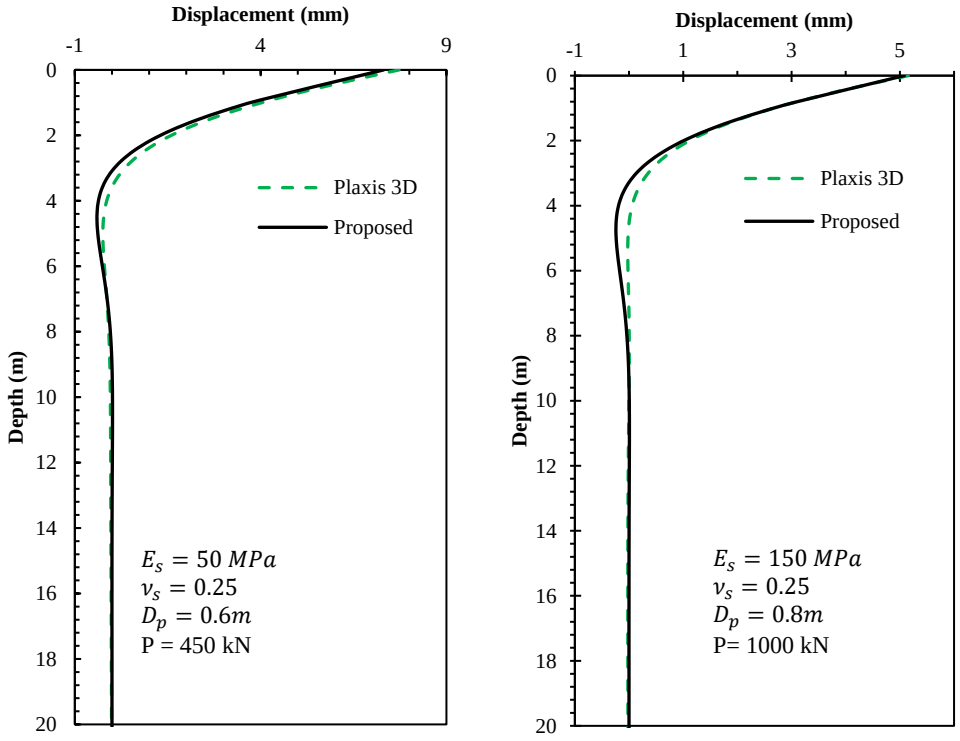

Figure 4-18: Deflection profile for free-head piles: comparison between proposed model and PLAXIS 3D

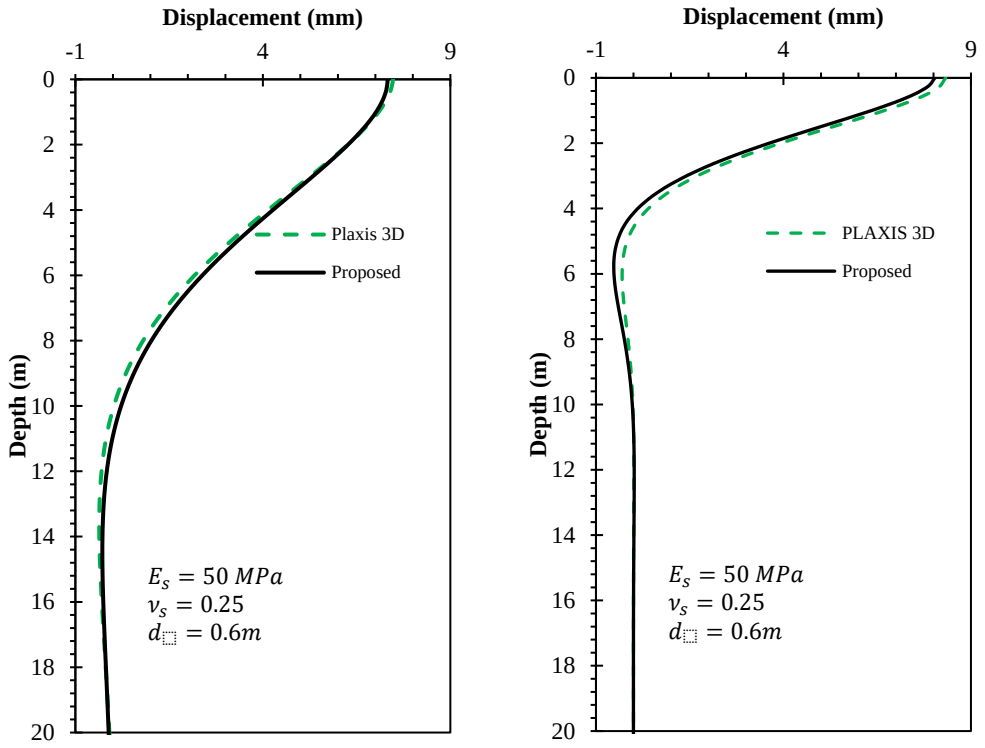

Figure 4-19: Deflection profile for fixed-head piles: comparison between proposed model and PLAXIS 3D

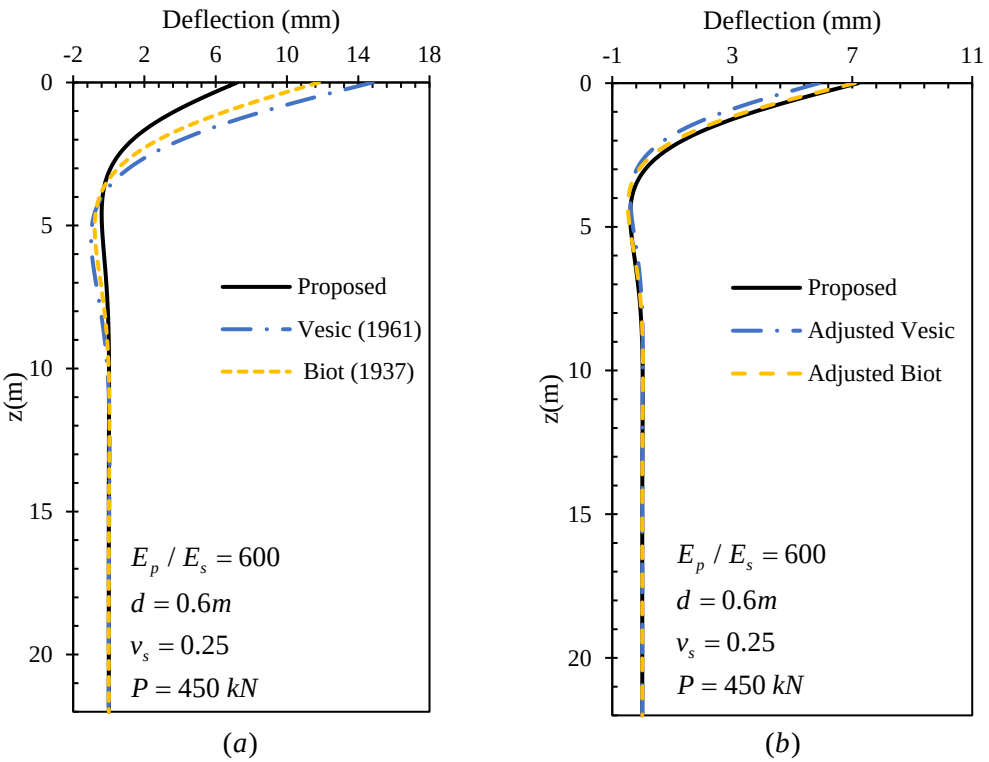

Figure 4-20: Deflection profile for free-head piles: (a) before adjustment factor (b): after adjustment factor

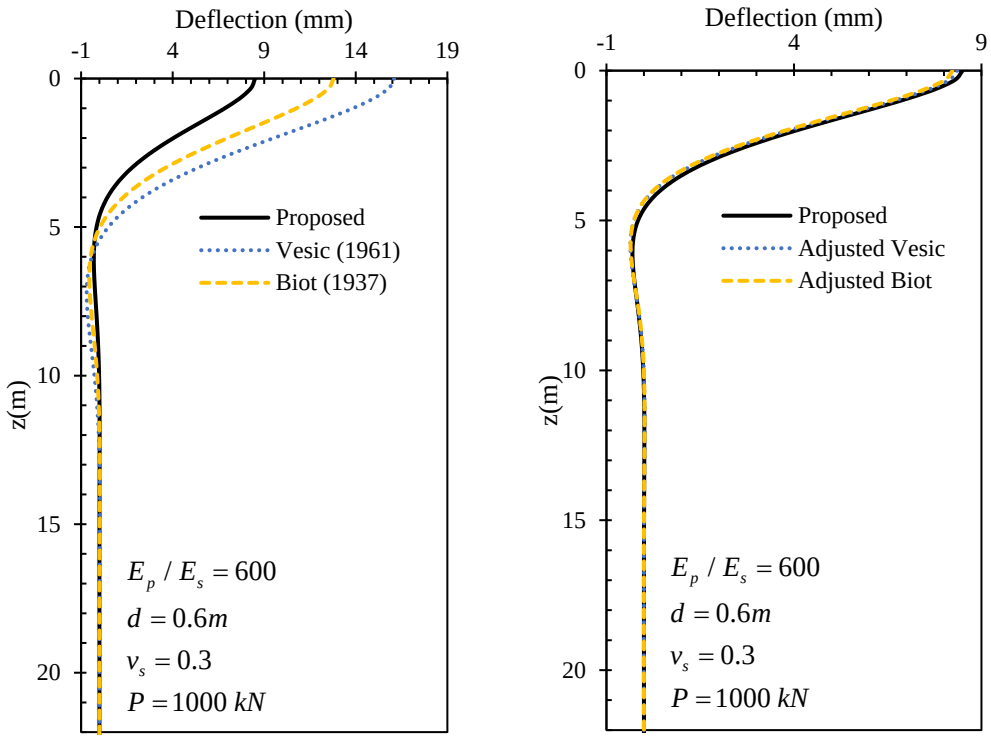

Figure 4-21: Deflection profile for free-head piles in homogeneous soil profiles subjected to applied lateral.

4.4 Critical pile length

The response of single piles can be determined using the relationships derived in Section 4.2.5 and their derivatives. The equations can be much simplified for long flexible piles because there exists a critical length, L_c, beyond which the pile head response and the maximum bending moment stay unaffected (Randolph 1981).

Kuhlemeyer (1979) defined the critical pile length for free head piles, as the length corresponding to the point where a fixed tip pile and a pinned tip pile have the same pile head swaying stiffness. This length is a function of the pile-soil relative stiffness, and for static conditions, it is equal to (Kuhlemeyer 1979):

$$\frac{L_c}{d} = 1.7\left(\frac{E_p}{E_s}\right)^{0.25} \tag{4.33}$$

Similarly, Randolph (1981) and Gazetas (1991b), as cited by Syngros (2004), defined the active length as the depth below which pile deflections are less than one-thousandth of the top deflections and came up with different expressions. The formulas are given in Equation (4.34) and Equation (4.35) for Randolph (1981) and Gazetas (1991b), respectively (for a Poisson's ratio of 0.4):

$$\frac{L_c}{d} = 1.25\left(\frac{E_p}{E_s}\right)^{\frac{2}{7}} \tag{4.34}$$

$$\frac{L_c}{d} = 2\left(\frac{E_p}{E_s}\right)^{0.25} \tag{4.35}$$

In this work, a different approach using pile head stiffness variation as a criteria is employed in order to find the critical pile length for all soil-pile boundary conditions.

For piles with $L \leq L_c$, referred to as "short piles", the pile head deformation varies with change in length. This implies the pile-head stiffness also varies with change in length. But for piles with $L > L_c$, which is referred as "long piles", the pile head stiffness remains constant because there will not be any change in pile head deformation due to length variation. Using this principle, a new parameter called variation factor (Φ) is introduced. The variation factor

represents the ratio between pile head stiffness as calculated using expressions in Section 4.2.5 and pile head stiffness of long flexible piles.

4.4.1 Pile-head stiffness for long flexible piles

4.4.1.1 Deflection equation for long flexible piles

For long flexible piles, the value of C_1 and C_3 in Equation (4.6) has to be zero because the $\lim_{z\to\infty} w(z) = 0$, in which case the pile base boundary conditions have no importance in calculating the deflection. Using this additional boundary condition, the deflection equation given in Equation (4.6) is solved using the pile head boundary conditions listed in Section 4.2.4.1. In doing this, the deflection equation given in Equation (4.15) and Equation (4.16) can be further simplified to give Equation (4.36) which can be used as the deflection equation for both fixed-head floating pile and fixed-head fixed-base pile.

$$w(z) = \frac{P}{4(EI)_p \alpha\beta\lambda^2}\left[\beta\cos(\beta z) + \alpha\sin(\beta z)\right]\left[\cosh(\alpha z) - \sinh(\alpha z)\right] \tag{4.36}$$

The same procedure can be used for determining the pile-head stiffness for the case of free-head piles. Using the additional boundary conditions specified in Section 4.2.4.1, Equation (4.13) and Equation (4.14) are further simplified to give Equation (4.37) which can be used as the deflection equation for both free-head floating piles and free-head fixed-base piles.

$$w(z) = \frac{P}{2\beta\lambda^2\left(2\lambda^2(EI)_p + T\right)}\begin{pmatrix} 2\alpha\beta\cos(\beta z) \\ +(\alpha^2 - \beta^2)\sin(\beta z)\end{pmatrix}\begin{pmatrix}\cosh(\alpha z) \\ -\sinh(\alpha z)\end{pmatrix} \tag{4.37}$$

4.4.1.2 Static pile head stiffness for long flexible piles

The definition of the beam on an elastic foundation is used. Winkler (1867) developed a relation between contact pressure and surface deformation ($P = Kw$), where K is the spring stiffness in the direction of loading and w is the surface deformation. Using the same principle for piles, the swaying stiffness of a pile at a given point is related using the Equation (4.38).

$$K_{HH} = \frac{P}{w(z)} \tag{4.38}$$

Evaluating Equation (4.38) at $z=0$ for Equation (4.36) and Equation (4.37), the pile head stiffness for fixed-head and free-head piles are given in Equation (4.39) and Equation (4.40) respectively.

Fixed-head:

$$K_{HH}=\lim_{z\to 0}\left(EI\right)_P\left(\frac{\frac{d^3}{dz^3}w(z)}{w(z)}\right)=4\alpha\lambda^2\left(EI\right)_P \tag{4.39}$$

Free-head:

$$K_{HH}=\lim_{z\to 0}\left(\frac{\left(EI\right)_P\frac{d^3}{dz^3}w(z)-T\frac{d}{dz}w(z)}{w(z)}\right)=\frac{\lambda^2\left(2\lambda^2\left(EI\right)_P+\tilde{T}\right)}{\alpha} \tag{4.40}$$

4.4.2 Generalized pile head stiffness

The difference between the pile-head stiffness calculated above and the one calculated in this section is that the former will not be affected by the variation of length, which implies that it only works for long piles. So, it is necessary to calculate a generalized pile-head stiffness which incorporates the effect of pile length variation. Using Equation (4.38) and the deflection equation provided in Section 4.2.5, the pile head stiffness for all soil-pile boundary conditions is determined and provided below.

For free-head floating-base pile

$$K_{HH}=\frac{\begin{pmatrix}\alpha^2\sin(L\beta)\begin{pmatrix}4\sqrt{k_s\tilde{T}}\begin{pmatrix}\alpha\left(\tilde{T}-2\left(EI\right)_p\alpha^2\right)\beta^2\cos(L\alpha)\\+2\beta\left(\alpha^2-\beta^2\right)\begin{pmatrix}\tilde{T}-\left(EI\right)_p\alpha^2\\+3\left(EI\right)_p\beta^2\end{pmatrix}\cos(L\beta)\end{pmatrix}\\+2\left(EI\right)_p\left(\alpha^2-3\beta^2\right)\lambda^2\left(2\left(EI\right)_p\lambda-\tilde{T}\right)\sin(L\beta)\end{pmatrix}\\+2\beta^2\lambda^2\left(\tilde{T}+2\left(EI\right)_p\lambda^2\right)\begin{pmatrix}\sqrt{k_s\tilde{T}}\alpha\sinh(2L\alpha)\\+2\left(EI\right)_p\left(3\alpha^2-\beta^2\right)\lambda^2\sinh(L\alpha)\sinh L\beta\end{pmatrix}\end{pmatrix}}{4\alpha\beta\lambda^2\begin{pmatrix}\alpha\begin{pmatrix}2\left(EI\right)_p\left(\alpha^2-3\beta^2\right)\lambda^2\cos(L\beta)\\+2\sqrt{k_s\tilde{T}}\beta\sin(L\alpha)\end{pmatrix}\sin(L\beta)\\+2\left(EI\right)_p\beta\left(3\alpha^2-\beta^2\right)\lambda^2\cosh(L\alpha)\sinh(L\beta)\\+2\sqrt{k_s\tilde{T}}\alpha\beta\sinh^2(L\alpha)\end{pmatrix}} \tag{4.41}$$

For free-head fixed-base pile

$$K_{HH} = -\frac{\begin{pmatrix} 2\lambda^2 (EI)_P \begin{pmatrix} -\alpha^4 + 6\alpha^2\beta^2 - \beta^4 + 2\lambda^2\alpha^2 \cos(2L\beta) \\ +2\lambda^2\beta^2 \cosh(2L\alpha) \end{pmatrix} \\ +4\tilde{T}\lambda^2 \left(\alpha^2 \sin^2(L\beta) + \beta^2 \sinh^2(L\alpha)\right) \end{pmatrix}}{2\alpha\beta\left(\alpha \sin(2L\beta) - \beta \sinh(2L\alpha)\right)} \tag{4.42}$$

For fixed-head floating base-pile

$$K_{HH} = \frac{4\alpha\beta\lambda^2 (EI)_P \begin{pmatrix} -2\alpha\beta\sqrt{k_s\tilde{T}} \left(\cos(2L\beta) + \cosh(2L\alpha)\right) \\ +\left(\alpha^2 + \beta^2\right)(EI)_P \begin{pmatrix} \alpha\left(\alpha^2 - 3\beta^2\right)\sin(2L\beta) \\ +\beta\left(\beta^2 - 3\alpha^2\right)\sinh(2L\alpha) \end{pmatrix} \end{pmatrix}}{(EI)_P \begin{pmatrix} -\left(\alpha^2 + \beta^2\right) \begin{pmatrix} -4\lambda^4 + \alpha^2\left(\alpha^2 - 3\beta^2\right)\cos(2L\beta) \\ +\beta^2\left(-3\alpha^2 + \beta^2\right)\cosh(2L\alpha)) \end{pmatrix} \end{pmatrix} + 2\alpha\beta\sqrt{k_s\tilde{T}} \left(-\alpha \sin(2L\beta) + \beta \sinh(2L\alpha)\right)} \tag{4.43}$$

For fixed-head fixed-base pile

$$K_{HH} = \frac{2\alpha\beta\lambda^2 (EI)_P \left(\alpha \sin(2L\beta) + \beta \sinh(2L\alpha)\right)}{-\alpha^2 \sin^2(L\beta) + \beta^2 \sinh^2(L\alpha)} \tag{4.44}$$

4.4.3 Variation factor

This variation factor Φ can be calculated using the ratio of the generalized pile head stiffness (Section 4.4.2) to the pile head stiffness of long flexible pile (Section 4.4.1.2). For piles with $L > L_c$, the value of Φ is one. However, for piles with $L \le L_c$, the value of Φ varies.

$$\Phi = \frac{Generalized\ pile\ head\ stiffness}{Pile\ head\ stiffness\ for\ long\ flexible\ piles} \tag{4.45}$$

4.4.3.1 Variation factor for all soil-pile boundary conditions

The variation factor for all soil-pile boundary conditions has been determined using both the generalized pile head stiffness and the pile head stiffness for long flexible pile (for FxHFBP using Equation (4.43) and Equation (4.39), for FxHFxBP Equation (4.44) and Equation (4.39),

for FHFBP Equation (4.41) and Equation (4.40) and for FHFxBP Equation (4.42) and Equation (4.40).

Free-head floating base pile

$$\Phi = \frac{\begin{pmatrix}\alpha^2\sin(L\beta)\begin{pmatrix}4\sqrt{k_s\tilde{T}}\begin{pmatrix}\alpha\left(\tilde{T}-2(EI)_p\alpha^2\right)\beta^2\cos(L\alpha)\\+2\beta\left(\alpha^2-\beta^2\right)\left(\tilde{T}-(EI)_p\alpha^2+3(EI)_p\beta^2\right)\cos L\beta\end{pmatrix}\\+2(EI)_p\left(\alpha^2-3\beta^2\right)\lambda^2\left(2(EI)_p\lambda-\tilde{T}\right)\sin(L\beta)\end{pmatrix}\\+2\beta^2\lambda^2\left(\tilde{T}+2(EI)_p\lambda^2\right)\begin{pmatrix}\sqrt{k_s\tilde{T}}\alpha\sinh[2L\alpha]\\+2(EI)_p\left(3\alpha^2-\beta^2\right)\lambda^2\sinh(L\alpha)\sinh L\beta\end{pmatrix}\end{pmatrix}}{2\beta\lambda^2\left(\tilde{T}+2(EI)_p\lambda^2\right)\begin{pmatrix}\alpha\begin{pmatrix}2(EI)_p\left(\alpha^2-3\beta^2\right)\lambda^2\cos(L\beta)\\+2\sqrt{k_s\tilde{T}}\beta\sin(L\alpha)\end{pmatrix}\sin(L\beta)\\+2(EI)_p\beta\left(3\alpha^2-\beta^2\right)\lambda^2\cosh(L\alpha)\sinh(L\beta)\\+2\sqrt{k_s\tilde{T}}\alpha\beta\sinh^2(L\alpha)\end{pmatrix}}$$

Free-head fixed-base pile

$$\Phi = -\frac{\begin{pmatrix}(EI)_P\left(\alpha^2+\beta^2\right)\begin{pmatrix}-\alpha^4+6\alpha^2\beta^2-\beta^4+2\lambda^2\alpha^2\cos(2L\beta)\\+2\lambda^2\beta^2\cosh(2L\alpha)\end{pmatrix}\\+4\tilde{T}\lambda^2\left(\alpha^2\sin^2(L\beta)+\beta^2\sinh^2(L\alpha)\right)\end{pmatrix}}{2\beta\lambda^2\left(\tilde{T}+2(EI)_p\lambda^2\right)\left(\alpha\sin(2L\beta)-\beta\sinh(2L\alpha)\right)} \tag{4.46}$$

Fixed-head floating base pile

$$\Phi = \frac{\begin{pmatrix}\beta\begin{pmatrix}-2\alpha\beta\sqrt{k_s\tilde{T}}\left(\cos(2L\beta)+\cosh(2L\alpha)\right)\\+\left(\alpha^2+\beta^2\right)(EI)_P\begin{pmatrix}\alpha\left(\alpha^2-3\beta^2\right)\sin(2L\beta)\\+\beta\left(\beta^2-3\alpha^2\right)\sinh(2L\alpha)\end{pmatrix}\end{pmatrix}\\(EI)_P\left(-\left(\alpha^2+\beta^2\right)\begin{pmatrix}-4\lambda^4+\alpha^2\left(\alpha^2-3\beta^2\right)\cos(2L\beta)\\+\beta^2\left(-3\alpha^2+\beta^2\right)\cosh(2L\alpha)\end{pmatrix}\right)\\+2\alpha\beta\sqrt{k_s\tilde{T}}\left(-\alpha\sin(2L\beta)+\beta\sinh(2L\alpha)\right)\end{pmatrix}} \tag{4.47}$$

Fixed-head fixed base pile

$$\Phi = \frac{\beta\left(\alpha\sin(2L\beta)+\beta\sinh(2L\alpha)\right)}{2\left(-\alpha^2\sin^2(L\beta)+\beta^2\sinh^2(L\alpha)\right)} \tag{4.48}$$

Using Mathematica 12, the variation of Φ for all soil-pile boundary conditions is plotted. The results are given in Figures 4.22 to 4-25. Figure 4-26 provides the three-dimensional version of the same plots.

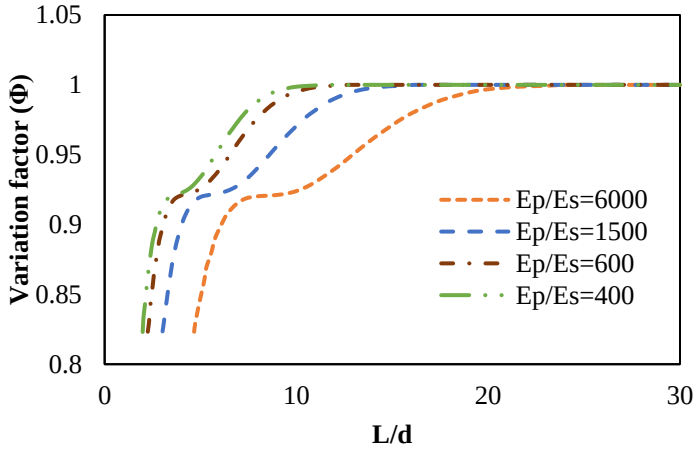

Figure 4-22: Variation factor for fixed-head floating-base pile

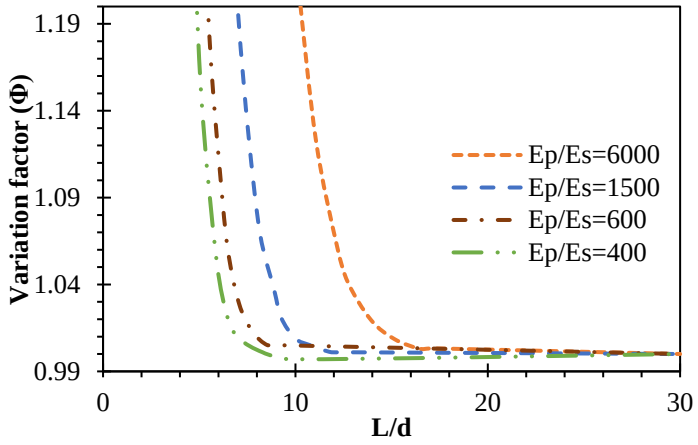

Figure 4-23: Variation factor for fixed-head fixed-base pile

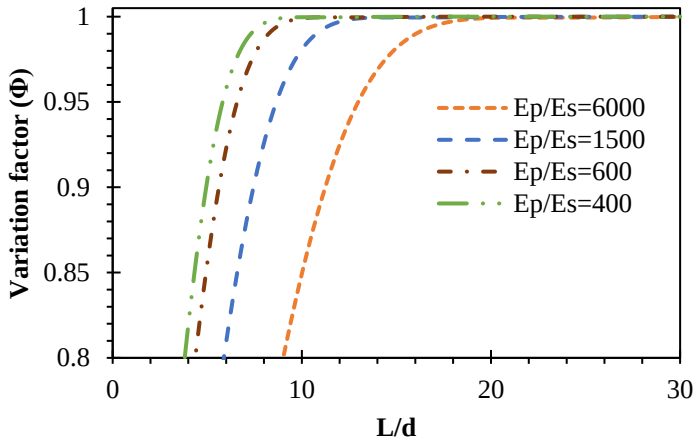

Figure 4-24: Variation factor for free-head floating-base pile

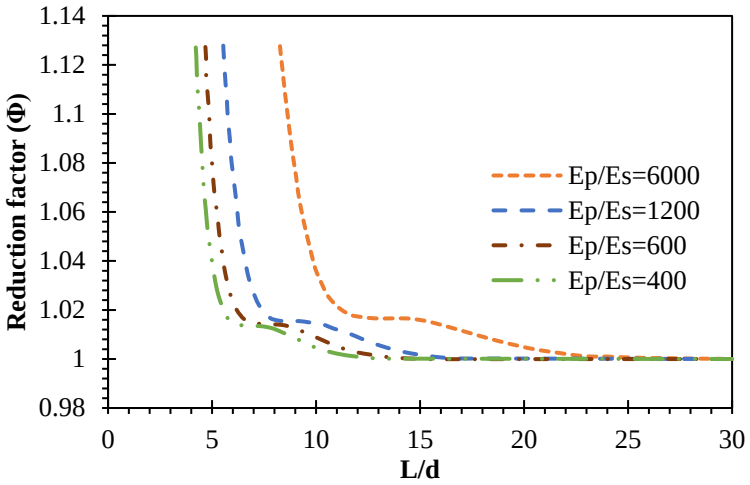

Figure 4-25: Variation factor for free-head fixed-base pile

Based on Figures 4-22 through 4-25, the following observations can be made:

- In all cases, the value of the variation factor remains one, after some value of pile slenderness ratio (L/d). The point at which the variation factor starts to change, for a given pile-soil stiffness ratio, is the critical slenderness ratio (L_c/d). This can be readily estabilised from the plots.
- For fixed-head floating-base piles and free-head floating base piles, the the stiffness variation factor decreases for L/d less than the threshold value (critical slenderness ratio).
- For the fixed-base piles, the variation factor increases for L/d less than the threshold value (critical slenderness ratio) regardless of the head condition.
- In all cases, whether Φ is increasing or decreasing, there exists a transition curve (responsible for about 5% of stiffness change) before a sudden change in head stiffness occurs. For this reason, an additional classification “transitional state” is introduced in addition to the “long piles” and “short piles”.

4.4.4 Expression for critical pile length

As it can be seen from Figure 4-22 to Figure 4-25, even if the value is dependent on the pile-soil relative stiffness ratio, there always exists a threshold value beyond which the stiffness variation factor varies. So, in order to determine the expressions for the critical length, first the critical pile slenderness ratio values (threshold) for different E_p/G_s is determined. The discrete points are then fitted to give simplified expressions for L_c. The reason for using E_p/G_s over

E_p/E_s is to incorporate the effect of Poisson's ratio on the critical pile length by using minimum parameters possible.

The same procedure was also implemented for determining L'_c (the lower bound of the "transitional state"). The detailed procedure is given in Appendix C.

Fixed-head floating base pile

$$\frac{L_c}{d} = 1.4\left(\frac{E_p}{G_s}\right)^{0.2817} \tag{4.49}$$

$$\frac{L'_c}{d} = 1.05\left(\frac{E_p}{G_s}\right)^{0.224} \tag{4.50}$$

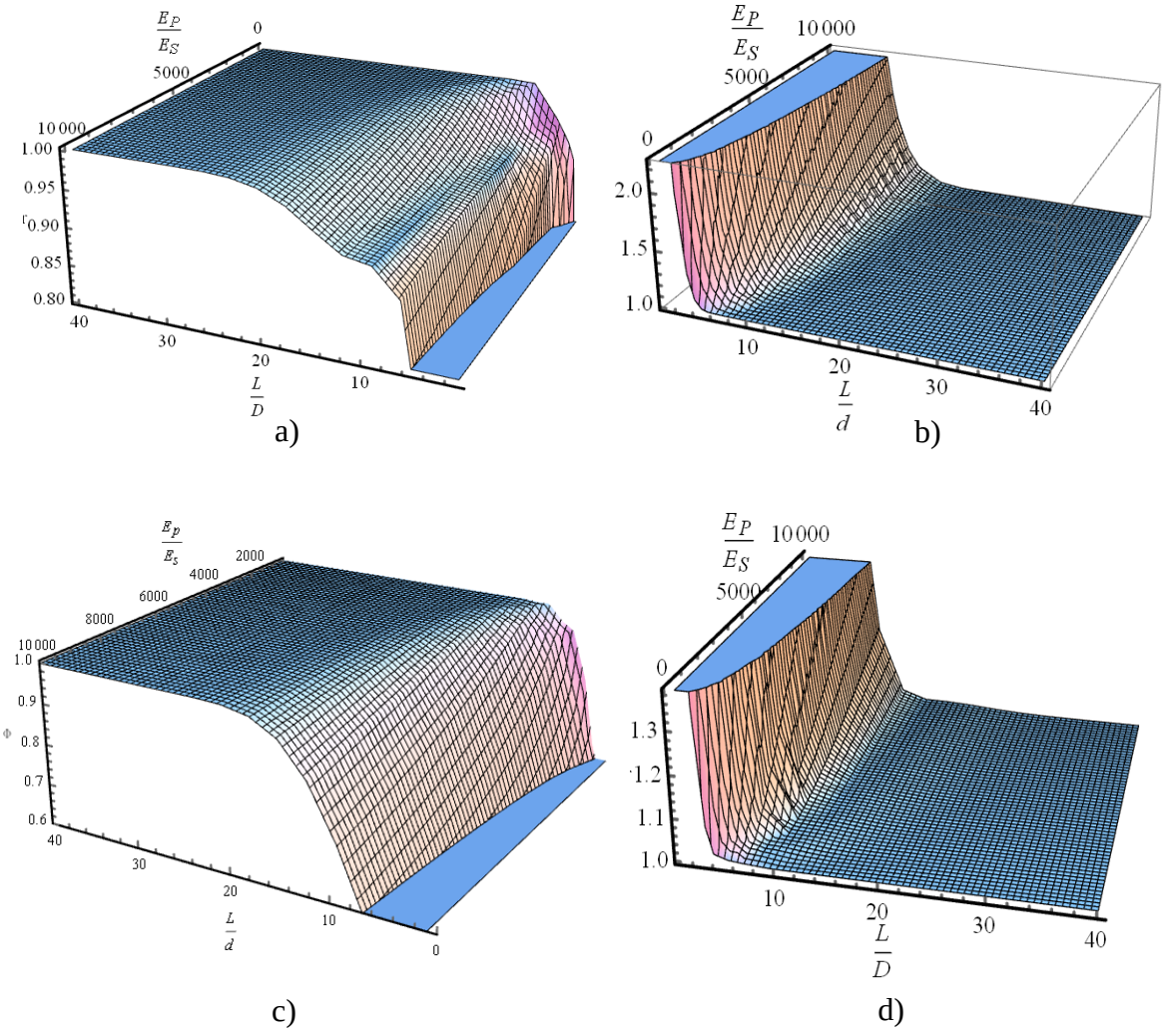

Figure 4-26: 3D plot for variation factor for a) FxHFBP b) FxHCBP c) FHFBP d) FHCBP.

Fixed-head fixed base pile

$$\frac{L_c}{d} = 1.08\left(\frac{E_p}{G_s}\right)^{0.28} \tag{4.51}$$

$$\frac{L'_c}{d} = 0.65\left(\frac{E_p}{G_s}\right)^{0.29} \tag{4.52}$$

If we compare the results given in Equation (4.49) and Equation (4.51), we can see the effect of pile base fixity (Figure 4-27). Due to base fixity at the base, the critical length decreases approximately by 23%.

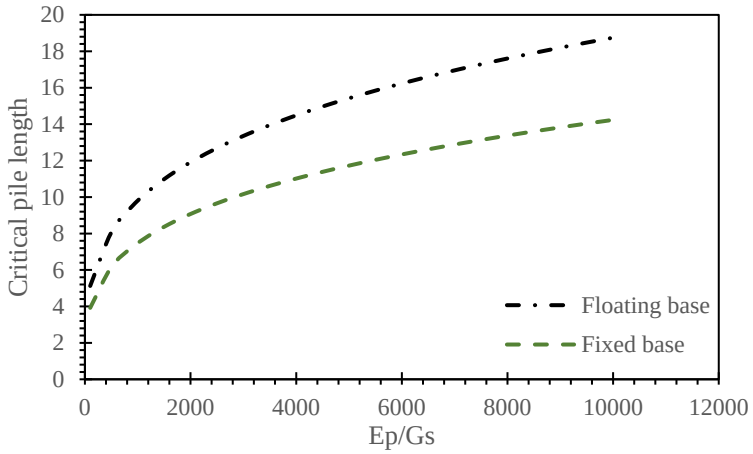

Figure 4-27: Variation of critical pile slenderness ratio for fixed-head pile

Free-head floating-base pile

$$\frac{L_c}{d} = \left(\frac{E_p}{G_s}\right)^{0.3236} \tag{4.53}$$

Free-head fixed-base pile

$$\frac{L_c}{d} = 1.14\left(\frac{E_p}{G_s}\right)^{0.3} \tag{4.54}$$

The effect of base fixity also has an effect on the critical pile length for free-head piles, even though the effect is smaller when compared to fixed-head piles. As we can see from Figure 4-28, the effect of fixity is considerably lower for smaller pile-soil stiffness ratio (for piles embedded in stiff soil), and the difference reaches up to 9% for piles embedded in soft soils.

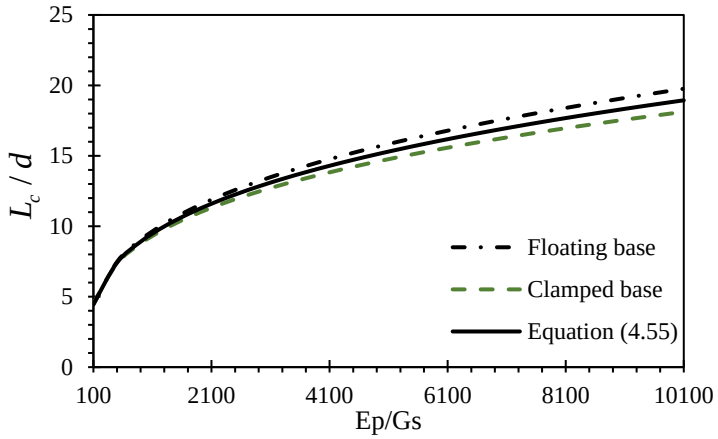

Figure 4-28: Variation of critical pile slenderness ratio for free head piles

Hence, for all practical purposes, the following single relationship may be used to determine the critical length of a free-head pile regardless of the base boundary condition;

$$\frac{L_c}{d} = 1.07\left(\frac{E_p}{G_s}\right)^{0.312} \tag{4.55}$$

4.4.5 Comparison of critical pile length with other models form literature

With the aim of comparing the proposed critical length, different critical lengths from the literature are used (Table 4-4 and Table 4-9).

Table 4-4: Critical pile slenderness ratio for free-head piles

Model	Kuhlemeyer (1979)	Syngros (2004)	Gazetas (1991)	Guo (2001)
L_c/d	$1.7\left(E_p/E_s\right)^{0.25}$	$1.6\left(E_p/E_s\right)^{0.28}$	$2\left(E_p/E_s\right)^{0.25}$	$1.057\left(E_p/G_s\right)^{0.25}$

Table 4-5: Critical pile slenderness ratio for fixed-head piles

Model	Guo (2001)	Syngros (2004)	Mylonakis G. (2001)
L_c/d	$1.5\left(E_p/G_s\right)^{0.25}$	$2.4\left(E_p/E_s\right)^{0.25}$	$1.5\left(E_p/E_s\right)^{0.25}$

The plots are given in Figure 4-29 and Figure 4-30 for free-head and fixed-head piles, respectively. From the result, it is clear that the proposed critical pile slenderness, for free head piles (both fixed and free base piles), is in excellent agreement with the critical pile length of Gazetas (1991b) and Syngros (2004). In the case of fixed-head piles, the proposed critical pile length for the floating base pile is in excellent agreement with Syngros (2004). At the same time, the proposed critical pile length for the fixed base pile is in good agreement with Guo (2001). This shows that the base condition is an important condition that the critical length,

especially for fixed-head piles. Besides, this work showed that some relationships in literature could be erroreous.

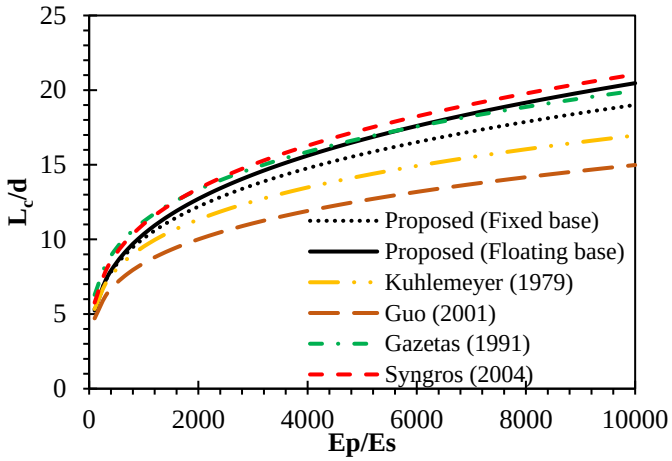

Figure 4-29: Comparison of critical slenderness ratio for free head piles

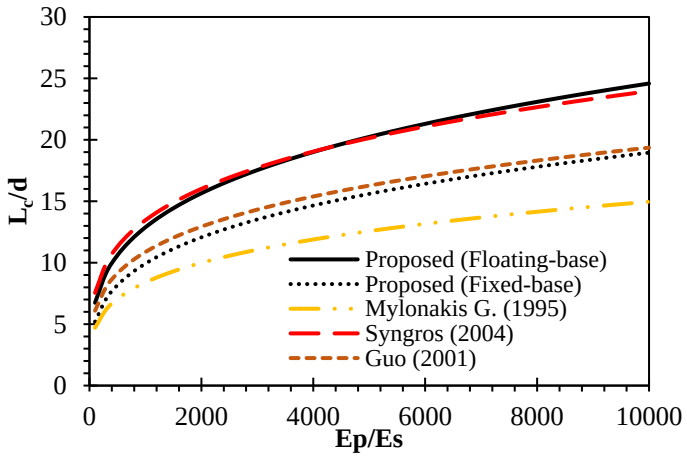

Figure 4-30: Comparison of critical slenderness ratio for fixed head piles

4.5 Static pile head stiffness for piles in "transitional" state

The value of pile head stiffness for the transitional state can be determined using the generalized stiffness expressions given in Section (4.4.2). However, the expression given is lengthy, making it difficult for hand calculation. Thus, it is found important to provide a simplified expression.

For free-head piles, as it can be seen from Figure 4-24 and Figure 4-25, the range of translational state is very narrow (contributing only 2% to the stiffness variation). This implies that the stiffness variation within this range is almost negligible. Hence, static stiffness in a transitional state for free-head piles is not formulated.

In the case of fixed-head piles, the "transitional" state is responsible for considerable stiffness variation for floating-base pile (Figure 4-22). For this reason, the static pile head stiffness in "transitional" state for the case of fixed-head floating-base piles is only formulated.

The generalized pile head stiffness can be expressed as a function of variation factor, Φ, and $K_{HH(Long)}$ (Equation (4.56)), where $K_{HH(Long)}$ is pile head stiffness for long flexible piles. The value of Φ as expressed earlier is lengthy and challenging to work with. So, with the aim of obtaining a simplified expression of Φ within the range of the "translational" state ($L'_c \le L \le L_c$), the curve under this range is fitted to give simplified expressions given in Equation (4.57).

$$Generalized\ pile\ head\ stiffness = \Phi K_{HH(Long)} \tag{4.56}$$

The result shown in Equation (4.57) is the curve fitting output of fixed-head floating-base piles, and it is a function of two dimensionless parameters (E_p / E_s and L / d).

$$\Phi = 0.9903\left(\frac{L}{d}\right)^{0.05}\left(\frac{E_p}{E_s}\right)^{-0.045} \tag{4.57}$$

To express Equation (4.57) interms of critical pile length, an additional computation is performed. Rearranging the expression of critical pile length of the fixed-head floating-base pile (Equation (4.49)), we have

$$\frac{E_p}{E_s} = 0.1514\left(\frac{L_c}{d}\right)^{3.5491}\frac{1}{1+\nu_s} \tag{4.58}$$

Substituting back Equation (4.58) into Equation (4.57) and simplifying;

$$\Phi = 1.08 d^{0.11}\left(\frac{L_c}{L^{3.19}}\right)^{-0.05}\left(1+\nu_s\right)^{0.045} \tag{4.59}$$

Therefore, the static stiffness of fixed-head floating-base pile in "transition" state is obtained by substituting back Equation (4.39) and Equation (4.58) in Equation (4.55), and the expression is given in Equation (4.59).

The expression for the stiffness variation factor contains only two parameters (L_c and L), as shown in Equation (4.58). However, this does not mean the value is independent E_p / E_s and ν_s. The effect of E_p / E_s and ν_s is included in calculating the value of the critical pile length.

$$K_{HH} = 4\alpha\lambda^2 \left(EI\right)_p \Phi \quad for \quad L'_c < L < L_c \tag{4.60}$$

4.6 Comparison of pile head stiffness

In this chapter, a continuum subgrade model proposed by Worku (2014) is calibrated for the analysis of laterally loaded piles. So, it is important at this stage to compare the horizontal head stiffness for the proposed model against published results. The complete threatment of pile-head stiffness that accounts for the coupling of the translational and rotational degrees of freedom at the head is presented in Chapter 5 for the static case and Chapter 8 for dynamic case.

First, pile head stiffness for long flexible piles is compared. In order to make the comparison more manageable, the expressions of pile head stiffness given in Equation (4.39) and Equation (4.40) are converted to a form similar to Syngros (2004) and Gazetas (1991b) (Table 4-10). The new expressions for pile-head stiffness for both free-head and fixed-head are given below.

Table 4-6: Expressions for pile head stiffness of long flexible piles in a homogenous soil.

Model	$\frac{K_{HH}}{E_s d}$	
	Free-head	Fixed-head
Syngros (2004)	$0.72\left(\frac{E_p}{E_s}\right)^{0.18}$	$1.2\left(\frac{E_p}{E_s}\right)^{0.18}$
Gazetas (1991b)	-	$1.0\left(\frac{E_p}{E_s}\right)^{0.21}$

Free-head

In order to obtain a simplified pile-head stiffness expression for free-head long flexible piles, Equation (4.38) was evaluated using pile head displacement equation given in Equation (4.23), and the result is given below.

$$\frac{K_{HH}}{E_s d} = 0.5376 \frac{(0.98+v_s)}{(1+v_s)} \left(\frac{E_P}{E_s} \right)^{0.214} \tag{4.61}$$

Equation (4.61) can be simplified to

$$\frac{K_{HH}}{E_s d} = 0.527 \left(\frac{E_P}{E_s} \right)^{0.214} \tag{4.62}$$

Fixed head

Following a similar procedure one obtains the expression for pile-head stiffness of the fixed-head pile using Equation (4.24).

$$\frac{K_{HH}}{E_s d} = 1.19 \frac{(1.15+v_s)}{(1+v_s)} \left(\frac{E_P}{E_s} \right)^{0.171} \tag{4.63}$$

This can be similarly simplified to obtain

$$\frac{K_{HH}}{E_s d} = 1.357 \left(\frac{E_P}{E_s} \right)^{0.171} \tag{4.64}$$

The pile head stiffness of Randolph (1981) and Higgins et al. (2013) is obtained from their pile head deflection given in Equation (4.20) through Equation (4.22). The results are given in Equation (4.65) and Equation (4.66) for Higgins et al. (2013) for fixed-head and free-head piles, respectively, and for Randolph (1981) in Equation (4.67) for free head piles.

$$\frac{K_{HH}}{E_s d} = \left(1.18 - 0.13 v_s \right) \left(\frac{E_P}{E_s} \right)^{0.2} \tag{4.65}$$

$$\frac{K_{HH}}{E_s d} = \left(0.82 - 0.1 v_s \right) \left(\frac{E_P}{E_s} \right)^{0.18} \tag{4.66}$$

$$\frac{K_{HH}}{E_s d} = \left(1.0854 - 0.13\nu_s\right)\left(\frac{E_P}{E_s}\right)^{\frac{1}{7}} \tag{4.67}$$

These relations of the head stiffness are plotted in Figure 4-31and Figure 4-32 for fixed-head and free-head piles, respectively, in which the relations in Table 4-10 are also included .

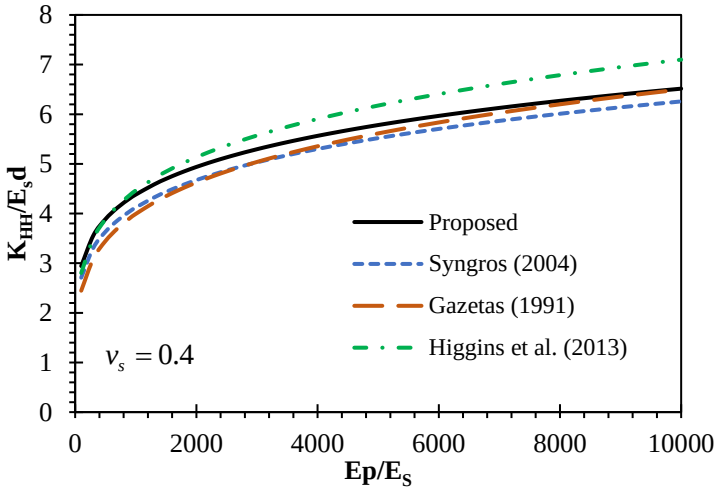

Figure 4-31: Normalized horizontal (swaying) stiffness of a fixed-head pile in a homogenous soil profile.

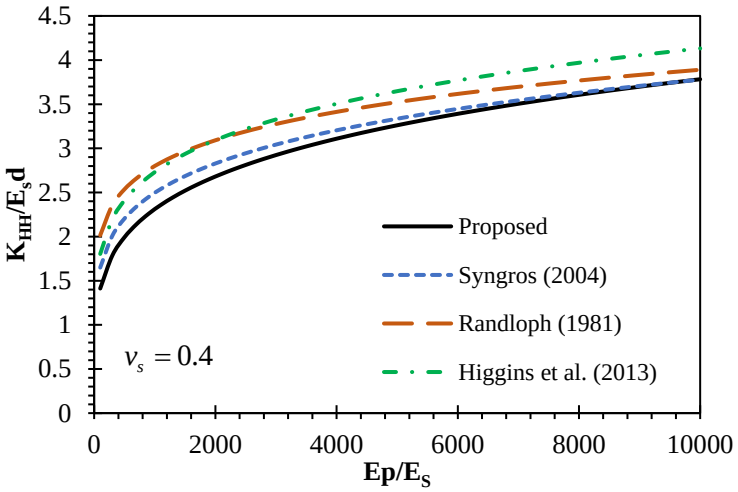

Figure 4-32: Normalized horizontal (swaying) stiffness of a free-head pile in a homogenous soil profile

From the plots, it is important to point out the following

- It can be seen that the results from the present study follow closely that of Syngros (2004) for both free and fixed head piles. In the case of a fixed head pile, the results

have about 6% over the entire range of E_p / E_s. On the other hand, the free head pile results have an exelent result for E_p / E_s values greater than 4000.

- It can be seen from Figure 4-31 that the results from the present study and other literature follow closely that of Higgins et al. (2013) for pile-soil stiffness ratio less than 2000, but for pile-soil stiffness ratio greater than 2000, the result form Higgins et al. (2013) diverges from all the results. The same trend can be seen in Figure 4-32. Thus, the Higgins et al. (2013) relations lead to deformation predictions that are on the unsafe side for piles of large relative rigidity.

All the above analyses are for infinitely long flexible piles. It is also important to compare the proposed model against published results for the general case of finite-length piles. In order to calculate the pile head stiffness for the general case, the values of α, β and λ given in Equation (4.7) are inserted into the pile-head stiffness given in Equation (4.41) to Equation (4.44). The relationships for the subgrade modulus given in Table 4-5 are used to draw comparison.

The general case's pile head stiffness is plotted for selected values of pile slenderness ratio and different soil-pile boundary conditions. The results are organized in sections for the four different combinations of soil-pile boundary conditions.

To study the variation of the pile head stiffness using non-dimensional parameters, the four dimensional parameters (E_p, E_s, L and d) are converted to two dimensionless parameters (E_p / E_s and L / d).

The pile-soil stiffness ratio is assigned to be 'x' ($E_p / E_s = x$). So, for any value of E_p, the value of E_s can be expressed as a function of E_p and 'x' ($E_s = E_p / x$). This help us to plot the response of piles as a fuction of 'x'.

The same approach was used for pile slenderness ratio ($L / d = y$). Which in turn give a pile length as a function of d and 'y' ($L = yd$). So, in Mathematica 12, using this relationships different plots as a fuction of E_p / E_s and L / d.

a) Free-head floating-base piles

Pile head swaying stiffness for laterally loaded free-head floating-base piles is presented in this section. The results are obtained using Equation (4.41) and plotted in Figure 4-33 to Figure 4-36 for different values of L/d, along with other literature results.

- Syngro (2004), after performing a series of runs on FE software called K-PAX, through curve fitting, obtained a relationship for the swaying static stiffness of piles due to different pile head restraints (Table 4-10). To make the model easier to use, he also provided a subgrade modulus, k_s, (Table 4-5) to be used in Beam on Elastic Foundation (BEF) method. So, one may expect to obtain approximately the same result by using both relationships. However, as it can be seen from Figure 4-33, the results are different.
- As shown in Figure 4-33 and Figure 4-34, for long piles, the result from the present study agrees with those obtained using the adjusted Vesic (1961) and Syngros (2004). However, the results obtained using Dobry and O'Rourke (1983) give consistently smaller stiffness.
- Figures 4-35 and 4-36 portray piles' transition from flexible to rigid piles. According to Higgins et al. (2013), the behavior of rigid piles depends only on the pile slenderness ratio. However, as shown in Figure 4-35 and Figure 4-36, the other models' results vary with the pile-soil stiffness ratio. Which implies, none of the models used for comparison are suitable for capturing the pile response in the rigid zone. The presence of shear interaction in the present study helped the model capture the pile's rigid response under consideration. So, this is one of the contributions of this model for the analysis of laterally loaded piles.

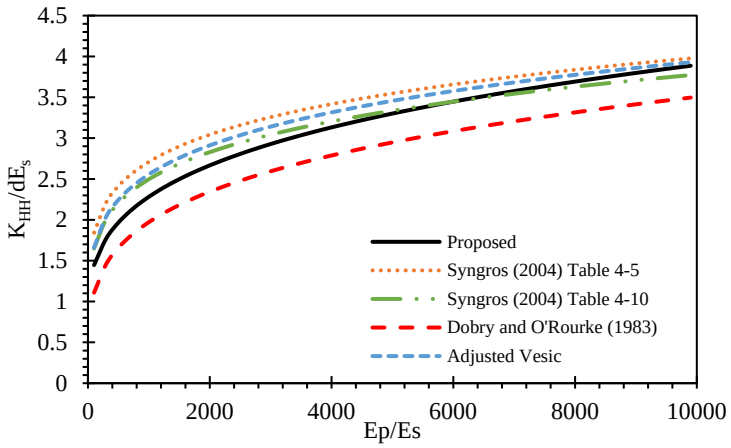

Figure 4-33: Normalized swaying stiffness of a free-head floating-base pile in homogenous soil profile: L/d = 50

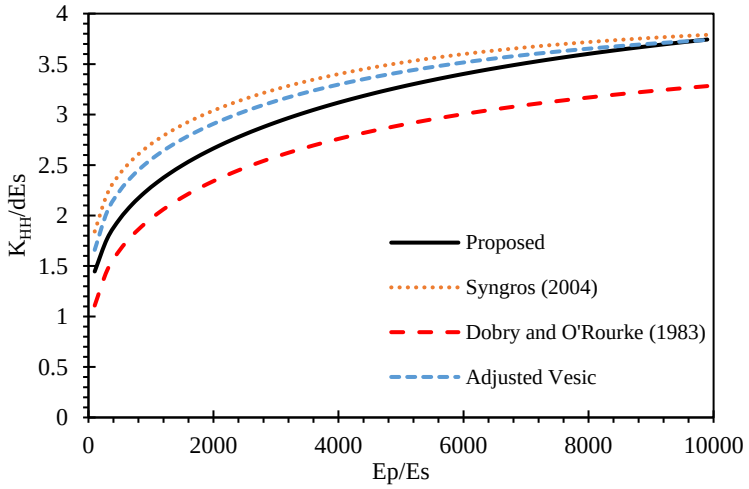

Figure 4-34: Normalized swaying stiffness of a free-head floating-base pile in homogenous soil profile: L/d = 15

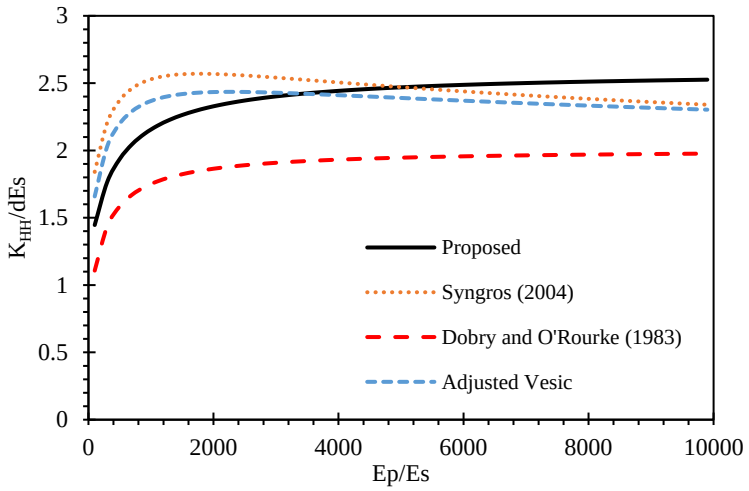

Figure 4-35: Normalized swaying stiffness of a free-head floating-base pile in homogenous soil profile: L/d = 7.5

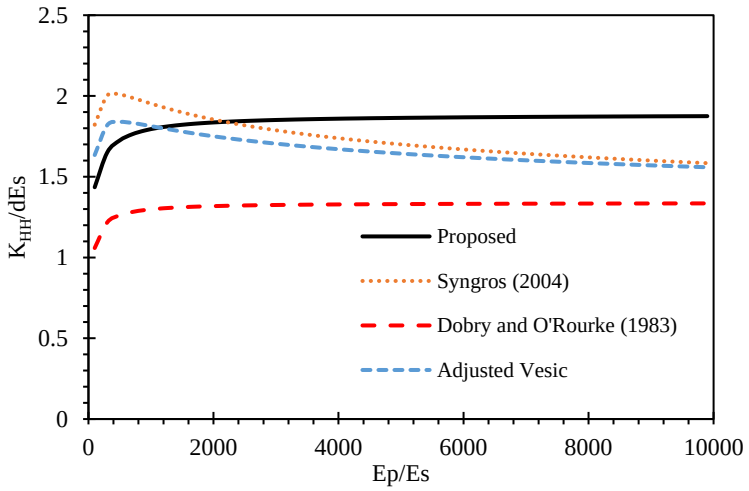

Figure 4-36: Normalized swaying stiffness of a free-head floating-base pile in homogenous soil profile: L/d = 5

b) Free-head fixed-base piles

The results are obtained using Equation (4.42) and plotted in Figures 4-37 to 4-40 along with the literature results.

- As discussed before, Kuhlemeyer (1979) has stated that for long piles ($L > L_c$), the pile base condition does not affect the pile head stiffness. The above statement can be supported by comparing the results of FHFBP and FHFxBP for long flexible piles. So, by comparing Figure 4-33 with Figure 4-37 and Figure 4-34 with Figure 4-38, one observes almost identical plots. Hence, based on this observation, it can be concluded that the pile base condition for long flexible piles does not affect the pile response.
- As shown in Figure 4-37 and Figure 4-38, for $E_p / E_s > 4000$, the result from the present study follows those of adjusted Vesic (1961) and Syngros (2004) closely. Also, the results obtained using Dobry and O'Rourke (1983) do not deviate as significantly as in the previous case.
- As illustrated in Figures 4-39 and 4-40, short pile does not necessarily mean rigid piles for fixed-base pile. In the figures, as E_p / E_s increase (stiff piles embedded in soft soil) the pile swaying stiffness increases almost linearly. Within the realm of this study for free-head fixed-base piles, rigid pile response is not encountered. The head stiffness of FHFxBP is much larger than FHFBP as the pile contribution is much larger.
- For short fixed-base piles (Figure 4-39 and Figure 4-40), even the result obtained by Dobry and O'Rourke (1983) is in good agreemet. This implies that, for short fixed-base piles, the pile is not much dependent on the subgrade model used because the pile base fixity contributes to the pile head response.

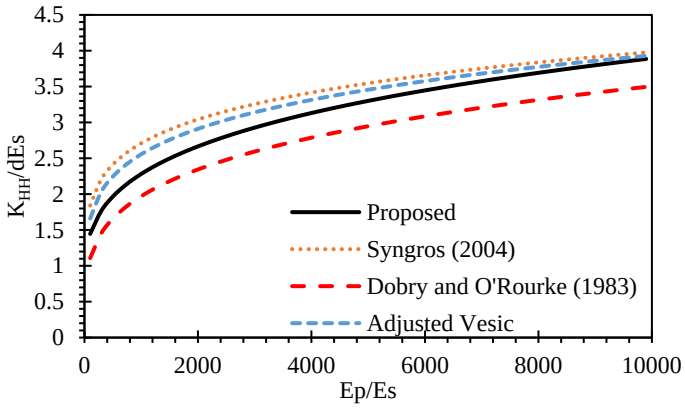

Figure 4-37: Normalized swaying stiffness of a free-head fixed-base pile in homogenous soil profile: L/d = 50

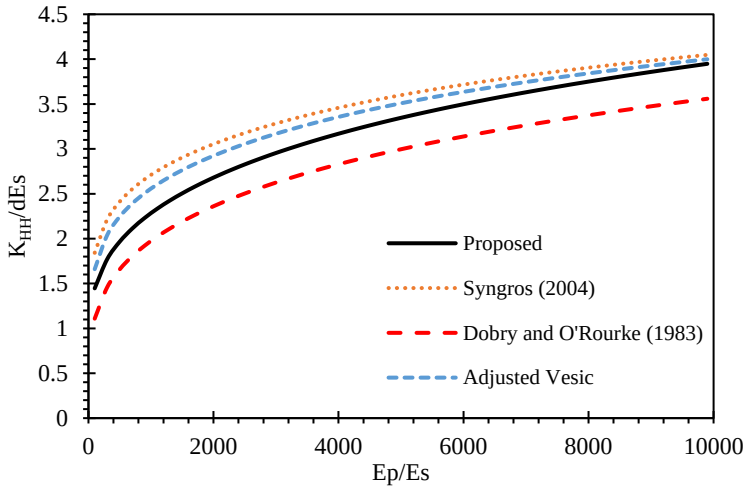

Figure 4-38: Normalized swaying stiffness of a free-head fixed-base pile in homogenous soil profile: L/d = 15

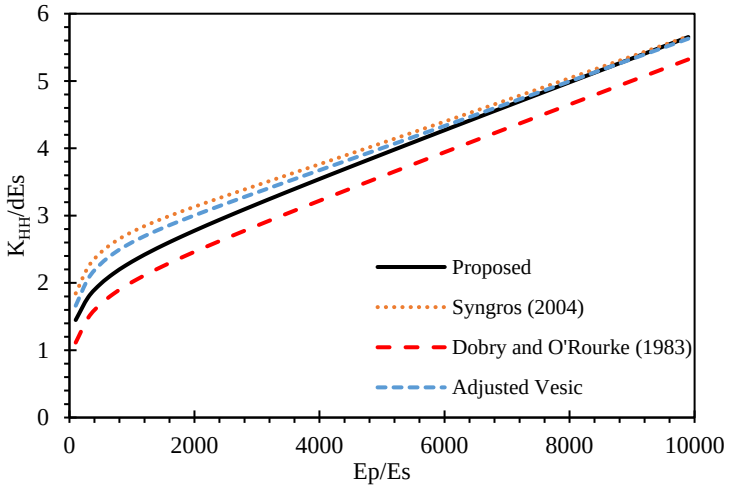

Figure 4-39: Normalized swaying stiffness of a free-head fixed-base pile in homogenous soil profile: L/d = 7.5

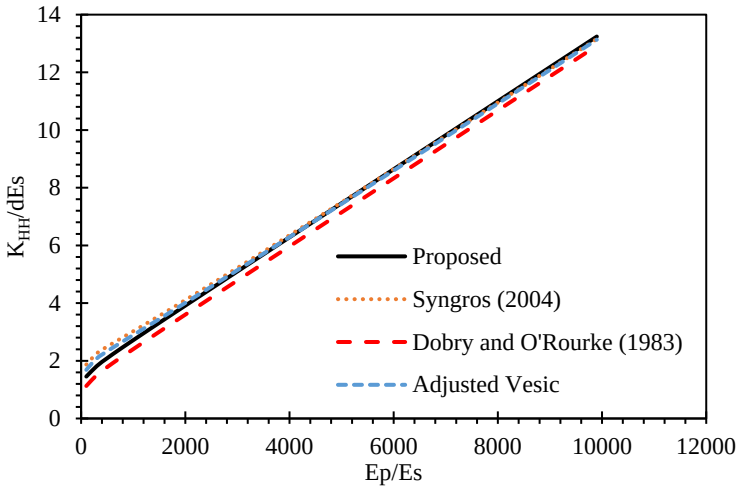

Figure 4-40: Normalized swaying stiffness of a free-head fixed-base pile in homogenous soil profile: L/d = 5

c) Fixed-head floating-base piles

Pile head swaying stiffness for laterally loaded fixed-head floating-base piles is presented in this section. The results are obtained using Equation (4.43) and plotted in Figures 4-41 to 4-44 along with other literature results. The observations on the results are given below:

- Figure 4-41 and Figure 4-42 portray that for long flexible piles ($L > L_c$), the results from the present study closely follow the adjusted Vesic (1961) and Syngros (2004).
- The result obtained using Dobry and O'Rourke (1983) for fixed head piles is more in agreement than with results obtained for free head piles using the same model. So, it is recommended to use the model proposed by Dobry and O'Rourke (1983) only for the case of fixed-head piles.
- Like in free-head floating-base piles, for fixed-head floating-base piles as portrayed in Figure 4-43 and Figure 4-44, there exists a pile-soil stiffness ratio for particular pile slenderness ratio, which serves as a threshold between flexible and rigid piles. As discussed before, the response of rigid piles should depend only on the pile slenderness ratio. However, as shown in Figures 4-43 and 4-44, the results obtained using the other models, except Dobry and O'Rourke (1983), vary with pile-soil stiffness ratio.
- For the present study the shear interaction and for the case of Dobry and O'Rourke (1983), the absence of pile-soil stiffness ratio in their expression of subgrade modulus has helped both models to capture the response of rigid piles.

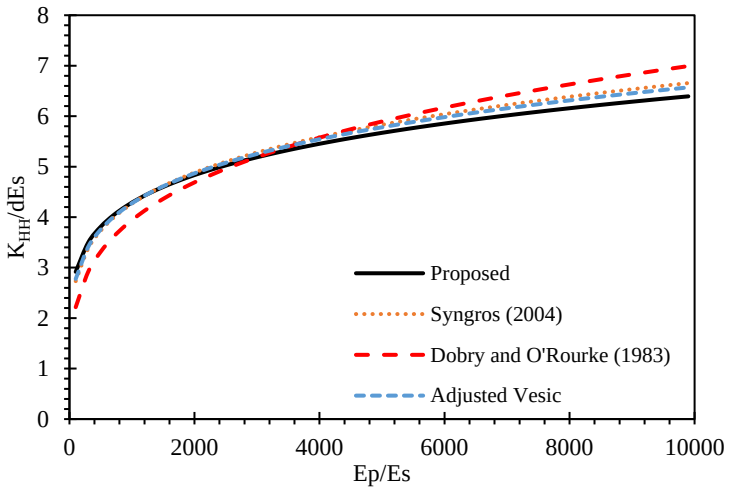

Figure 4-41: Normalized swaying stiffness of a fixed-head floating-base pile in homogenous soil profile: L/d = 50

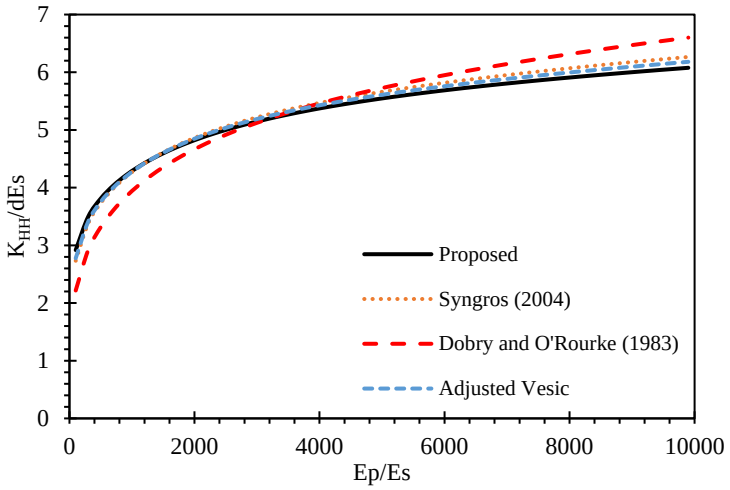

Figure 4-42: Normalized swaying stiffness of a fixed-head floating-base pile in homogenous soil profile: L/d = 15

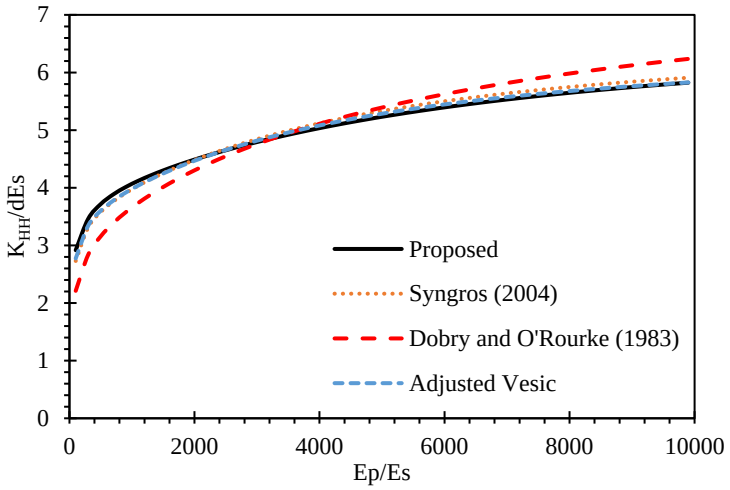

Figure 4-43: Normalized swaying stiffness of a fixed-head floating-base pile in homogenous soil profile: L/d = 7.5

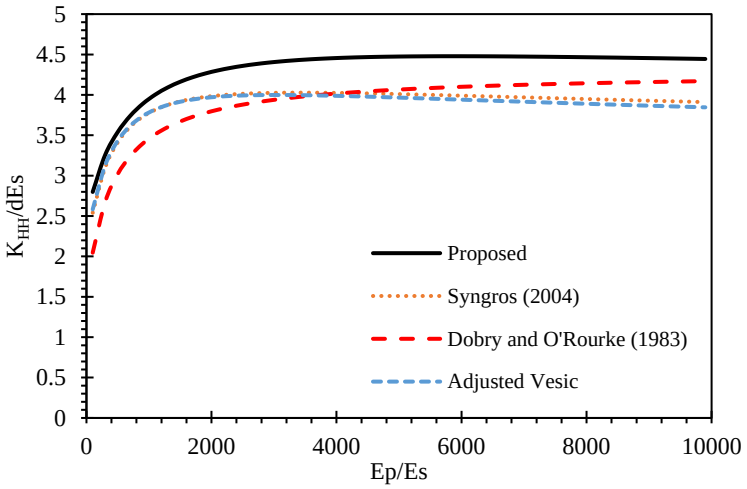

Figure 4-44: Normalized swaying stiffness of a fixed-head floating-base pile in homogenous soil profile: L/d = 4

d) Fixed-head fixed-base piles

Pile head swaying stiffness for laterally loaded fixed-head fixed-base piles is dealt with in this section. The results are obtained using Equation (4.44), and the observation on the results are given below.

- The results in Figure 4-45 and Figure 4-46 are similar to that of Figures 4-41 and 4-42. The reason as described earlier, for long piles, pile base condition has no effect.
- From Figure 4-45 through 4-48, it can be seen that for both long and short piles, the results from the present study closely follow those Syngros (2004) and Dobry and O'Rourke (1983).

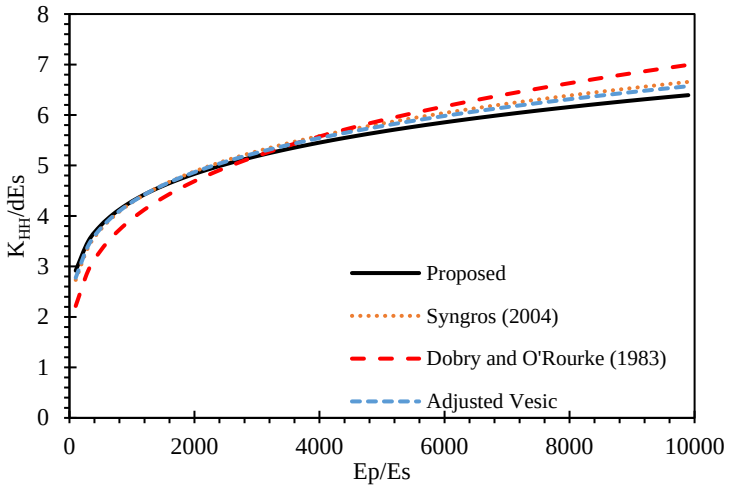

Figure 4-45: Normalized swaying stiffness of a fixed-head fixed-base pile in homogenous soil profile: L/d = 50

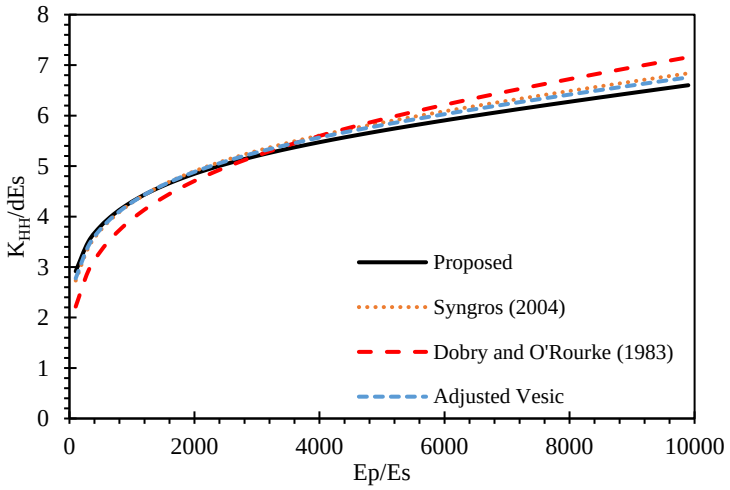

Figure 4-46: Normalized swaying stiffness of a fixed-head fixed-base pile in homogenous soil profile: L/d = 15

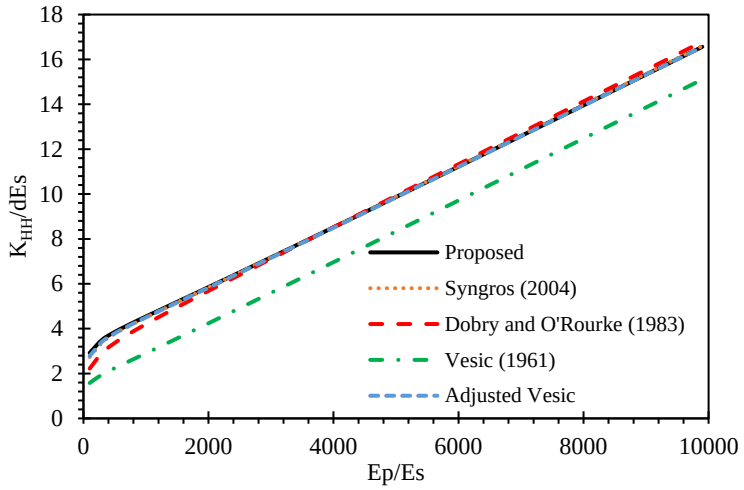

Figure 4-47: Normalized swaying stiffness of a fixed-head fixed-base pile in homogenous soil profile: L/d = 7.5

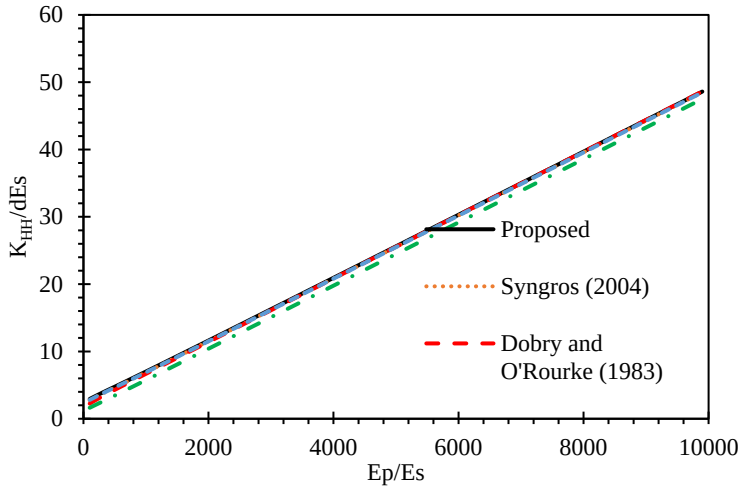

Figure 4-48: Normalized swaying stiffness of a fixed-head fixed-base pile in homogenous soil profile: L/d = 5

General notes:

1. A fixed-head pile's head stiffness is always larger than that of the free-head pile for similar pile tip conditions.
2. For fixed-base piles, the pile-head stiffness becomes less influenced by the subgrade model employed with decreasing slenderness ratio, the reason being it becomes more dependent on the pile rigidity than on the soil.

4.7 Non-linear lateral response

The analytical model studied in the previous sections applies only to the deflection of piles within the range of elastic response of soil caused by lateral loading on the piles. This section deals with the possibility of extending the use of the model in the inelastic range by integrating it with *p-y* curves that represent soil deformation at any given depth for a range of horizontally applied loads on the piles.

In the current practice, laterally loaded piles are often analyzed using the finite-difference method. The model uses the classical beam theory to represent the pile and uncoupled, non-linear load transfer functions called *p-y* curves, to represent the soil. For a better understanding of the application of the *p-y* method, a brief review of selected models is conducted.

4.7.1 *p-y* models

The beam on elastic foundation method attempts to use the discrete load transfer approach with the assumption of a linear load transfer function for the soil, which assumes the pressure p and deflection y at any discrete point along the pile are related through a modulus of subgrade reaction. In the *p-y* method, a non-linear load transfer function called "*p-y* curves" is used.

One distinct advantage of the *p-y* model-based design is its capability of simulating the soil's non-linear stress-strain response (Kondner 1963). The concept of the *p-y* model was originally proposed by Mcclelland and Focht (1956) and developed by Matlock (1970), Reese et al. (1974), Reese and Welch (1975), and others. The following sections are dedicated to discussing the non-linear models of pressure/deflection relation, called *p-y* curves.

4.7.1.1 p-y Criteria – Cohesive Soils

The *p-y* curves used for calibrating the current model for cohesive soils are presented in the following table:

Table 4-7: *p-y* models for cohesionless soils

p-y model	Applicability
Matlock (1970)	Soft Clay
Reese and Welch (1975)	Stiff Clay
API (2011)	All Clays

API: American Petroleum Institute

Matlock (1970) Criteria: The Matlock Criteria was first developed based on a research program on laterally loaded piles for offshore structures. The program included field tests on an instrumented

pile, laboratory model testing, and the development of correlations. As a result of his research program, Matlock proposed the following *p-y* curve for short-term static loading;

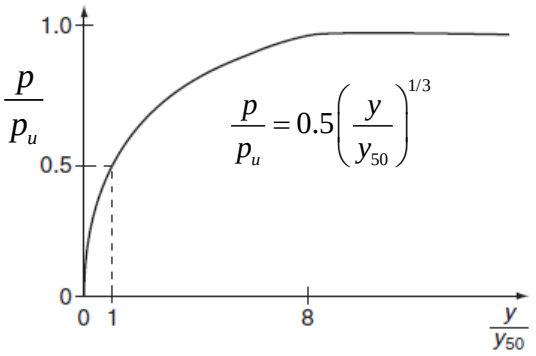

Figure 4-49: Characteristic shapes of *p-y* curves for soft clay (Matlock 1970)

For the construction of the non-dimensional curve, as Matlock suggested in Figure 4-49, the following expressions can be used:

$$y_{50} = 2.5\varepsilon_{50}d \tag{4.68a}$$

$$p_u = N_p C_u d \tag{4.68b}$$

$$N_p = \min\left\{\begin{matrix}\left(3+\frac{\gamma z}{C_u}+0.5\frac{z}{d}\right)\\ 9\end{matrix}\right\} \tag{4.68c}$$

Where; $p=$ lateral soil resistance, $p_u=$ ultimate lateral soil resistance, $y=$ lateral pile deflection, $y_{50}=$ deflection at one-half the ultimate soil resistance, and $\varepsilon_{50}=$ strain at one-half the maximum deviator stress in an undrained test.

Reese and Welch (1975) Criteria: The experimental research program conducted by Reese and Welch was to propose criteria for predicting the behavior of stiff clay around a deep foundation subjected to short-term static or cyclic loading. As a result of their research program, Reese and Welch proposed the following *p-y* curve for short-term static loading;

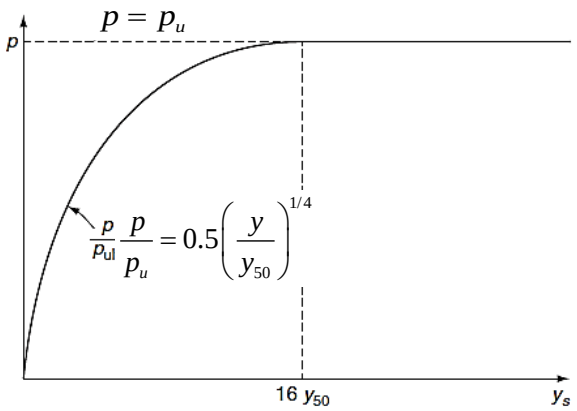

Figure 4-50: Characteristic shapes of *p-y* curves for stiff clay Reese (Reese and Welch 1975)

***API Criteria*:** The API criterion is the modified version of soft clay (Matlock 1970) and stiff clay (Reese and Welch 1975) criteria. The suggested method distinguishes soft clays from stiff clays by introducing boundary shear strength of C_u equal to 100kPa. The ultimate soil resistance is obtained from Equations (1.1b) and (1.1c).

The following are the procedures for the construction of *p-y* curves for stiff and soft clay subject to short-term static loading;

a) Obtain the best possible estimate of soils parameters, i.e., the variation of shear strength and unit weight with depth, and the value of ε_{50}.
b) Calculate the ultimate soil resistance per unit length of the shaft, p_u, using Equation (4.68b) and (4.68c)
c) Calculate y_{50} by using Equation (4.68a)
d) *p-y* curve points can be computed by using the equation provided in Figure 4-49 and Figure 4-50:

4.7.1.2 p-y Criteria – Cohesionless Soils

The basic ascribed models used to define *p-y* curves for cohesionless soils are presented in the following table:

Table 4-8: *p-y* models for sand

p-y model	Applicability
Reese et al. (1974)	Clean fine sand to silty fine sand
API (2011)	All sands

Reese et al. (1974) ***Criteria*:** Reese and his colleagues used the data obtained from the lateral loading of two 60.96cm (24-inch) diameter piles installed at the site where the soil consisted

of clean fine sand to silty fine sand. The tests were performed under static and cyclic loadings, and the families of *p-y* curves were developed. Then, the authors suggested a semi-empirical method for predicting *p-y* curves based on the properties of the sand and the pile diameter.

The typical family of *p-y* curves is shown in Figure 4-51.

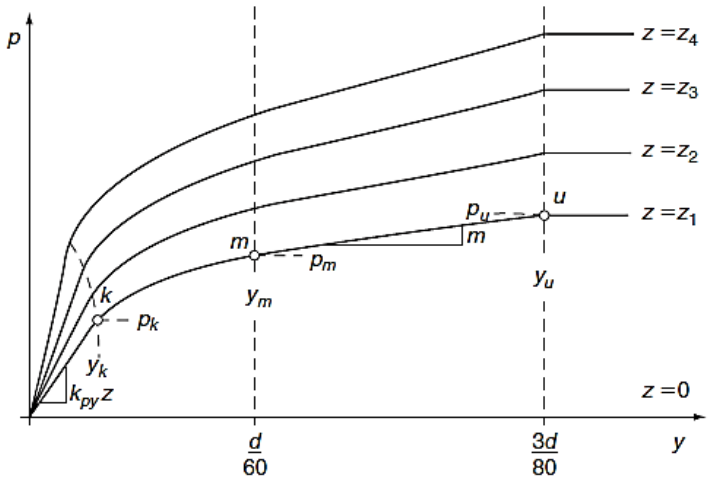

Figure 4-51: Characteristic shapes of *p-y* curves for sand (Reese et al. 1974)

The following procedure can be used in developing a *p-y* curve for laterally loaded piles in sand

a) Obtain values for the friction angle, the soil unit weight, and pile diameter.
b) Make the following preliminary computations using Equation (4.69).

$$\alpha_s = \frac{\phi}{2};\ \beta_r = 45 + \frac{\phi}{2};\ K_o = 0.4 \text{ and } K_a = \tan^2\left(45 - \frac{\phi}{2}\right) \tag{4.69}$$

c) Compute the ultimate soil resistance per unit length of the pile using the smaller of the values given by the following equations

$$p_s = \begin{pmatrix} \gamma z\left[\dfrac{K_o z \tan\phi \sin\beta_r}{\tan(\beta_r - \phi)\cos\alpha_s} + \dfrac{\tan\beta_r}{\tan(\beta - \phi)}(d + z\tan\alpha_s)\right] \\ +\gamma z\left[K_o z \tan\beta_r(\tan\phi\sin\beta_r - \tan\alpha_s) - K_a d\right] \end{pmatrix} \tag{4.70a}$$

$$p_s = K_a d\gamma z\left(\tan^8\beta_r - 1\right) + K_0 d\gamma z \tan^4\beta_r \tag{4.3b}$$

d) Establish y_u as $3d/80$. Compute p_u by the following equation:

$$p_u = \bar{A}_s p_s \tag{4.71}$$

e) Establish y_u as $d/60$. Compute p_m by the following equation

$$p_m = B_s p_s \tag{4.72}$$

the values of $\bar{A}_s$ and B_s are given in

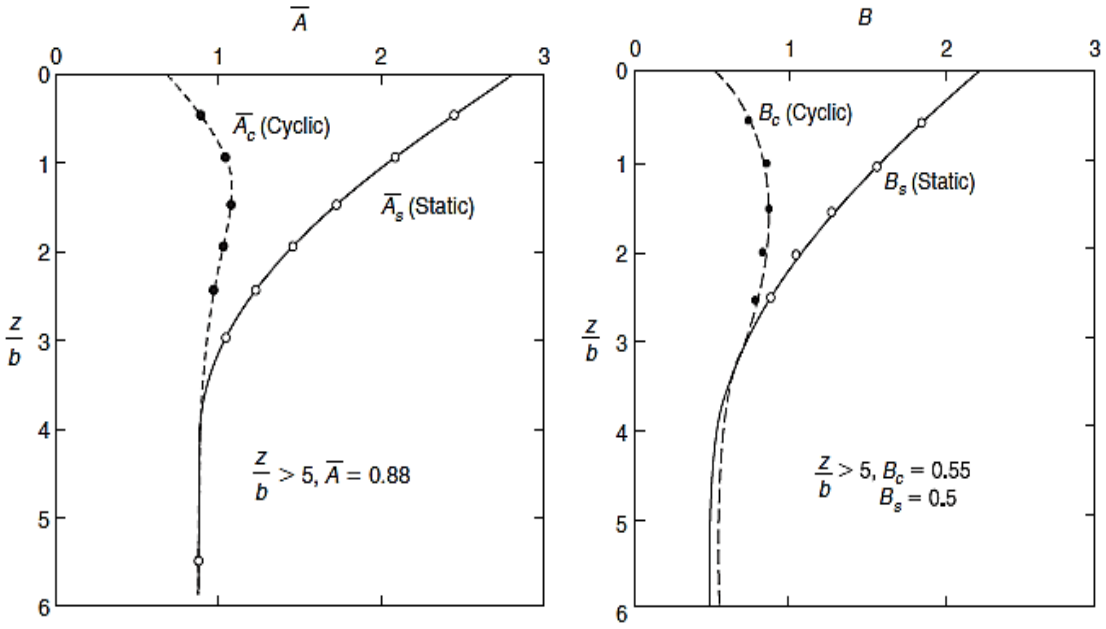

Figure 4-52: Values of coefficient $\bar{A}_c$ and B_c (Reese et al. 1974)

f) Establish the initial straight-line portion of the *p-y* curve

$$p = \left(k_{py} z\right) y \tag{4.73}$$

where k_{py} is the initial stiffness of the *p-y* curve. Recommended values of k_{py} are given in

Table 4-9: Representative values of k_{py} for sand above the water table

Relative density	Loose	Medium	Dense
Recommended k_{py} (MPa/m^3)	6.8	24.4	61

g) Establish the parabolic section of the *p-y* curve.

API (2011) Criteria: The latest editions of API provide the same approach proposed by Bogard and Matlock (1980). The ultimate lateral capacity for sands at a given depth is the smallest value of P_u from Equations (4.74a) and (4.74b)

$$P_u = \left(\bar{C}_1 z + \bar{C}_2 d\right)\gamma' z \tag{4.74a}$$

$$P_u = \bar{C}_3 d\gamma' z \tag{4.7b}$$

Where $\bar{C}_1$, $\bar{C}_2$ and $\bar{C}_3$ are coefficients which are functions of the angle of friction, and can be calculated from the following equations:

$$\bar{C}_1 = \frac{\tan^2\beta_r \tan\alpha_s}{\tan\left(\beta - \phi'\right)} + K_0\left(\begin{array}{l}\dfrac{\tan\phi'\sin\beta_r}{\cos\alpha_s \tan\left(\beta_r - \phi'\right)} \\ +\tan\beta_r\left(\tan\phi\sin\beta_r - \tan\alpha\right)\end{array}\right) \tag{4.75a}$$

$$\bar{C}_2 = \frac{\tan\beta_r}{\tan\left(\beta_r - \phi'\right)} - K_a \tag{4.8b}$$

$$\bar{C}_3 = K_a\left[\left(\tan^8 - 1\right) + K_0\tan\phi'\tan^4\beta\right] \tag{4.8c}$$

API suggests the use of Equation (4.76) for developing the *p-y* curve

$$\frac{p}{p_u} = \bar{\eta} A \tanh\left(\frac{K_{py} z}{A\bar{\eta} p_u} y\right) \tag{4.76}$$

where; $\bar{\eta} =$ shape factor ($\bar{\eta} = 1$ for circular piles) and $A =$ static or cyclic loading factor ($A = 0.9$ for cyclic and $A = 3 - 0.8z/d \geq 0.9$ for static).

4.7.2 Proposed non-linear model

In the preceding sections, a detailed introduction to the ascribed *p-y* models is presented. In this section, the non-linear aspect of the two-parameter subgrade model, calibrated earlier, is studied. But prior to that a non-linear soil response together with stress-strain characteristics of pile-soil system is discussed.

4.7.2.1 Soil response and Stress-deformation of soil

In the p-y approach, the reaction modulus is the main soil parameter used for assessing the lateral pile response. And it is defined as the resistance of the soil, *p*, at a point along the pile

divided by the deflection of the pile at that point, *y*, (Equation (4.77)). From the p-y curve given in Figure 4-53(a), it can be seen that the slope of the secant is the reaction modulus of the system.

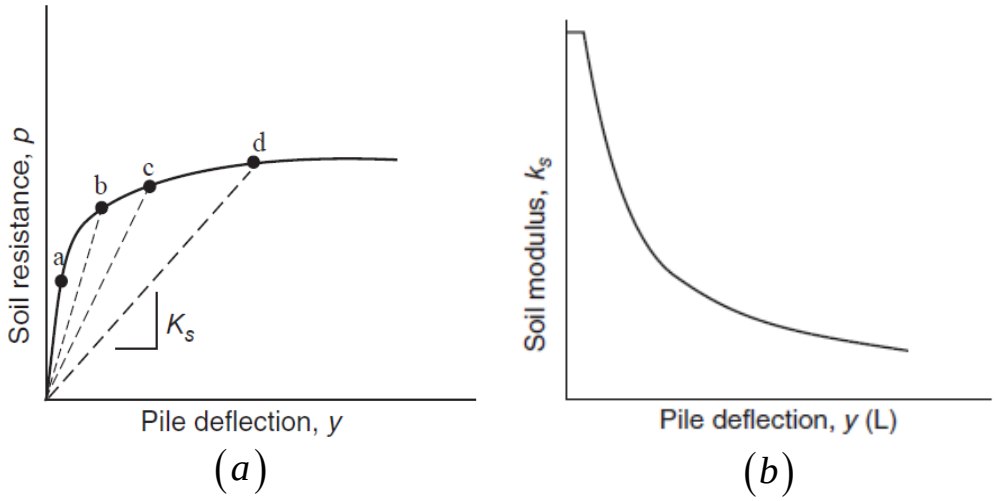

Figure 4-53: (a) Typical *p-y* curve (b) Resulting soil modulus

It is evident that the soil reaction modulus value is constant for small deflections (up to, say, point 'a') but decreases with increased deflection (points b, c, and d). This decay in stiffness is depicted in Figure 4-53(b). The expression for the subgrade modulus of the *p-y* curve is Equation (4.77) is identical to the one shown in Equation (4.38). The basic difference between the two expressions being, in the case of the *p-y* model, the applied load is replaced by the resistance of the soil (*p*).

$$k_s = \frac{p}{y} \tag{4.77}$$

Focusing now on to the non-linear stress-strain relationship, according to Vardanega and Bolton (2013), the non-linear behavior of soil is often expressed in the form of hyperbolic stress-strain relationships. The stress-strain relationship of any soil can be depicted by the curve given in Figure 4-54. The slope of the line, termed E_s, is the secant soil modulus and represents the stiffness of the soil. The magnitude of E_s is related to the value of strain to which the line is drawn.

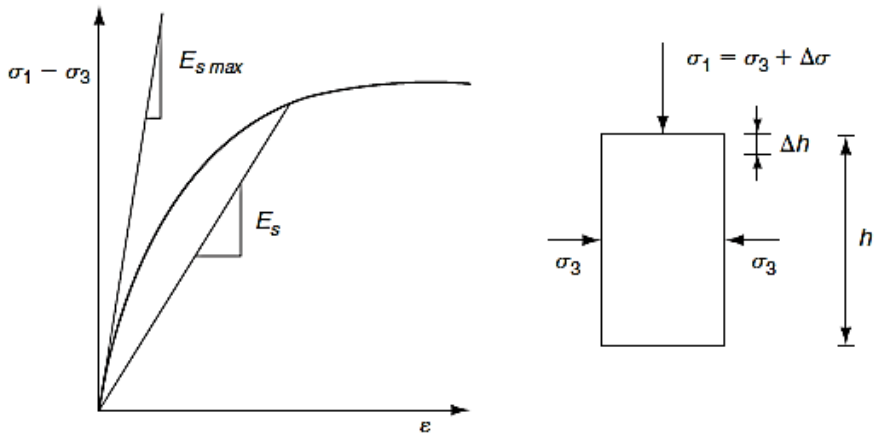

Figure 4-54: Typical non-linear stress-strain relationship

The decay of soil reaction modulus (subgrade modulus) reflects the same phenomena but with different units. The decay in both cases is undoubtedly due to the same phenomenon: a decrease in stiffness of a soil element with increased strain.

Furthermore, the above phenomenon can be observed in the shear stress reduction curve shown in Figure 4-55. The hyperbolic relationships describe the reduction of normalized secant shear modulus G_s/G_{s0} of soil as a function of engineering shear strain induced in the soil (G_s is the secant shear modulus of soil at any value of shear strain, and G_{s0} is the initial (or small-strain) shear modulus of soil at a very small value of shear strain, typically less than 10^{-6} (Atkinson, 2000)).

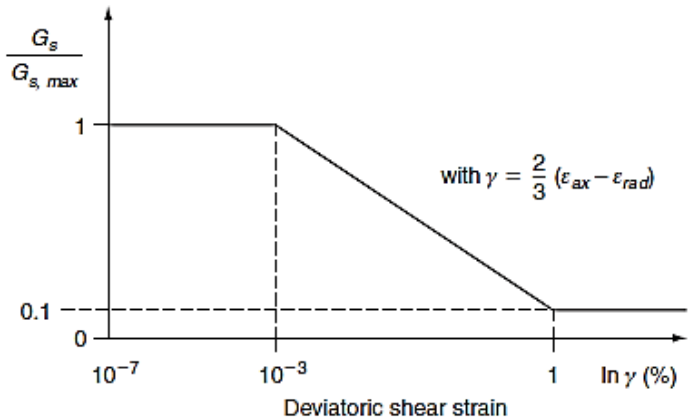

Figure 4-55: Model for decay of Gs (Van Impe 1991)

In the case of the current elastic subgrade model, a linear relationship exists between the pile deflection and subgrade modulus as shown in Figure 4-56.

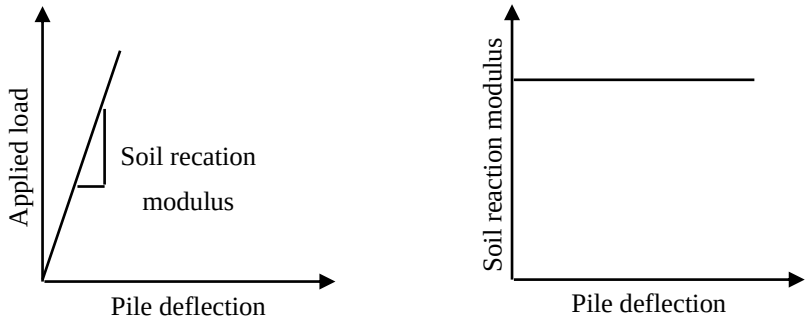

Figure 4-56: Typical load versus deflection curve and resulting soil modulus: for the current model

In order to incorporate the response un the non-linear range, the subgrade modulus expressions, given in Equations (4.9) and (4.10), should be modified using non-linear soil properties. For convenience, both equations are provided below

$$k_s = \frac{(0.4\nu_s + 0.67)}{\chi}\frac{E_s}{d}; \qquad G_P = T = (1.36\nu_s + 2.28)\chi G_s d \tag{4.78}$$

As can be seen from Equation (4.78), the subgrade parameters are only dependent on the elastic soil parameters, ν_s and E_s, the calibration factor (which is also a function of the soil and pile elastic parameters), and the pile diameter.

In order to capture the non-linear aspect of a given pile-soil system, we have to use a non-linear soil reaction modulus instead of elastic subgrade parameters. Of the soil parameters involved in the current model (Equation (4.78)), only the modulus of elasticity can be expressed as a function of load and deflection (Figure 4-54). And also it is important to consider the effect of the pile diameter.

In the *p-y* methods discussed earlier, the effect of the pile diameter is incorporated by using different parameters (y_{50} and p_u for clay and p_s, $\bar{A}_s$ and B_s for sand). In both cases the functions used to incorporate the contribution of the pile diameter are different from the current model. So, in order to account additional effect of the pile diameter, if any, on the non-linear response, a new parameter, δ, is introduced.

So, for the case of non-linear lateral response, the parameters given in Equation (4.78) are rewritten by changing E_s with $\bar{E}_s$. Where $\bar{E}_s$ is a parameter containing a variable secant modulus (E^*_{sec}) and also the effect of pile diameter (δ).

$$\bar{E}_s = \delta E^*_{sec} \tag{4.79}$$

In order to find the expressions of both parameters the computer program LPILE is used. LPILE is a program specifically designed for analyzing a single pile under lateral loading using the p-y method. The program uses internally generated p-y curves to computes deflection, bending moment, shear force and soil response over the length of the pile.

The values of E^*_{sec} and δ are obtained through parallel analyses of the current model and the LPILE model of a sufficiently large number of cases by varying soil and pile parameters and subjecting the pile to a horizontal force of varying magnitude. The value of E^*_{sec} and δ is then determined in each case by equating the pile head deflection from the two models.

4.7.2.2 P-y model used

The load-deflection behavior of a laterally loaded pile is dependent on the type of *p-y* curve used (Section 4.7.1). LPILE provides around 14 different load-transfer (*p-y* curves) models. So that the user can choose a suitable *p-y* curve type based as needed. because their wide acceptance, the following *p-y* curves are used in this study for the analysis using LPILE.

- For soft clay: Matlock (1970)
- For medium and Stiff clay: Reese et al. (1975)
- Sand: Reese, et al. (1974)

The details about the above three models can be seen in Section 4.7.1.

4.7.2.3 Material and geometric properties used in the non-linear analysis

The following sufficiently wide rages of material properties are used.

Pile properties

- Pile modulus of elasticity , E_p (GPa): 25, 28 and 30
- Pile slenderness ratio, L/d : 5 to 50

Soil Properties

Cohesive Soil (Clay)

- Soil Poisson's ratio, v_s: 0.25 to 0.49
- Effective Unit weight, γ' (kN/m^3): 15-20
- Cohesion: C_u (kN/m^2): According to Reese and Sullivan (1984), given clay soil can be categorized as a soft, medium, and stiff based on the value of the undrained cohesion. The range of each category is shown in Table 4-1. However, in this study, selected undrained shear strength values representing each soil consistency group are used which are given in Table 4-11

Table 4-10: Relationship between Cohesion and clay consistency

Clay Consistency	Cohesion (kPa)	ε_{50}
Soft	10 to 25	0.02
Medium	25 to 50	0.01
Stiff	50 to 100	0.007
	100 to 200	0.005
	200 to 400	0.004

Table 4-11: Soil data used in the parametric study

Soil Consistency	Cohesion (kPa)	ε_{50}
Soft	15	0.02
	20	0.02
Medium	30	0.01
	45	0.01
Stiff	70	0.007
	150	0.005
	250	0.004

The value ε_{50} in Table 4-1 and Table 4-11 is the strain at one-half of the deviator stress (Skempton 1984).

Cohesionless Soil (Sand)

- Soil Poisson's ratio, v_s: 0.25 to 0.4
- Effective Unit weight, γ' (kN/m^3): 15-18
- The angle of internal friction, ϕ (^{0}): 25-40

4.7.2.4 Ultimate lateral pile load

As portrayed in Figure 4-53, the lateral response of a pile is dependent on the magnitude of the applied load P. Therefore, it is predestined to have the effect of P in the expression of E^*_{sec}. For this purpose, a new parameter $\bar{P}$ is introduced, defined as the ratio of the applied load P to P_{ult}. P_{ult} is the ultimate load that the pile can carry before a total failure or before surpassing an allowable displacement. The expressions for the ultimate load used in this study are presented next.

Ultimate load for clay

The ultimate load, per unit length of the pile in clay used in this study is proposed by Matlock (1970), who recommended the use of the smaller of the values given in Equation (4.80) and Equation (4.81).

$$P_{ult} = \left[3 + \frac{\gamma'}{C_u} z + \frac{J}{d} z \right] C_u d \tag{4.80}$$

$$P_{ult} = 9 C_u d \tag{4.81}$$

where $\gamma' =$ average effective unit weight from the ground surface to the depth, where the *p-y* curve is used; $z =$ depth from the ground surface to the *p-y* curve. Matlock (1970) stated that the value of J was determined experimentally to be 0.5 for a soft clay and about 0.25 for a medium clay.

Because the pile head response is the primary concern of this study (at $z = 0$), the ultimate load of $P_{ult} = 3 C_u d$ as obtained from Equation (4.80) is taken throughout the following sections.

Ultimate load for sand

According to Broms (1964), the ultimate lateral resistance of a pile is directly related to the passive Rankine earth pressure. Therefore, unless there is a considerable surcharge load, the ultimate resistance of the soil at the pile head is approximately zero. The above statement can be supported by evaluating the ultimate load capacity expression by McClelland and Focht (1956), given by Equation (4.82) at $z = 0$.

$$P_{ult} = \begin{pmatrix} \gamma z \left[\dfrac{K_o z \tan\phi \sin\beta_r}{\tan(\beta_r - \phi)\cos\alpha_s} + \dfrac{\tan\beta_r}{\tan(\beta - \phi)}(d + z\tan\alpha_s) \right] \\ + \gamma z \left[K_o z \tan\beta_r (\tan\phi \sin\beta_r - \tan\alpha_s) - K_a d \right] \end{pmatrix} \quad (4.82)$$

where $K_a = \tan^2(45^0 - \phi'/2) =$ active earth pressure coefficient; $K_o =$ at-rest earth pressure coefficient; $\beta_r = 45^0 + \phi'/2$; $\alpha_s =$angle defining wedge shape; and $\phi' =$ effective internal friction angle.

This shows that, using soil reaction for estimating the ultimate load at the pile head is not the right approach. Instead, the maximum allowed pile head deflection is used as the limiting criteria in this study. The recommendation of Okahara et al. (1991a, 1991b) as cited by Shirato et al. (2009) is used to this end. Okahara et al. (1991a, 1991b), using in-situ test data on piles subjected to horizontal loads and examining the elastic limit displacement on the observed load-displacement curves, suggested the use of the larger value of 1% of the pile diameter or 15mm.

LPILE is used to plot the load versus displacement relationship of a range of pile-soil cases. And as it can be seen from Figure 4-57 to Figure 4-59 for selected cases the ultimate load corresponding to the displacement of 15mm or 1% of pile diameter is dependent on d, ϕ and γ. A regression analysis of the data results in the expression given in Equation (4.83).

$$P_{ult} = (31.1 + 5.85\gamma) K_p^{1.15} d^{2.1} \quad (4.83)$$

where $K_p = \tan^2(45^0 + \phi'/2)$, $\gamma =$ unit weight in kN/m^3, kPa and $d =$ pile diameter in m and $P_{ult} =$ ultimate load in kN.

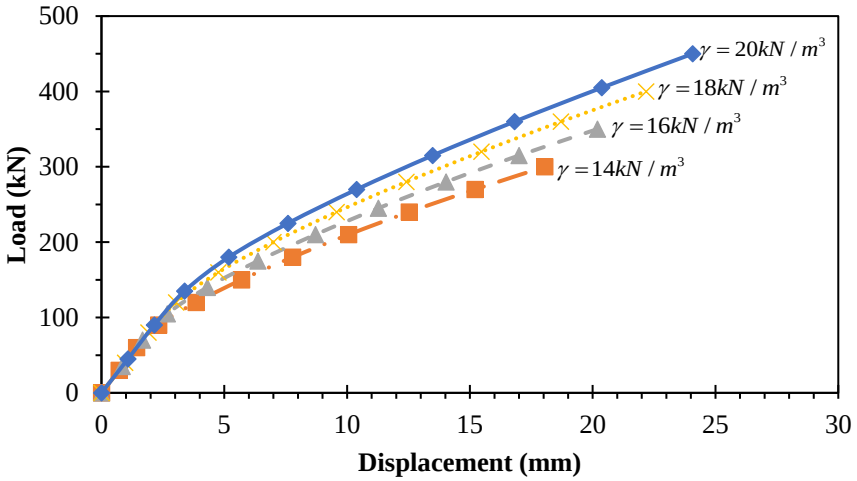

Figure 4-57: Load vs. Displacement: Effect of unit weight ($\phi = 30^0$, $d = 0.8m$, $E_p = 25GPa$ and $L = 25m$)

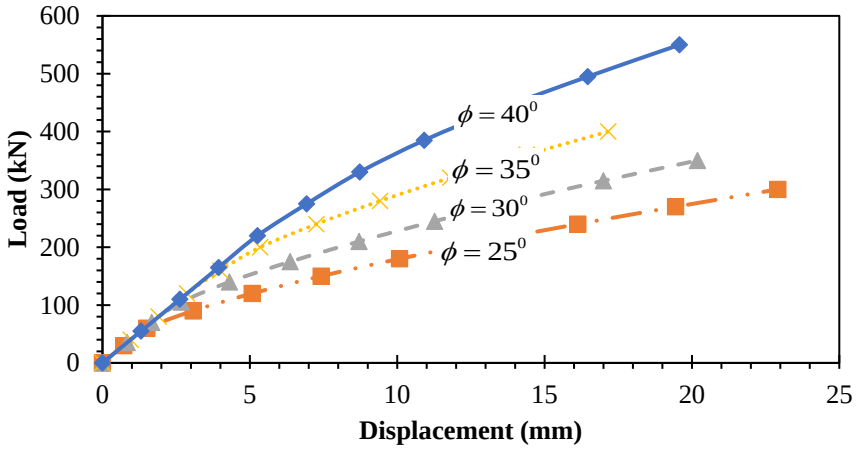

Figure 4-58: Load vs. Displacement: Effect of angle of internal friction ($\gamma = 16kN/m^3$, $d = 0.8m$, $E_p = 25GPa$ and $L = 25m$)

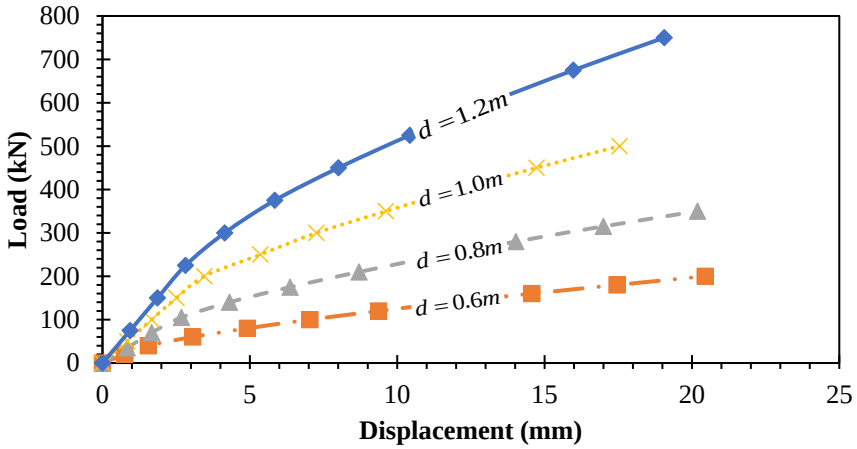

Figure 4-59: Load vs. Displacement: Effect of angle of internal friction ($\gamma = 16kN/m^3$, $\phi = 30^o$, $E_p = 25GPa$ and $L = 25m$)

4.7.2.5 Proposed secant modulus, E^*_{sec}

Up to this point, the primary input parameters and the *p-y* model are discussed. In this section, through parallel analyses, the secant modulus that gives equal pile head deflection as the *p-y* curve is determined (different based on the pile-soil property). The summarized procedure used in the process is presented below.

4.7.2.5.1 For cohesive soil

The non-linear lateral response of the pile-soil system shown in Figure 4-53 can be divided into two parts. For the first part, up to point a, the relation between the applied load and the pile deflection can be expressed using a linear expression. Which implies, a constant slope can be used for representing points within this range.

Skempton (1984) developed an expression for the secant modulus of the linear range using the soil undrained shear strength and ε_{50} (Equation (4.84)).

$$E_{sec} = \frac{C_u}{\varepsilon_{50}} \tag{4.84}$$

Using the secant modulus proposed by Skempton (1984), as $\bar{E}_s$ in the current model, the load versus deflection relationship for a range of pile-soil properties are plotted in Figure 4-60 to Figure 4-62. And form the plots it is evident that the secant modulus proposed by Skempton (1984) gives a very gentle slope compared to the *p-y* curve. Therefore, a multiplier, $\tilde{\delta}$, is introduced to increase the slope by adjusting the value of E_{sec}. The adjusted expression of the secant modulus is given in Equation (4.85). The secant modulus proposed by Skempton (1984) is found by setting $\tilde{\delta}$ in Equation (4.85) to one.

$$E_{sec} = \tilde{\delta}\frac{C_u}{\varepsilon_{50}} \tag{4.85}$$

Load versus deflection relationship for different values of $\tilde{\delta}$ is plotted From Figure 40-60 to Figure 40-63.

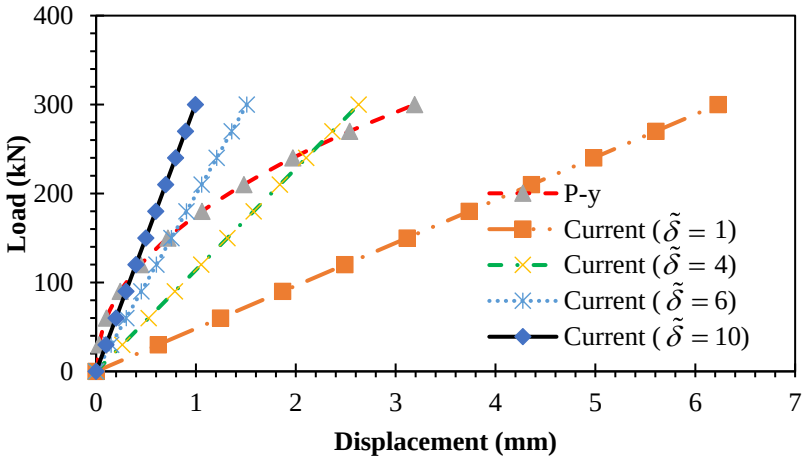

Figure 4-60: Load vs. Displacement: for stiff clay soil ($\gamma = 16kN/m^3$, $d = 1.0m$, $C_u = 100kPa$, $E_p = 25GPa$ and $L = 25m$)

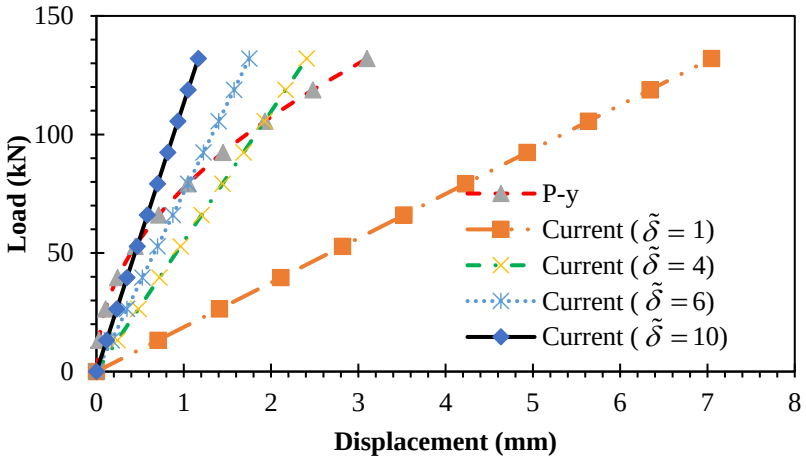

Figure 4-61: Load vs. Displacement: for medium clay ($\gamma = 16kN/m^3$, $d = 0.8m$, $C_u = 50kPa$, $E_p = 25GPa$ and $L = 25m$)

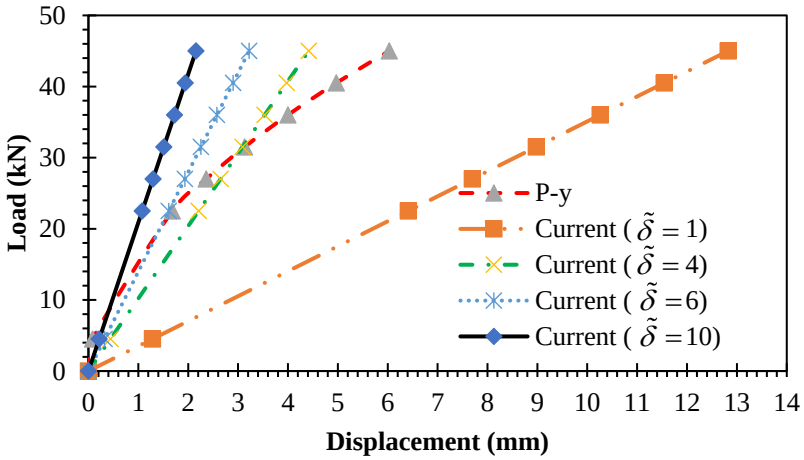

Figure 4-62: Load vs. Displacement: for soft clay ($\gamma = 16kN/m^3$, $d = 0.6m$, $C_u = 25kPa$, $E_p = 25GPa$ and $L = 25m$)

As it can be seen from the plots, for all soil consistencies, for $\tilde{\delta}=10$, the linear part of the current model and the p-y curve are in good agreement. Hence, the slope of the linear part, hereinafter referred as $E_{\max}$, is expressed as

$$E_{\max}=10\frac{C_u}{\varepsilon_{50}} \tag{4.86}$$

For the second part, discrete $\bar{E}_s$ values that gives equal pile deflection as the *p-y* curve are obtained. Some representative values are given in Table 4-7. As can be seen from the table, $\bar{E}_s$ is a function of d, C_u and $\bar{P}$.

Table 4-12: Representative values of $\bar{E}_s$ for stiff soils

$d\,(m)$	$\bar{P}$	$C_u\,(kPa)$			
		70	100	150	200
0.6	0.3	81.764	97.425	123.527	149.629
	0.5	41.089	48.960	62.077	75.195
	0.7	26.115	31.118	39.455	47.792
	0.9	18.616	22.181	28.124	34.067
	0.1	16.153	19.247	24.403	29.560
1.0	0.3	191.188	227.809	288.844	349.879
	0.5	96.079	114.483	145.155	175.828
	0.7	61.065	72.762	92.257	111.751
	0.9	43.529	51.867	65.763	79.659
	0.1	37.770	45.004	57.062	69.119

By fitting the discrete $\bar{E}_s$ values, the following empirical equation is obtained.

$$\bar{E}_s\,(MPa)=\delta_{dc}\left(0.104C_u+\kappa\right)\left[\bar{P}\right]^{-1.347} \tag{4.87}$$

where $C_u=$ undrained shear strength in kPa, and $\kappa=$ a dimensionless constant value representing soil consistency ($\kappa=2.5$ for soft, $\kappa=6.5$ for medium, and $\kappa=9$ for stiff clay soil) and $\delta_{dc}=$ pile size factor ($\delta_{dc}=3.321d-1$) and $d=$ pile diameter in m

As it is difficult to identify the range of the linear part, note that $\bar{E}_s$ should be taken as the minimum of the values obtained from Equation (4.86) and (4.87). In Figure 4-63, the normalized $\bar{E}_s$ ($\bar{E}_s/E_{\max}$) versus $\bar{P}$ for the three soil consistencies is plotted. From the figure

it can be seen that the stiffness reduction, for all soil consistencies, is very much dependent on the pile diameter. Form Figure 4-63c, it is evident that for piles with bigger diameters, the normalized $\bar{E}_s$ converges to one. Implying, for softer soils, the lateral response of a given pile-soil system is highly influenced by the pile property. So, for large diameter piles in soft soil, the load-displacement relationship, can be treated by using linear elastic subgrade modulus.

The plot of $\bar{E}_s/E_{\max}$ versus $\bar{P}$ for different undrained shear strength values is given in Figure 4-64. From the plot it is evident that, for stiff soils, the non-linear response is predominant. When compared to piles embedded in stiff soils, linear range of piles embedded in soils with medium or soft consistency, covers a significant range of $\bar{P}$.

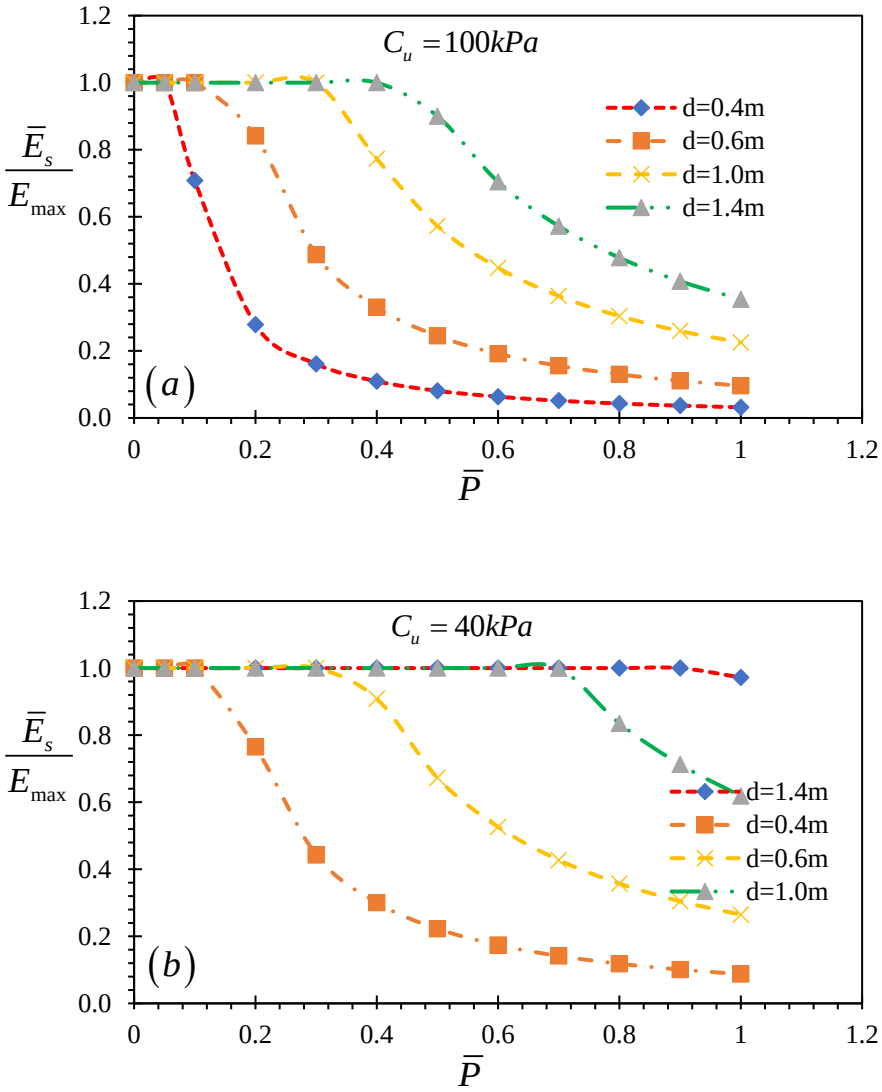

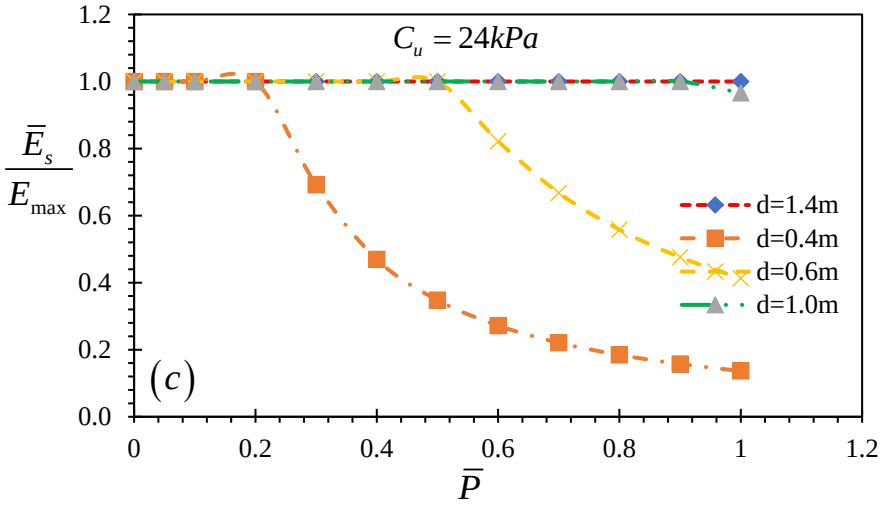

Figure 4-63: Normalized secant modulus reduction: Effect of diameter (a) Stiff clay (b) Medium clay and (c) Soft clay

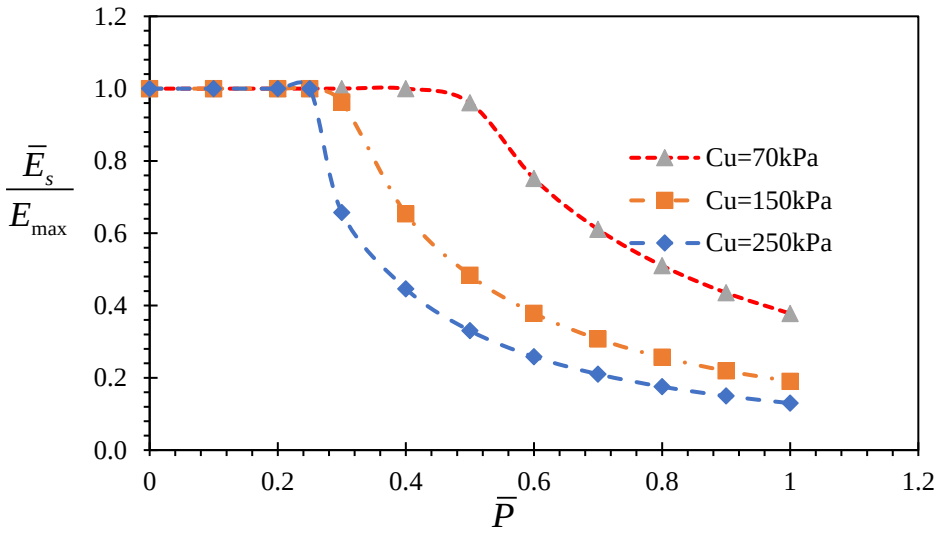

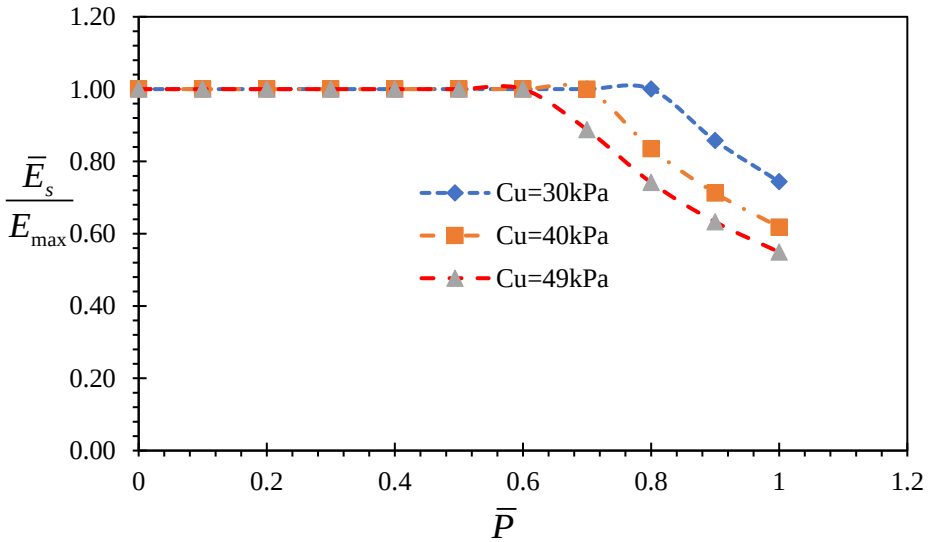

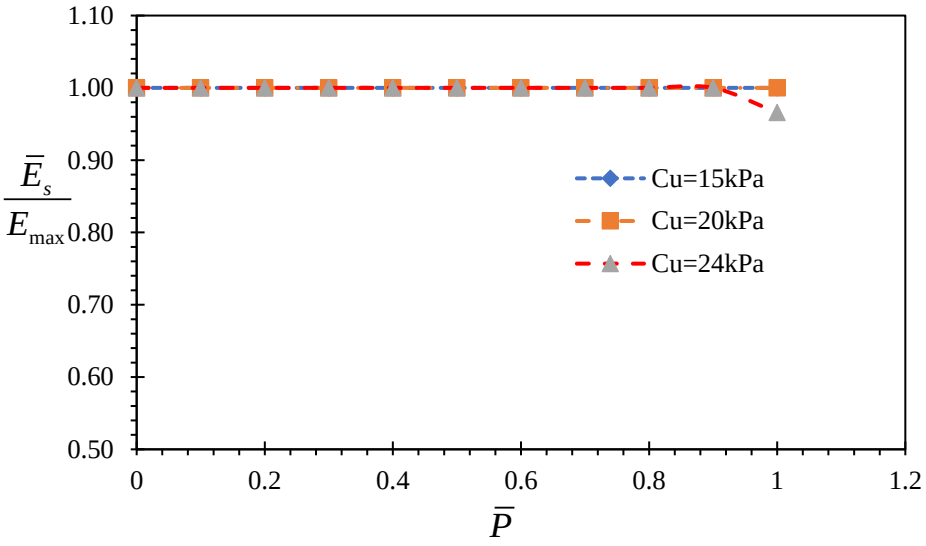

Figure 4-64: Normalized secant modulus reduction: Effect of undraind shear strength (a) Stiff clay (b) Medium clay and (c) Soft clay ($d = 1.0m$)

4.7.2.5.2 For cohesionless soils

During pile installation, as a result of a mechanical vibration induced during driving the pile or the casing, relatively dense soil will form around the pile. So, it can be assumed that it is not practical to have piles in loose sand. Therefore, in the following sections $\bar{E}_s$ is derived only for piles in medium or dense sand.

The non-linear lateral response of the pile-soil system shown in Figure 4-51 can be divided into four parts. The linear part, as discussed in Section 4.7.1.2, is dependent on the value of K_{py}.

The lateral response of piles embedded in medium dense and dense sand is studied using LPILE (Figure 4-68). From the figure it is evident that for dense sands, the non-linear response starts at $\bar{P} = 0.4$. Whereas for medium dense sands, the threshold $\bar{P}$ value varies $\bar{P} = 0.5$. Therefore, for the linear part, two relationships of $\bar{E}_s$ representing medium dense and dense soils are derived. For the second part of the *p-y* curve, as can be seen from the figure, one expression is sufficient to express the *p-y* curve for both medium dense and dense soils.

Using parallel analysis with LPILE, discrete $\bar{E}_s$ values that gives equal pile deflection as the *p-y* curve are obtained. And those descrete points are fitted to give expressions given the empreical relationship given in Equation (4.88) and (4.89).

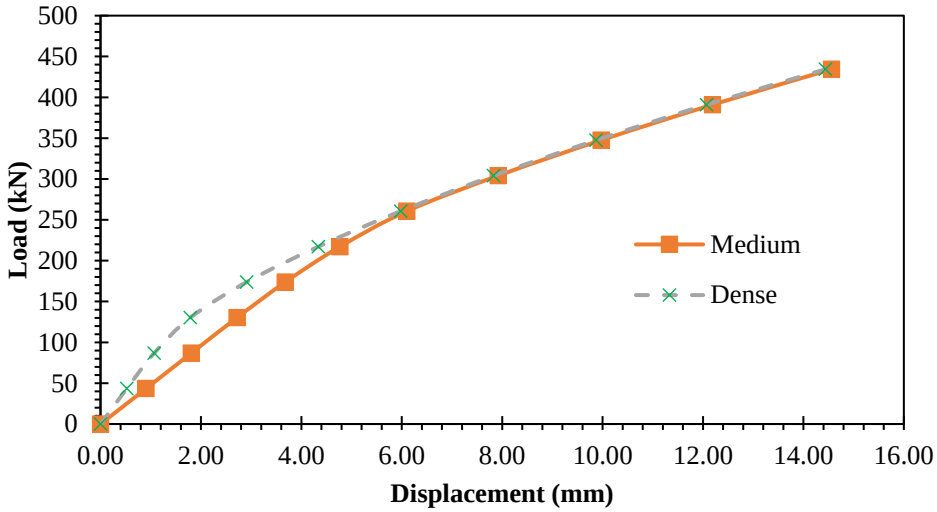

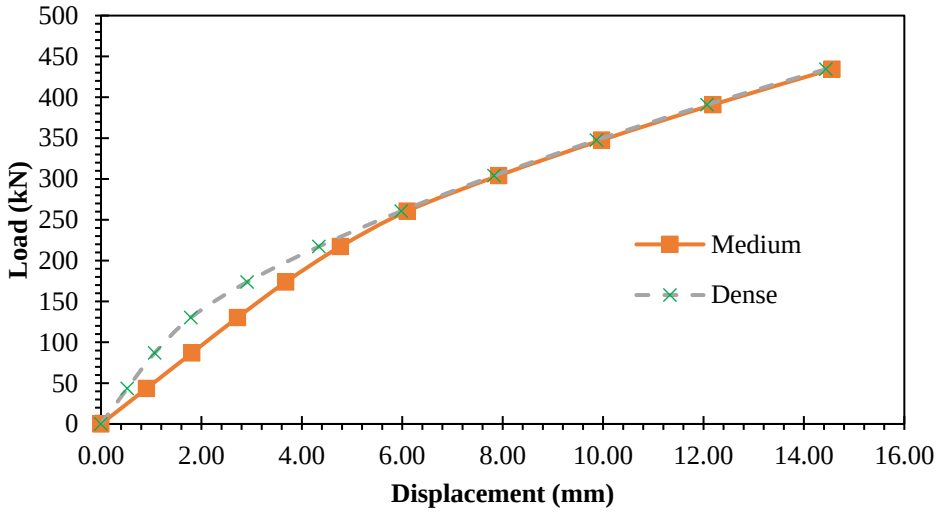

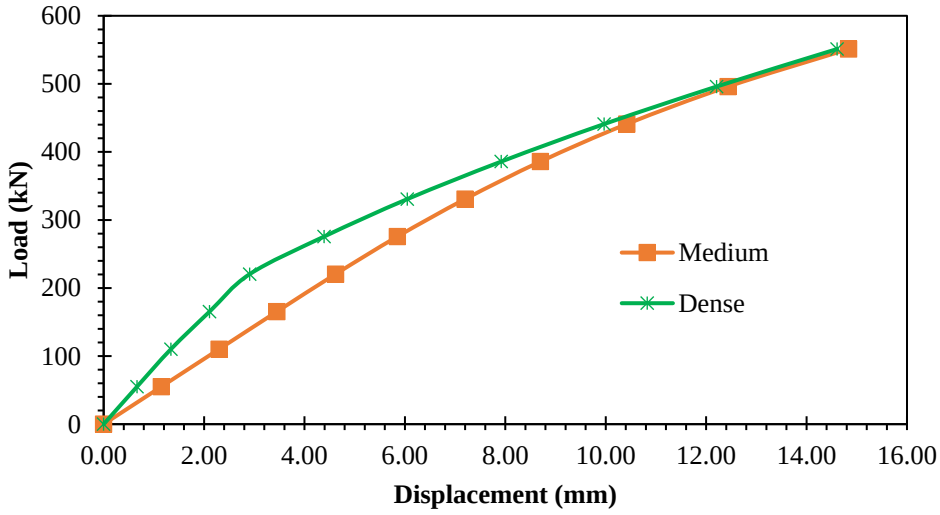

Figure 4-65: Load Vs Deflection : For medium dense and dense sand (a) $\phi = 25^0$

(b) $\phi = 30^0$ **and (c)** $\phi = 35^0$ **(**$d = 1.0m$**)**

Dense Sand

$$\bar{E}_s\left(MPa\right)=\begin{cases}\delta_d\,6.76\mathrm{e}^{\left(0.462K_p\right)} & \text{for} \quad \bar{P}<0.4\\ \delta_d\,6.76\mathrm{e}^{\left(0.462K_p-\bar{P}\right)} & \text{for} \quad \bar{P}\geq 0.4\end{cases} \tag{4.88}$$

Medium Dense Sand

$$\bar{E}_s\left(MPa\right)=\begin{cases}\delta_d\left(36.592K_P\mathrm{e}^{\left(-0.286K_p\right)}-19.6\right) & \text{for} \quad \bar{P}<0.5\\ \delta_d\,6.76\mathrm{e}^{\left(0.462K_p-\bar{P}\right)} & \text{for} \quad \bar{P}\geq 0.5\end{cases} \tag{4.89}$$

where δ_d = parameter controlling the effect of diameter ($\delta_d=1$ for $d=1m$, $\delta_d=1.25d-0.25$ for $d<1m$, and $\delta_d=1.5d-0.5$ for $d>1m$) and d = pile diameter in m.

Using the expressions given in Equation (4.88) and (4.89), the non-dimensional $\bar{E}_s$ ($\bar{E}_s/E_{\max}$) is ploted for both medium dense and dense sands (Figure 4-66). In this case, $E_{\max}$ is the $\bar{E}_s$ values sudggusted for the linear range.

As can be seen from Figure 4-66, for dense sand the variation of $\bar{E}_s/E_{\max}$ is independent of angle of internal friction. Whereas, for the case of medium dense sand, it increases with increase in angle of internal friction.

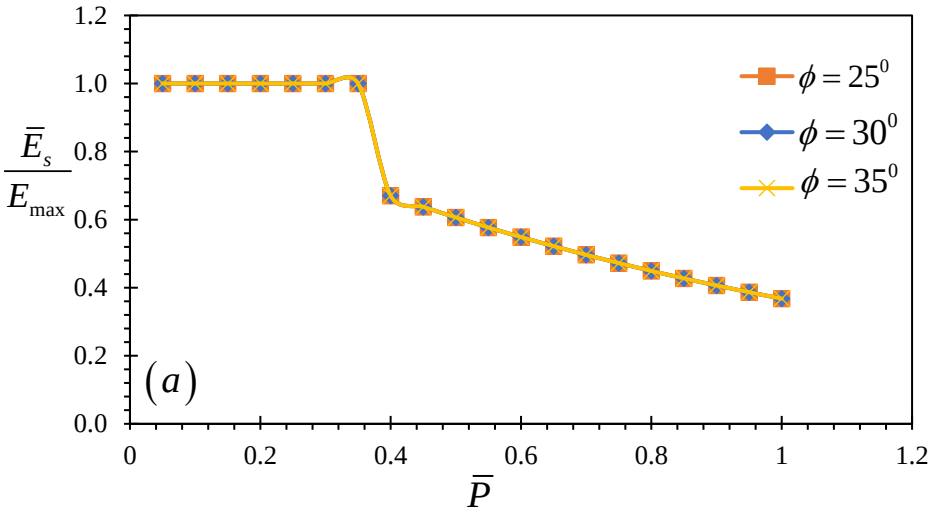

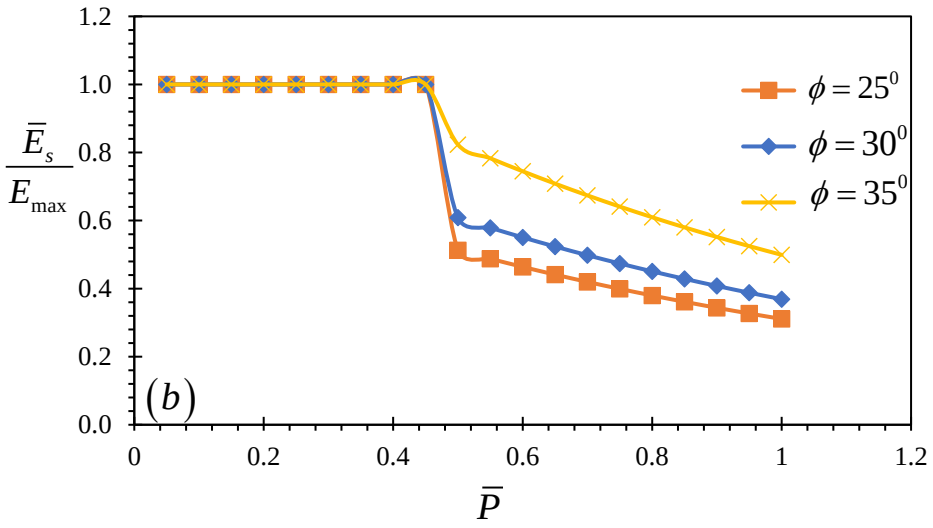

Figure 4-66: Normalized secant modulus reduction: Effect of ϕ (a)Dense sand

(b) Medium dense sand

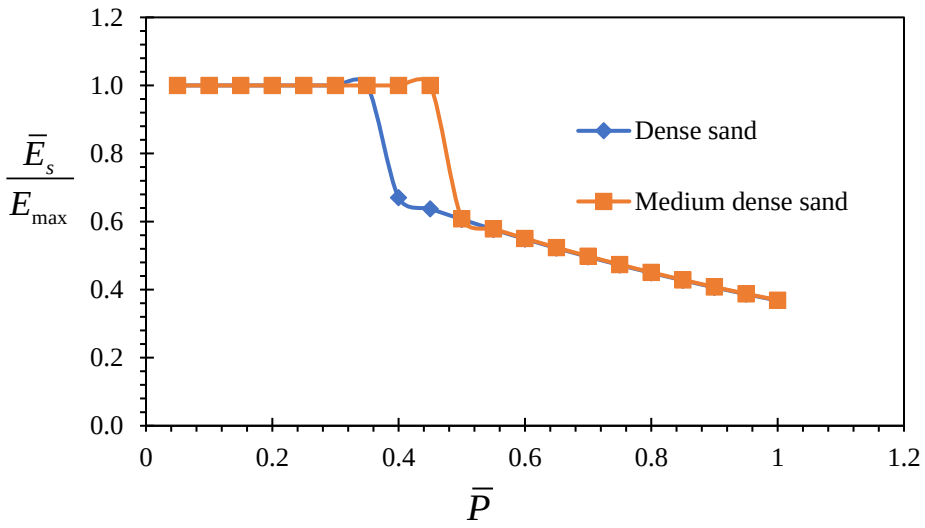

Figure 4-67: Normalized secant modulus reduction: Effect of sand relative density ($\phi = 30$)

In Figure 4-67, the non-dimensional $\bar{E}_s$ variation of both medium dense and dense sand is plotted together. Form the plot it is evident that the variation of the stiffness reduction of a medium dense and dense sand varies with in small range.

4.7.2.6 Non-linear subgrade parameters

For non-linear aspect of the current two parameter subgrade model, as stated earlier, the elastic subgrade parameters in Equation (4.78) should be modified by using $\bar{E}_s$ instade of E_s. Using the simplified expressions of the elastic parameters, given in Section 4.3.2, the following expressions are obtained.

For Clay

$$k_s\left(MPa\right)=\min\begin{cases}\left(1.28-0.25\nu_s\right)\left(0.104C_u+\kappa\right)\left[\bar{P}\right]^{-1.347}\dfrac{\delta_{dc}}{d}\\ \left(12.8-2.5\nu_s\right)\dfrac{C_u}{\varepsilon_{50}}/d\end{cases} \tag{4.90}$$

$$T\left(MPa\right)=\min\begin{cases}\left(0.32\nu_s+0.58\right)\left(0.104C_u+\kappa\right)\left[\bar{P}\right]^{-1.347}\delta_{dc}d\\ \left(3.2+0.58\nu_s\right)\dfrac{C_u}{\varepsilon_{50}}d\end{cases} \tag{4.91}$$

For Dense Sand

$$k_s=\min\begin{cases}\left(1.28-0.25\nu_s\right)6.76\mathrm{e}^{\left(0.462K_p\right)} & \text{for} \quad \bar{P}<0.4\dfrac{\delta_d}{d}\\ \left(12.8-2.5\nu_s\right)6.76\mathrm{e}^{\left(0.462K_p-\bar{P}\right)} & \text{for} \quad \bar{P}\geq 0.4\dfrac{\delta_d}{d}\end{cases} \tag{4.92}$$

$$T=\min\begin{cases}\left(0.32\nu_s+0.58\right)6.76\mathrm{e}^{\left(0.462K_p\right)}\delta_d d & \text{for} \quad \bar{P}<0.4\\ \left(3.2+0.58\nu_s\right)6.76\mathrm{e}^{\left(0.462K_p-\bar{P}\right)}\delta_d d & \text{for} \quad \bar{P}\geq 0.4\end{cases} \tag{4.93}$$

For Dense Sand

$$k_s=\min\begin{cases}\left(1.28-0.25\nu_s\right)\left(36.592K_P\mathrm{e}^{\left(-0.286K_p\right)}-19.6\right)\dfrac{\delta_d}{d} & \text{for } \bar{P}<0.5\\ \left(12.8-2.5\nu_s\right)6.76\mathrm{e}^{\left(0.462K_p-\bar{P}\right)}\dfrac{\delta_d}{d} & \text{for} \quad \bar{P}\geq 0.4\end{cases} \tag{4.94}$$

$$T=\min\begin{cases}\left(0.32\nu_s+0.58\right)\left(36.592K_P\mathrm{e}^{\left(-0.286K_p\right)}-19.6\right)\delta_d d & \text{for } \bar{P}<0.4\\ \left(3.2+0.58\nu_s\right)6.76\mathrm{e}^{\left(0.462K_p-\bar{P}\right)}\delta_d d & \text{for} \quad \bar{P}\geq 0.4\end{cases} \tag{4.95}$$

4.7.3 Parametric investigation

In the previous sections, the expressions for $\bar{E}_s$ are derived based on different *p-y* curves. And in this section, the performance of the proposed non-linear model is examined by varying the pile-soil properties. The plots for sand and clay are given separately in the following subsections.

As shown in Figure 4-67 and 68, the proposed model is in excellent agreement with the *p-y* curve used in the study. This indicates that if the subgrade model is calibrated with care, we can use it also in the inelastic range of a wide range of geotechnical problems.

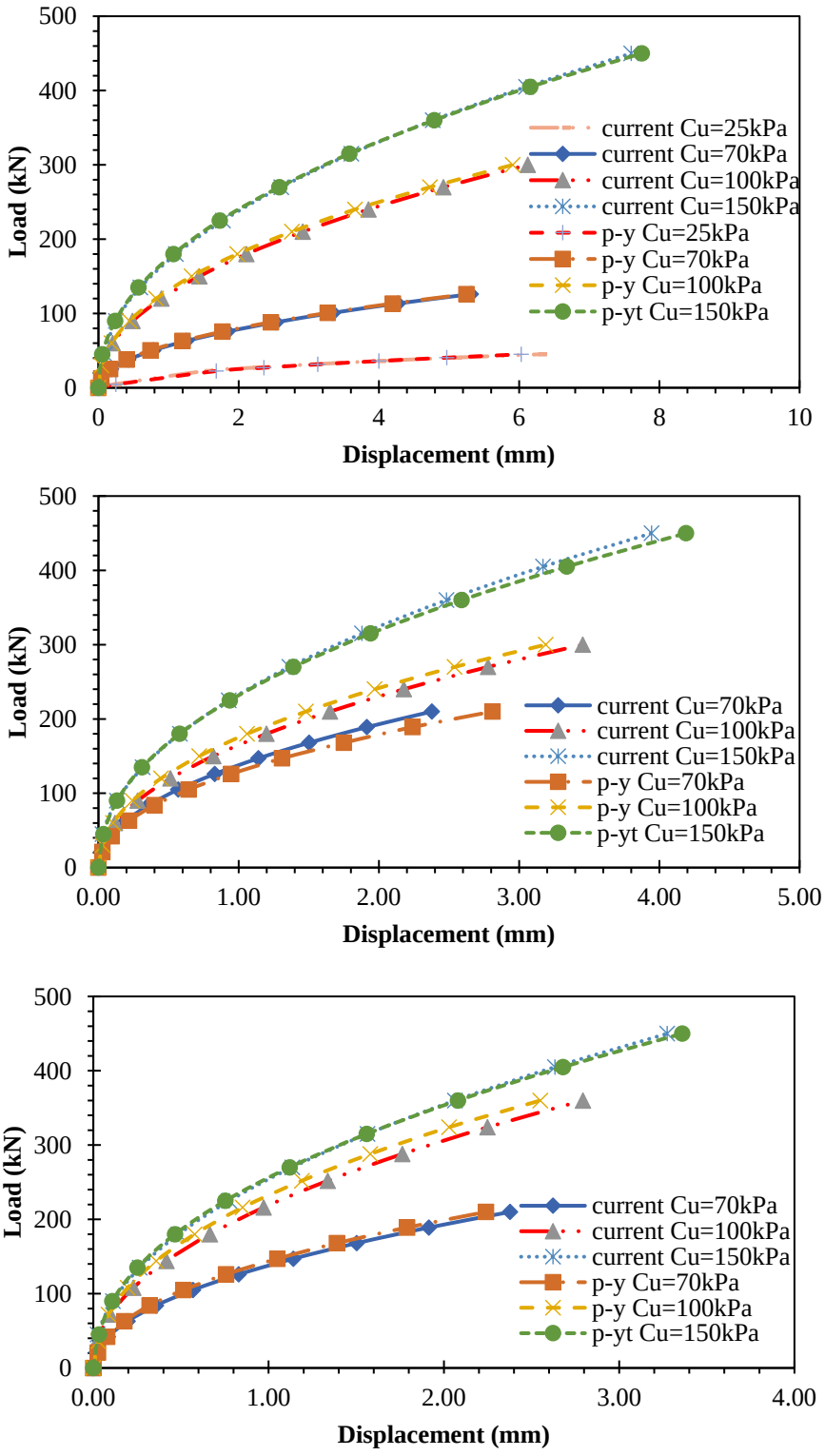

Figure 4-68: Load vs. Displacement fro cohesive soil: (a) d=0.6m (b) d=1.0m and (c)d=1.2m (

$\gamma = 16kN/m^3$, $E_p = 25GPa$ **and** $L = 25m$**)**

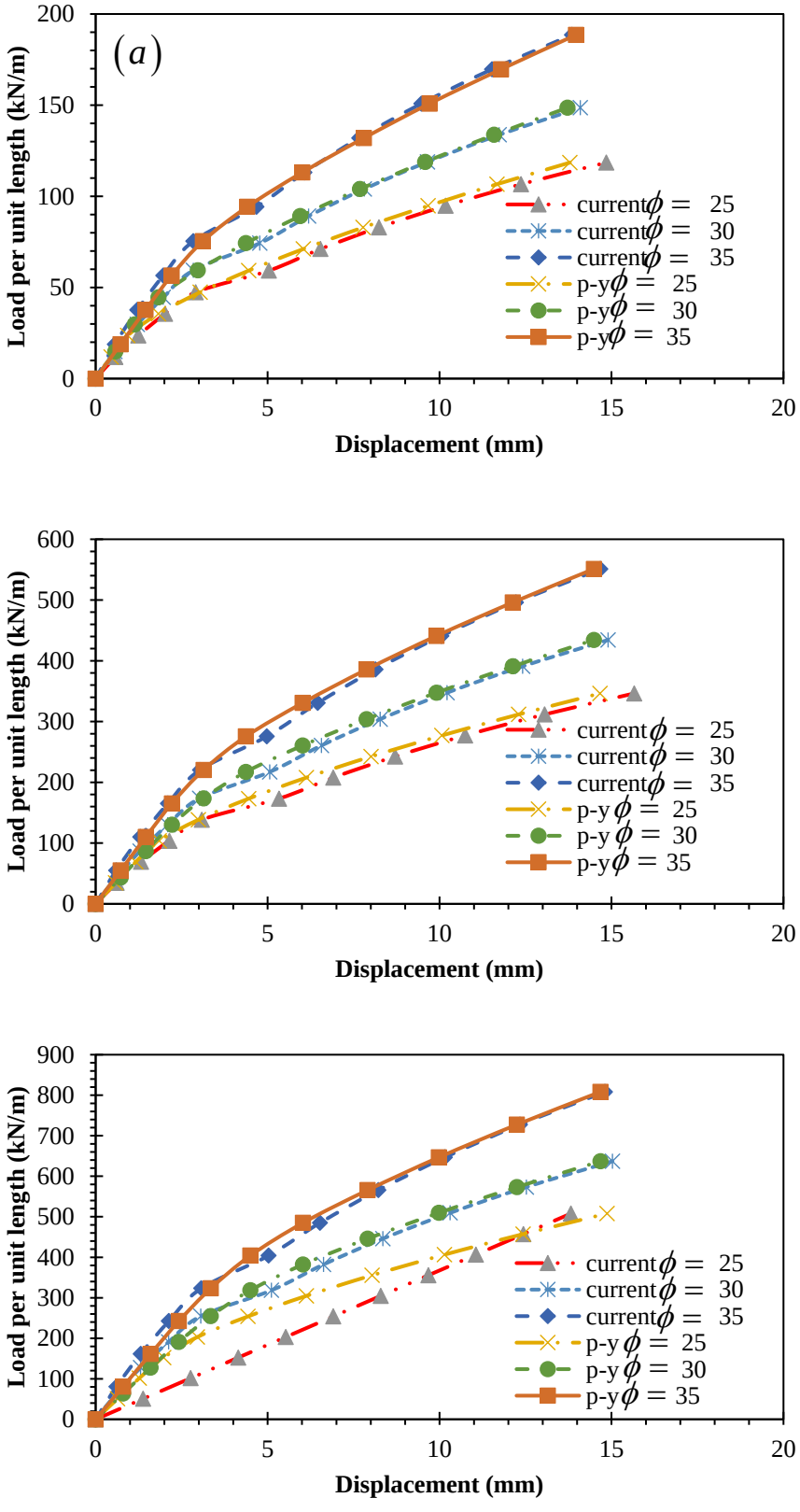

Figure 4-69: Load vs. Displacement for sand: (a) d=0.6m (b) d=1.0m and (c)d=1.2m

($\gamma = 16kN/m^3$**,** $E_p = 25GPa$ **and** $L = 25m$**)**

4.8 Illustrative examples

In the previous section, the model used in this study is compared against other models from published results. It is clear that the model used in this study is capable of satisfactorily modeling the elastic response of laterally loaded piles for a wide range of pile-soil properties.

In this section, to show how to use the proposed model in the analysis of laterally loaded piles, two illustrative examples are presented.

Illustrative example 1

Let us consider the analysis of a 15 m long reinforced concrete drilled shaft, with a diameter of 0.6 m and pile modulus $E_P = 25\ GPa$, embedded in a homogenous soil deposit with a soil modulus $E_S = 25\ MPa$ and Poisson's ratio of 0.3. It is intended to determine the swaying static stiffness at the pile-head for a) a fixed-head and b) a free-head pile

a) First, the critical pile length must be calculated. Using Equation (4.49) (fixed-head), the critical pile length is 7.69 m, less than the pile's length; thus, this is a "flexible" (or "long") pile. Similarly, for free-head pile, using Equation (4.53), the critical pile length is 7.42 m, also less than the pile length.
b) The pile-head stiffness K_{HH} is given by Equation (4.43) that yields $65,263\ kN/m$ for the fixed-head pile. Similarly, a value of $34,646\ kN/m$ is obtained for the free-head pile using Equation (4.41). Thus, the dimensionless pile-head stiffnesses, K_{HH}/dE_s, are approximately equal to 4.37 and 2.31 for the fixed and free-head pile, respectively. These values can also be read from Figure 4-43 and 4-35, respectively, using the plot $L/d = 7.5$.

Illustrative example 2

Let us consider an illustration, the analysis of a 25 m long reinforced concrete drilled shaft, with a diameter of 0.8 m and pile modulus $E_p = 28\ GPa$, embedded in a homogenous soil deposit with a soil modulus $E_s = 50\ MPa$ and Poisson's ratio of 0.35. It is intended to determine the swaying static stiffness at the pile-head for a) a fixed-head and b) a free-head pile

a) First, the critical pile length must be calculated. Using Equations (4.49) (fixed-head), the critical pile length is 8.8 m, less than the pile's length; thus, this is a "flexible" (or "long") pile. Similarly, for free-head pile, using Equation (4.53), the critical pile length is 8.55 m, also less than the pile length.

b) The pile-head stiffness K_{HH} is given by Equation (4.43) that yields $165,448\ kN/m$ for the fixed-head pile similarly a value of $80,970\ kN/m$ is obtained for the free-head pile using Equation (4.41). Thus, the dimensionless pile-head stiffnesses, K_{HH}/dE_s , are approximately equal to 3.9 and 2.02 for the fixed and free-head pile, respectively. These values can also be approximately read from Figure 4-43 and 4-35, respectively, using the plot $L/d = 7.5$.

CHAPTER 5
STATIC PILE HEAD STIFFNESS

5.1 Introduction

The static response of a single pile in an elastic soil, as dealt with in Chapter 4, is related to the pile head stiffness. In Section 4.4.1 and 4.4.2, the swaying pile-head stiffness (K_{HH}) is presented. However, due to the presence of rotation in addition to swaying, it is necessary to drive expressions for the complete pile-head stiffness. So, as shown in Figure 5-1 and Figure 5-2, the complete set of three pile-head stiffnesses (translation, K_{HH}, rocking, K_{RR}, and cross swaying–rocking, $K_{RH} = K_{HR}$) need to be determined. The reason for dealing with the swaying stiffness, K_{HH}, separately in Chapter 4, is its importance in calculating critical pile length.

The procedures for the derivation of the closed-form pile-head stiffness relations are presented. The derivation is based on a closed-from analytical solution of the force-deformation matrix for two sets of boundary conditions at the pile head. The details are presented below.

5.2 Problem definition

The model studied is depicted in Figure 5-1 and Figure 5-2 for fixed-head and free-head piles, respectively: a laterally loaded pile embedded in a homogenous soil profile, loaded by a concentrated force and/or a moment at the head. The pile is idealized as a linearly solid cylindrical beam of diameter d, Young's modulus E_p, and Length L. The soil is modeled as a homogenous medium of Young's modulus E_s, Poisson's ratio ν_s.

For both fixed-head and free-head piles given in Figure 5-1 and Figure 5-2, respectively, four different pile-soil boundary conditions similar to the boundary conditions used in Chapter 4 are studied in this section. In doing so, the pile-head stiffnesses for "long" and "short" piles under different pile head and base boundary conditions are determined.

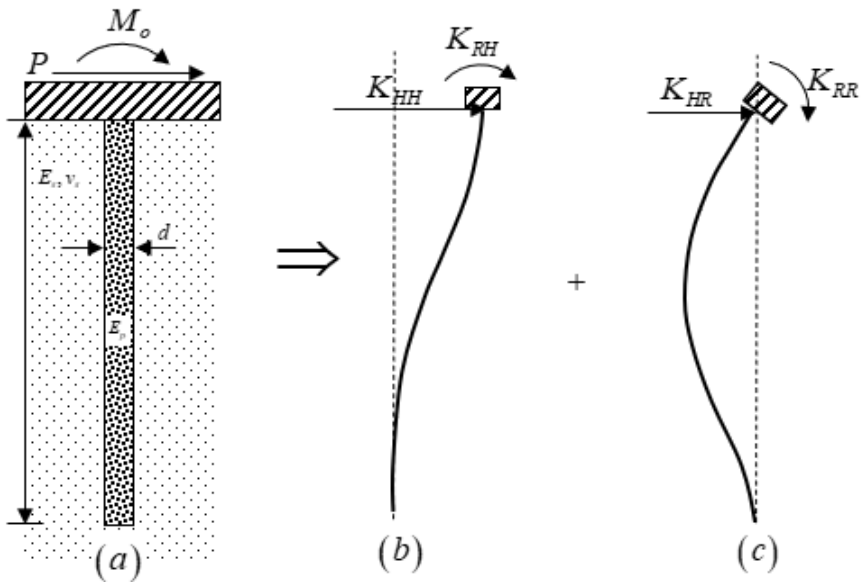

Figure 5-1: (a) Problem definition for fixed-head pile (b) shape function for pile deflection due to unit head displacement under zero rotation (c) corresponding shape function due to unit head rotation under zero displacement

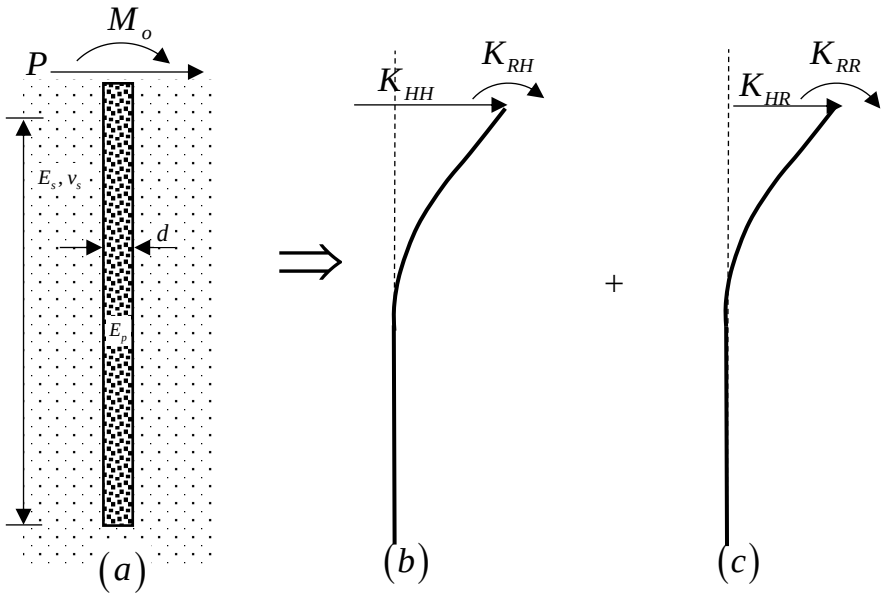

Figure 5-2: (a) Problem definition for free-head pile (b) shape function for pile deflection due to a unit head displacement under zero rotation (c) shape function due to a unit head rotation under zero displacement

The expressions of the slope, $\theta(z)$, shear, $Q(z)$, and moment, $M(z)$, from the generalized deflection equation (Equation (4.6)) are derived. Then, using the required matrix operations, all stiffness components are formulated. The results obtained using the closed-form analytical method are presented in the following sections.

5.3 Pile-head stiffness for "long" flexible piles

In Chapter 4, it was discussed that for "long" flexible piles, $\lim_{z\to\infty} w(z) = 0$. In order to satisfy this condition, the values of C_1 and C_3 in the general deflection equation (Equation (4.6)) have to be zero. As a result, the general deflection equation simplifies to Equation (5.1). This implies that the pile base boundary conditions have no importance in calculating the pile-head deflection and stiffness. The deflected shape is thus obtained as.

$$w(z) = e^{-\alpha z}\left(C_2\cos(\beta z) + C_4\sin(\beta z)\right) \tag{5.1}$$

5.3.1 Free-head long piles

The free-head pile responses given in Figure 5-2 can be determined by imposing the boundary conditions on Equation (5.1) and its derivatives. Subsequent differentations result in

$$\theta(z) = \frac{d}{dz}w(z) = -\mathrm{e}^{-z\alpha}\begin{pmatrix}\sin(z\beta)(\beta C_2 + \alpha C_4)\\ +\cos(z\beta)(\alpha C_2 - \beta C_4)\end{pmatrix} \tag{5.2}$$

$$M(z) = -EI\frac{d^2}{dz^2}w(z) = -\mathrm{e}^{-z\alpha}EI\begin{pmatrix}\cos(z\beta)\begin{pmatrix}\alpha^2 C_2 - \beta^2 C_2\\ -2\alpha\beta C_4\end{pmatrix}\\ +\sin(z\beta)\begin{pmatrix}2\alpha\beta C_2 + \alpha^2 C_4\\ -\beta^2 C_4\end{pmatrix}\end{pmatrix} \tag{5.3}$$

$$Q(z) = EI\frac{d^3}{dz^3}w(z) - T\frac{d}{dz} = -\mathrm{e}^{-z\alpha}EI\begin{pmatrix}\sin(z\beta)\begin{pmatrix}(3\alpha^2\beta - \beta^3)C_2\\ +\alpha(\alpha^2 - 3\beta^2)C_4\end{pmatrix}\\ +\cos(z\beta)\begin{pmatrix}(\alpha^3 - 3\alpha\beta^2)C_2\\ +\beta(-3\alpha^2 + \beta^2)C_4\end{pmatrix}\end{pmatrix} \tag{5.4}$$

The free-head single pile lateral response, as it can be seen from Figure 5-2, can be treated using superposition. Hence, the influence of the applied moment and horizontal load can be studied separately. Using this principle, Pender (1993) expressed the deflection equation as:

$$w(z) = f_{uH}P + f_{uM}M \tag{5.5}$$

And the slope as:

$$\theta(z) = f_{\theta H}P + f_{\theta M}M \tag{5.6}$$

where f_{uH}, f_{uM}, $f_{\theta H}$ and $f_{\theta M}$ are the flexibility coefficients

Equation (5.5) and Equation (5.6) can be rewritten in a matrix form as

$$\begin{Bmatrix} w(z) \\ \theta(z) \end{Bmatrix} = [F] \begin{Bmatrix} P \\ M \end{Bmatrix} \tag{5.7}$$

where $[F] = \begin{bmatrix} f_{uH} & f_{uM} \\ f_{\theta H} & f_{\theta M} \end{bmatrix}$ is the flexibility matrix

Using the inverse of the flexibility matrix, we can rewrite Equation (5.7) as

$$[F]^{-1} \begin{Bmatrix} w(z) \\ \theta(z) \end{Bmatrix} = \begin{Bmatrix} P \\ M \end{Bmatrix} \tag{5.8}$$

By definition, the inverse of the flexibility matrix is the stiffness matrix, $[K]$. Therefore;

$$[K] \begin{Bmatrix} w(z) \\ \theta(z) \end{Bmatrix} = \begin{Bmatrix} P \\ M \end{Bmatrix} \tag{5.9}$$

where

$$[K] = [F]^{-1} = \begin{bmatrix} K_{HH} & K_{RH} \\ K_{HR} & K_{RR} \end{bmatrix} \tag{5.10}$$

The stiffness matrix is easily obtained from the flexibility matrix

$$[K] = [F]^{-1} = \frac{1}{f_{uH} f_{\theta M} - f_{uM} f_{\theta H}} \begin{bmatrix} f_{\theta M} & -f_{uM} \\ -f_{\theta H} & f_{uH} \end{bmatrix}$$

The value of $\left[F\right]^{-1}$ is determined after solving the value of C_2 and C_4 in Equation (5.1) to (5.4), and this is done by using two sets of loading conditions and adding them together for the superposition effect. The two sets of loading condition are given below

First case: pure horizontal force (P) at the pile head with zero moment;

$$\left(EI\right)_p \frac{d^3}{dz^3} w\left(z\right) - T\frac{d}{dz}\bigg|_{z=0} = P \text{ and } -\left(EI\right)_p \frac{d^2}{dz^2} w\left(z\right)\bigg|_{z=0} = 0$$

Using the above boundary conditions, the value of C_2 and C_4 are obtained and substituted back to Equation (5.1) and (5.2) to give;

$$w\left(z\right)_p = \frac{\mathrm{e}^{-z\alpha} P\left(2\alpha\beta\cos\left(z\beta\right) + \left(\alpha^2 - \beta^2\right)\sin\left(z\beta\right)\right)}{\beta\left(\alpha^2+\beta^2\right)\left(T + \left(EI\right)_p\left(\alpha^2+\beta^2\right)\right)} \tag{5.11}$$

$$\theta\left(z\right)_p = -\frac{\mathrm{e}^{-z\alpha} P\left(\beta\cos\left(z\beta\right) + \alpha\sin\left(z\beta\right)\right)}{\beta\left(T + \left(EI\right)_p\left(\alpha^2+\beta^2\right)\right)} \tag{5.12}$$

where $w\left(z\right)_p$ and $\theta\left(z\right)_p$ are displacement and slope due to an applied pure horizontal loading without a head moment.

Second case: pure moment (M_o) at the pile head with zero horizontal force;

$$\left(EI\right)_p \frac{d^3}{dz^3} w\left(z\right) - T\frac{d}{dz}\bigg|_{z=0} = 0 \text{ and } -\left(EI\right)_p \frac{d^2}{dz^2} w\left(z\right)\bigg|_{z=0} = M_o$$

Using the above boundary conditions, the value of C_2 and C_4 are obtained and substituted back to Equation (5.1) and (5.2) to give;

$$w\left(z\right)_M = \frac{\mathrm{e}^{-z\alpha} M \begin{pmatrix} \beta\left(T + \left(EI\right)_p\left(-3\alpha^2+\beta^2\right)\right)\cos\left(z\beta\right) \\ +\alpha\left(T + \left(EI\right)_p\left(-\alpha^2+3\beta^2\right)\right)\sin\left(z\beta\right) \end{pmatrix}}{\left(EI\right)_p \beta\left(\alpha^2+\beta^2\right)\left(T + \left(EI\right)_p\left(\alpha^2+\beta^2\right)\right)} \tag{5.13}$$

$$\theta(z)_M = \frac{e^{-z\alpha} M \begin{pmatrix} 2(EI)_p \alpha\beta \cos(z\beta) \\ -\left(T + (EI)_p \left(-\alpha^2 + \beta^2\right)\right) \sin(z\beta) \end{pmatrix}}{(EI)_p \beta \left(T + (EI)_p \left(\alpha^2 + \beta^2\right)\right)} \tag{5.14}$$

where $w(z)_M$ and $\theta(z)_M$ are displacement and slope due to the applied moment at the pile head loading without a head force.

By adding the pile's response due to the horizontal force and moment, we can get the total response of the system, and it will have the form given in Equation (5.5) and Equation (5.6).

The pile-head stiffnesses, as discussed above, can be determined from the inverse of the flexibility matrix $[F]$. In order to do this, the value of f_{uH}, f_{uM}, $f_{\theta H}$ and $f_{\theta M}$ are evaluated by solving Equation (5.11) to (5.14) at $z = 0$.

The total displacement at the pile-head is calculated as $w(z)\big|_{z=0} = w(z)_p\big|_{z=0} + w(z)_M\big|_{z=0}$ and the result is given as;

$$w(z)\big|_{z=0} = P\frac{\alpha}{\lambda^2\left(T + 2(EI)_p \lambda^2\right)} + M\frac{T + (EI)_p\left(\beta^2 - 3\alpha^2\right)}{2(EI)_p \lambda^2\left(T + 2(EI)_p \lambda^2\right)} \tag{5.15}$$

And the slope at the pile-head can also be calculated as $\theta(z)\big|_{z=0} = \theta(z)_p\big|_{z=0} + \theta(z)_M\big|_{z=0}$, and the result is given as

$$\theta(z)\big|_{z=0} = -P\frac{1}{T + 2(EI)_p \lambda^2} + M\frac{2\alpha}{\left(T + 2(EI)_p \lambda^2\right)} \tag{5.16}$$

From Equation (5.15) and Equation (5.16), the values of f_{uH}, f_{uH}, $f_{\theta H}$ and $f_{\theta M}$ are evident and given as follows:

$$f_{uH} = \frac{\alpha}{\lambda^2\left(T + 2(EI)_p \lambda^2\right)} \quad f_{uM} = \frac{T + (EI)_p\left(\beta^2 - 3\alpha^2\right)}{2(EI)_p \lambda^2\left(T + 2(EI)_p \lambda^2\right)} = -\frac{1}{T + 2(EI)_p \lambda^2}$$

$$f_{\theta H} = -\frac{1}{T + 2(EI)_p \lambda^2}, \quad f_{\theta M} = \frac{2\alpha}{T + 2(EI)_p \lambda^2}$$

Using the relationship between the flexibility and the stiffness matrix given in Equation (5.10), the pile head stiffnesses are determined.

$$K_{HH} = \frac{1}{f_{uM} f_{\theta M} - f_{uM} f_{\theta H}} f_{\theta M} = \frac{\lambda^2 \left(T + 2(EI)_p \lambda^2\right)}{\alpha} \tag{5.17a}$$

$$K_{RH} = \frac{1}{f_{uM} f_{\theta M} - f_{uM} f_{\theta H}} - f_{uM} = \frac{\lambda^2 \left(T + 2(EI)_p \lambda^2\right)}{2\alpha^2} \tag{5.17b}$$

$$K_{HR} = \frac{1}{f_{uM} f_{\theta M} - f_{uM} f_{\theta H}} - f_{\theta H} = \frac{\lambda^2 \left(T + 2(EI)_p \lambda^2\right)}{2\alpha^2} \tag{5.17c}$$

$$K_{RR} = \frac{1}{f_{uM} f_{\theta M} - f_{uM} f_{\theta H}} f_{uH} = \frac{\left(T + 2(EI)_p \lambda^2\right)}{2\alpha} \tag{5.17d}$$

Note that both the flexibility and stiffness matrices are symmetrical, as would be expected. Furthermore, it is also worth mentioning that the expression of K_{HH} given in Equation (5.17a) is the same as the one obtained in Chapter 4.

5.3.2 Fixed-head long piles

In the case of fixed-head piles, unlike the free-head piles, as shown in Figure 5-1, the effect of the applied horizontal force and moment is different. The force produces only lateral translation under zero rotation, whereas the moment creates rotation without horizontal translation. The two loading cases are considered separately.

First case: pure horizontal force (P) at the pile head with zero external moment;

$$(EI)_p \frac{d^3}{dz^3} w(z)\Big|_{z=0} = P, \quad -(EI)_p \frac{d^2}{dz^2} w(z)\Big|_{z=0} = M(z)\Big|_{p,z=0} = M \quad \text{and}$$

$$\theta(z)\Big|_{P,z=0} = \frac{d}{dz} w(z)\Big|_{z=0} = 0$$

Solving the displacement equation given in Equation (5.1) using the above boundary conditions, we can get a deflection equation at the pile head as a function of force.

$$w(z)\Big|_{z=0} = P \frac{1}{4(EI)_p \alpha \lambda^2} \tag{5.18}$$

Furthermore, by using the relation between deflection and moment, the moment at the pile head can be expressed as:

$$-(EI)_p \frac{d^2}{dz^2} w(z)\Big|_{z=0} = M \Rightarrow M = \frac{P}{2\alpha} \Rightarrow P = 2\alpha M$$

Substituting back the value of P given above in Equation (5.17) yields;

$$w(z)\big|_{z=0} = M \frac{1}{2(EI)_p \lambda^2} \tag{5.19}$$

Second case: pure moment at the pile head (M_o) with zero external horizontal force (P);

$(EI)_p \frac{d^3}{dz^3} w(z)\Big|_{z=0} = Q(z)\big|_{z=0} = Q$, $-(EI)_p \frac{d^2}{dz^2} w(z)\Big|_{z=0} = M_0$ and

$w(z)\big|_{z=0} = 0$

As discussed earlier, the moment will only create rotation at the pile head without translation (Figure 5.1). So, after solving the deflection equation given in Equation (5.1), the expression of the slope due to the applied moment at the pile head is presented as:

$$\theta(z)\big|_{z=0} = \frac{M_o}{2(EI)_p \alpha} \tag{5.20}$$

Using the relation between deflection and shear, the moment at the pile head can be expressed as

$$(EI)_p \frac{d^3}{dz^3} w(z) - T \frac{d}{dz}\Big|_{z=0} = Q(z)\big|_{z=0} \Rightarrow M_o = Q \frac{\alpha}{\lambda^2}$$

Substituting the above expression of M is Equation (5.20), we get;

$$\theta(z)\big|_{z=0} = \frac{Q}{2(EI)_p \lambda^2} \tag{5.21}$$

The pile head stiffnesses can be calculated by applying both cases in Equation (5.9).

For the first case;

$$\begin{bmatrix} K_{HH} & K_{RH} \\ K_{HR} & K_{RR} \end{bmatrix} \begin{Bmatrix} w(z)\big|_{z=0} \\ 0 \end{Bmatrix} = \begin{Bmatrix} P \\ M \end{Bmatrix}$$

where $M = P/2\alpha$ (derived earlier). Expanding the matrix

$$K_{HH}\, w(z)\big|_{z=0} = P \text{ and } K_{HR}\, w(z)\big|_{z=0} = M$$

Therefore;

$$K_{HH} = \left.\frac{P}{w(z)}\right|_{z=0} = 4(EI)_p\, \alpha\lambda^2 \tag{5.22a}$$

$$K_{HR} = \left.\frac{M}{w(z)}\right|_{z=0} = 2(EI)_p\, \lambda^2 \tag{5.22b}$$

For the second case

$$\begin{bmatrix} K_{HH} & K_{RH} \\ K_{HR} & K_{RR} \end{bmatrix} \begin{Bmatrix} 0 \\ \theta(z)\big|_{z=0} \end{Bmatrix} = \begin{Bmatrix} Q \\ M_o \end{Bmatrix}$$

where $Q = M_o\lambda^2/\alpha$ (derived earlier). Expanding the matrix

$$K_{RH}\, \theta(z)\big|_{z=0} = Q \text{ and } K_{RR}\, \theta(z)\big|_{z=0} = M_o$$

Rearranging and substituting $Q = M_o\lambda^2/\alpha$.

$$K_{RH} = \frac{Q}{\theta(z)\big|_{z=0}} = 2(EI)_p\, \lambda^2 \tag{5.23a}$$

$$K_{RR} = \frac{M_o}{\theta(z)\big|_{z=0}} = 2(EI)_p\, \alpha \tag{5.23b}$$

5.3.3 Parametric investigation of the proposed stiffnesses

In the above sections, the pile head stiffnesses for "long" flexible piles were derived. In this section, the performance of the derived pile head stiffnesses is studied. In the previous sections, the pile head stiffnesses for both free and fixed head piles are swaying, rotation and cross-swaying were determined. Because it is not the practical interest of almost all engineering works and there is no available literature for free-head piles under rotation and cross-swaying, only the proposed pile-head stiffness of fixed-head piles is investigated.

The derived expressions given in Equation (5.23a) and (5.23b) are simplified using curve-fitting to make the analysis of pile head stiffnesses simpler. The swaying stiffness given in (5.2a) is identical to the one obtained in Chapter 4. The simplified expression for swaying stiffness for fixed-head has been treated in section 4.6 (Equation (4.65)), so in this section, only the detailed procedures for cross swaying–rocking and rocking stiffness are presented.

5.3.3.1 Cross swaying–rocking stiffness

First the expression given in Equation (22b) is plotted for wide range of relative stiffness and Poisson's ratio (0.25, 0.3, 0.35, 0.4 and 0.45) and the plots are given in Figure 5-3.

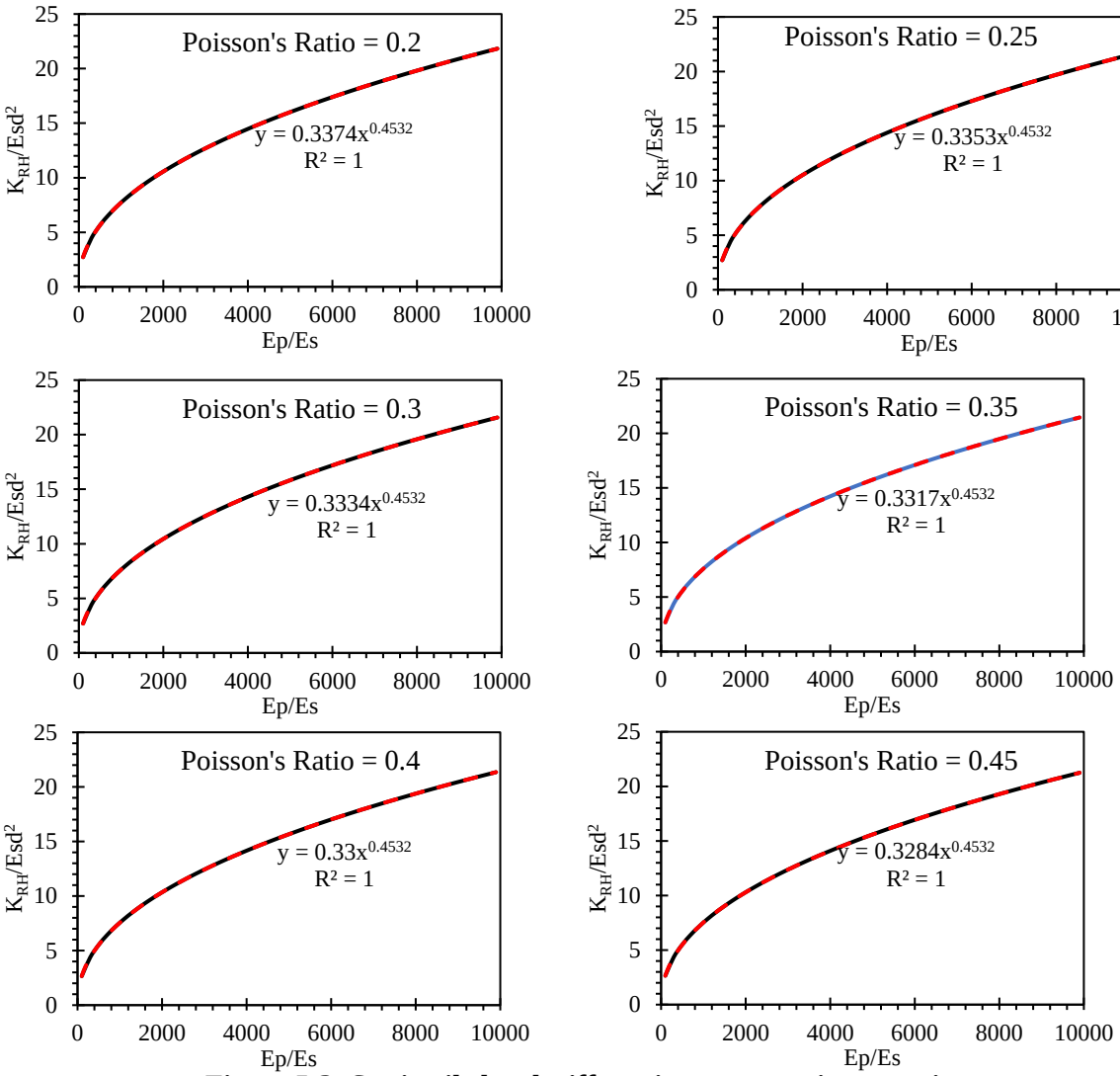

Figure 5-3: Static pile head stiffness in cross swaying–rotation.

As can be seen from Figure 5-3, the expression for the cross swaying-rotation can be expressed using the form

$$\frac{K_{RH}}{E_s d^2} = \gamma_{HR}\left(\frac{E_P}{E_s}\right)^{\alpha_{HR}} \tag{5.24}$$

where γ_{HR} and α_{HR} are a function of Poisson's ratio, and their variation is presented in Table 5-2

Table 5-1: Frequency-independent expressions

Poisson's ratio	γ_{HR}	α_{HR}
0.45	0.3284	0.4532
0.4	0.33	0.4532
0.35	0.3317	0.4532
0.3	0.3334	0.4532
0.25	0.3353	0.4532
0.2	0.3374	0.4532
Standard deviation	**0.0031**	**0**

From Table 5-1, it is evident that the variation of α_{HR} is independent of Poisson's ratio, so $\alpha_{HR} = 0.4532$ is taken. However, in the case of γ_{HR} the standard deviation is 0.0031. Even if the standard deviation is small, an expression as a function of ν_s is obtained using curve-fitting, which resulted in the best-fitted relationship sown in Figure 5-4.

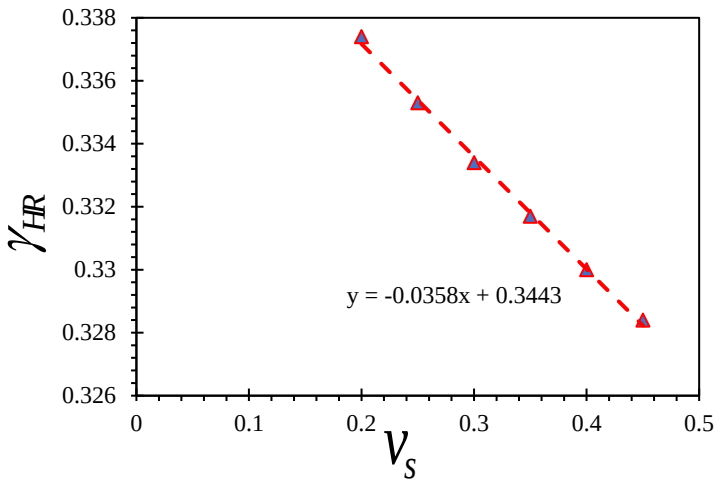

Figure 5-4: Variation of γ_{HR} with Poisson's ratio.

The expression for γ_{HR} obtained from the curve-fitting is given as

$$\gamma_{HR} = 0.3443 - 0.0358 v_s \tag{5.25}$$

The second term of equation (5.25) contributes less than 1.6% to the value of γ_{HR}. Hence, an average value is taken to give $\gamma_{HR} = 0.3443$. Substituting both γ_{HR} and α_{HR} into Equation (5.24), the simplified cross swaying-rotation at the pile head can be expressed as;

$$\frac{K_{RH}}{E_s d^2} = 0.3327 \left(\frac{E_P}{E_s} \right)^{0.4532} \tag{5.26}$$

5.3.3.2 Rocking stiffness

Using the same procedure with that of the cross swaying-rocking stiffness (Section 5.3.3.2), the simplified expression for pile head stiffness against rotation is determined, and the expression is given as;

$$\frac{K_{RR}}{E_s d^3} = 0.1954 \left(\frac{E_P}{E_s} \right)^{0.7208} \tag{5.27}$$

5.3.3.3 Comparison of the proposed stiffnesses with other models from literature

So far, in this chapter, pile head stiffnesses under cross swaying-rotation and rotation were obtained. So, in this section, the proposed stiffnesses are compared against published results.

The expressions for the static Winkler moduli presented in Table 4-5 are inserted in the proposed model (Equation (5.22a) - (5.23b)) to compute static pile head stiffnesses in rotation K_{RR} and cross swaying-rotation K_{HR}. The results are then compared to the proposed models given in Equations (5.26) and (5.27). Also, results from the simplified expressions of Gazetas (1991b) and Syngros (2004) (Table 5-2) are included. These simple expressions are obtained through curve fitting of FE results of piles embedded in a homogeneous half-space.

Table 5-2: Simple expressions for static pile head stiffness from literature.

Model	Pile head stiffness		
	$\frac{K_{HH}}{E_s d}$	$\frac{K_{RH}}{E_s d^2}$	$\frac{K_{RR}}{E_s d^3}$
Syngros (2004)	$1.2\left(\frac{E_p}{E_s}\right)^{0.18}$	$0.21\left(\frac{E_p}{E_s}\right)^{0.5}$	$0.15\left(\frac{E_p}{E_s}\right)^{0.75}$
Gazetas (1991b)	$1.0\left(\frac{E_p}{E_s}\right)^{0.21}$	$0.22\left(\frac{E_p}{E_s}\right)^{0.5}$	$0.16\left(\frac{E_p}{E_s}\right)^{0.75}$

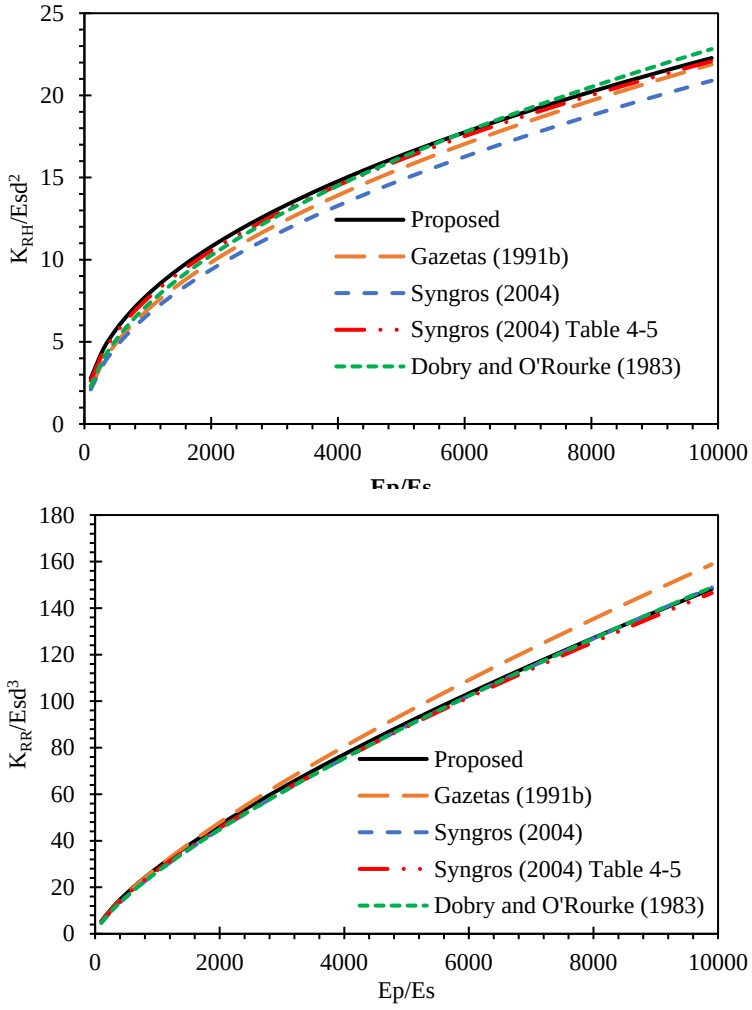

Figure 5-5: Static pile head stiffness in rotation K_{RR} and cross swaying–rotation K_{RH}.

The proposed solutions for pile head stiffness in cross swaying–rotation are in good agreement with all models except the one proposed by Syngrose (2004) (Table 5-2). The proposed pile-head stiffness in rotation provides a close agreement to all models used in the comparison (Figure 5-5) for $E_p / E_s \le 5000$. For $E_p / E_s > 5000$, the one proposed by Gazetas (1991b) diverges.

5.4 Generalized pile head stiffnesses in rotation and cross swaying-rotation

In Section 5-3, pile head stiffness in rotation and cross swaying-rotation for "long" flexible piles were obtained. In this section, the set of generalized pile head stiffness that incorporates pile length is determined.

In order to obtain the expressions for the generalized pile head stiffness, the same procedure used in Section 5.3.2 is followed. However, for this case, the generalized displacement equations given in equation (4.6) are used, and the results are given below. The expressions for the swaying stiffness obtained in this section is the same as the one obtained in Chapter 4.

Fixed-head fixed-base piles

$$K_{HR} = 2(EI)_p \lambda^2 \frac{-\left(\alpha^2 \sin^2(L\beta) + \beta^2 \sinh^2(L\alpha)\right)}{\alpha^2 \sin^2(L\beta) - \beta^2 \sinh^2(L\alpha)} \tag{5.28}$$

$$K_{RR} = 2(EI)_P \alpha \frac{\left(\left(\alpha^2 - \beta^2\right)\sin(2L\beta) + 2\alpha\beta \sinh(2L\alpha)\right)}{2\alpha\beta\left(\cos(2L\beta) + \cosh(2L\alpha)\right)} \tag{5.29}$$

Fixed-head floating-base piles

$$K_{HR} = 2(EI)_p \lambda^2 \frac{\left(\begin{array}{l}\left(\begin{array}{l}-\alpha^4 + \beta^4 + \alpha^2\left(\alpha^2 - 3\beta^2\right)\cos(2L\beta) \\ -\beta^2\left(-3\alpha^2 + \beta^2\right)\cosh(2L\alpha)\end{array}\right) \\ +2\dfrac{\sqrt{k_s \tilde{T}}}{(EI)_p\left(\alpha^2 + \beta^2\right)}\alpha\beta\left(\begin{array}{l}\alpha\sin(2L\beta) \\ +\beta\sinh(2L\alpha)\end{array}\right)\end{array}\right)}{\left(\begin{array}{l}\left(\begin{array}{l}\left(\alpha^2 + \beta^2\right)^2 - \alpha^2\left(\alpha^2 - 3\beta^2\right)\cos(2L\beta) \\ -\left(-3\alpha^2\beta^2 + \beta^4\right)\cosh(2L\alpha)\end{array}\right) \\ +2\dfrac{\sqrt{k_s \tilde{T}}}{(EI)_p\left(\alpha^2 + \beta^2\right)}\alpha\beta\left(\begin{array}{l}-\alpha\sin(2L\beta) \\ +\beta\sinh(2L\alpha)\end{array}\right)\end{array}\right)} \tag{5.30}$$

$$K_{RR}=2\left(EI\right)_p\,\alpha\frac{\left(\begin{array}{l}\left(EI\right)_p\left(\alpha^2+\beta^2\right)^2\left(\begin{array}{l}-\alpha^2+3\beta^2\\+\left(\alpha^2-\beta^2\right)\cos\left(2L\beta\right)\\-2\beta^2\cosh\left(2L\alpha\right)\end{array}\right)\\-2\sqrt{k_s\tilde{T}}\,\beta\left(\begin{array}{l}\left(-\alpha^2+\beta^2\right)\sin\left(2L\beta\right)\\-2\alpha\beta\sinh\left(2L\alpha\right)\end{array}\right)\end{array}\right)}{\left(\begin{array}{l}2\sqrt{k_s\tilde{T}}\,\alpha\beta\left(\cos\left(2L\beta\right)+\cosh\left(2L\alpha\right)\right)\\2\beta\left(\begin{array}{l}-\left(EI\right)_P\left(\alpha^2+\beta^2\right)^2\left(\begin{array}{l}\alpha\sin\left(2L\beta\right)\\+\beta\sinh\left(2L\beta\right)\end{array}\right)\end{array}\right)\end{array}\right)} \tag{5.31}$$

5.4.1 Parametric investigation of the proposed stiffnesses

The generalized stiffness equations in Equation (5.28) to Equation (5.31) are plotted for different pile slenderness ratio values and given in Figure 5-6, 5-7, 5-8, and 5-9.

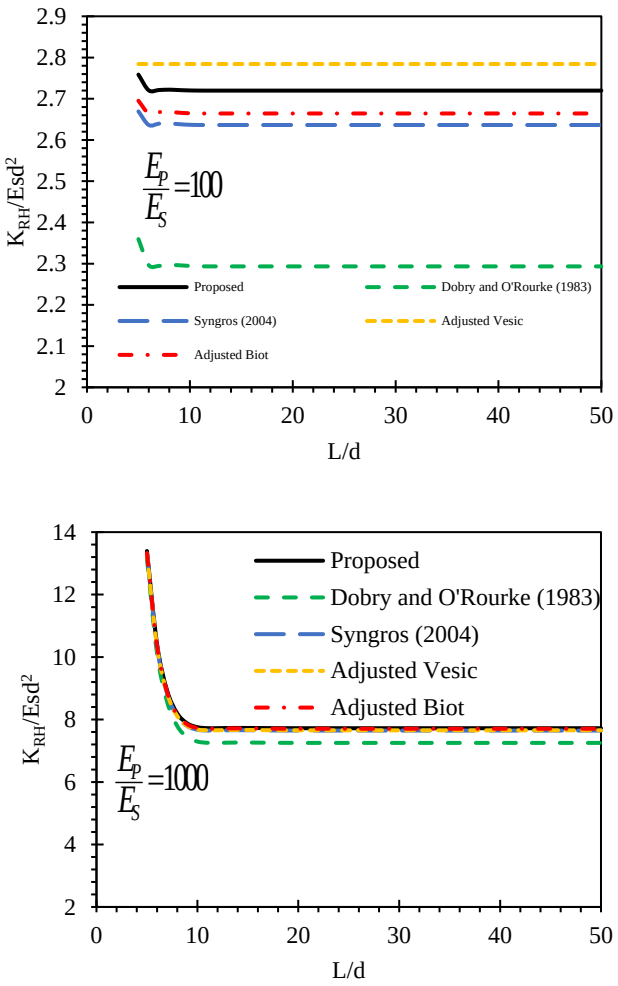

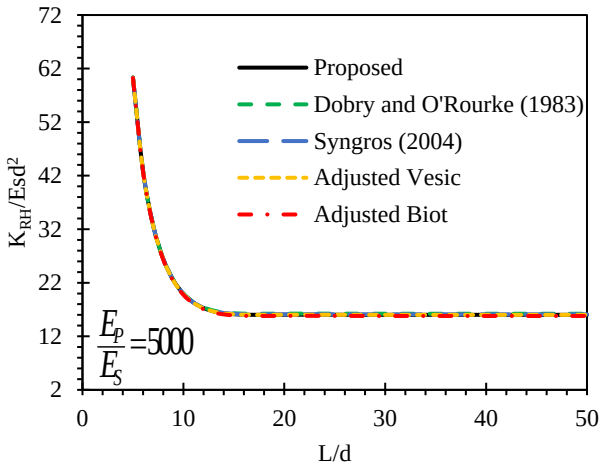

Figure 5-6: Static pile head stiffness for FxHFxBP in cross swaying–rotation K_{RH}

From Figure 5-6, it is worth mentioning.

- For very stiff soils, the one proposed by Dobry and O'Rourke (1983) always give comparatively smaller values.

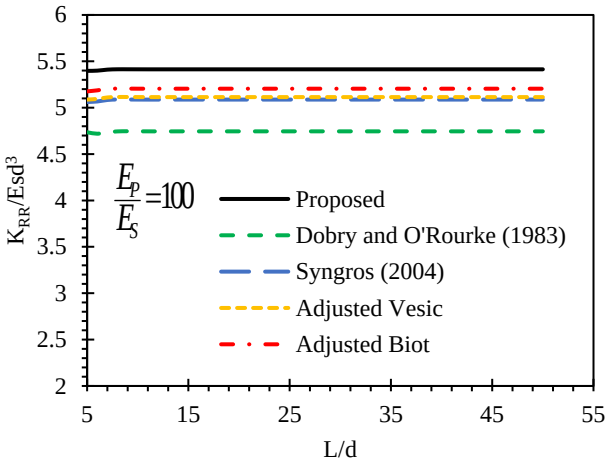

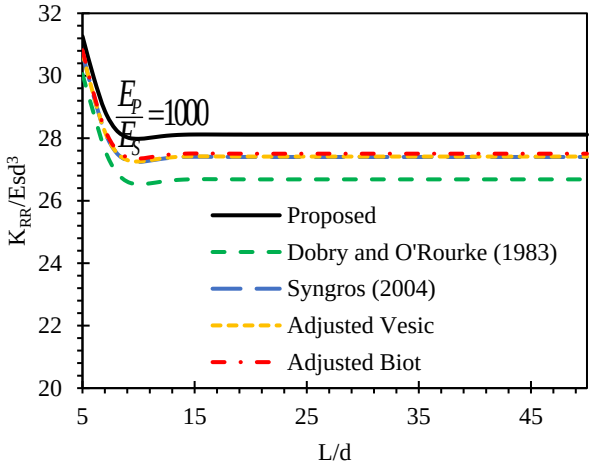

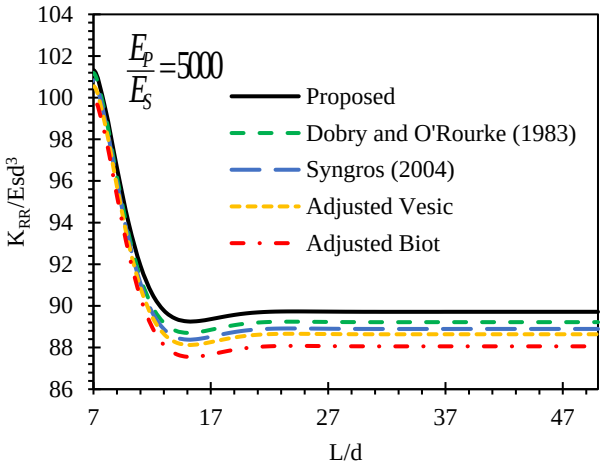

Figure 5-7: Static pile head stiffness for FxHFxBP in rotation K_{RR}

From Figure 5-7, it is worth mentioning.

- For soils with moderate and high stiffness, the one proposed by Dobry and O'Rourke (1983) always give comparatively smaller values.

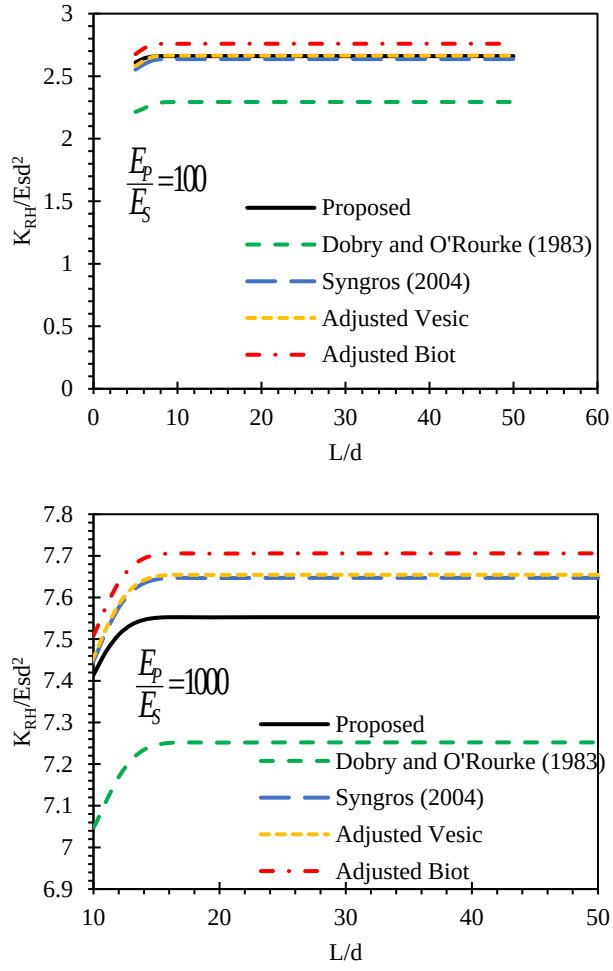

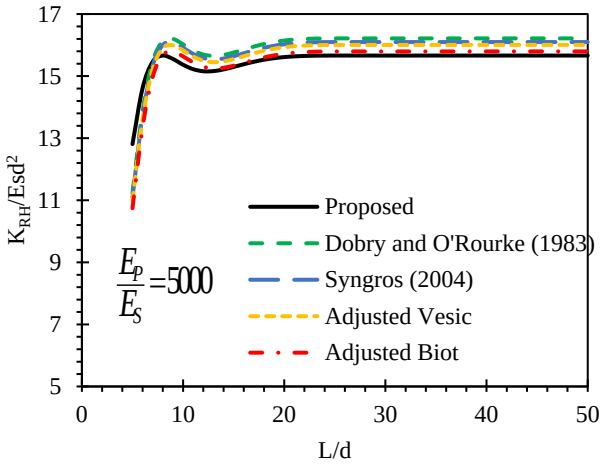

Figure 5-8: Static pile head stiffness for FxHFBP in cross swaying–rotation K_{RH}

From Figure 5-8, it is worth mentioning.

- For soils with moderate and high stiffness, the one proposed by Dobry and O'Rourke (1983) always give comparatively smaller values. Whereas the once proposed by other authors predict K_{RH} with a difference of 3%, when compared to the proposed model.

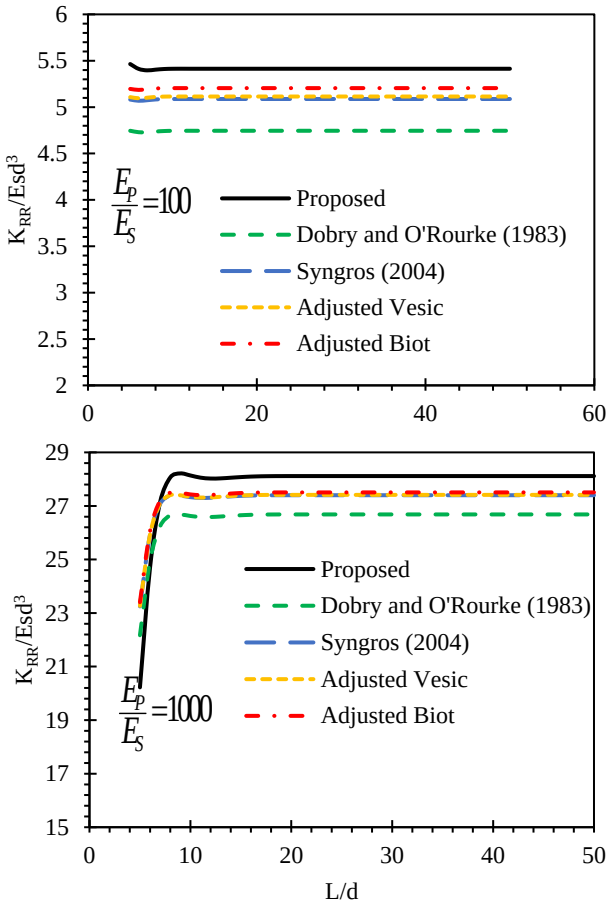

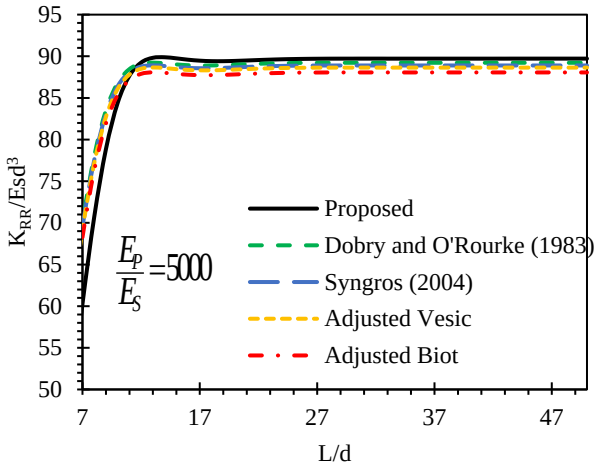

Figure 5-9: Static pile head stiffness for FxHFBP in rotation K_{RR}

From Figure 5-9, it is worth mentioning.

- For soils with high stiffness, the one proposed by Dobry and O'Rourke (1983) always give considerably smaller values. Whereas the one proposed by Syngros (2004) givens K_{RH} with a difference of 5%, when compared to the proposed model.

In general, as shown in the figures above (Figure 5-6 - Figure 5-9), the proposed model, except the one proposed by Dobry and O'Rourke (1983), is in good agreement with all Winkler models used in the comparison. For stiff soils, Dobry and O'Rourke (1983) model gives smaller values of pile head stiffness.

Depending on the pile base condition, there is an increase or a decrease in pile head stiffness with pile slenderness. The decrease in stiffness is more pronounced in very soft soil (i.e., $E_p / E_S = 5000$ and $E_p / E_S = 1000$), and occurs predominantly in the range $L \le L_c$.

Dynamic Response

CHAPTER 6
DAMPING MODEL

6.1 Introduction to soil damping

Material (or hysteretic) and geometric (or radiation) damping acting along the length of a pile contribute to the equivalent damping coefficient at the top of the pile. Material damping accounts for energy loss due to internal friction in soil, and radiation damping accounts for energy loss due to waves propagating away from the pile.

The swaying dynamic stiffness at the pile head k_x^* , which encompasses both spring and dashpot coefficients, can be expressed in two ways: a) a viscous model and b) a hysteretic model. These models and their incorporation in the present study are discussed below.

6.1.1 Viscous model

According to Molenkamp and Smith (1980), the soil is viscous when both shear modulus and bulk modulus of the soil are independent of the frequency. For this model, the dynamic stiffness at the top of the pile is given by Equation (6.1) after Vicente (1982).

$$k_x^* = K_x + i\omega C_x \tag{6.1}$$

where

C_x : viscous dashpot coefficient, which may generally include the effect of both hysteretic and radiation damping (force/velocity)

K_x is equivalent spring coefficient for horizontal mode of vibration (force/length).

6.1.2 Hysteretic model

According to Molenkamp and Smith (1980), a material is hysteretic when the dissipated energy per cycle is independent of the frequency. They also defined and gave expressions for a parameter called critical or hysteretic damping ratio β . The expression of dynamic swaying stiffness of piles using a hysteretic model is given by equation (6.2).

$$k_x^* = K_x(1+2i\beta_x) \tag{6.2}$$

where

β_x is the damping ratio which includes the effect of both hysteretic and radiation damping.

Equating the imaginary parts of Equation (6.1) and Equation (6.2), the following relationship can be obtained:

$$\beta_x = \frac{\omega c_x}{2K_x} \tag{6.3}$$

According to Vicente (1982), β_x is especially useful for the case in which the soil surrounding the pile is assumed to have a constant material damping (piles in homogeneous soil). Since both material (β_s) and radiation (β_{rad}) damping contribute to the total damping, the value of β_x is expressed as:

$$\beta_x = \beta_s + \beta_{rad} \tag{6.4}$$

According to Whitman (1979), as cited by Vicente (1982) and Gazetas (1984), at low frequency ($f < f_n$), there is no radiation damping. This is because, at low frequency, it is not possible for horizontally propagating waves to develop (Vicente, 1982; Gazetas, 1984). Therefore, for $f < f_{nat}$, $\beta_{rad} = 0$ and $\beta_x = \beta_s$

6.2 Proposed damping model

O'Rourke and Dobry (1982) proposed a simplified approach based upon wave propagation considerations to determine an equivalent damping coefficient at the top of the pile subjected to horizontal dynamic loading.

For this purpose, radiation dashpots are considered to be distributed along the length of the pile. These radiation dashpots are arranged parallel with the springs, as shown in Figure 6-1. The effect of these distributed radiation dashpots (Figure 6-1(a)) can be replaced by an equivalent radiation dashpot at the top of the pile $(C_x)_{rad}$ (Figure 6-1(b)). Figure 5-1a

represents distributed spring and dashpot along the pile's length, where c_x is distributed damping ratio and k_x is distributed spring stiffness for lateral loading. Whereas, Figure 6-1b represents the equivalent spring and dashpot coefficients at the pile

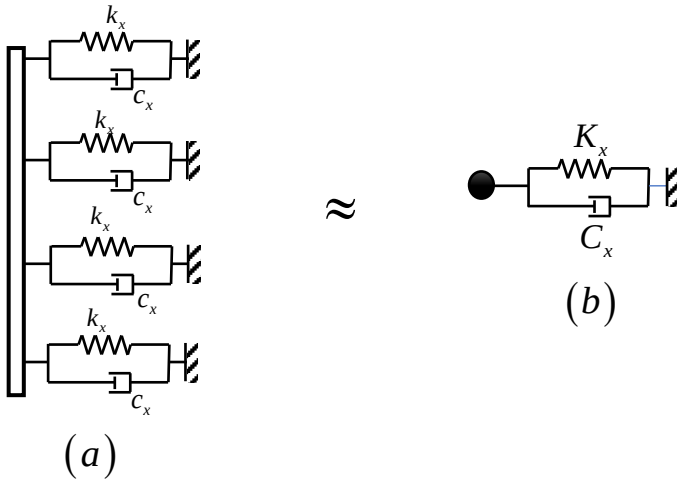

Figure 6-1: a) Spring and dashpot distribution along the pile length b) Equivalent spring and dashpot at the pile head.

According to Gazetas and Dobry (1984), the overall damping coefficient is computed from the distributed dashpot coefficients along the pile length. They proposed an expression for the pile shaft's overall damping value based on the principle of a weighted averaging process. In this way, the soil surrounding the top of the pile shaft makes the damping's most significant contribution. The detailed procedures followed for the weighted averaging process are given below.

The whole pile length in Figure 6-1 is divided into a finite number of horizontal slices. Using the area under each slice, we can determine the damping each slice contributes to the system's overall damping. So, to get the overall damping, the damping contribution of each slice should be added together.

$(c_x)_i = \left((c_x)_{rad} + (c_x)_m\right) Y_i(z)\,dz$ is damping contribution of i^{th} slice

using weighted averaging;

$$C_x = \sum_{i=1}^{n} \left((c_x)_i\, Y_i(z)\,dz\, \frac{Y_i(z)}{Y(0)} \right) = \sum_{i=1}^{n} c_x Y_i^2(z)\,dz$$

Changing the summation function into integration, we have

$$C_x = c_x \int_0^L Y^2(z)\,dz \tag{6.5}$$

or

$$C_x = \left((c_x)_{rad} + (c_x)_m\right) \int_0^L Y^2(z)\,dz \tag{6.6}$$

where

$(c_x)_m$ distributed material damping coefficient in the horizontal direction

$Y(z) = w(z)/w(0)$ is static deflection profile normalized to a unit top amplitude.

The determination of the dashpot coefficients $(c_x)_{rad}$ and $(c_x)_m$ has been the research topic for many researchers for many years.

Proposed radiation dashpot coefficient:

In this study, a new radiation damping coefficient based on the one-dimensional wave propagation assumption is proposed. To define the radiation damping coefficient, c_x , it is useful to recall the analogy between one-dimensional (1-D) wave propagation in an elastic space and a viscous dashpot, as schematically illustrated in Figure 5-2. Considering a harmonic wave of form

$$u = u_o \exp\left(i\omega\left(t - \frac{x}{V}\right)\right) \tag{6.7}$$

where u_o is wave amplitude, ω is circular frequency, t is time, and V is the corresponding wave velocity (V_p or V_s, depending on the type of wave). The total force induced by this wave on a perpendicular surface of the area A, at a location x, can be expressed in the form given in Equation (6.8) (Berger et al. (1977)).

$$F = (\rho_s V A)\dot{u} \tag{6.8}$$

Therefore, one could replace the semi-infinite portion of the space or cylinder located to the right of x by a viscous dashpot having a constant coefficient

$$c_{rad} = \rho_s V A \tag{6.9}$$

The motion of all points to the left of x would not be affected. In other words, this dashpot fully absorbs the energy of the traveling wave, causing no reflection to occur.

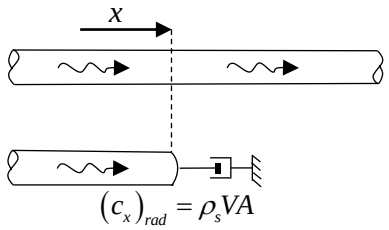

Figure 6-2: Radiation damping for one-dimensional (1-D) wave propagation (Gazetas and Dobry, 1984)

Berger et al. (1977) adopted this 1-D model to estimate the radiation damping coefficients of a laterally oscillating pile. Their model assumed that a horizontally moving pile section of effective width b and thickness Δz generates 1-D P-waves traveling in the direction of shaking and 1-D SH-waves traveling in the direction perpendicular to shaking as sketched in Figure 6-3. Therefore, adding radiation dashpot coefficients in both directions (two in the loading direction and two in the perpendicular direction), we get

$$V = 2\left(V_p + V_s\right) \tag{6.10}$$

Substituting Equation (6.10) into Equation (6.10)

$$c_{rad} = 2\rho_s A\left(V_p + V_s\right) \tag{6.11}$$

For circular piles, as shown in Figure 6-3, the value of A given in Equation (6.11) is an arc with an angle of 45^o. So, the area under consideration is the multiplication of the arc length, $x = d\frac{\pi}{4}$, and thickness, dz.

$$A = d\frac{\pi}{4}dz \tag{6.12}$$

Substituting Equation (6.12) back into Equation (6.11), we get the radiation damping per a single horizontal slice of thickness, dz.

$$c_{rad} = 2\rho_s d\left(V_p + V_s\right)\frac{\pi}{4} \tag{6.13}$$

The relationship in Equation (6.13) is identical to that in Berger et al. (1977), except for the presence of $\pi/4$.

The values of V_p and V_s are related through Poisson's ratio , v_s , of the soil as

$$V_p = \sqrt{\frac{2(1-v_s)}{(1-2v_s)}} \tag{6.14}$$

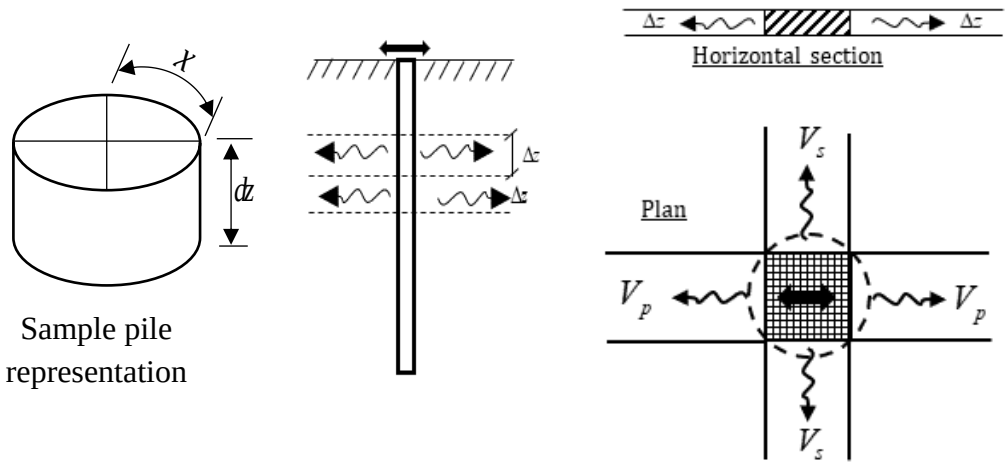

Figure 6-3: Radiation damping for 1-D wave propagation (Berger et al. 1977)

The above model (Equation (6.13) has two main drawbacks. First, using V_p as wave velocity in the compression-extension zone makes the proposed radiation damping sensitive to the variation of soil Poisson's ratio, even jumping to infinity as Poisson's ratio approaches 0.5 (Gazetas and Dobry, 1984). So, Gazetas and Dobry (1984) proposed to use V_{La} instead of V_p , where V_{La} is Lysmer's analog wave velocity which is expressed as

$$V_{La} = \frac{3.4}{\pi(1-v_s)} V_s \tag{6.15}$$

Second, the proposed damping model in Equation (6.13) is independent of frequency. However, as it was shown by Novak and Nogami (1977), Gazetas and Dobry (1984), Anoyatis et al. (2016, 2017), radiation damping is dependent on frequency. For this reason, using the dimensionless frequency ratio, a_o, adjustment is made to the damping model proposed. In order to adjust the proposed model, the well-known and widely accepted damping model for piles on an elastic foundation, proposed by Gazetas and Dobry (1984), given in Table (6.1) is used.

Table 6-1: Frequency-independent expressions for Winkler spring k and frequency-dependent damping ratio β from literature ($\beta = \beta_s + \beta_{rad}$).

Studies	Spring k	Radial damping
Dobry et al. (1982)	$k = 1.67E_s\left(\frac{E_P}{E_s}\right)^{-0.053}$	$\beta = \beta_s + 1.55\left(\frac{1+v_s}{2}\right)\left(\frac{E_P}{E_s}\right)^{0.124} a_o\, G_s/k$
Gazetas and Dobry (1984)	Fixed head $k = 1\ to\ 1.2E_s$ Free head $k = 1.5\ to\ 2.5E_s$	For deep depths ($z > 2.5d$) $\beta = \beta_s + 2\left(\frac{\pi}{4}\right)^{\frac{3}{4}} * (a_o)^{\frac{3}{4}}\left[1 + \left(\frac{3.4}{\pi(1-v_s)}\right)^{\frac{5}{4}}\right] G_s/k$ For shallow depths ($z \leq 2.5d$) $\beta = \beta_s + 4\left(\frac{\pi}{4}\right)^{\frac{3}{4}} * (a_o)^{\frac{3}{4}} G_s/k$
Makris and Gazetas (1992)	$k = 1.2E_s$	$\beta = \beta_s + 3 * (a_o)^{\frac{3}{4}} G_s/k$
Kavvadas et al. (1993)	$k = \frac{3E_s}{1-v_s^2}\left(\frac{E_P}{E_s}\right)^{-\frac{1}{8}}\left(\frac{L_P}{D_P}\right)^{-\frac{1}{8}}$	For deep depths ($z > 2.5d$) $\beta_{rad} = \beta + 2 * (a_o)^{\frac{3}{4}}\left[1 + \left(\frac{3.4}{\pi(1-v_s)}\right)^{\frac{5}{4}}\right] G_s/k$ For shallow depths ($z \leq 2.5d$) $\beta = \beta_s + 4 * (a_o)^{\frac{3}{4}} G_s/k$

Gazetas and Dobry (1984), using a plain-strain radiation damping model proposed by Novak et al. (1978) (Table 6-2), have further improved their model. Novak et al. (1978) obtained a rigorous solution to the corresponding elastodynamic boundary value problem of an infinite soil space subjected to horizontal oscillations from an infinitely long circular pile. Gazetas and Dobry (1984) curve fitted a plot of the radiation damping, c_{rad}, normalized by $2\rho_s dV_s$. After the curve fitting, they found $c_{rad} / 2\rho_s dV_s = 2.58a_o^{0.25}$ for Poisson's ratio of 0.4 and $2.15a_o^{0.25}$. Finally, using the curve-fitted expressions, they proposed a simplified radiation damping model given in Equation (6.18) and (6.19). In this study, a similar approach using the model proposed by Gazetas and Dobry (1984) is followed, and radiation damping given in Equation (6.16) is obtained.

$$\left(c_x\right)_{rad} = 2\rho_s dV_s \left(1+\frac{3.4}{\pi\left(1-\nu_s\right)}\right)^{1.15} \frac{\pi}{4} a_o^{-0.25} \tag{6.16}$$

Gazetas and Dobry (1984) and Kavvadas et al. (1993) suggested that for shallow depth piles ($z \le 2.5d$), due to the presence of the "stress-free" ground surface, surface type waves in addition to plane-strain body waves, will be generated. Furthermore, according to both authors, the surface wave generated propagate with velocities closer to V_s than to V_{La}. To account for this phenomenon, they proposed to use V_s as a propagating wave in all four quarter planes (Figure 6-3). By using this suggestion, the radiation dashpot coefficient given in Equation (6.17) is modified for piles with $z \le 2.5d$ to give

$$\left(c_x\right)_{rad} = \rho_s dV_s \pi a_o^{-0.25} \tag{6.17}$$

A dimensionless plot of the proposed radiation damping model and that of Gazetas and Dobry (1984) is presented for selected soil Poisson's ratio values in Figure 6-4. In order to get a similar expression for the radiation dashpot coefficient proposed by Gazetas and Dobry (1984), given in Table 6-1, with that of Equation (6.16) and (6.17), a relation between c_{rad} and β_{rad} given in Equation (6.3) is used, and the results are given in Equation (6.18) and (6.19) for piles with $z > 2.5d$ and $z \le 2.5d$ respectively.

$$\left(c_x\right)_{rad} = 2\rho_s dV_s\left(1+\left(\frac{3.4}{\pi\left(1-\nu_s\right)}\right)^{5/4}\right)\left(\frac{\pi}{4}\right)^{3/4} a_o^{-1/4} \tag{6.18}$$

$$\left(c_x\right)_{rad} = 4\rho_s dV_s\left(\frac{\pi}{4}\right)^{3/4} a_o^{-1/4} \tag{6.19}$$

The proposed radiation dashpot coefficients and the once proposed by Gazetas and Dobry (1984) are plotted in Figure 6-4 and 6-5 and from the plots it is evident that the proposed model is in good agreement with by Gazetas and Dobry (1984).

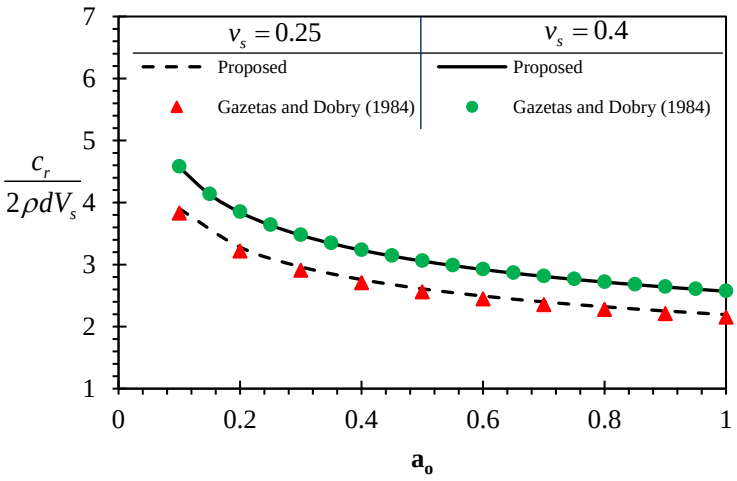

Figure 6-4: Radiation dashpot coefficient of circular pile cross-section ($z > 2.5d$)

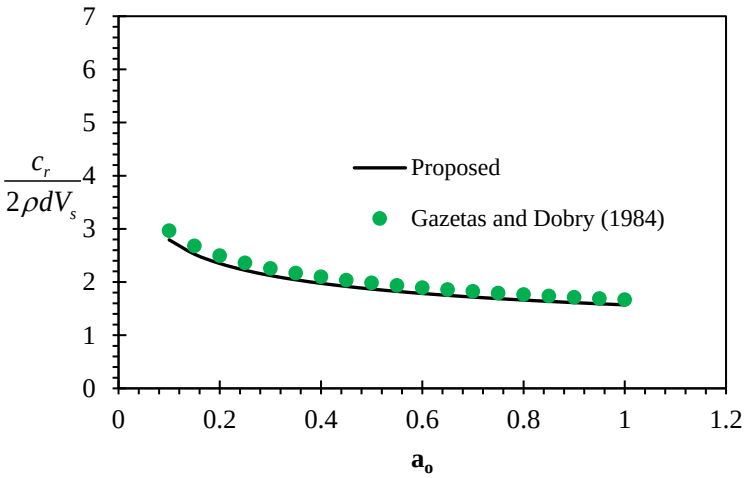

Figure 6-5: Radiation dashpot coefficient of circular pile cross-section ($z \leq 2.5d$)

Material damping

The dashpot coefficient, c_m, is related to, β_s, by an expression similar to Equation (6.3), in which β_x is replaced by β_s, c_x is replaced by $(c_x)_m$.

$$(c_x)_m = 2k_x \frac{\beta_s}{\omega} \tag{6.20}$$

The value of β_s can be determined depending on the strain levels. According to Richart and Wylie (1977), as referred by Gazetas and Dobry (1984), typical values for β_s at different levels of strain, γ_e, are: for $\gamma_e = 10^{-5}$, $\beta_s = 0.02$; for $\gamma_e = 10^{-4}$, $\beta_s = 0.05$; and for $\gamma_e = 10^{-3}$, β_s = 0.10-0.15.

Using both radiation damping and material damping models proposed earlier, the dashpot coefficient, c_x, is given as

$$c_x = 2k_x \frac{\beta_s}{\omega} + 2\rho_s d V_s \left(1 + \frac{3.4}{\pi(1-\nu_s)}\right)^{1.15} \frac{\pi}{4} a_o^{-0.15} \qquad z > 2.5d \tag{6.21}$$

$$c_x = 2k_x \frac{\beta_s}{\omega} + \rho_s d V_s \pi a_o^{-0.25} \qquad z \le 2.5d \tag{6.22}$$

Equation (6.21) can be rewritten using the hysteretic damping model as

$$\beta_x = \frac{c_x \omega}{2k_x} = \frac{(c_x)_m \omega}{2k_x} + \frac{(c_x)_{rad} \omega}{2k_x}$$

$$= \beta_s + \frac{2\rho_s d V_s \left(1 + \frac{3.4}{\pi(1-\nu_s)}\right)^{1.15} \frac{\pi}{4} a_o^{-0.25} \omega}{2k_x}$$

Using $a_o = \omega d / Vs$ and $V_s = \sqrt{G_s / \rho_s}$ the equation can be simplified;

$$\beta_x = \beta_s + \left(1 + \frac{3.4}{\pi(1-\nu_s)}\right)^{1.15} \frac{\pi}{4} a_o^{0.75} G_s / k_x \qquad z > 2.5d \tag{6.23}$$

Equation (6.22) can also be rewritten using the hysteretic damping model as

$$\beta_x = \beta_s + \frac{\pi}{2} a_o^{0.75} G_s / k_x \quad z > 2.5d \tag{6.24}$$

All the formulations done up to this point are only for damping coefficients distributed along the length. The equivalent damping coefficient at the pile head is formulated in the next section.

6.3 Overall damping at the pile head

Gazetas and Dobry (1984), using a simple energy-conservation approach, developed a method to formulate the overall damping coefficient, and the expression is given in Equation (6.6). As it can be seen from Equation (6.18), (6.19) and (6.20), $c_x = (c_x)_{rad} + (c_x)_m$ is not a function of z so, Equation (6.6) can be rewritten as

$$C_x = c_x \int_0^L \gamma dz \tag{6.25}$$

where γ is

$$\gamma = \int_0^L Y^2(z) dz \tag{6.26}$$

The value of γ for each boundary condition studied in the static case is determined using Mathematica 12. Because the output is lengthy, only the results are presented here. Still, the expressions with their derivation are given in Appendix D. During the process of deriving the expressions for γ, the same expressions for γ is obtained for both floating base and fixed base piles. For this reason, the results presented below are presented based on pile head conditions.

Free-head

For free-head (floating-base and fixed-base) piles, the deflection equations given in Equation (4.13) and Equation (4.14) were used. As shown in Appendix D, the value of γ is lengthy, so simplified expression is obtained by fitting the plot of γ given in Figure 6-6.

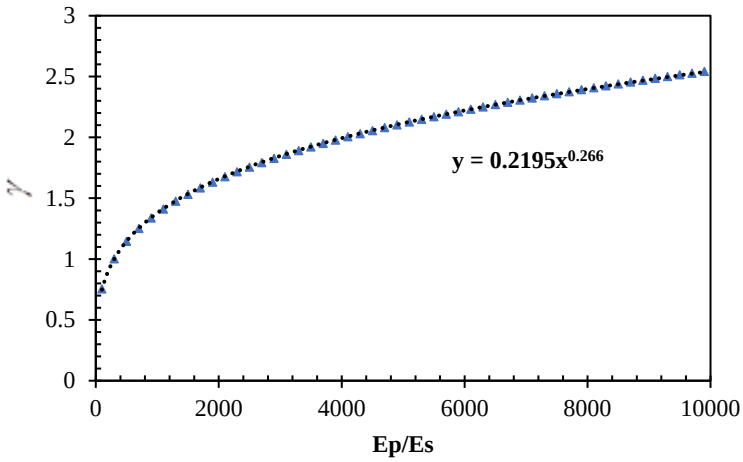

Figure 6-6: Variation of γ for free-head piles

The fitted equation is given as

$$\gamma = 0.2195\left(\frac{E_p}{E_s}\right)^{0.2666} \tag{6.27}$$

Fixed-head

For fixed-head floating-base and fixed-base piles, the deflection equation given in Equation (4.15) and Equation (4.16) are used. As of the free-head case, the value of γ is lengthy, so simplified expression is found by fitting the plot of γ given in Figure 6-7.

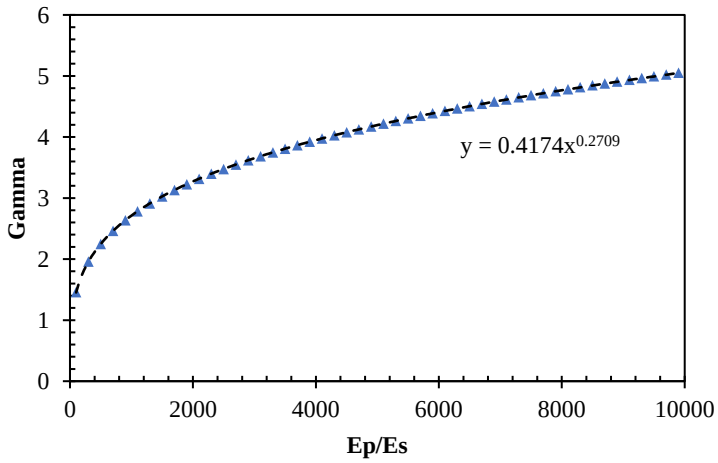

Figure 6-7: Variation of γ for free-head piles

The fitted equation is given as

$$\gamma = 0.4174 * \left(\frac{E_p}{E_s} \right)^{0.2709} \tag{6.28}$$

The value of the equivalent damping coefficient at the pile head can be found by substituting Equation (6.27) and Equation (6.28) into Equation (6.25).

6.4 Comparison of the proposed damping model with literature

An overview of the dynamic Winkler moduli (spring and dashpots) proposed in the past are given in Table 6-1 and Table 6-2. Two groups of expression can be seen among the presented Winkler springs

a) **Frequency-independent**: This type of expressions of spring and dashpot can be seen in the early works (Dobry et al. (1982), Gazetas and Dobry (1984), Makris and Gazetas (1992), Kavvadas et al. (1993)). In their expressions, only the value of damping is dependent on frequency.
b) **Frequency-dependent**: This types of expression can be seen in the more recent publication of Anoyatis and Lemnitzer (2017) and also in the early works of Novak (Novak 1974, Novak et al. 1978), and Mylonakis (2001)

While frequency-independent spring formulations are accompanied by simplified expressions for the radiation damping β_{rad}, frequency-dependent spring formulation offers complex-valued springs that integrally account for dynamic stiffness and damping (the real part being the dynamic stiffness and the imaginary part being associated with damping).

The damping ratio β in Table 6-1 embodies both material and radiation damping. In the original studies of Dobry et al. (1982), Gazetas and Dobry (1984), Makris and Gazetas (1992), Kavvadas et al. (1993), the dashpots are represented by damping coefficient c. However, for consistency reasons, as it can be seen in Table 6-1, all the expressions are presented as the damping ratio β.

For the expressions in Table 6-2, the material damping is incorporated using complex-valued shear modulus $G_s^* = G_s\left(1+i2\beta_s\right)$. Therefore, as it can be seen from Equation

(6.2), the value of the damping ratio can be obtained as $\beta = \mathrm{Im}(k^*) / 2\mathrm{Re}(k^*)$. The damping ratio includes loss of energy due to radiation damping. The expression K_n in all the expressions in Table 6-2 is the n^{th} order modified Bessel function of the second kind (Novak et al., 1978). The solution for the modified Bessel function of the second kind is computed using Wolfram Mathematica 12.

Selected radiation damping models from both Table 6-1 and Table 6-2 are plotted in Figure 6-8.

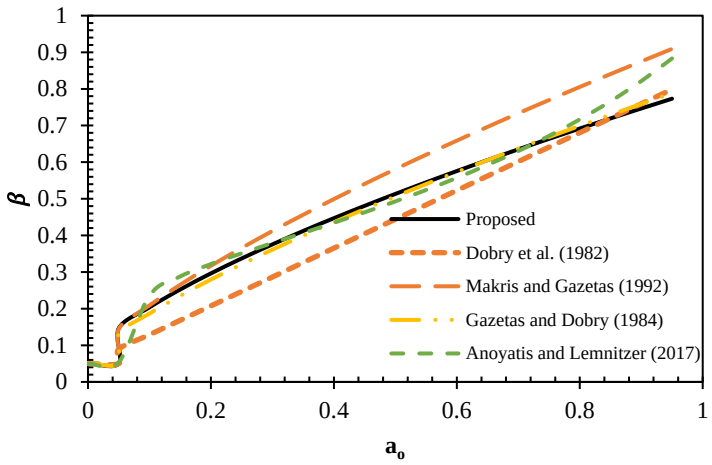

Figure 6-8: Damping ratio: $L/D = 20$ and $E_p/E_s = 1000$

Figure 6-8 shows that the proposed model gives damping in close agreement with Anoyatis and Lemnitzer (2017) and Gazetas and Dobry (1984).

The bend at low frequency is because, at low cyclic frequencies ($a_o < a_{cutoff}$), there is no radiation damping, but at $a_o = a_{cutoff}$ the radiation damping starts to develop and jump from zero to some value ($\beta = \beta_m + \beta_{rad}$).

Table 6-2: Frequency-dependent expressions for dynamic Winkler spring k^*.

Studies	Dynamic Winkler Spring k^*
Novak (1974) Novak et al. (1978)	$k^* = \pi G^*_s s^2 \frac{4K_1(q)K_1(s)+sK_1(q)K_0(s)+qK_0(q)K_1(s)}{qK_0(q)K_1(s)+sK_1(q)K_0(s)+qsK_0(q)K_0(s)}$ $s = \frac{ia_o}{2\sqrt{1+2i\beta_s}}$, $q = \frac{s}{\eta_s}$ and $\eta_s = \sqrt{\frac{2*(1-\nu_s)}{1-2\nu_s}}$
Mylonakis (2001)	$k^* = \pi G^*_s s^2 \frac{4K_1(q)K_1(s)+sK_1(q)K_0(s)+qK_0(q)K_1(s)}{qK_0(q)K_1(s)+sK_1(q)K_0(s)+qsK_0(q)K_0(s)}$ $s = \frac{1}{2}\sqrt{a^2_{cutoff} - \frac{a^2_o}{1+2i\beta_s}}$, $q = \frac{s}{\eta_s}$, $\eta_s = \sqrt{\frac{2*(1-\nu_s)}{1-2\nu_s}}$ and $a_{cutoff} = \frac{\pi d}{2L}$
Anoyatis and Lemnitzer (2017)	$k^* = \pi G^*_s s\left(s + 4\frac{K_1(s)}{K_0(s)}\right)$ $s = \frac{1}{2\eta^{\chi}_s}\sqrt{a^2_{cutoff} - \frac{a^2_o}{1+2i\beta_s}}$, $\eta_s = \sqrt{\frac{2-\nu_s}{1-\nu_s}}$

CHAPTER 7
KINEMATIC RESPONSE

7.1 Introduction

According to modern design criteria, piles should be designed to withstand two types of seismic actions. (1) kinematic forces induced due to deformation of the surrounding soil along the entire pile length because of the incoming seismic waves; and (2) inertial forces at pile head induced by oscillations of the superstructure (Gazetas et al. 1992, Rovithis et al. 2009). According to CEN/TC 250 (2004), this issue is addressed by soil-pile-structure interaction through superposition for allowing interaction between kinematic and inertial effects in the domain of the substructure method.

Mylonakis et al. (1997), as referred by Rovithis et al. (2013), has decomposed soil-pile-structure into three consecutive steps (a) determination of the pile head response due to seismic load using a kinematic interaction analysis. (b) computation of dynamic stiffness associated with the rocking, cross swaying–rocking and swaying motions of the pile and; (c) analysis of the superstructure supported on the dynamic model consisting of springs and dashpots. According to Rovithis et al. (2013), the kinematic interaction's output motion serves as an input motion for the inertial interaction.

7.2 Kinematic response

As described above, kinematic soil-pile interaction is generated by soil motion capable of exciting the pile across its entire length, even when no superstructure is present. This kind of loading may result from earthquake motions, operating frequency from the vibration of high-frequency machineries, and blast loading. According to Anoyatis and Lemnitzer (2017), various computational tools are used to study soil-pile kinematic interaction. Out of the various methods available, rigorous finite element (FE), boundary element (BE), and beam on dynamic Winkler foundation (BDWF) are widely-used models.

The BDWF method is the most widely used methodology but its accuracy and performance are much dependent on the input dynamic Winkler modulus values. That is why it has been the focus of many studies for the last decades (Anoyatis and Lemnitzer 2017).

A comprehensive literature review on the kinematic response of piles has been made. And in all the literature reviewed, the interaction between the individual Winkler springs in the BDWF approach is neglected. So, with the aim of studying the dynamic response of piles considering shear interaction between Winkler springs, the model proposed by Worku (2014) is employed.

7.2.1 Problem definition

The kinematic soil-pile interaction problem considered in this study is represented in Figure 7-1. A single flexible cylindrical pile with length L, and diameter d, is embedded in a homogeneous soil layer of thickness H resting on a rigid base. The soil is modeled as a linear elastic material with a modulus of elasticity, E_s, Poisson's ratio, ν_s, mass density, ρ_s and material damping, β_s.

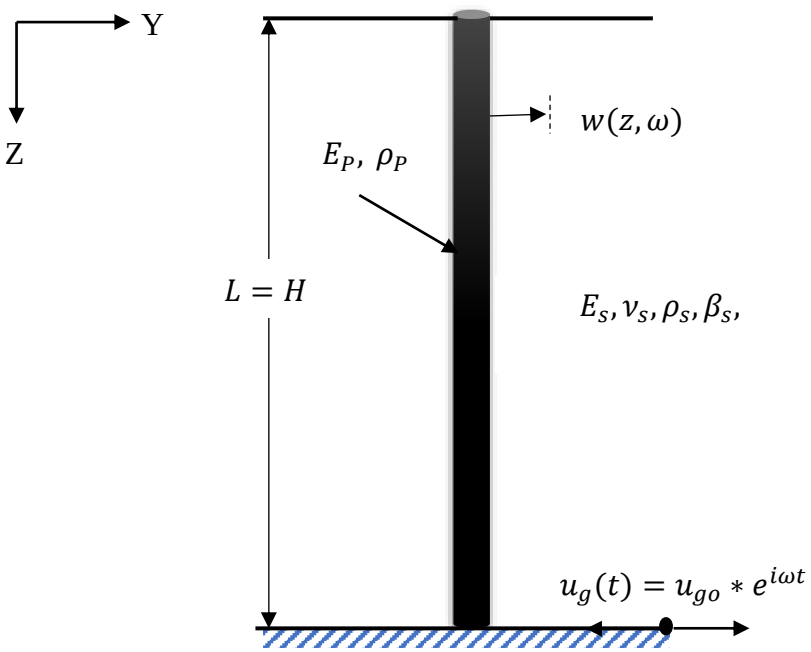

Figure 7-1: Problem considered in kinematic response of single piles.

The pile is loaded with vertically propagating shear-waves expressed in the form of harmonic base excitation, which can be described through base displacement, $u_g(t) = u_{go}e^{iwt}$. Considering different boundary conditions at the pile tip and the pile head, we have four distinct cases to be studied (the same boundary conditions used for the static

case). Nine parameters govern this problem out of those, seven are dimensional parameters ($L, d, E_p, \rho_p, E_s, \rho_s$ and ω), and the rest two are dimensionless parameters (β_s and v_s) (Anoyatis et al. 2013).

Using the theory of Buckingham (1914), given that three dimensions of basic physical quantities are involved (time, mass, and length), the system can be represented using six dimensionless ratios. ($L/d, E_p/E_s, \rho_p/\rho_s$ and $\omega d/V_s$) (Anoyatis et al., 2013).

The effect of kinematic response is mainly expressed in the form of kinematic response factors I_u (translational kinematic response factor) and I_ϕ (rotational kinematic response factor) defined respectively as the maximum translation and rotation of the pile head normalized by the maximum free-field displacement of soil layer (Gazetas 1984, Rovithis et al. 2013, Anoyatis and Lemnitzer 2017).

$$I_u = \frac{w(0,\omega)}{u_{ff}(0,\omega)} \tag{7.1}$$

$$I_\phi = \frac{w'(0,\omega) r_p}{u_{ff}(0,\omega)} \tag{7.2}$$

Where $w(0,\omega)$ and $u_{ff}(0,\omega)$ are frequency-dependent translations of the pile head and the free-field soil, respectively. The kinematic response can also be expressed using the curvature ratios CR_o and CR_L (Anoyatis et al. (2013)).

$$CR_0 = \frac{w''(0,\omega) V_s^2}{a_s(0,\omega)} \tag{7.3}$$

$$CR_L = \frac{w''(L,\omega) V_s^2}{a_s(0,\omega)} \tag{7.4}$$

Where V_s and a_s are shear wave velocity (constant throughout soil layer) and soil acceleration.

7.2.2 Model development

From earlier studies (Gazetas 1984, Rovithis et al. 2013, Anoyatis and Lemnitzer 2017), it is clear that the problem is addressed in the domain of two modular problems. The first

module is a free-field soil response, and the second is a pile response. Both parts are studied separately, and the results are given in the following sections.

7.2.2.1 Free-Field soil response

In one-dimensional linear ground response analysis, in which the soil is modeled as a linear viscoelastic medium, the stress-strain relationship is given by

$$\tau(z,t) = G_s^* \frac{\partial u_{ff}(z,t)}{\partial z} \tag{7.5}$$

where

- $G_s^* = G_s(1+2i\beta_s)$ is complex valued shear modulus.
- τ is shear stress, and
- $u_{ff(z,t)}$ is time and depth dependent displacement of the free-field.

The motion considered has a form of forced harmonic motion of the form $u_{ff}(z,t) = u_{ff}(z)e^{i\omega t}$ when subjected to a harmonic base motion.

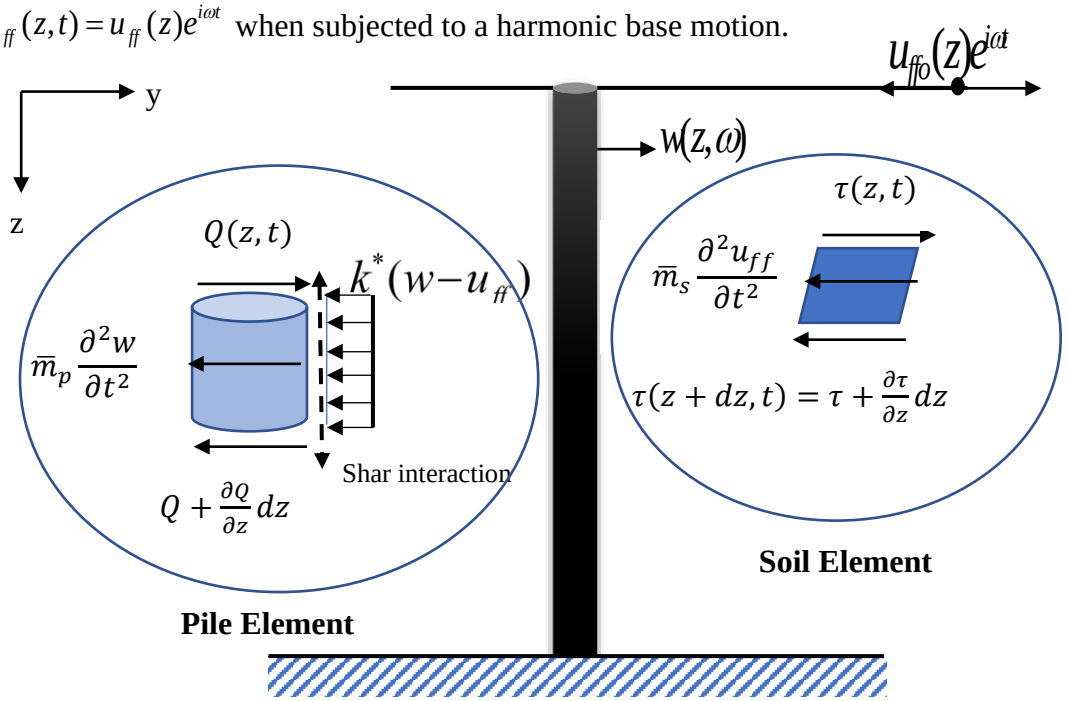

Figure 7-2: Force and stresses in soil and pile for a kinematic response.

From the equilibrium of forces in the horizontal direction for the soil element shown in Figure 7-2, one can find the familiar second order differential equation of the one-dimensional wave equation:

$$\frac{\partial^2 u_{ff}}{\partial z^2} + q^2 u_{ff} = 0 \tag{7.6}$$

Where $q = \frac{\omega}{V_s}$ is the wave number. Note that $\bar{m}_s$ and $\bar{m}_p$ are mass per unit length of the soil and the pile, respectively.

The differential equation in Equation (7.6) is solved to give the well-known solution given by Equation (7.7).

$$u_{ff}(z) = A_1 \cos(qz) + A_2 \sin(qz) \tag{7.7}$$

where A_1 and A_2 represent the amplitudes of the harmonic shear-wave propagating upward and downward. Using the boundary condition, at the free-field the shear stress is zero ($\tau(0) = G_s \gamma(0) = G_s \frac{du_{ff}}{dz} = 0$), the value of A_2 becomes zero. Hence, the amplitude of the standing wave becomes A_1. So, substituting $A_1 = u_{ff0}$ and $A_2 = 0$ back into Equation (7.7), and the equation of motion can be expressed using the form of forced harmonic motion ($u_{ff}(z,t) = u_{ff}(z)e^{i\omega t}$) as

$$u_{ff}(z,t) = u_{ff0} \cos(qz) e^{i\omega t} \tag{7.8}$$

The transfer function with respect to the bedrock motion is obtained by evaluating Equation (7.8) for $z = 0$ and $z = H$ and applying its definition

$$\frac{u_{ffo}}{u_{go}} = \frac{1}{\cos(qH)} = \frac{1}{\cos(\omega H / V_s)} \tag{7.9}$$

7.2.2.2 Pile response

Within this study's realm, soil–pile interaction is modeled by a set of springs, dashpots, and shear interaction. The springs and dashpots are distributed along the pile axis, representing dynamic stiffness and damping, respectively, while the shear interaction

embodies the soil shear. For homogeneous soil conditions, the equation of motion of a pile under harmonic base excitation is derived based on Figure 7-2. A similar approach to that of Section 4.2.2 with some additional considerations is followed.

First, it must be noted that the subgrade modulus used in this dynamic problem is different from that of the static case (i.e. $k_x^* = k_x + i\omega c$, where the static case is only represented by k_x). Another consideration taken before driving the expression is the net displacement of the pile. Because of the base excitation, the pile displaces a total of $(u_{ff} + w)$. Applying all these considerations in Equation (4.5), we obtain

(7.10)

The governing differential equation given in Equation (7.10) is solved using Mathematica 12, and the general solution is given by

$$w(z) = \begin{pmatrix} \left(C_1 e^{\alpha z} + C_2 e^{-\alpha z}\right)\cos(\beta z) \\ +\left(C_2 e^{\alpha z} + C_4 e^{-\alpha z}\right)\sin(\beta z) \end{pmatrix} + \Gamma_p u_{ff}(z) \tag{7.11}$$

where

$$\alpha = \sqrt{\lambda^2 + \frac{\tilde{T}}{4(EI)_P}},\ \beta = \sqrt{\lambda^2 - \frac{\tilde{T}}{4(EI)_P}} \text{ and } \lambda = \sqrt[4]{\frac{k_x + i\omega c_x - \bar{m}_p \omega^2}{4(EI)_P}} \tag{7.12}$$

$$\tilde{T} = TB \ ,\ k_x = k_p B \quad \text{and} \quad \Gamma_p = \frac{k_x + i\omega c_x}{(EI)_p\left(q^4 + 4\lambda^4\right) + \tilde{T}q^2} \tag{7.13}$$

Note that the last term of Equation (7.11) is a particular solution.

The parameters k_p and T are the subgrade model parameters given by Worku (2014) given in Equation (4.9) and Equation (4.10) of the static problem.

The complex-valued kinematic response factor, Γ_p, which is part of the particular solution of Equation (7.10), and given in Equation (7.13) (other than the presence of shear parameter in the denominator), is the same as the expressions given by Flores-Berrones and Whitman (1982) as referred by (Anoyatis et al. 2013, Rovithis et al. 2013).

7.2.3 Boundary conditions

a) Free head: - this boundary condition is described in Section 4.2.4.1. The only difference here is there is no applied load at the pile head. Hence,

$$(EI)_p\left(\frac{d^2}{dz^2}w(z)\right)_{z=0}=0$$

$$(EI)_p\left(\frac{d^3}{dz^3}w(z)\right)_{z=0}-T\left(\frac{d}{dz}w(z)\right)_{z=0}=0$$

b) Fixed head

For fixed-head piles, rotation is not allowed. So, the slope at the pile head is zero, and because there is no applied load at the pile head, the shear force at the pile head is also zero.

$$\left(\frac{d}{dz}w(z)\right)_{z=0}=0 \text{ and } (EI)_p\left(\frac{d^3}{dz^3}w(z)\right)_{z=0}=0$$

c) Fixed base

For fixed base piles, because of pile-base fixity, rotation is zero, but because the pile base moves with the bedrock, the pile base translation is equal to the bedrock translation.

$$\left(\frac{d}{dz}w(z)\right)_{z=L}=0 \text{ and } w(L)=u_{go}$$

d) Floating base

The boundary conditions are the same as in the static case.

$$-T\left(\frac{d}{dz}w(z)\right)_{z=L}-\sqrt{Tk_s}\,w(L)=0$$

$$(EI)_p\left(\frac{d^2}{dz^2}w(z)\right)_{z=L}=0$$

7.2.4 Kinematic response factors

7.2.4.1 Translational kinematic response factors

The expressions for translational kinematic response factors for different soil-pile boundary conditions are obtained by dividing the pile head displacement, $w(0,\omega)$, by the free-field soil displacement, $u_{ff}(0,\omega)$, (Equation (7.1). Hence, before any formulation using the boundary conditions given in Section 7.2.3, the displacement equation given in Equation (7.10) is derived. After this, obtaining the expression of, I_u, is a straight forward procedure. Like the static case, for deriving the expressions, Mathematica 12 is used.

The derived translational kinematic response factors for each boundary condition are given below. For detail, see Appendix E.

Fixed-head floating-base pile

$$I_u = \Gamma_p + \frac{\left(2q^2\Gamma_p\left(\begin{array}{l}\alpha\cosh(\alpha L)\left(\begin{array}{l}2q\beta\cos(\beta L)\sin(qL)\\+(\alpha^2-3\beta^2)\cos(qL)\sin(\beta L)\end{array}\right)\\+\sinh(\alpha L)\left(\begin{array}{l}-\beta(-3\alpha^2+\beta^2)\cos(qL)\cos(\beta L)\\+q(\alpha^2-\beta^2)\sin(qL)\sin\beta L\end{array}\right)\end{array}\right)\right)}{(\alpha^2+\beta^2)^2(\alpha\sin(2\beta L)+\beta\sinh(2\alpha L))} \tag{7.14}$$

Fixed-head fixed-base pile

$$I_u = \Gamma_p + \frac{\left(2\left(\begin{array}{l}\alpha\cosh(\alpha L_p)\sin(\beta L)(\cos(Hq)-\Gamma_p\cos(qL))\\+\left(\beta\cos(Hq)\cos(\beta L)-\Gamma_p\sinh(\alpha L)\left(\begin{array}{l}\beta\cos(qL)\cos(\beta L)\\+q\sin(qL)\sin(\beta L)\end{array}\right)\right)\end{array}\right)\right)}{(\alpha\sin(2\beta L)+\beta\sinh(2\alpha L))} \tag{7.15}$$

The second terms of Equation (7.14) and Equation (7.15) are plotted, as shown in Figures 7-3 and 7-4 for fixed-base and free-base piles. Because both Equation (7.14) and Equation (7.15) are complex-valued functions, the complex-valued function's absolute value is used for plotting them.

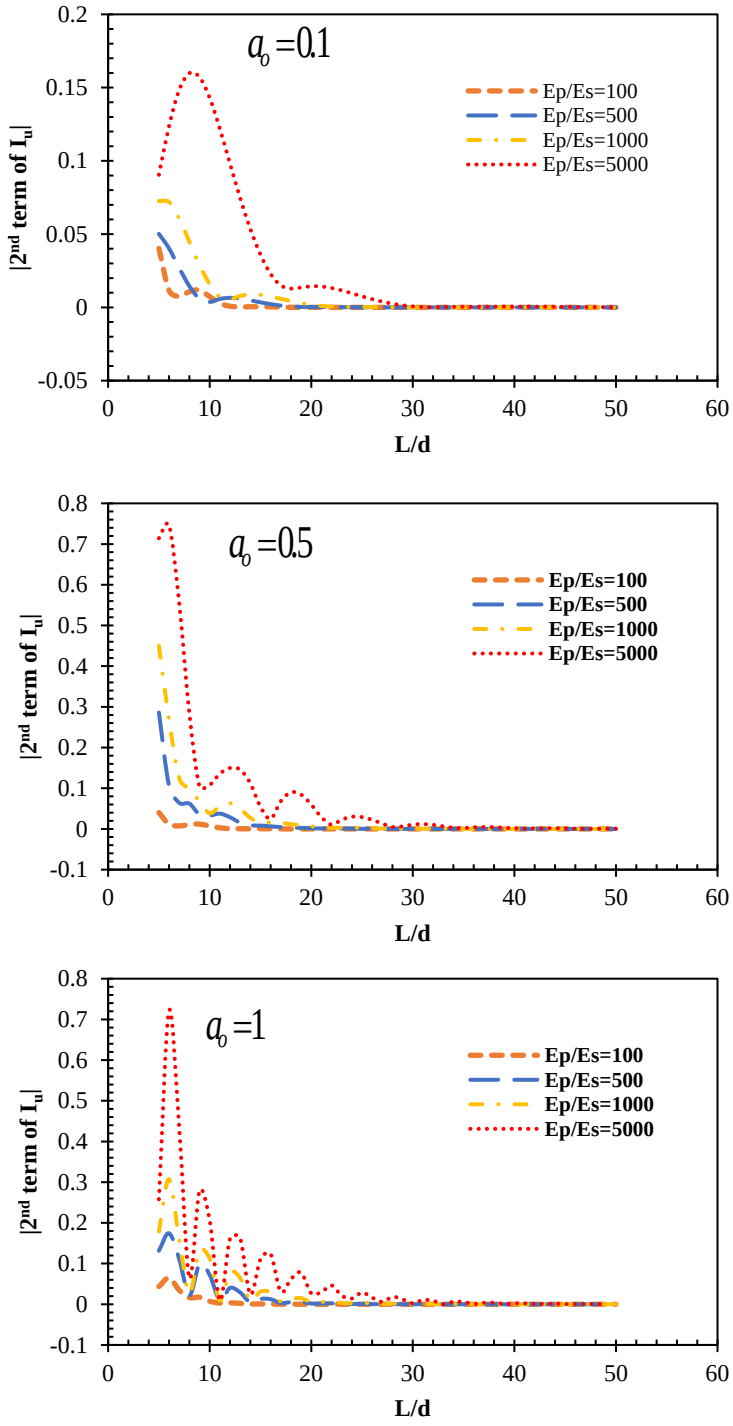

Figure 7-3: The second term of kinematic response factor of fixed-head fixed-base single pile in a homogeneous soil with; $\beta_s = 0.05$, $v_s = 0.4$ **and** $\rho_s = 1900\,kg/m^3$.

As it could be seen from both Figure 7-3 and 7-4, the second terms of Equation (7.14) and Equation (7.15) converge to zero for long pile ($L > L_c$). So, both Equation (7.14) and Equation (7.15) are reduced to a simple solution given in Equation (7.16).

$$I_u = \Gamma_p = \frac{k_x + i\omega c_x}{(EI)_p\left(q^4 + 4\lambda^4\right) + Tq^2} \qquad L > L_c \tag{7.16}$$

For piles on one parameter subgrade model ($T = 0$), the expression given in Equation (7.16) converges to the kinematic response factor, Γ_W, proposed by Flores-Berrones and Whitman (1982).

$$\Gamma_W = \frac{k_x + i\omega c_x}{(EI)_p\left(q^4 + 4\lambda^4\right)} \tag{7.17}$$

As it can be seen from both Figure 7-3 and 7-4, like the static case, there always exists a critical pile length, L_c, increasing the pile length beyond it does not affect the kinematic response of the pile.

The critical pile length of fixed-head free-base piles given in Equation (4.51) of the static case can also be used in studying the kinematic response of fixed-head free-base piles. For the case of fixed-head fixed-base piles, the critical pile length given in Equation (4.51), as shown in Figure 7-3, always under predicts the value of L_c. This difference is mainly the result of the pile base excitation. As a result of the base excitation, the increase in stiffness due to pile base fixity observed in the static case, which decreased the value of the critical pile length, cannot be achieved. So, in studying the kinematic response of fixed-head fixed-base piles, the critical pile length given Equation (4.51) should not be used. Instead, the author recommends to use L_c of fixed-head floating-base piles given in Equation (4.49).

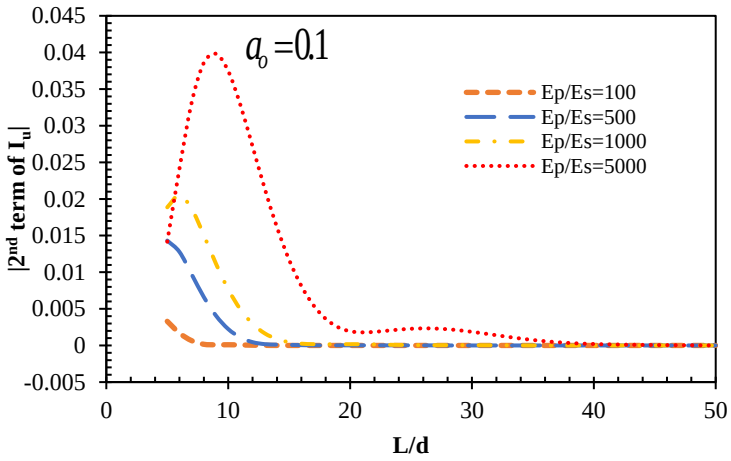

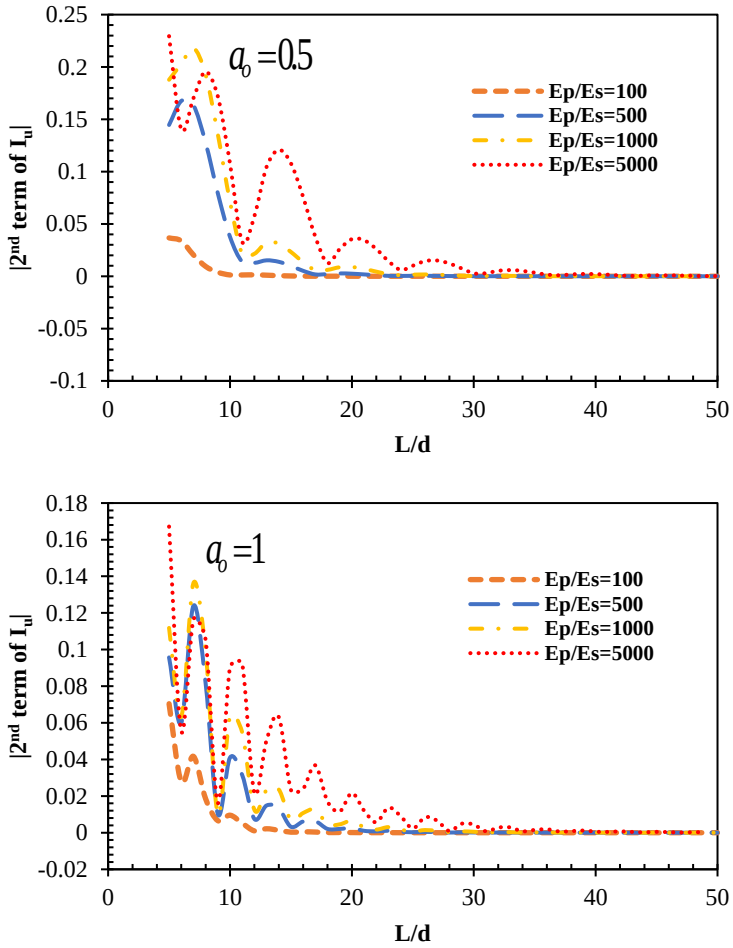

Figure 7-4: The second term of kinematic response factor of fixed-head floating-base single pile in a homogeneous soil with; $\beta_s = 0.05$, $v_s = 0.4$ and $\rho_s = 1900\,kg/m^3$.

For free-head fixed base pile

$$I_u = \frac{\left((EI)_p \left(4\alpha\beta\cos(Hq) \left(\begin{array}{l} 4\alpha\beta\lambda^2\cos(\beta L)\cosh(\alpha L) \\ +\left(-\alpha^4+\beta^4\right)\sin(\beta L)\sinh(\alpha L) \end{array} \right) + A_{\Gamma 1} \right) \right.}{\left. +\tilde{T}\left(8\alpha\beta\lambda^2\cos(Hq)\sin(\beta L)\sinh(\alpha L) + A_{\Gamma 2}\right) \right)} \qquad (7.18)$$
$$\left(2(\mathrm{EI})_p \lambda^2 \left(\begin{array}{l} -\alpha^4+6\alpha^2\beta^2-\beta^4+2\alpha^2\lambda^2\cos(2\beta L) \\ +2\beta^2\lambda^2\cosh(2\alpha L) \end{array} \right) \right.$$
$$\left. +2\lambda^2\tilde{T}\left(\alpha^2-\beta^2-\alpha^2\cos(2\beta L)+\beta^2\cosh(2\alpha L)\right) \right)$$

where

$$A_{\Gamma 1}=\Gamma_p\begin{pmatrix}-2\lambda^2\left(\alpha^4-6\alpha^2\beta^2+\beta^4+q^2\left(\alpha^2-\beta^2\right)\right)+\alpha^2\left(q^2\left(\alpha^2-3\beta^2\right)+4\lambda^4\right)\cos\left(2\beta L_p\right)\\-16\alpha^2\beta^2\lambda^2\cos\left(qL\right)\cos\left(\beta L\right)\cosh\left(\alpha L\right)+\beta^2\cosh\left(\alpha L\right)\left(q^2\left(3\alpha^2-\beta^2\right)+4\lambda^4\right)\\+4q\alpha^2\beta\cosh\left(\alpha L\right)\sin\left(qH\right)\sin\left(\beta L\right)\left(\alpha^2-3\beta^2\right)\\4q\alpha\beta^2\left(-3\alpha^2+\beta^2\right)\cos\left(\beta L\right)\sin\left(qH\right)\sinh\left(\alpha L\right)\\+4\alpha\beta\cos\left(qH\right)\sin\left(\beta L\right)\sinh\left(\alpha L\right)\left(\alpha^4-\beta^4\right)\\+\beta^2\left(q^2\left(3\alpha^2-\beta^2\right)+4\lambda^4\right)\sinh^2\left(\alpha L\right)\end{pmatrix}$$

$$A_{\Gamma 2}=\Gamma_p\begin{pmatrix}2\left(q^2+\alpha^2-\beta^2\right)\lambda^2-\alpha^2\left(q^2+2\lambda^2\right)\cos\left(2\beta L\right)-\beta^2\left(q^2-2\lambda^2\right)\cosh^2\left(\alpha L\right)\\-4q\alpha^2\beta\cosh\left(\alpha L\right)\sin\left(qH\right)\sin\left(\beta L\right)+4q\alpha\beta^2\cos\left(\beta L\right)\sin\left(qH\right)\sinh\left(\alpha L\right)\\-8\alpha\beta\lambda^2\cos\left(qH\right)\sin\left(\beta L\right)\sinh\left(\alpha L\right)-\beta^2\sinh^2\left(\alpha L\right)\left(q^2-2\lambda^2\right)\end{pmatrix}$$

For free-head floating base pile

$$I_u=\Gamma_p\frac{\begin{pmatrix}2\left(EI\right)_p\left(\alpha^2+\beta^2\right)\left(\left(\alpha^2+\beta^2\right)^2\begin{pmatrix}-\alpha^2-\beta^2\\+\alpha^2\cos\left(2L\beta\right)\\+\beta^2\cosh\left(2L\alpha\right)\end{pmatrix}-q^2\left(A_{q1}\right)\right)\\+2\tilde{T}\left(-\left(\alpha^2+\beta^2\right)^2\begin{pmatrix}-\alpha^2+\beta^2\\+\alpha^2\cos\left(2L\beta\right)-\beta^2\cosh\left(2L\alpha\right)\end{pmatrix}+q^2\left(A_{q2}\right)\right)\end{pmatrix}}{\begin{pmatrix}2\left(\alpha^2+\beta^2\right)^2\begin{pmatrix}\tilde{T}\begin{pmatrix}\alpha^2-\beta^2-\alpha^2\cos\left(2L\beta\right)\\+\beta^2\cosh\left(2L\alpha\right)\end{pmatrix}\\+\left(EI\right)_p\left(\alpha^2+\beta^2\right)\begin{pmatrix}-\alpha^2-\beta^2+\alpha^2\cos\left(2L\beta\right)\\+\beta^2\cosh\left(2L\alpha\right)\end{pmatrix}\end{pmatrix}\end{pmatrix}} \tag{7.19}$$

where,

$$A_{q1}=\begin{pmatrix}\alpha^4-\beta^4-\alpha^4\cos\left(2L\beta\right)+3\alpha^2\beta^2\cos\left(2L\beta\right)\\+\left(-3\alpha^2\beta^2+\beta^4\right)\cosh^2\left(L\alpha\right)+4q\alpha^2\beta\cosh\left(L\alpha\right)\sin\left(Hq\right)\sin\left(L\beta\right)\\+4\alpha\beta\left(-q\beta\cos\left(L\beta\right)\sin\left(Hq\right)+\left(\alpha^2+\beta^2\right)\cos\left(Hq\right)\sin\left(L\beta\right)\right)\sinh\left(L\alpha\right)\\+\left(-3\alpha^2\beta^2+\beta^4\right)\sinh^2\left(L\alpha\right)\end{pmatrix}$$

$$A_{q2}=\begin{pmatrix}\alpha^4-6\alpha^2\beta^2+\beta^4-\alpha^4\cos(2L\beta)-\alpha^2\beta^2\cos(2L\beta)-\beta^2(\alpha^2+\beta^2)\cosh^2(L\alpha)\\+4\alpha^2\beta\cosh(L\alpha)(2\beta\cos(Hq)\cos(L\beta)+q\sin(Hq)\sin(L\beta))\\+4\alpha\beta(q\beta\cos(L\beta)\sin(Hq)+(\alpha^2-\beta^2)\cos(Hq)\sin(L\beta))\sinh(L\alpha)\\-\beta^2(\alpha^2+\beta^2)\sinh^2(L\alpha)\end{pmatrix}$$

For long flexible free-head piles, Mylonakis (1999), as reported in Nikolaou et al. (2001), has derived a simplified expression for I_u given in Equation (7.19)

$$I_u=\Gamma_W\left(1+\frac{1}{2}\left(\frac{q}{\lambda}\right)^2\right) \tag{7.20}$$

With the aim of determining simplified expression for I_u of long free-head piles similar to the one proposed by Mylonakis (1999), the expression of I_u given in Equation 7.20 (using Γ_p instead of Γ_w) is plotted together with Equation (7.18) and (7.19) in Figure 7-5. And from the figure, it is evident that for long piles ($L > L_c$), the translational kinematic response factor proposed by Mylonakis (1999) can be used only by replacing the value of Γ_W by Γ_p.

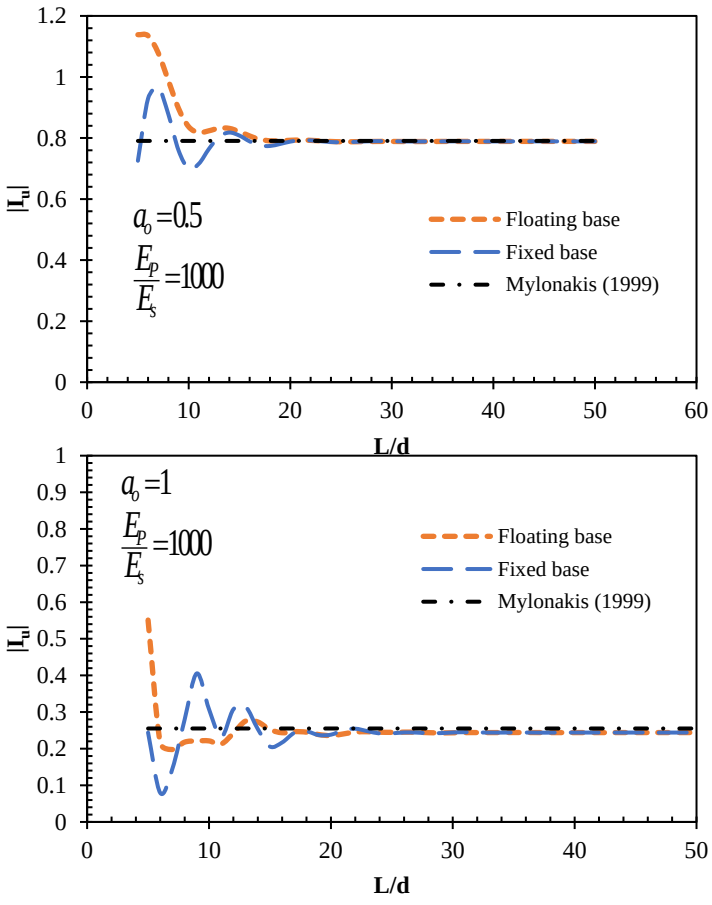

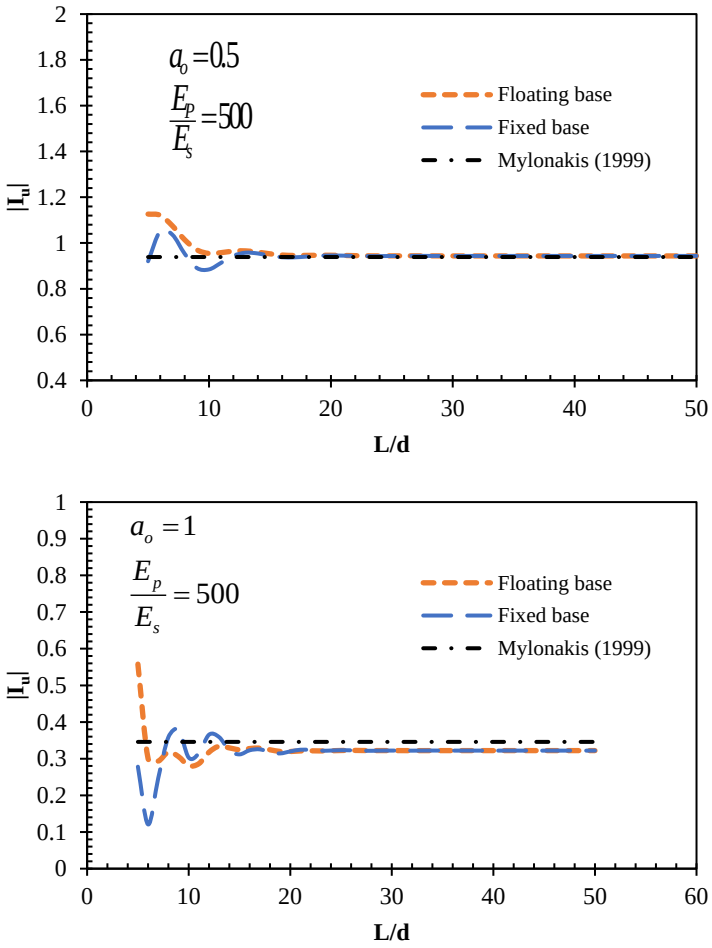

Figure 7-5: Translational kinematic response factor of free-head floating and fixed base single pile in a homogeneous soil with; $\beta_s = 0.05$, $v_s = 0.4$ and $\rho_s = 1900\,kg/m^3$.

The critical pile length, L_c, of both free-head fixed and floating base piles, for the same reason stated in the fixed-head case, is the one given for free-head floating base piles (Equation (4.53)).

7.2.4.2 Parametric investigation of translational response factor

Four translational response factors for both free and fixed-head piles are obtained in the preceding section. In this section, the variation of each translational response factor is examined by varying the different soil and pile properties.

Contribution of the shear element (T)

As discussed earlier, the subgrade model used in this study has a shear element introduced to interconnect the individual springs. So, the shear interaction contribution to the translational kinematic response factors is studied prior to any parametric study.

As it can be seen in all of the expressions provided for translational kinematic response factors (Equation (7.14), (7.15), (7.18) and (7.19)), all of them are a function of the kinematic response factor, Γ_p. So, with the aim of studying the effect of the shear parameter, T, the ratio between Γ_p and Γ_W for different pile-soil stiffness ratio is plotted in Figure 7-6.

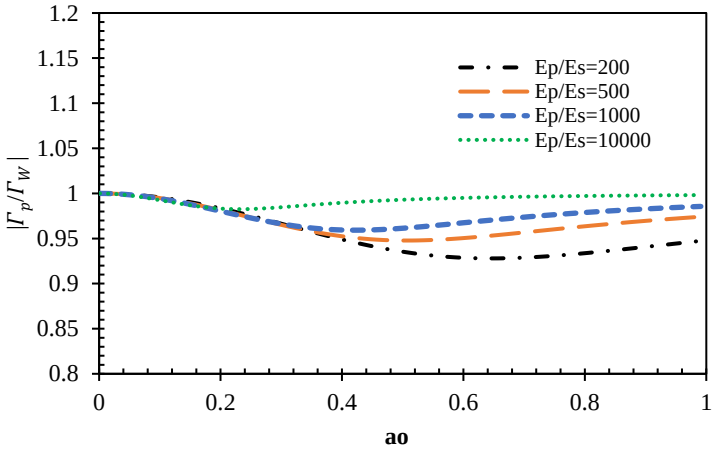

Figure 7-6: The ratio between kinematic response factors on two and one parameter subgrade models; $\beta_s = 0.05$, $\nu_s = 0.4$ and $\rho_s = 1900\,kg/m^3$.

Figure 7-5 shows that the contribution of shear interaction becomes very significant for most practical pile-soil stiffness ratios ($100 < E_p / E_s < 2000$). But for piles in very soft soil ($5000 \le E_p / E_s \le 10000$) the contribution can be neglected. Therefore, for piles in very soft soil, the analytical solutions proposed based on one parameter subgrade models can be used.

The result presented in Figure 7-6 is independent of pile length, L. So, with the aim of studying the contribution of the shear element, T, on the kinematic response of piles with different pile slenderness, Equation (7.14), (7.15), (7.18), and (7.19) are plotted (by considering the contribution of shear interaction ($T \neq 0$) and without it ($T = 0$)) for three different pile slenderness. And the results are given in Figure 7-7, Figure 7-8, Figure 7-9, and Figure 7-10.

Figure 7-7 and Figure 7-8 show that for free-head piles, the effect of the shear interaction becomes predominant for pile in stiff or moderately stiff soils. And also, its effect increase with a decrease in pile length.

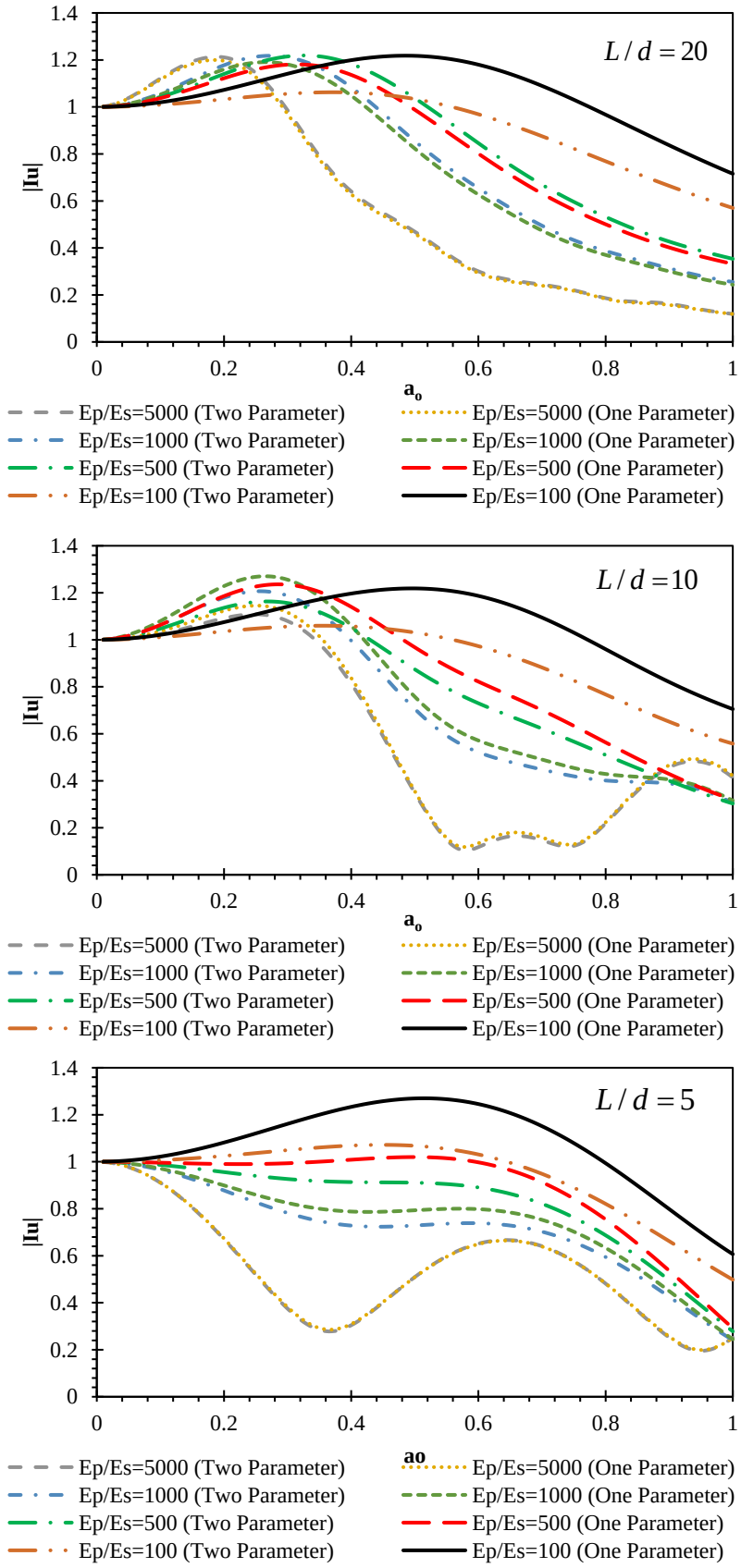

Figure 7-7: The translational kinematic response factor for FrHFxBP : $\beta_s = 0.05$, $v_s = 0.4$ **and** $\rho_s = 1900\,kg/m^3$.

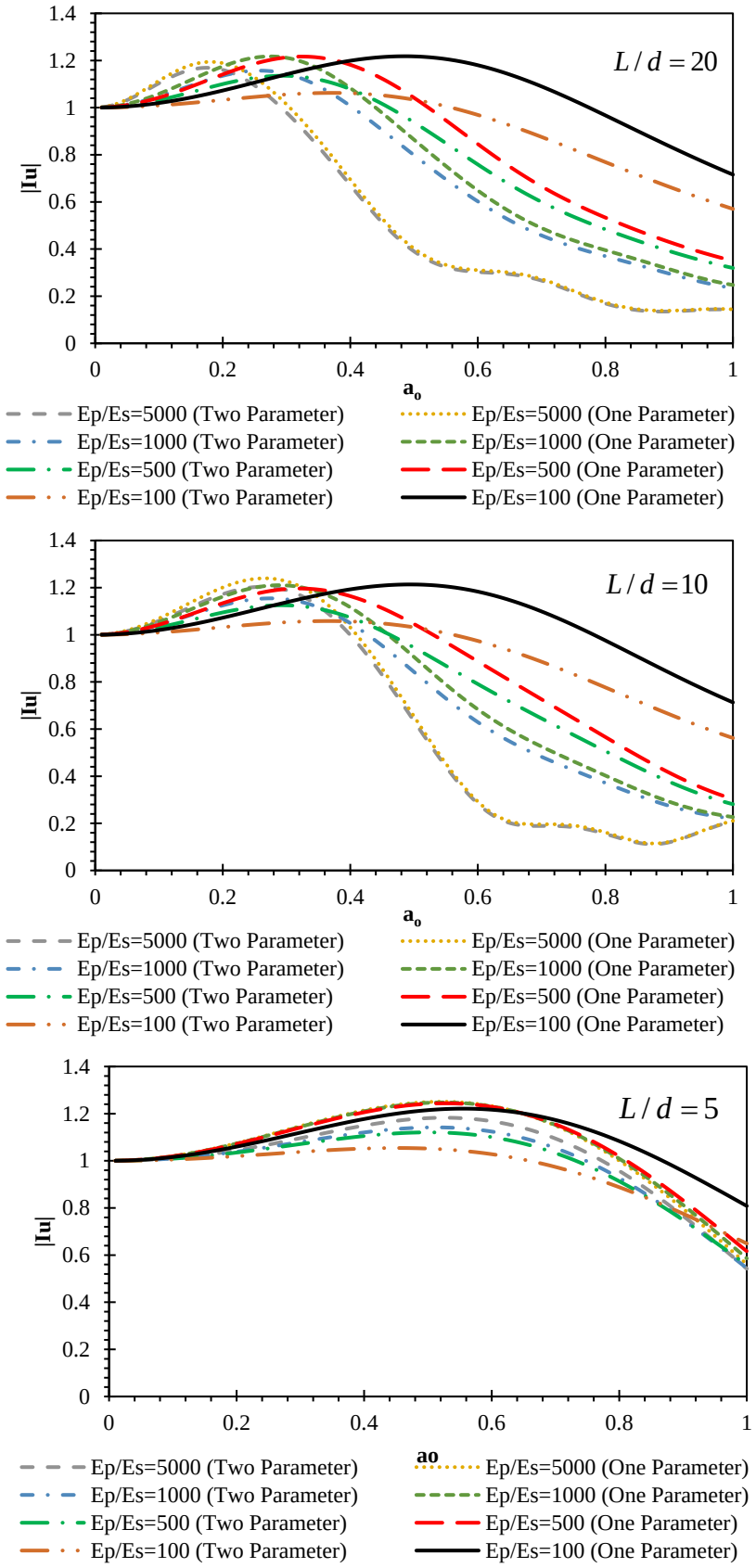

Figure 7-8: The translational kinematic response factor for FrHFBP ; $\beta_s = 0.05$, $\nu_s = 0.4$ **and** $\rho_s = 1900\,kg/m^3$.

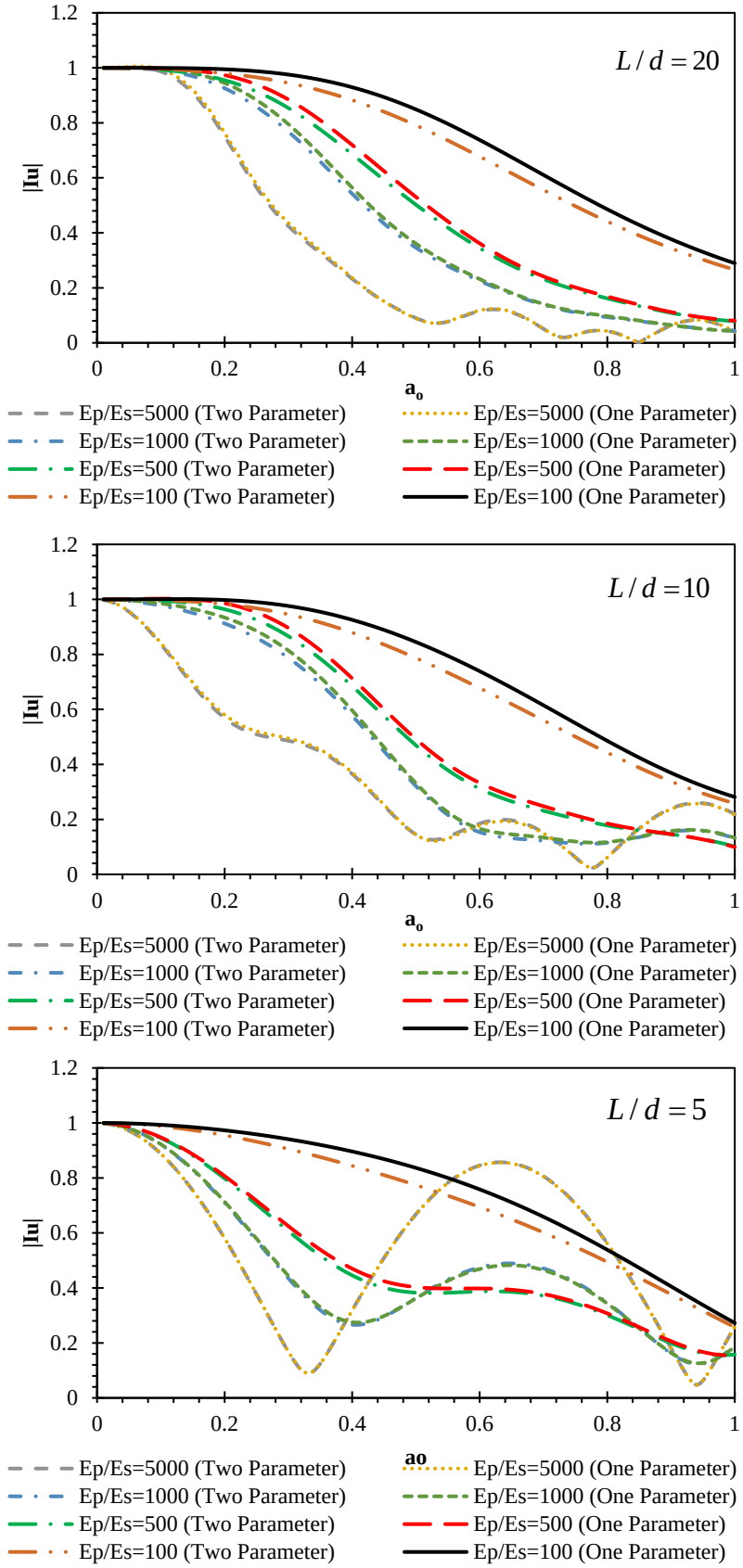

Figure 7-9: The translational kinematic response factor for FxHFxBP ; $\beta_s = 0.05$, $v_s = 0.4$ **and** $\rho_s = 1900\,kg/m^3$.

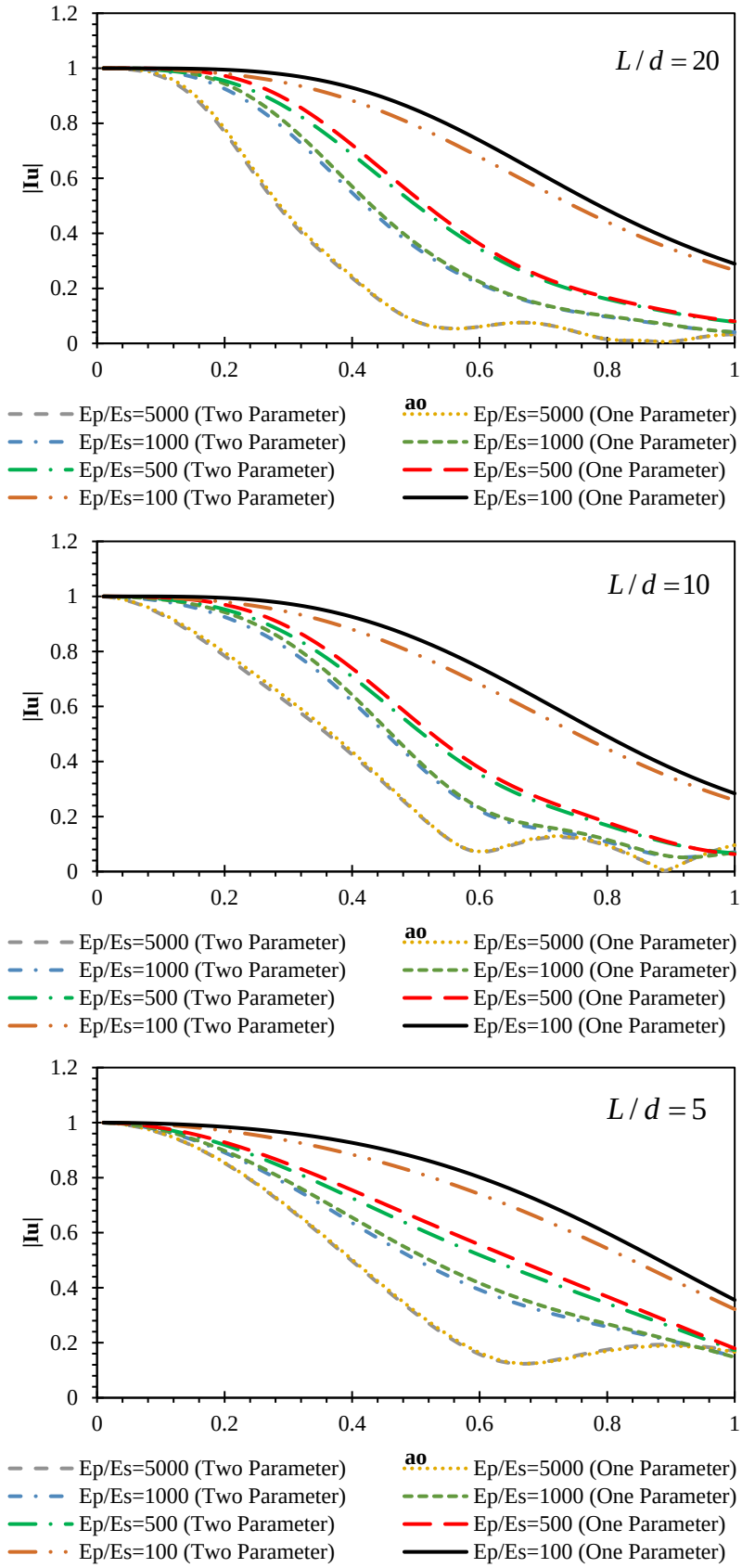

Figure 7-10: The translational kinematic response factor for FxHFxBP ; $\beta_s = 0.05$**,** $v_s = 0.4$ **and** $\rho_s = 1900\,kg/m^3$**.**

In the case of fixed-head piles (Figure 7-9 and Figure 7-10), the shear element's contribution becomes appreciable for only a very short pile. Hence, for long and intermediate fixed-head floating and fixed base piles, the expression of the translational kinematic response factor given in Equation (7.14) and Equation (7.15) can be simplified by neglecting shear interaction ($G_P = 0 \;\; \Rightarrow \alpha = \beta = \lambda$).

In the preceding section, the shear element's contribution is studied, and its contribution is portrayed for different pile slenderness and pile-soil stiffness ratio. In the following sections, the proposed model is evaluated for different soil-pile properties.

Effect of slenderness ratio, L/d

Using Equation (7.14), (7.15), (7.18) and (7.19), the influence of L/d is studied, and the results are given in Figure 7-9 and 7-10 , for a pile having $E_p / E_s = 1000$, embedded in a homogeneous soil having $v_s = 0.4$, $\rho_s = 1900\, kg/m^3$ and $\beta_s = 0.05$. The 3D plot is also given in Figure 7-13 as a function of L/d and a_o .

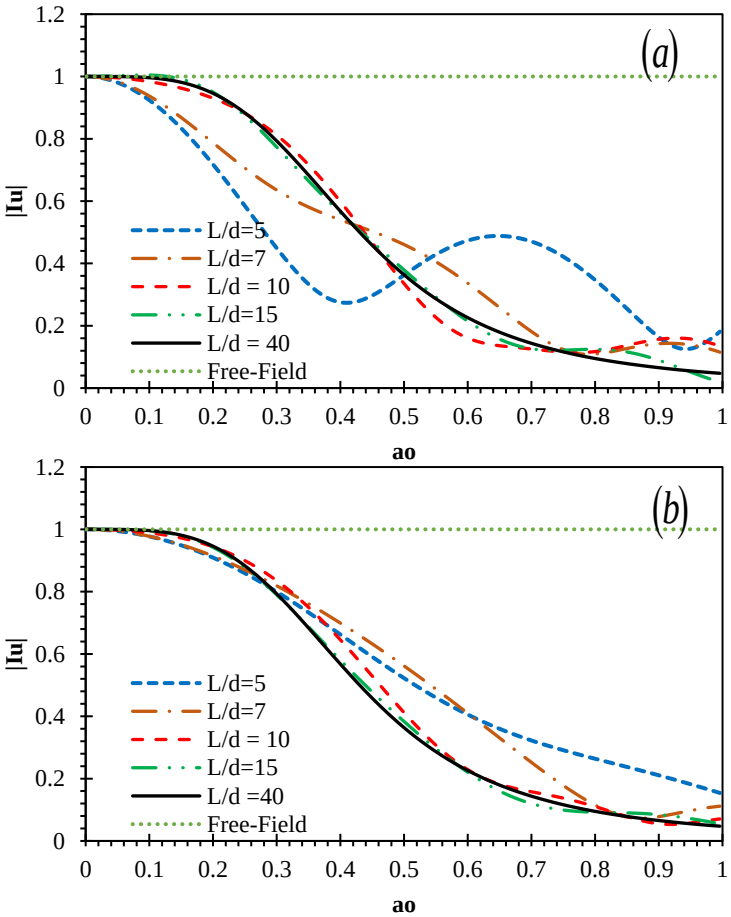

Figure 7-11: Translational kinematic response factor for (a) fixed-head fixed-base (b) fixed-head free-base piles: effect of slenderness

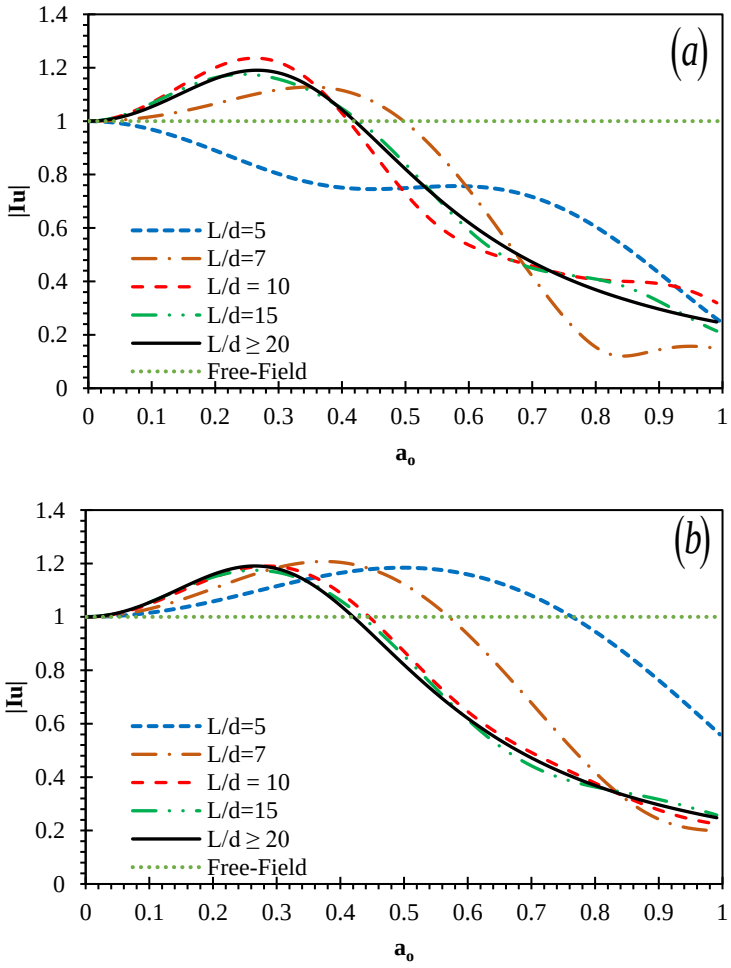

Figure 7-12: Translational kinematic response factor for (a) free-head fixed-base (b) free-head free-base piles: effect of slenderness

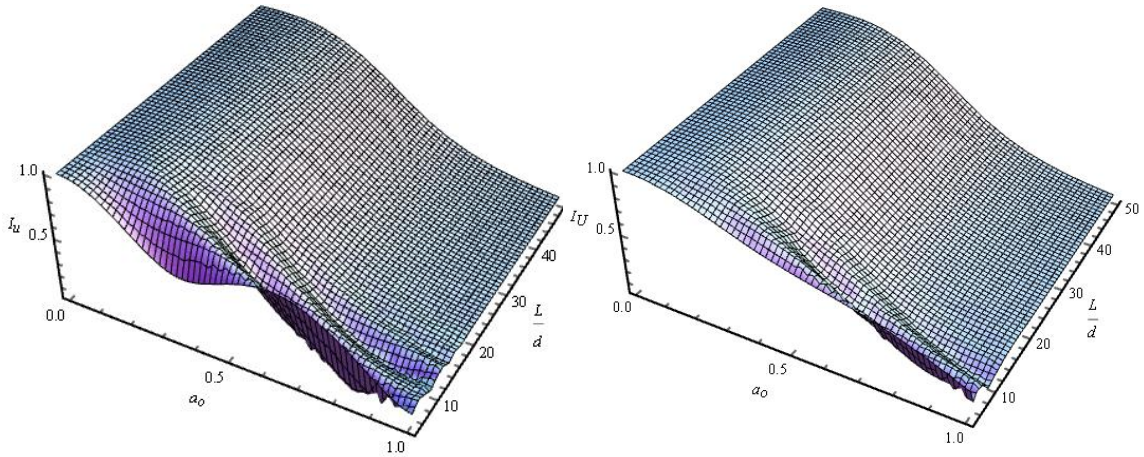

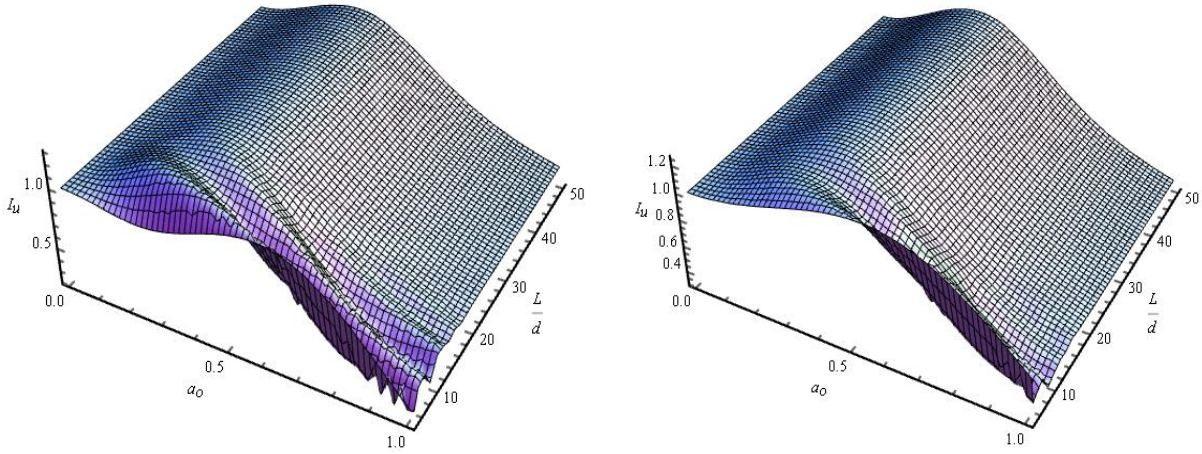

Figure 7-13: 3D plot for translational kinematic response factor a) FxHCBP b)FxHFBP c)FHCBP d)FHFBP : effect of slenderness

Figures 7-11 and 7-12 portray the effect of L/d the translational kinematic response for piles with $E_p/E_s = 1000$ in a homogeneous soil. Five values of L/d are examined (5, 7, 10, 15 and 20), which cover a relatively wide range of slenderness ratios of actual piles, and the following trends are worthy of note

- It is evident that for long fixed-head piles ($L > L_c$) independent of the pile base boundary condition, L/d has a profound effect on its translational kinematic response only at frequencies greater than about $a_o = 0.15$, whereas for the shorter piles ($L \le L_c$), the effect starts at frequencies greater than about $a_o = 0.1$.
- In the case of free-head piles, L/d has a profound effect on its translational kinematic response, independent of the piles slenderness and piles base boundary condition, only at frequencies greater than about $a_o = 0.1$.
- For both free-head and fixed-head piles, the effect of pile slenderness becomes appreciable after some threshold point. Before that point, the translational kinematic response remains approximately one, implying that piles of all slenderness appear to follow the ground's movement. Hence, their presence has no practical effect on the translational motion at the ground surface level.

Effect of stiffness ratio, E_p/E_s

Using Equation (7.14), (7.15), (7.18) and (7.19), the influence of E_p/E_s is portrayed in Figure 7-14 and Figure 7-15 for fixed-head and free-head piles, respectively for pile having $L > L_c$ (long piles), embedded in a homogeneous soil having $v_s = 0.4$, $\rho_s = 1900\,kg/m^3$

and $\beta_s = 0.05$. The three-dimensional plot is also given in Figure 7-14 as a function of E_p / E_s and a_o.

In this section, because only the effect of pile-soil stiffness ratio was studied. So, pile with $L > L_c$ is used. For the free-head pile, Equation (4.53) and the fixed-head pile, Equation (4.49) are used to get the critical pile length and the resulting maximum critical pile length values are 20 and 22 for free and fixed head piles, respectively. So, as discussed above, long piles are used to assess only the effect of pile-soil stiffness ratio; pile with a slenderness ratio of 40 is used.

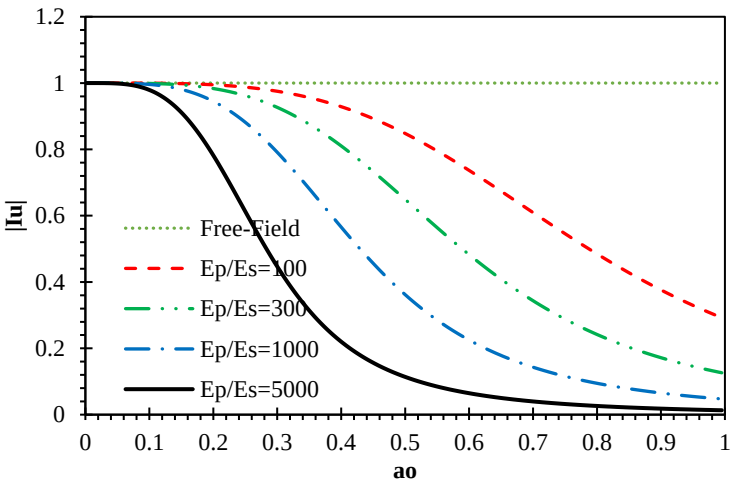

Figure 7-14: Translational kinematic response factors for fixed-head pile: effect of pile-soil stiffness ratio.

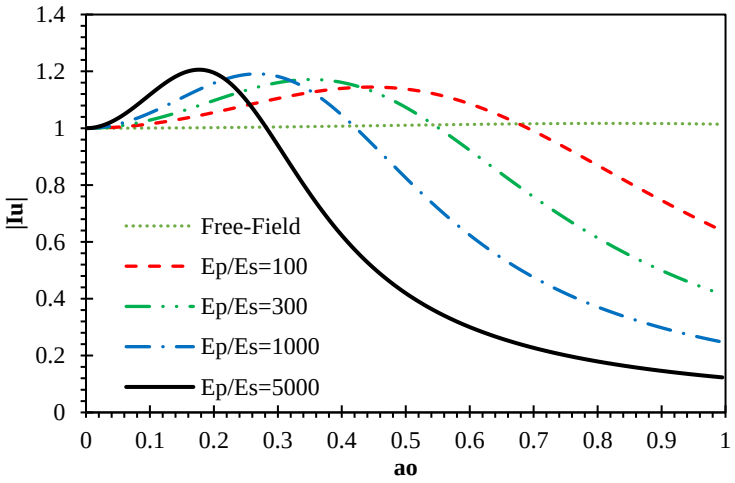

Figure 7-15: Translational kinematic response factors for free-head pile: effect of pile-soil stiffness ratio.

Figure 7-14 and 7-15 portray the effect of E_p / E_s on the translational kinematic response for piles with $L/d = 40$ in a homogeneous soil. Four values of E_p / E_s are examined (100, 300, 1000, and 5000), which cover a fairly wide range of relative pile stiffness of actual piles and the following trends are worthy of note

- Up to some threshold values of frequency, piles of all relative stiffness appear to essentially follow the ground's movement. This trend implies, their presence has no practical effect on the seismic motion at the free-field.
- According to Gazetas (1984), at higher frequencies, even practically flexible piles may not be able to follow the wavy movements of the free-field, which in turn produces considerable variation in the relative deformations between the ground and the pile. This phenomenon can be observed for both free and fixed-base in Figure 7-14 and 7-15, respectively.
- For fixed-head piles, as shown in Figure 7-14, after the threshold frequency ($a_o = 2a_{cutoff} = 0.08$), a considerable decrease in pile deformation is observed. Especially for piles in very soft soils ($E_p / E_s = 1000$ and 5000), a substantial reduction in deformation is observed. This observation is in agreement with the pile deformation (on actual earthquake) reported by Otha et al. (1980) and Tajimi (1977) as cited by Gazetas (1984).

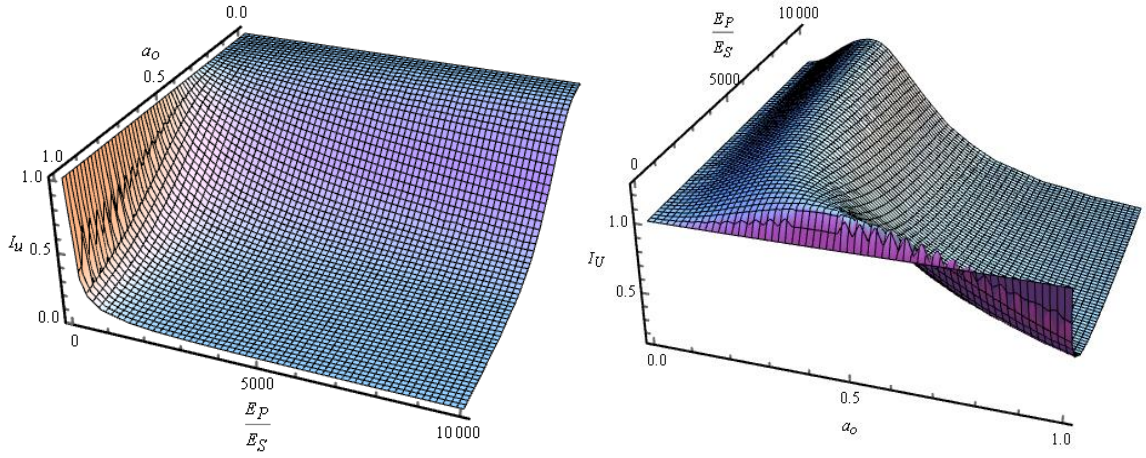

Figure 7-16: 3D plot for translational kinematic response factor a) fixed-head b)free- head: effect of pile-soil stiffness ratio.

- For free-head piles, as shown in Figure 7-15, the piles move with the ground up to a frequency $a_o = a_{cutoff} = 0.04$. On the other hand, for $a_o > a_{cutoff}$ the pile undergoes two different variations of deformation. First, there is an increase in pile deformation up to a certain threshold (different for different types of soils). After that point, a considerable decrease in pile deformation is observed.

As discussed above, for free-head piles, there is a threshold beyond which a decrease in deformation is observed. With the aim of obtaining a simplified expression for the point of the threshold, the discrete points of curvature are fitted to give

$$a'_o = 1.35\left(\frac{E_P}{E_s}\right)^{-0.237} \tag{7.21}$$

7.2.4.3 Rotational Kinematic response factors

For fixed-head piles, the slope at the pile head is zero; therefore, the expression, $w'(0,w)$, in Equation (7.2), is zero, which leads to zero rotational kinematic factors for fixed-head piles.

The rotational kinematic response factor for the case of the free-head pile has been derived using Equation (7.2), and the expressions for the rotational kinematic factor of fixed base and floating base piles are given in Equation (7.22) and Equation (7.23), respectively.

$$I_\phi = -4q^2\alpha\beta\Gamma(\mathrm{EI})_p\begin{pmatrix}\cosh(2\alpha L)\\ +\sinh(2\alpha L)\end{pmatrix}\frac{\begin{pmatrix} \\ -2\alpha\cos(qL)\cosh(\alpha L)\sin(\beta L)\\ +\alpha\sin(2\beta L)+\beta\sinh(2\alpha L)\\ -2\sinh(\alpha L)\begin{pmatrix}\beta\cos(qL)\cos(\beta L)\\ +q\sin(qL)\sin(\beta L)\end{pmatrix}\end{pmatrix}}{\begin{pmatrix}(\mathrm{EI})_p\begin{pmatrix}\alpha^4-6\alpha^2\beta^2+\beta^4\\ -2\alpha^2\lambda^2\cos(2\beta L)\\ -2\beta^2\lambda^2\cosh(2\alpha L)\end{pmatrix}\\ +T\begin{pmatrix}-\alpha^2+\beta^2+\alpha^2\cos(2\beta L)\\ -\beta^2\cosh(2\alpha L)\end{pmatrix}\end{pmatrix}}r_p \tag{7.22}$$

$$I_\phi = 2q^2\alpha\beta\Gamma\left(\mathrm{EI}\right)_p \frac{\left(\begin{array}{l}-2\left(\cosh\left(2\alpha L\right)+\sinh\left(2\alpha L\right)\right)\\ \left(\begin{array}{l}-2\alpha\cos\left(qH\right)\cosh\left(\alpha L\right)\sin\left(\beta L\right)\\ +\alpha\sin\left(2\beta L\right)+\beta\sinh\left(2\alpha L\right)\\ -2\left(\begin{array}{l}\beta\cos\left(qH\right)\cos\left(\beta L\right)\\ +q\sin\left(qH\right)\sin\left(\beta L\right)\end{array}\right)\sinh\left(\alpha L\right)\end{array}\right)\end{array}\right)}{\left(\begin{array}{l}2\lambda^2\left(\mathrm{EI}\right)_p\left(\begin{array}{l}-\alpha^2-\beta^2\\ +\alpha^2\cos\left(2\beta L\right)\\ +\beta^2\cosh\left(2\alpha L\right)\end{array}\right)\\ +T\left(\begin{array}{l}\alpha^2-\beta^2-\alpha^2\cos\left(2\beta L\right)\\ +\beta^2\cosh\left(2\alpha L\right)\end{array}\right)\end{array}\right)} r_p \qquad (7.23)$$

7.2.4.4 Parametric investigation of rotational kinematic response factor

Effect of pile slenderness

Using Equation (7.22) and (7.23), the influence of pile slenderness on the rotational kinematic response is portrayed in Figure 7-17 for pile having $E_P / E_s = 1000$, embedded in a homogeneous soil having $v_s = 0.4$, $\rho_s = 1900 kg/m^3$ and $\beta_s = 0.05$. The three-dimensional plot is also given in Figure 7-18

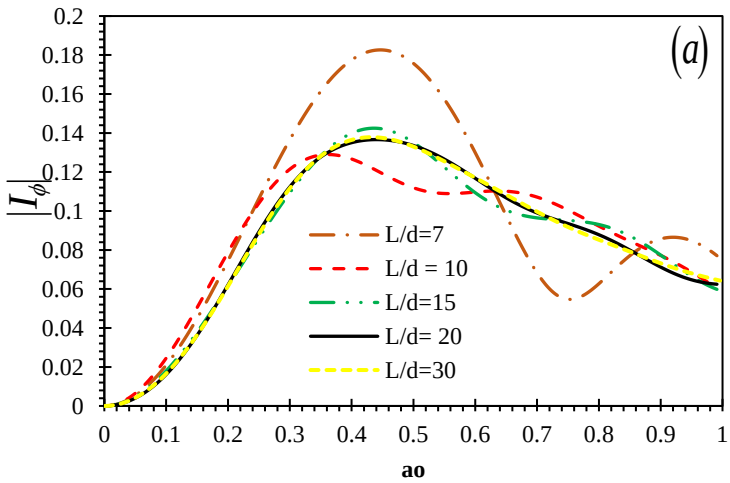

Figure 7-17: Rotational kinematic response factor for free-head fixed-base piles: effect of pile slenderness

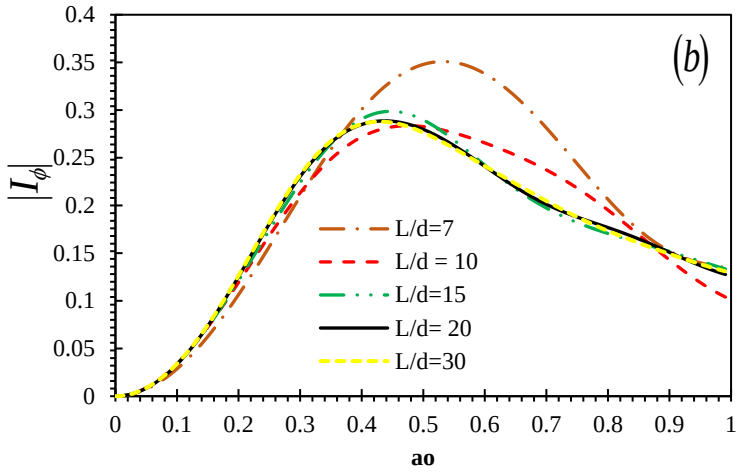

Figure 7-18: Rotational kinematic response factor for free-head floating-base piles: effect of pile slenderness

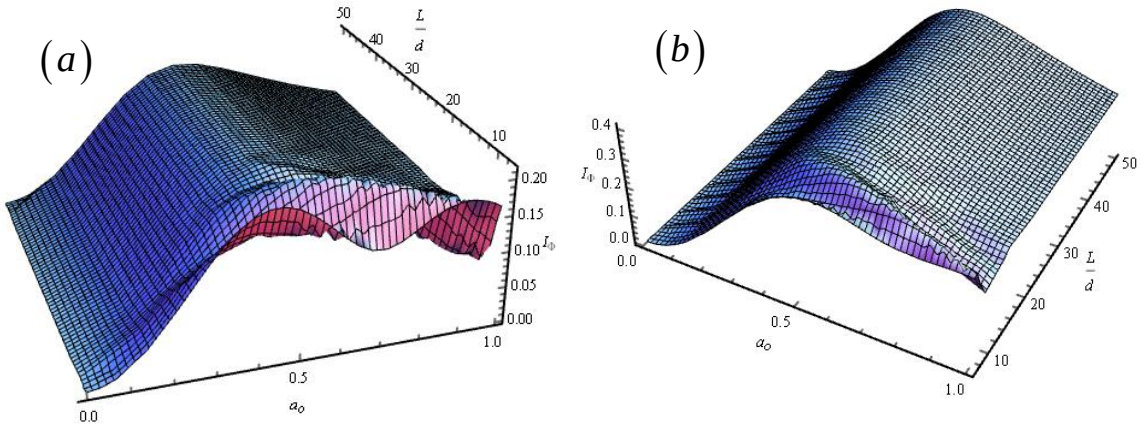

Figure 7-19: 3D plot of rotational kinematic response factor for free-head a) fixed-base b)free- base: effect of pile slenderness

Figure 7-17 portray the effect of L/d on the rotational kinematic response for piles with $E_p/E_s = 1000$ in a homogeneous soil. Five values of L/d are examined (7, 10, 15, 20 and 30), which cover a fairly wide range of slenderness ratios of actual piles, and the following trends are worthy of note

- It is evident that for free-head piles ($L > L_c$) independent of the pile base boundary condition and pile slenderness, L/d has a profound effect on its rotational kinematic response only at frequencies greater than about $a_o = 0.04$.
- For higher frequencies ($a_o > 0.04$), the pile goes under two different phases. In the first case, there is an increase in piles rotation up to a threshold point (for long free-

head fixed and floating base piles, it is approximately $a_o = 0.42$); after that point decrease in the rotation is observed.

- As shown in Figure 7-17, fixed base piles for the same frequency, experience rotation is always less than that of floating base piles.

Effect of stiffness ratio, E_p/E_s

Using Equation (7.22) and (7.23), the influence of E_P / E_s on the rotational kinematic response is portrayed in Figure 7-20 for pile having $L > L_c$, embedded in a homogeneous soil having $v_s = 0.4$, $\rho_s = 1900 kg/m^3$ and $\beta_s = 0.05$. The three-dimensional plot is also given in Figure 7-21. In this section, only the effect of pile-soil stiffness ratio was needed. For this reason, $L/d = 40$ is used.

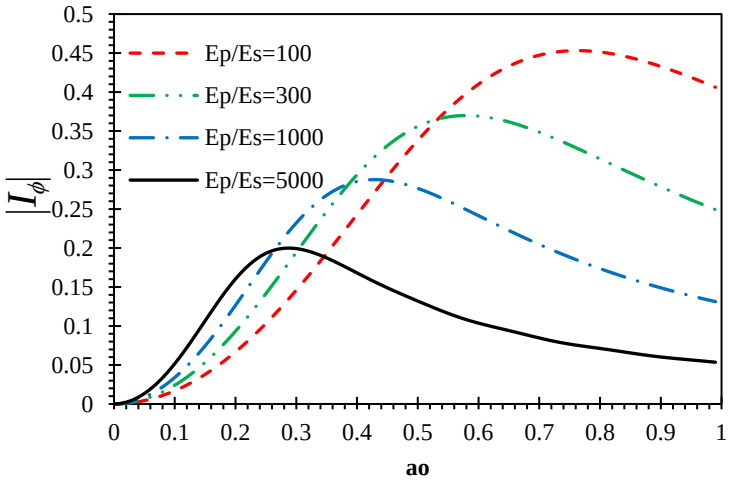

Figure 7-20: Rotational kinematic response factor for free-head piles: effect of pile-soil stiffness ratio

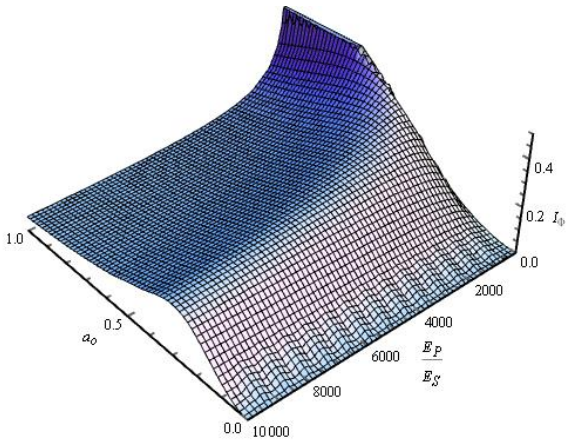

Figure 7-21: 3D plot for variation of rotational kinematic response factor (I_φ): effect of pile-soil stiffness ratio

Figure 7-20 portrays the effect of E_p / E_s on the rotational kinematic response for piles with $L/d = 40$ in a homogeneous soil. Four values of E_p / E_s are examined (100, 300, 1000 and 5000), which cover a fairly wide range of relative pile stiffness of actual piles and the following trends are worthy of note

- It is evident from Figure 7-20, up to a frequency $a_o = a_{cutoff} = 0.04$, the piles move with the ground. On the other hand, for $a_o > a_{cutoff}$ the pile goes under two different variations of rotation. First, there is an increase in pile deformation up to a certain threshold (different for different types of soils). After that point, a considerable decrease in pile rotation is observed. According to Anoyatis et al. (2013), this trend is explained in light of the wavelengths developing in the soil at different frequencies. The wave lengh becomes shorter for a higher frequency, which forces the pile to a stronger rotation at the free-head (Anoyatis et al.,2013).

As discussed above, a point of the threshold is beyond which a decrease in the rotation is observed. With the aim of obtaining a simplified expression for the point of the threshold, the discrete points of curvature are fitted to give

$$a'_o = 2.44\left(\frac{E_P}{E_s}\right)^{-0.252} \tag{7.24}$$

7.2.5 Comparison of the proposed model with FE results

Finite element analysis result from Anoyatis et al. (2013) is used to compare the proposed model. The plots are given in Figure 7-22.

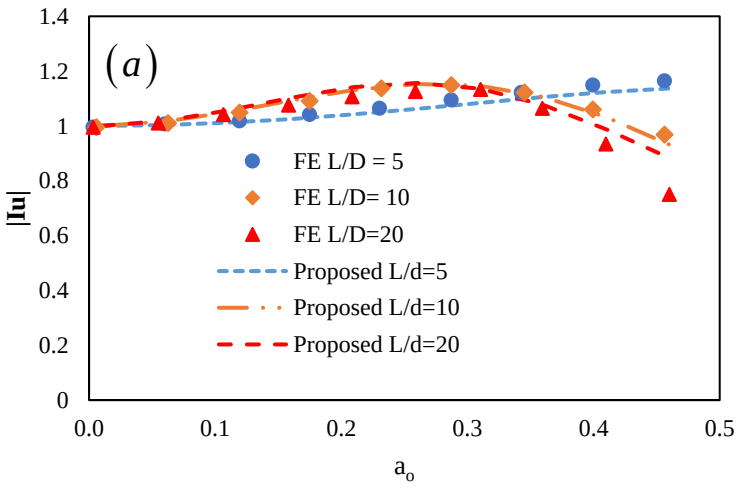

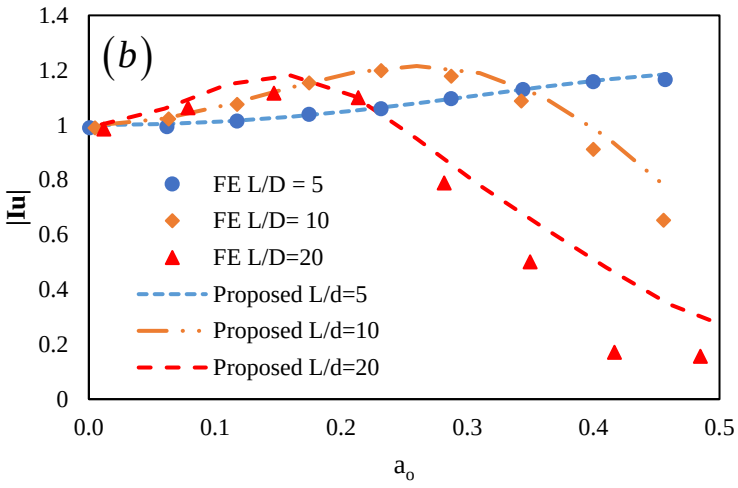

Figure 7-22: Variation of translational kinematic response factor for free-head floating-base piles: comparisons of rigorous elastodynamic FE results with the proposed model.

$\beta_s = 0.05$ **(a)** $E_p / E_s = 1000$ **(b)** $E_p / E_s = 10000$

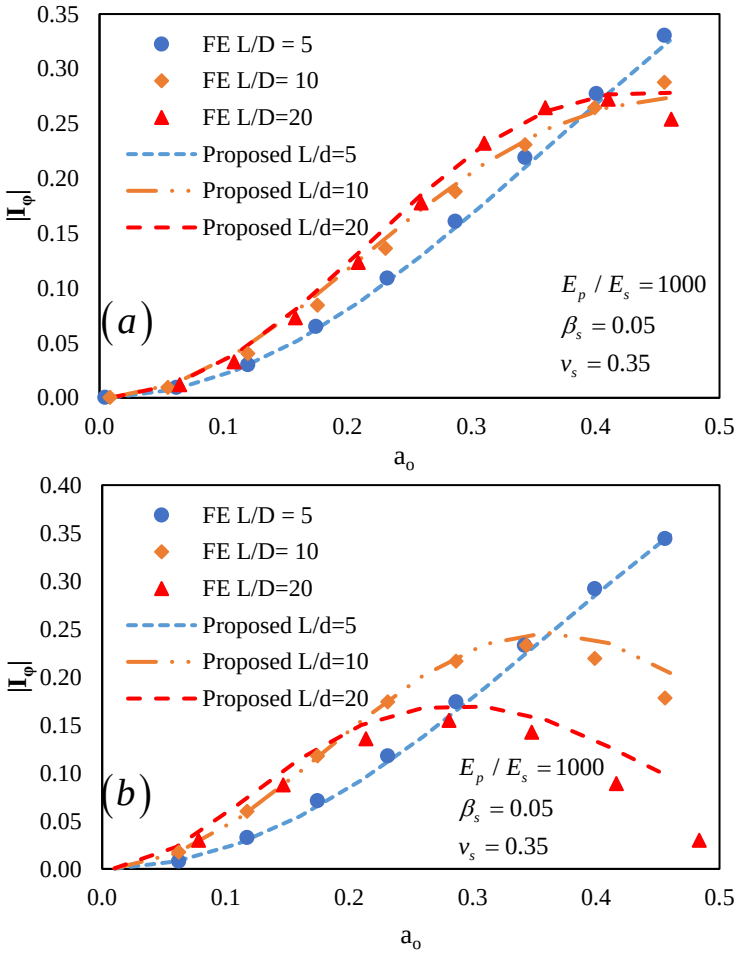

Figure 7-23: Variation of rotational kinematic response factor for free-head floating-base piles: comparisons of rigorous elastodynamic FE results with the proposed model.

$\beta_s = 0.05$ **(a)** $E_p / E_s = 1000$ **(b)** $E_p / E_s = 10000$

As it can be seen from the figures, the proposed model is in good agreement with the FE result indicating that the subgrade model with the calibration factors established in this study is an excellent alternative to conduct quick yet reliable analysis.

CHAPTER 8
INERTIAL RESPONSE

8.1 Introduction

In the past 40 years, many theoretical methods have been developed for the dynamic analysis of piles and pile groups subjected to lateral loads. These methods treat the soil as an elastic continuum; they require significant computational effort and, therefore, are used primarily for research rather than as design tools (Mylonakis 1995).

Approximate solutions have also been developed. Most of them use the Beam on Winkler-Foundation (BWF) model in which the soil reaction with depth to lateral pile movement, is represented through independent soil springs. For-static loads, as stated in the literature section, these springs are calibrated using field load tests. For dynamic loads, theoretically-calculated soil springs and dashpots have been proposed (Novak 1974, Nogami and Novak 1977, Novak and Nogami 1977).

Novak (1974) proposed a simple method for calculating the dynamic lateral pile response. According to this approach, the soil consists of an infinite number of independent horizontal slices. Neglecting the vertical soil deformation, the soil reaction (per unit pile length) due to a horizontal pile movement can be determined by solving a plane-strain elastodynamic problem. This leads to a set of frequency-dependent springs and dashpots which represent the stiffness and the radiation (and material) damping of the soil.

The lateral soil impedance, according to plane-strain theory, is given by (Novak et al, 1978):

$$k_x^* = k_x + i\omega c_x \tag{8.1}$$

Alternatively, frequency-dependent springs and dashpots can be calculated by matching the dynamic pile response from Winkler and finite-element (FE) analysis. As cited by Mylonakis (1995), Dobry et al. (1982) derived the following expression:

$$k_x = \delta E_s \tag{8.2}$$

where

$$\delta = 1.67\left(\frac{E_p}{E_s}\right)^{-0.053} \tag{8.3}$$

Makris and Gazetas (1992) proposed the following approximate expressions for the distributed springs and dashpots:

$$k_x = 1.2E_s \tag{8.4}$$

and

$$c_x = 6a_o^{-0.25}\rho_s V_s d + 2\beta_s \frac{k_x}{\omega} \tag{8.5}$$

In this work, the expressions for both the spring and dashpot coefficients are derived considering shear interaction between the individual springs as presented in Chapters 4 to 6.

8.2 Problem definition

The problem studied is that of a floating or end-bearing fixed-head or free-head flexible pile embedded in a homogenous soil layer of thickness *H* (=L) and subjected to lateral harmonic excitation at the top which causes a harmonic horizontal pile displacement of $w(z,t) = w_o e^{i\omega t}$ as sown in Figure 8-1.

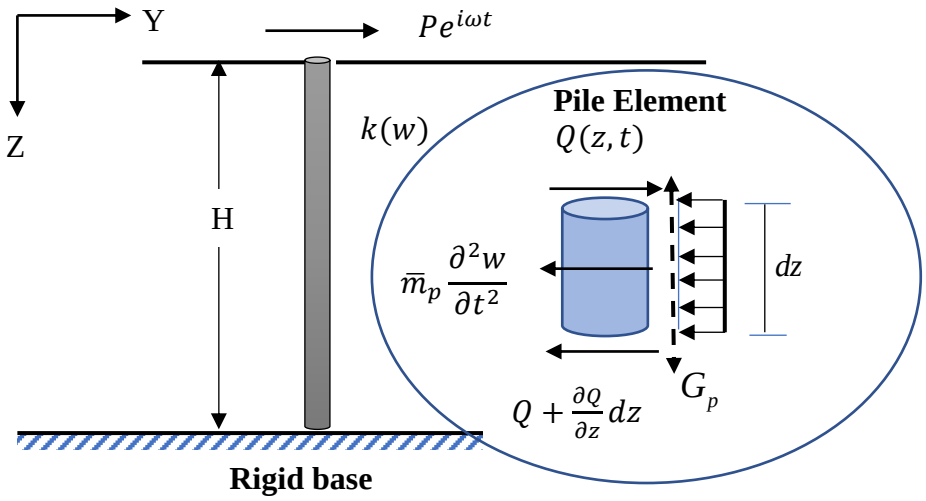

Figure 8-1: Problem considered for an inertial response of piles.

Where t is the time variable, $\omega = 2\pi f$, is the circular excitation frequency and i $(= \sqrt{-1})$ is the imaginary number. The pile is modeled as a linear elastic material with Young's Modulus, E_P and mass density, ρ_P. The soil is modeled as a linear elastic material with modulus of elasticity, E_s, Poisson's ratio, v_s, mass density ρ_s and material damping β_s.

8.3 Dynamic pile stiffness

The inertial response of a head-loaded pile is determined using a beam on a modified Kerr-equivalent Pasternak type model described in Chapter 4. By definition, dynamic pile stiffness is expressed in a matrix form as (Rovithis et al., 2013)

$$\kappa = \begin{vmatrix} K_{HH} & K_{RH} \\ K_{HR} & K_{RR} \end{vmatrix}$$

Where the complex-valued impedances K_{HH}, K_{HR} $(= K_{RH})$ and K_{RR} correspond to the swaying, cross swaying-rocking and rocking modes respectively. All impedance functions can be determined using a harmonic horizontal excitation force $P(t) = P_o e^{i\omega t}$ and a harmonic horizontal displacement $w(z,t) = w_o e^{i\omega t}$ (Gazetas and Dobry 1984), from which the ratio is easily obtained as

$$\frac{P_o}{w_o} = K_x + i\omega C_x \tag{8.6}$$

in which P_o is the amplitude of the forcing function, w_o is the amplitude of the horizontal motion and K_x and C_x are pile head equivalent spring and dashpot coefficients; they are both functions of frequency. In the realm of this study, all impedance values are studied.

The main difference between the equation of motion for a dynamically loaded pile and statically loaded pile (Chapter 4 and Chapter 5) is the presence of dynamic spring stiffness and inertial force. Including this two in Equation (4.5) or just from the equilibrium of a small pile element shown in Figure 8-1, one obtains the governing differential equation:

$$(EI)_P \frac{d^4 w(z)}{dz^4} - G_p \frac{d^2 w(z)}{dz^2} + \left(k_x + i\omega c_x - \bar{m}_p \omega^2\right) w = 0 \tag{8.7}$$

Solving the differential equation, one obtains a relationship identical to the well-known displacement equation of a beam on a two-parameter subgrade model.

$$w(z)=\left(C_1e^{\alpha^* z}+C_2e^{-\alpha^* z}\right)\cos\left(\beta^* z\right)+\left(C_2e^{\alpha^* z}+C_4e^{-\alpha^* z}\right)\sin\left(\beta^* z\right) \tag{8.8}$$

The DE in Equation (8.8) is solved in Chapter 4 and Chapter 5; the difference is mainly on the values of α, β and λ. For the dynamic case, all three quantities are changed to complex-valued functions. In order to distinguish between the static and dynamic case, the Asterix (*) is placed next to them (α^*, β^* and λ^*).

8.3.1 Pile impedance expressions for all soil-pile boundary conditions

Inertial interaction only exists if there is super-structure action, and most of the time, the joint between structure and foundation is fixed. For this reason, in this work, only dynamic pile impedance for the case of fixed-head pile is studied.

According to Velez et al. (1983), the dynamic pile impedance is the ratio between the magnitude of excitation (force or moment) having a frequency of ω and the resulting steady-state displacement or rotation at the pile head.

Using almost the same principle stated by Velez et al. (1983), with an exception of the excitation frequency, in section 5.3.2 the expressions for the static stiffness of the swaying, cross swaying-rocking and rocking modes were derived. The derivation of the pile impedances is similar to the one performed for the static case. Hence, no additional derivation was needed.

8.3.1.1 Swaying impedance, K_{HH}

The swaying impedance is defined as a ratio between the magnitude of excitation force, $P_oe^{i\omega t}$, and the resulting steady-state displacement when no rotation is allowed at the pile top (fixed-head pile), $w_oe^{i\omega t}$, (Velez, Gazetas et al. (1983).

$$K_{HH}=\frac{P_oe^{i\omega t}}{w_oe^{i\omega t}}=\frac{P_o}{w_o} \tag{8.9}$$

The expression for swaying pile impedance is similar to the expression of static pile-head stiffness given in Section 4.4.2 with α, β and λ replaced by α^*, β^* and λ^*, respectively. They are given below for the two tip conditions.

For fixed-head floating base pile

$$K_{HH} = 4\alpha^*\lambda^{*2}(EI)_P \left(\frac{\beta^* \begin{pmatrix} -2\alpha^*\beta^*\sqrt{k_s\tilde{T}}\left(\cos(2L\beta^*)+\cosh(2L\alpha^*)\right) \\ +2\lambda^{*2}(EI)_P \begin{pmatrix} \alpha^*\left(\alpha^{*2}-3\beta^{*2}\right)\sin(2L\beta^*) \\ +\beta^*\left(\beta^{*2}-3\alpha^{*2}\right)\sinh(2L\alpha^*) \end{pmatrix} \end{pmatrix}}{(EI)_P \begin{pmatrix} -2\lambda^{*2} \begin{pmatrix} -4\lambda^4+\alpha^{*2}\left(\alpha^{*2}-3\beta^{*2}\right)\cos(2L\beta^*) \\ +\beta^2\left(-3\alpha^{*2}+\beta^{*2}\right)\cosh(2L\alpha^*)) \end{pmatrix} \\ +2\alpha^*\beta^*\sqrt{k_s\tilde{T}}\left(-\alpha^*\sin(2L\beta^*)+\beta\sinh(2L\alpha^*)\right) \end{pmatrix}} \right) \tag{8.10}$$

For fixed-head fixed base pile

$$K_{HH} = 4\alpha^*\lambda^{*2}(EI)_P \left(\frac{\beta^*\left(\alpha^*\sin(2L\beta^*)+\beta^*\sinh(2L\alpha^*)\right)}{2\left(\beta^{*2}\sinh^2(L\alpha^*)-\alpha^{*2}\sin^2(L\beta^*)\right)} \right) \tag{8.11}$$

8.3.1.2 Cross swaying-rocking impedance, $K_{RH} = K_{HR}$

The cross swaying-rocking impedance, K_{HR}, is defined as a ratio between the magnitude of the moment, $Me^{i\omega t}$, induced by excitation force, $P_o e^{i\omega t}$, and the resulting steady-state displacement when no rotation is allowed at the pile top (fixed-head pile).

The cross swaying-rocking impedance, K_{RH}, can also be defined as a ratio between the magnitude of the shear, $Qe^{i\omega t}$, induced by excitation force, $M_o e^{i\omega t}$, and the resulting steady-state rotation when no translation is allowed at the pile top (fixed-head pile).

$$K_{HR} = \frac{Me^{i\omega t}}{w_o e^{i\omega t}} = \frac{M}{w_o} \tag{8.12}$$

$$K_{HR} = \frac{Qe^{i\omega t}}{\theta_o e^{i\omega t}} = \frac{Q}{\theta_o} \tag{8.13}$$

The expression for cross swaying-rocking impedance is similar to the one provided for the static cross swaying-rocking stiffness given in Section 5.3.2 with α, β and λ replaced by α^*, β^* and λ^*, respectively.

For fixed-head floating base pile

$$K_{RH}=K_{HR}=2(EI)_p\lambda^{*2}\frac{\left(\begin{array}{l}\left(\begin{array}{l}3\alpha^{*2}\beta^2\left(\cos\left(2L\beta^*\right)-\cosh\left(2L\alpha^*\right)\right)\\+2\left(\alpha^{*4}\sin^2\left(L\beta^*\right)-\beta^{*4}\sinh^2\left(L\alpha^*\right)\right)\end{array}\right)\\+\frac{\sqrt{k_s\tilde{T}}}{(EI)_p\lambda^{*2}}\alpha^*\beta^*\left(\begin{array}{l}\alpha^*\sin\left(2L\beta^*\right)\\+\beta^*\sinh\left(2L\alpha^*\right)\end{array}\right)\end{array}\right)}{\left(\begin{array}{l}\left(\begin{array}{l}4\lambda^{*4}+3\alpha^{*2}\beta^{*2}(\cos\left(2L\beta^*\right)+\cosh\left(2L\alpha^*\right)\\-\alpha^{*4}\cos\left(2L\beta^*\right)-\beta^{*4}\cosh\left(2L\alpha^*\right)\end{array}\right)\\+\frac{\sqrt{k_s\tilde{T}}}{(EI)_p\lambda^{*2}}\alpha^*\beta^*\left(\begin{array}{l}-\alpha^*\sin\left(2L\beta^*\right)\\+\beta^*\sinh\left(2L\alpha^*\right)\end{array}\right)\end{array}\right)} \tag{8.14}$$

For fixed-head fixed base pile

$$K_{RH}=K_{HR}=2(EI)_p\lambda^{*2}\left(\frac{-\alpha^{*2}\sin^2\left(L\beta^*\right)-\beta^{*2}\sinh^2\left(L\alpha^*\right)}{\alpha^{*2}\sin^2\left(L\beta^*\right)-\beta^{*2}\sinh^2\left(L\alpha^*\right)}\right) \tag{8.15}$$

8.3.1.3 Rocking impedance, K_{RR}

The rocking impedance, K_{RR}, is defined as a ratio between the magnitude of the excitation moment, $M_o e^{i\omega t}$, and the resulting steady-state rotation when no translation is allowed at the pile top (fixed-head pile).

$$K_{RR}=\frac{M_o e^{i\omega t}}{\theta_o e^{i\omega t}}=\frac{M_o}{\theta_o} \tag{8.16}$$

The rocking impedance expression is similar to the one provided for the static cross rocking stiffness given in Section 5.3.2 with α, β and λ replaced by α^*, β^* and λ^*, respectively.

For fixed-head floating base pile

$$K_{RR}=2(EI)_p\alpha^*\frac{\left(\begin{array}{l}4(EI)_p\lambda^{*4}\left(\begin{array}{l}-\alpha^{*2}+3\beta^{*2}\\+\left(\alpha^{*2}-\beta^{*2}\right)\cos\left(2L\beta^*\right)\\-2\beta^{*2}\cosh\left(2L\alpha^*\right)\end{array}\right)\\-2\sqrt{k_sT}\beta^*\left(\left(-\alpha^{*2}+\beta^{*2}\right)\sin\left(2L\beta^*\right)-2\alpha^*\beta^*\sinh\left(2L\alpha^*\right)\right)\end{array}\right)}{\left(\begin{array}{l}2\beta^*\left(\begin{array}{l}2\sqrt{k_sT}\alpha^*\beta^*\left(\cos\left(2L\beta^*\right)+\cosh\left(2L\alpha^*\right)\right)\\-4(EI)_P\lambda^{*4}\left(\begin{array}{l}\alpha^*\sin\left(2L\beta^*\right)\\+\beta^*\sinh\left(2L\beta^*\right)\end{array}\right)\end{array}\right)\end{array}\right)} \tag{8.17}$$

For fixed-head fixed base pile

$$K_{RR} = 2\left(EI\right)_P \alpha^* \left(\frac{\left(\alpha^{*2} - \beta^{*2}\right)\sin\left(2L\beta^*\right) + 2\alpha^*\beta^*\sinh\left(2L\alpha^*\right)}{2\alpha^*\beta^*\left(\cos\left(2L\beta^*\right) + \cosh\left(2L\alpha^*\right)\right)} \right) \tag{8.18}$$

8.3.2 Critical pile length

The critical pile length must be determined prior to any parametric investigation, because the dynamic response depends on it as the static case is. Following the same process as in Section 4.4, the critical pile length is determined using the stiffness variation factor. The dynamic stiffness variation factor Φ^* is the same as Φ but with α, β and λ replaced with α^*, β^* and λ^*. The expressions for both the floating and fixed base piles are given in Equation (8-19) and (8-120).

For fixed-head floating base pile

$$\Phi^* = \frac{\beta^* \left(\begin{array}{l} -2\alpha^*\beta^*\sqrt{k_s T}\left(\cos\left(2L\beta^*\right) + \cosh\left(2L\alpha^*\right)\right) \\ +\left(\alpha^{*2} + \beta^{*2}\right)\left(EI\right)_P \left(\begin{array}{l} \alpha^*\left(\alpha^{*2} - 3\beta^{*2}\right)\sin\left(2L\beta^*\right) \\ +\beta^*\left(\beta^{*2} - 3\alpha^{*2}\right)\sinh\left(2L\alpha^*\right) \end{array} \right) \end{array} \right)}{\left(EI\right)_P \left(-2\lambda^{*2} \left(\begin{array}{l} -4\lambda^4 + \alpha^{*2}\left(\alpha^{*2} - 3\beta^{*2}\right)\cos\left(2L\beta^*\right) \\ +\beta^2\left(-3\alpha^{*2} + \beta^{*2}\right)\cosh\left(2L\alpha^*\right)) \end{array} \right) \right)} \\ +2\alpha^*\beta^*\sqrt{k_s T}\left(-\alpha^*\sin\left(2L\beta^*\right) + \beta\sinh\left(2L\alpha^*\right)\right)} \tag{8.19}$$

For fixed-head fixed base pile

$$\Phi^* = \frac{\beta^*\left(\alpha^*\sin\left(2L\beta^*\right) + \beta^*\sinh\left(2L\alpha^*\right)\right)}{2\left(-\alpha^{*2}\sin^2\left(L\beta^*\right) + \beta^{*2}\sinh^2\left(L\alpha^*\right)\right)} \tag{8.20}$$

In order to visualize the effect of pile slenderness on the inertial interaction of piles, Equation (8-19) and (8-20) needed to be plotted. But both Equation (8-19) and (8-20) are complex-valued functions, and it is very complex to separate the real part from the imaginary one. Hence, only the separate plots are presented here. Using outputs from Mathematica 12, both the real and imaginary parts are plotted separately in Figure 7-2 through Figure 7-5. Also, the plot of the modulus of the dynamic stiffness variation factor is given in Figure

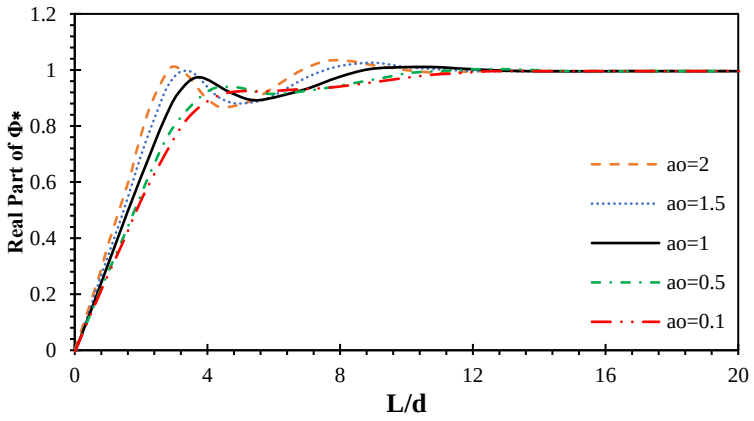

Figure 8-2: Stiffness reduction factor for fixed-head floating base piles in a homogeneous soil profiles subjected to harmonic lateral loading at the top (Real part).

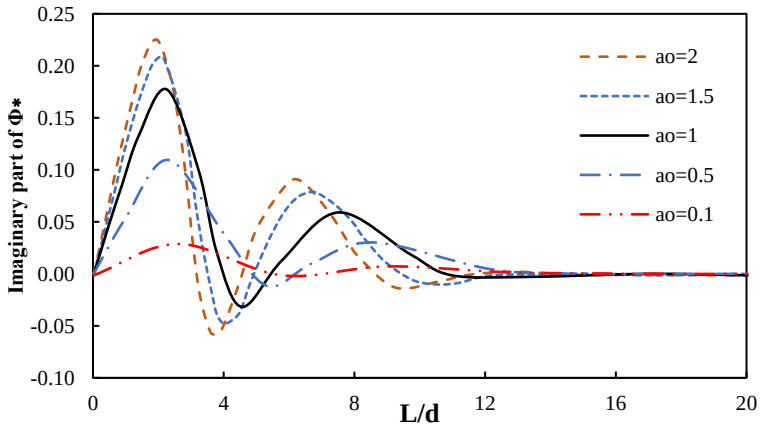

Figure 8-3: Stiffness reduction factor for fixed-head floating base piles in a homogeneous soil profiles subjected to harmonic lateral loading at the top: (Imaginary part).

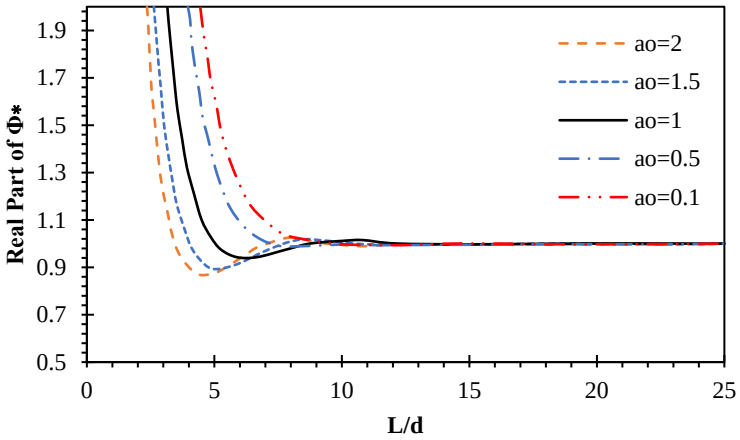

Figure 8-4: Stiffness reduction factor for fixed-head fixed base pile in homogeneous soil profiles subjected to harmonic lateral loading at the top: (Real part).

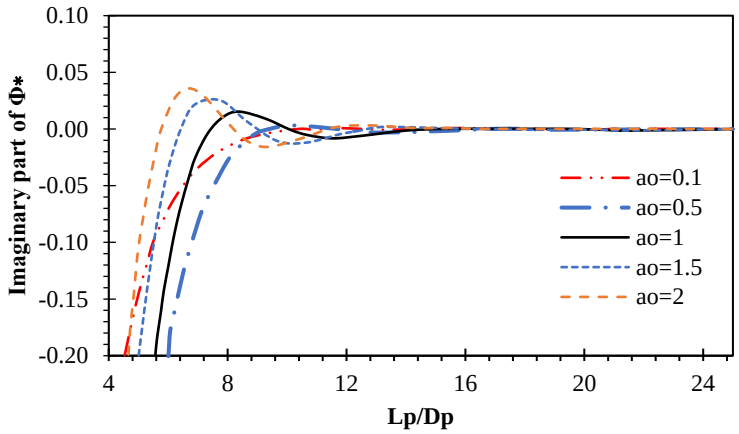

Figure 8-5: Stiffness reduction factor for fixed-head fixed base pile in homogeneous soil profiles subjected to harmonic lateral loading at the top: (Imaginary part).

Figures 8-2 through Figure 8-5 portray the variation of the real and imaginary part of dynamic stiffness variation factor for piles with $E_P / E_s = 1000$, embedded in a homogeneous soil having $\nu_s = 0.4$, $\rho_s = 1900 kg/m^3$ and $\beta_s = 0.05$. Five values of a_o are used (0.1, 0.5, 1, 1.5 and 2), which cover a relatively wide range of frequency, and the following trends are worthy of note

- After some threshold pile slenderness value, L_c, (approximately $L_c = 10$ for a floating base and $L_c = 8$ fixed head-fixed base piles), the real and imaginary parts' converge towards one and zero, respectively. We can find almost similar results by using the critical pile length formulas given in the static case (Equation (4.49) and (4.51) for floating and fixed base piles, respectively). Which implies that frequency has almost no effect on the value of critical pile length. Hence, the value provided for the static case can also be used for the dynamic case.
- Based on the plots, we can deduce that, for long piles ($L > L_c$), the value of K_{HH} can be simplified.

  Equation (8.10) and (8.11) can be rewritten using the complex-valued dynamic stiffness variation factor ($\Phi^* = \mathrm{Re}|\Phi^*| + \mathrm{Im}|\Phi^*|$) as

  $K_{HH} = 4\alpha^* \lambda^{*2} (EI)_P \left(\mathrm{Re}|\Phi^*| + \mathrm{Im}|\Phi \right)$, for long piles $\mathrm{Re}|\Phi^*| = 1$ and $\mathrm{Im}|\Phi^*| = 0$. Substituting back, we get a simplified expression for swaying impedance given in Equation (8.21).

$$K_{HH} = 4\alpha^{*}\lambda^{*2}\left(EI\right)_{P} \tag{8.21}$$

Equation (8.21) is similar to the expression of static swaying stiffness given in Equation (5.22a) with α and λ replaced by α^{*} and λ^{*}.

To provide simplified expressions for both cross swaying-rocking and rock impedance, the real and imaginary parts of the values in the brackets of Equation (8.14), (8.15), (8.17), and (8.19) are plotted below.

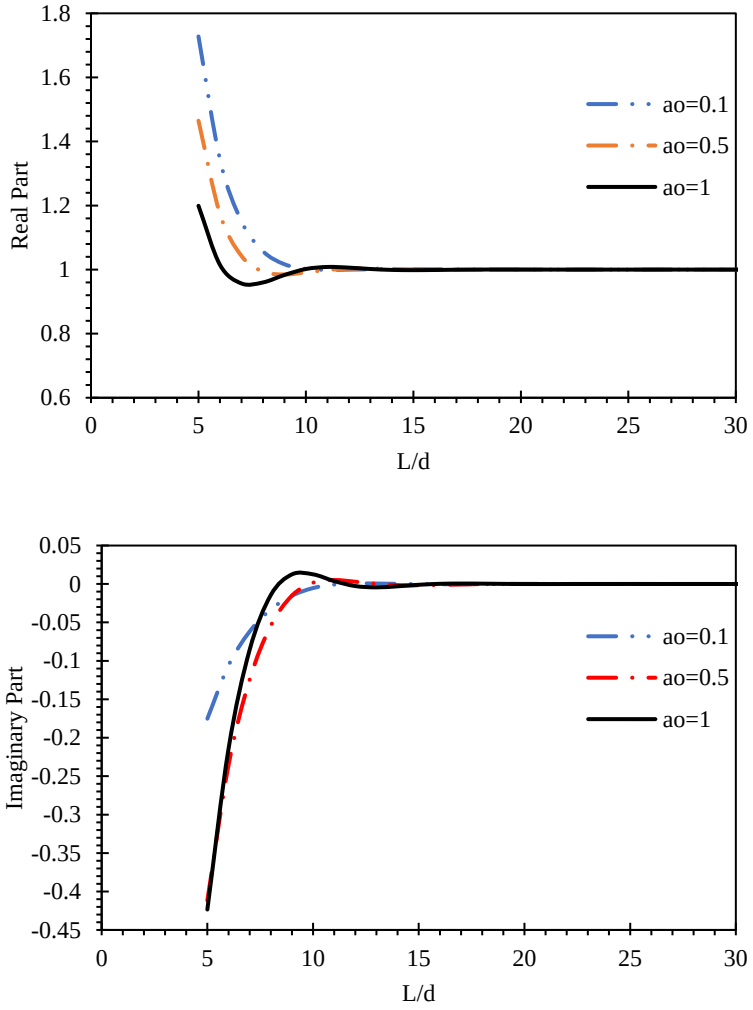

Figure 8-6: Values in the brackets of cross swaying-rocking impedance for fixed-head pile in a homogeneous soil profile subjected to harmonic lateral loading at the top

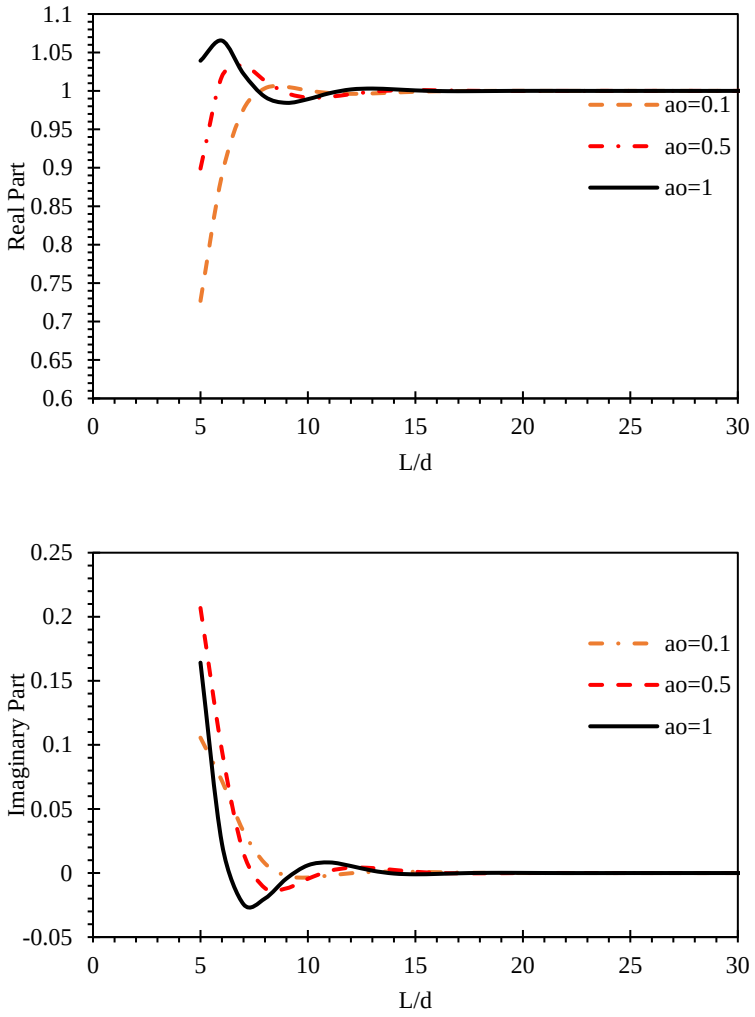

Figure 8-7: Values in the bracket of rocking impedance for fixed-head pile in a homogeneous soil profile subjected to harmonic lateral loading at the top

Figure 8-7 and Figure 8-7 portrays the variation of the real and imaginary part of the values in the bracket of Equation (8.14), (8.15), (8.17) and (8.19); for piles with $E_P / E_s = 1000$, embedded in a homogeneous soil having $v_s = 0.4$, $\rho_s = 1900 kg/m^3$ and $\beta_s = 0.05$. Three values of a_o are used (0.1, 0.5 and 1), and the following trend is worthy of note

- The same observation as the swaying impedance is observed. After some threshold pile slenderness value, the real and imaginary parts' value converges one and zero, respectively.

Following the same procedure used in the swaying case, the expressions for cross swaying-rocking and rocking impedance given in Equation (8.14), (8.15), (8.17) and (8.19) are

simplified, for long piles, to Equation (8.22) and Equation (8.23) for cross swaying-rocking and rocking impedance, respectively,

$$K_{RH} = K_{HR} = 2(EI)_p \lambda^{*2} \tag{8.22}$$

$$K_{RR} = 2(EI)_P \alpha^{*} \tag{8.23}$$

8.4 Model validation

The dynamic response of piles is dependent on the Winkler spring stiffness (k_s). Different literature uses different expressions for k_s . As cited by Rovithis et al. (2013), following the early work of Blaney et al. (1976), Roesset (1980) proposed the relationship:

$$k_s = 1.2E_s \tag{8.24}$$

The same relationships were provided by Makris and Gazetas (1992). Both sources provided the same relationship regardless of pile head condition. Later, Gazetas and Dobry (1984), by matching results from Winkler and elastic continuum analysis for long flexible pile, proposed the expressions in Equation (8.25) and (8.26) for fixed and free-head piles, respectively.

$$k_s = E_s \text{ to } k_s = 1.2E_s \tag{8.25}$$

$$k_s = 1.5E_s \text{ to } k_s = 2.5E_s \tag{8.26}$$

Syngros (2004) presented more improved formulas for fixed (Equation 8.27) and free-head (Equation 8.28) long flexible piles in the homogenous soil layer.

$$k_s = 2E_s \left(\frac{E_p}{E_s} \right)^{-0.075} \tag{8.27}$$

$$k_s = 3.5E_s \left(\frac{E_p}{E_s} \right)^{-0.11} \tag{8.28}$$

In this study, using the Kerr-equivalent Pasternak model proposed by Worku (2014), the Winkler spring (Chapter 4) are determined. So, in this section, the performance of the proposed subgrade model, for inertial interaction, in comparison to other subgrade models, is studied. But first, its performance is validated by using a recent finite element result of Anoyatis et al. (2017).

8.4.1 Validation using finite element

Comparison of the proposed dynamic pile head stiffnesses and damping ratios with results obtained by Anoyatis et al. (2017) using the FE commercial software ANSYS is presented in this section.

Swaying impedance

Various pile-soil systems with slenderness ratios , L/d, of 5, 10 and 20 and different pile-soil stiffness ratios, E_P / E_S, of 100, 1000, 5000 are selected to demonstrate the model performance across a wide range of non-dimensional frequencies a_o (from 0 to 1) in all cases β_S=0.05, ν_S= 0.4 .

From the results portrayed in Figures 8-8, 8-9 and 8-10, one can see that the proposed model is in a very good agreement with the finite element output. This implies that the proposed model can be used to calculate the swaying inertial response of the pile-soil system with a wide range of slenderness and pile stiffness ratio, especially when a quick but reliable result is needed.

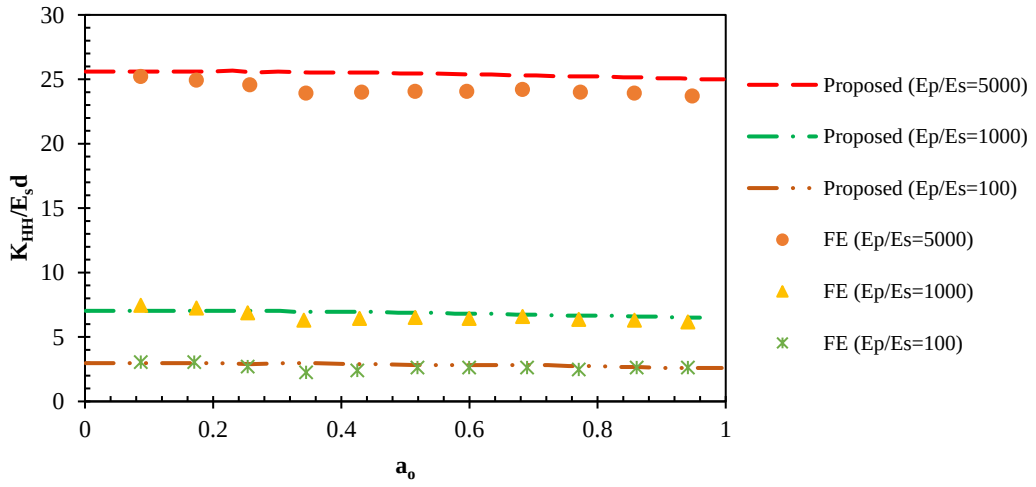

Figure 8-8: Comparison of results from the proposed swaying impedance against results from finite element analyses for $L/d = 5$.

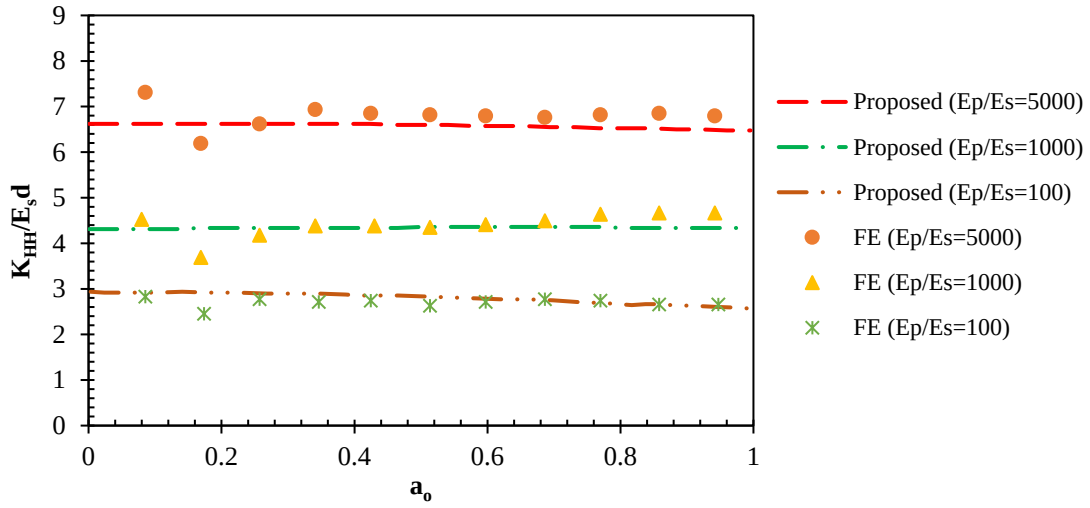

Figure 8-9: Comparison of results from the proposed swaying impedance against results from finite element analyses for $L/d = 10$

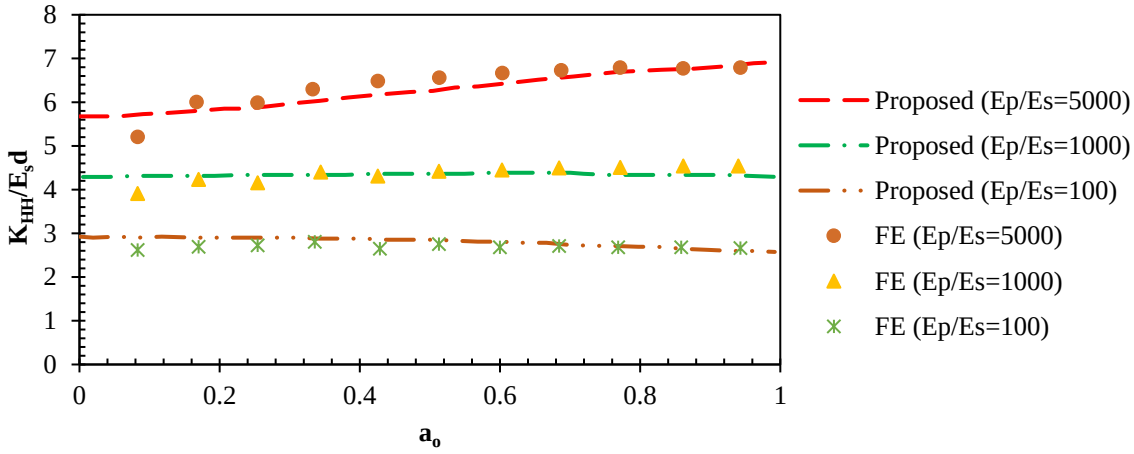

Figure 8-10: Comparison of results from the proposed swaying impedance against results from finite element analyses for $L/d = 20$.

Figure 8-9 and Figure 8-10 show that at low frequency, there is some discrepancy between the proposed model and FE results. This is mainly because of the first resonance ($a_o = a_{cutoff}$). The proposed model cannot capture the effects associated with the first resonance, so that additional correction should be given in future studies.

Cross swaying-rocking impedance

Various pile-soil systems with slenderness ratios, $L/d = 20$, and different pile-soil stiffness ratios, E_P/E_S, of 100, 1000, 5000 are selected to demonstrate the model performance across a wide range of non-dimensional frequencies a_o (from 0 to 1) in all

cases $\beta_s = 0.05$, $v_s = 0.4$. All the finite element data shown in Figure 8-11 are obtained from Anoyatis et al. (2017); as stated above,

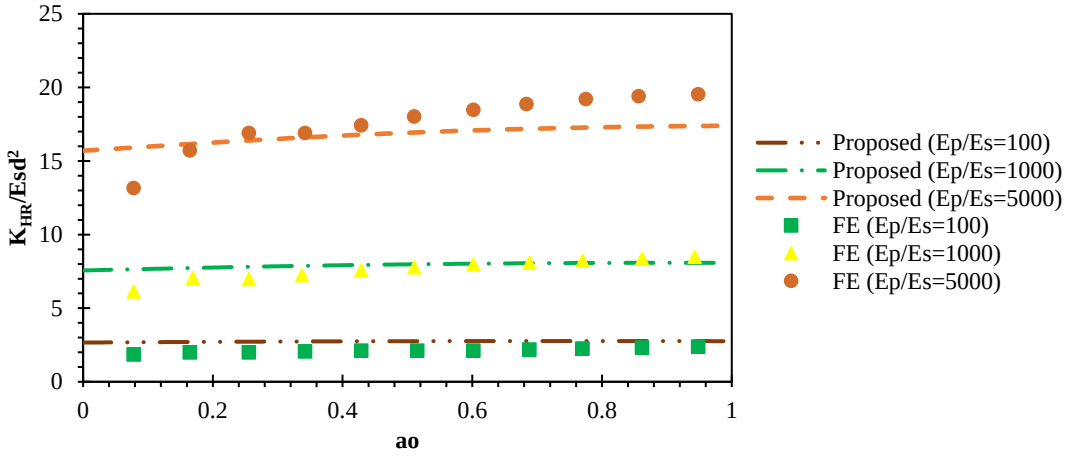

Figure 8-11: Comparison of the proposed cross swaying-rocking impedance against results from finite element result for $L/d = 20$.

From the results portrayed in Figure 8-11, the FE and the proposed model's comparisons indicate an excellent performance of the proposed model for soils with medium or high stiffness ($E_P / E_s = 100$ and $E_P / E_s = 1000$), and good performance was observed for soils with low stiffness ($E_P / E_s = 5000$).

Rocking impedance

Various pile-soil systems with slenderness ratios , $L/d = 20$, and different pile-soil stiffness ratios, E_P / E_S, of 100, 1000, 5000 are selected to demonstrate the model performance across a wide range of dimensionless frequencies a_o (from 0 to 1) in all cases $\beta_s = 0.05$, $v_s = 0.4$.

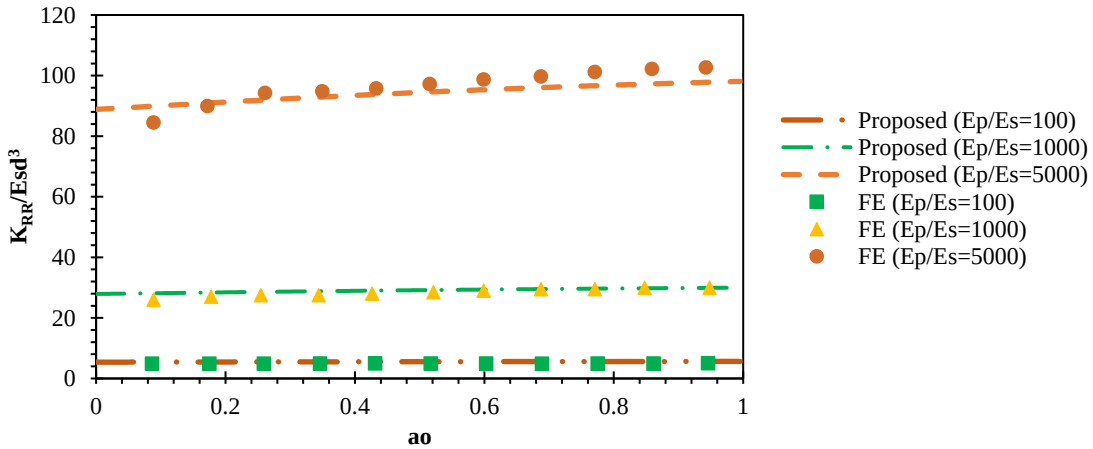

Figure 8-12: Comparison of the proposed rocking impedance against results from finite element result for $L/d = 20$.

Comparisons of the FE and the proposed model results, as shown in Figure 8-12, indicate the excellent performance of the proposed model for all three stiffnesses across the entire range of frequencies examined.

8.4.2 Comparison with Winkler models from literature

Using Winkler modulus from literature (Dobry et al. (1982), Makris and Gazetas (1992) and Kavvadas et al. (1993)), the dynamic pile head stiffnesses are similarly computed and compared with that of the proposed model.

8.4.2.1 Swaying impedance

The influence of E_P / E_S is portrayed in Figure 8-13, for pile having $L/d = 30$, embedded in a homogeneous soil having $v_s = 0.4$, $\rho_s = 1900\ kg/m^3$ and $\xi_s = 5\%$.

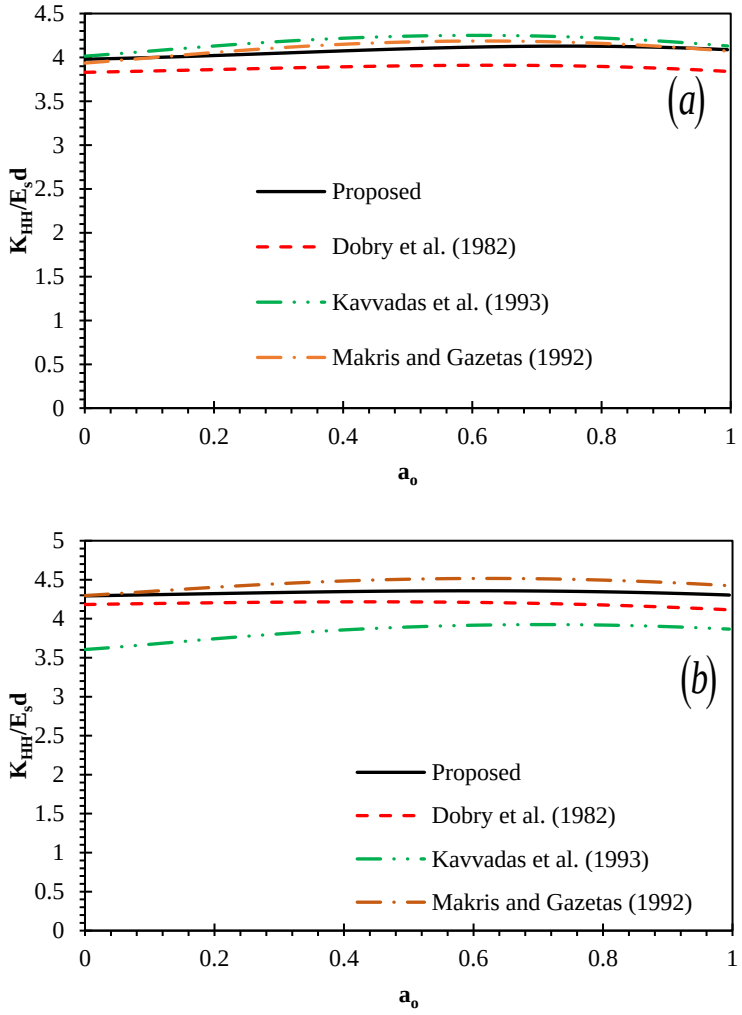

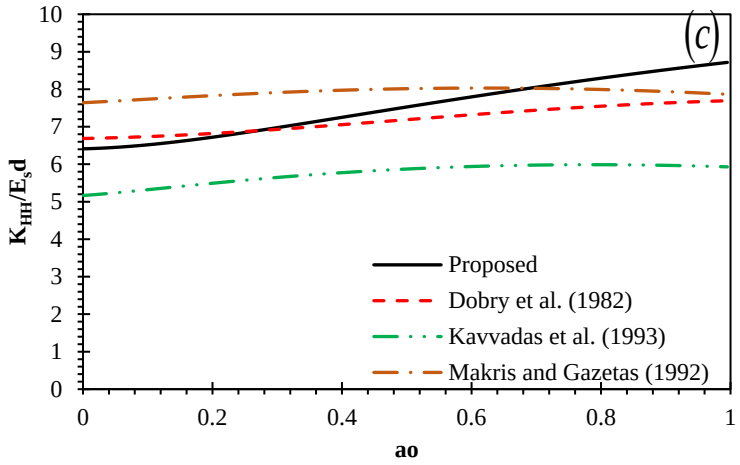

Figure 8-13: Comparison of the proposed model against results from literature for

(a) $E_P / E_s = 100$ **(b)** $E_P / E_s = 1000$ **(c)** $E_P / E_s = 10,000$

From the above three figures, the following points are worth noting

- We can see that the Winkler modulus proposed by the other researchers give close results for only stiff piles in medium or high stiffness soils. But for soils with low stiffness, only the proposed model produces a good result that agrees with FE results, as could be confirmed by the plots Figure 8-8, 8-9, and 8-10.
- Also, from the figures, the one proposed by Dobry et al. (1982) is in much better agreement to the proposed model and the Kavvadas et al. (1993) model significantly underestimated the swaying dynamic impedance.
- Finally, it's worth noting that all the analytical models used above can not capture the resonance effect observed in the FE result.

8.4.2.2 Cross swaying-rocking impedance

The influence of E_P / E_S is portrayed in Figure 8-14, for pile having $L / d = 30$, embedded in a homogeneous soil having $v_s = 0.4$, $\rho_s = 1900\ kg/m^3$ and $\xi_s = 5\%$.

From the figures, we can see that the Winkler modulus proposed by the other researchers give close results for only stiff piles in medium or high stiffness soils. But for soils with low stiffness, only the proposed model produces a good result that agrees with FE results, as could be confirmed by the plots Figure 8-11.

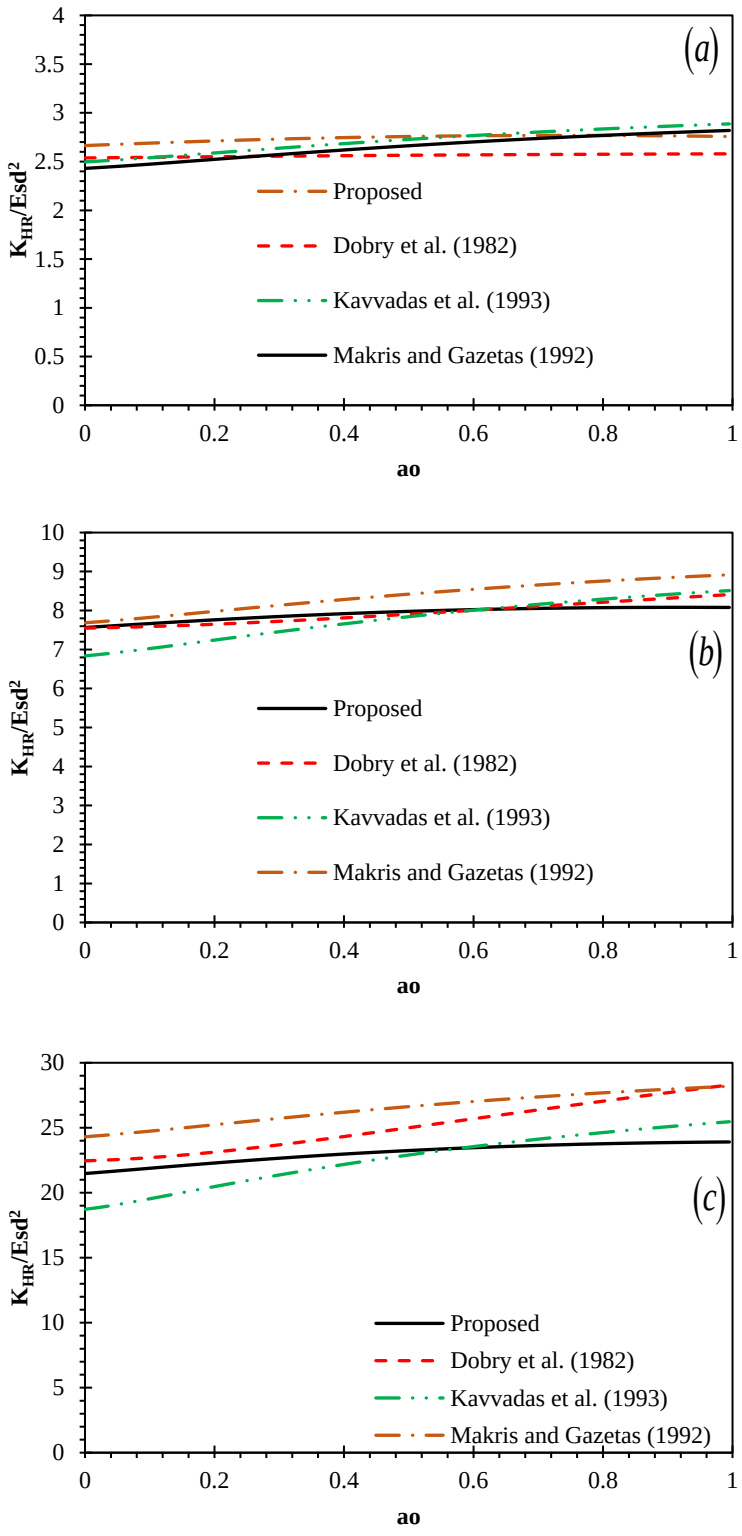

Figure 8-14: Comparison of the proposed cross swaying-rocking model against models from literature for (a) $E_P / E_s = 100$ **(b)** $E_P / E_s = 1000$ **(c)** $E_P / E_s = 10,000$

8.4.2.3 Rocking impedance

The influence of E_P / E_S is portrayed in Figure 8-15, for pile having $L/d = 30$, embedded in homogeneous soil having $v_s = 0.4$, $\rho_s = 1900\ kg/m^3$ and $\xi_s = 5\%$.

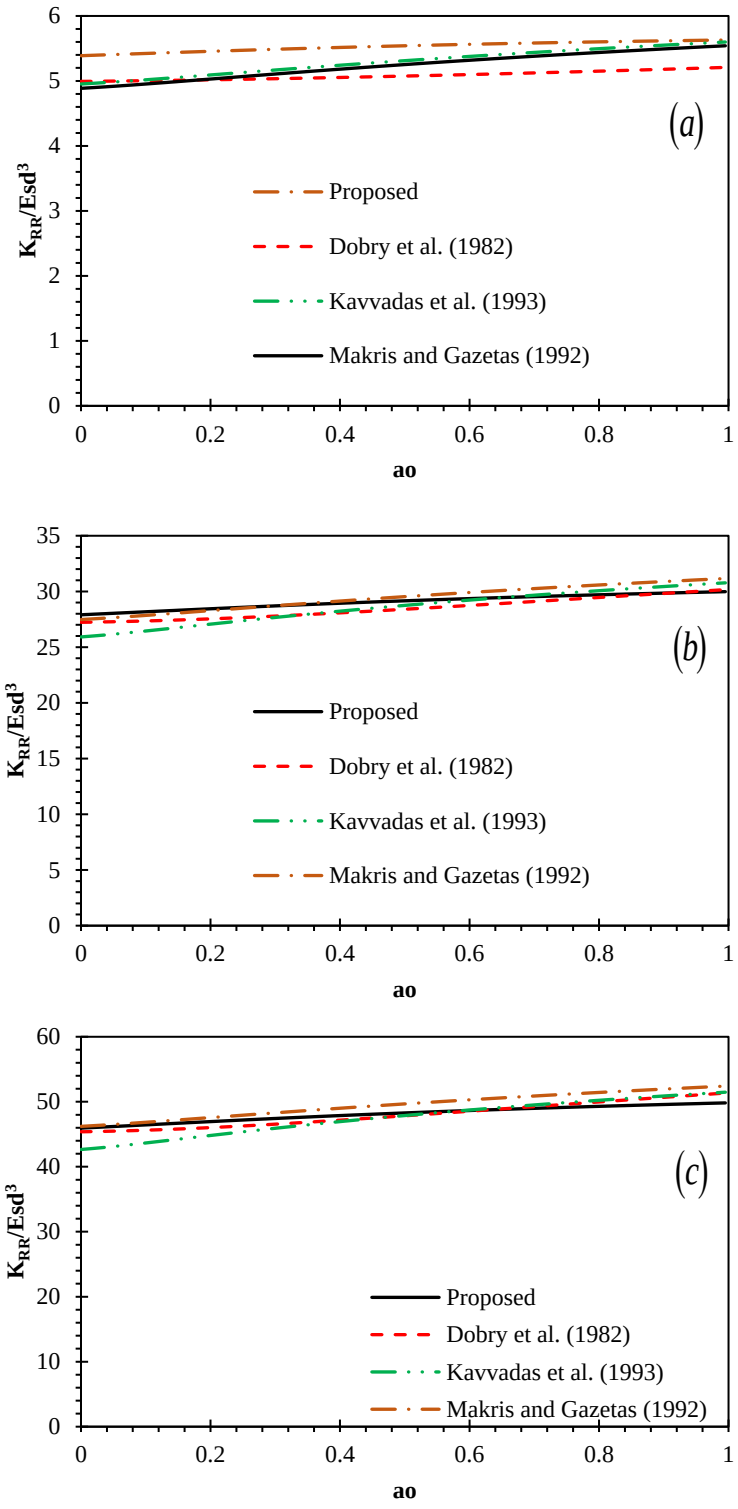

Figure 8-15: Comparison of the proposed rocking model against models from literature for (a) $E_P / E_s = 100$ **(b)** $E_P / E_s = 1000$ **(c)** $E_P / E_s = 2000$

From the figures, we can see that the Winkler modulus proposed by the other researchers give close results for all pile-soil stiffness ratios used.

CHAPTER 9
CONCLUSIONS AND RECOMMENDATIONS

9.1 Summary and Conclusions

This research aims to study single piles' static and dynamic response using a rigorous two-parameter subgrade model derived by Worku (2014). The subgrade model is complete with its own subgrade parameters given in closed-form while leaving a single factor, χ, open for calibration purpose. Some of the important findings are presented below:

Static response (Chapter 4)

Static lateral pile response is efficiently simulated for four different boundary conditions through the Kerr-equivalent Pasternak model. The model appears to provide excellent values of the equivalent spring coefficient K_{HH} (within 5 % margin of error as compared to FEM) for a single pile in a homogeneous soil for all four different boundary conditions.

The pertinent adjustment/calibration factor, χ, left open in the model has been established. It is obtained from rigorous parametric study and curve fitting with output from PLAXIS 3D. It has been found that its value is dependent on the pile slenderness ratio, L/d, pile-soil stiffness ratio, L/d, and the soil Poisson's ratio, v_s. Form the relations given in Equation (4.17) and Equation (4.18), it is clear that the calibration factor χ is more dependent on the pile stiffness ratio for fixed-head piles and on the soil's Poisson's ratio for free-head piles.

Furthermore, using a new approach which uses the pile head stiffness as a criterion, the critical (active) pile length for all soil-pile boundary conditions was also determined. In order to visualize the variation of the pile head stiffness a new parameter called variation factor, Φ, was introduced. The expression and the definition for Φ is unique to this work. The critical pile length established shows a very good agreement with the expression given in pertinent literature. It was also observed that the critical pile length is about 12% larger for fixed-head conditions as compared to the free head conditions. The trend is anticipated since a fixed head pile is stiffer and, thereby, mobilizes soil reaction at higher depths.

An additional classification to the conventional "short" and "long" pile is introduced based on the rate at which the pile-head stiffness varies. This new class is termed as a "transitional state" and exists between the "short" and "long" thresholds ($L'_c < L < L_c$). The corresponding expressions for the pile head stiffness was also provided for piles within the "transitional state". The simplified expressions use the stiffness variation factor and pile-head stiffness of long flexible piles.

Finally, a detailed parametric comparison is performed to assess the performance of the proposed model when compared to those in the literature. The model performance for static analysis of laterally loaded piles is strikingly excellent, while its ability to predict the response of rigid (stocky) piles is unique.

Static pile head stiffnesses (Chapter 5)

The two-parameter subgrade model proposed by Worku (2014) with the calibrated adjustment factor, χ, used in Chapter 4 was extended for cross swaying-rocking, K_{HR}, and rocking, K_{RR}, pile head stiffnesses.

First, by solving the stiffness matrix using different boundary and loading conditions, the expressions of all pile-head stiffnesses are obtained. Similar to the swaying pile head stiffness given in Chapter 4, the expression of the cross swaying-rocking, K_{HR}, and the rocking, K_{RR}, pile head stiffnesses for long piles and general case are shown separately.

Finally, a detailed parametric comparison is performed to assess the proposed model's performance with those in the literature. The model performance for the analysis of static both cross swaying-rocking, K_{HR}, and the rocking, K_{RR}, pile head stiffnesses was excellent.

Damping Model (Chapter 6)

A new model is developed for the distributed Winkler radiation damping coefficient based on a simplified approach proposed by Gazetas and Dobry (1984). The value of the damping coefficient obtained is in good agreement with that of Gazetas and Dobry (1984) and Anoyatis and Lemnitzer (2017).

Also, equivalent damping coefficient at the pile head for fixed-head and free-head piles is determined based on the approach proposed by Gazetas and Dobry (1984).

The following trends can be seen from the proposed damping model

- The dashpot coefficient, c_x, equals the material damping for forcing frequency less than or equal to the natural frequency of the soil layer.
- The proposed damping model is a function of Poisson's ratio, shear wave velocity, soil density, pile diameter and dimensionless frequency ratio.

Kinematic Soil-Pile Interaction (Chapter 7)

The Kerr-equivalent Pasternak model is also used for investigating the kinematic soil-pile interaction for a pile of length L embedded in a homogeneous soil layer for different boundary conditions at the head and base. Analytical solutions for pile response were derived in closed form.

Owing to its simplicity, the adopted analytical model can shed light on certain fundamental mechanisms controlling pile–soil interaction. Its performance, however, is related to the proper selection of calibration factor χ which depends on Poisson's ratio, pile–soil stiffness ratio and boundary conditions.

The proposed analytical solution with the factor χ, established in the static case, is compared with finite element results from Anoyatis et al. (2013). It is clear that the proposed analytical solution is in a very good agreement with FE results.

Inertial Soil-Pile Interaction (Chapter 8)

A simplified method for evaluating all pile head stiffnesses under inertial loading using the two-parameter subgrade model is used. It is established that the pile head stiffnesses obtained appear to be almost independent of the excitation frequency (f) for stiff to moderately stiff soils. In contrast, the excitation frequency (f) has a considerable effect on soft soils. The same trend is observed in the FE results of Anoyatis et al. (2017).

The effect of critical pile length is examined using detailed parametric studies. From the results, it is clear that the pile length is almost independent of the excitation frequency. For

this reason, the critical pile length expressions given in Chapter 4 are recommended for use in both static and dynamic cases.

The proposed analytical model allows closed-form solutions for the pile stiffness at the pile head to be obtained for homogeneous soil. Results for pile stiffness obtained with the proposed method are in good agreement with available numerical solutions and finite element output.

The proposed method can be implemented in hand calculations or simple computer spreadsheets and, thereby, can be used in routine calculations for designing piles against lateral dynamic loads.

9.2 Recommendations for future research

This study is limited to single piles' static and dynamic lateral response in a homogenous soil layer. The following main points can be suggested for future work.

- The current work focuses on piles in a homogenous soil layer. More work is needed to account for soil inhomogeneity in analyzing piles' static and dynamic lateral response.
- The current work studied only lateral response of single piles. Which is not true for most civil engineering problems. Further work is needed to study and improve pile group response. In doing so, it is expected to come up with improved interaction factors between two piles.

REFERENCE

Anoyatis, G., Di Laora, R. and Lemnitzer, A. (2017). "Dynamic pile impedances for fixed-tip piles." Soil Dynamics and Earthquake Engineering 97: 454-467.

Anoyatis, G., Di Laora, R., Mandolini, A. and Mylonakis, G. (2013). "Kinematic response of single piles for different boundary conditions: Analytical solutions and normalization schemes." Soil Dynamics and Earthquake Engineering 44: 183-195.

Anoyatis, G. and Lemnitzer, A. (2017). "Dynamic pile impedances for laterally–loaded piles using improved Tajimi and Winkler formulations." Soil Dynamics and Earthquake Engineering 92: 279-297.

Anoyatis, G. and Lemnitzer, A. (2017). "Kinematic Winkler modulus for laterally-loaded piles." Soils and Foundations 57(3): 453-471.

Anoyatis, G., Mylonakis, G. and Lemnitzer, A. (2016). "Soil reaction to lateral harmonic pile motion." Soil Dynamics and Earthquake Engineering 87: 164-179.

Ben Jamaa, S. and Shiojiri, H. (2000). "A Method for Three Dimensional Interaction Analysis of Pile-Soil System in Time Domain." Transactions of the Japan Society for Computational Engineering and Science 2000.

Berger, E., Mahi, S. A. and Pyke, R. (1977). Simplified Method For Evaluating Soil-Pile-Structure Interaction Effects. Offshore Technology Conference. Houston, Texas, Offshore Technology Conference: 10.

Biot, M. A. (1937). "Bending of an infinite beam on an elastic foundation." Journal of Applied Mathematics Mechanics 2(3): 165-184.

Bowles, L. (1997). Foundation analysis and design. Singapore, McGraw-hill.

Broms, B. B. (1964). "Lateral Resistance of Piles in Cohesionless Soils." JOrnal of the Soil Mechanics and Foundations Division 90(3): 123-156.

Buckingham, E. (1914). "On Physically Similar Systems; Illustrations of the Use of Dimensional Equations." Physical Review 4(4): 345-376.

CEN/TC 250 (2004). Eurocode 8: Design of structures for earthquake resistance Part 5: Foundations, retaining structures and geotechnical aspects. Brussels, Belgium, European Committee for Standardization.

Dobry, R. and O'Rourke, M. J. (1983). "Discussion of seismic response of end-bearing piles." Jornal of Geotechnical Engineering 109(5): 778-781.

Dobry, R., O'Rourke, M. J., Roesset, J. M. and Vicente, E. (1982). "Horizontal stiffness and damping of single piles." Journal of the Geotechnical Engineering Division 108(GT3): 439-459.

Filonenko-Borodich, M. M. (1950). "Some approximate theories of elastic foundations,." Uchenyie Zapiski Moskovskogo Gosudarstuennogo Universiteta Mekhanika 46: 3–18.

Flores-Berrones, R. and Whitman, R. V. (1982). "Seismic response of end-bearing piles." Journal of Geotechnical Geoenvironmental Engineering 108(GT4).

Francis (1964). "Analysis of pile groups with flexural resistance." Journal of Soil Mechanics 90(Proc. Paper 3887).

Gazetas, G. (1984). "Seismic response of end-bearing single piles." International Journal of Soil Dynamics and Earthquake Engineering 3(2): 82-93.

Gazetas, G. (1991a). "Formulas and Charts for Impedances of Surface and Embedded Foundations." Journal of Geotechnical Engineering 117(9): 1363-1381.

Gazetas, G. (1991b). Foundation Vibrations. Foundation Engineering Handbook. H.-Y. Fang. Boston, MA, Springer US: 553-593.

Gazetas, G. and Dobry, R. (1984). "Horizontal response of piles in layered soils." Jornal of Geotechnical Engineering 110(1): 20-40.

Gazetas, G., Fan, K., Tazoh, T., Shimizu, K., Kavvadas, M. and Makris, N. (1992). Seismic pile-group-structure interaction. Piles under dynamic loads, ASCE.

Guo, W. D. (2001). Subgrade modulus for laterally loaded piles. Proceedings of the Eighth International Conference on Civil and Structural Engineering Computing, Scotland.

Guo, W. D. and Lee, F.-H. (2001). "Load transfer approach for laterally loaded piles." International Journal for Numerical and Analytical Methods in Geomechanics 25: 1101-1129.

Gupta, B. and Basu, D. (2019). "Computationally Efficient Three-Dimensional Continuum-Based Model for Nonlinear Analysis of Laterally Loaded Piles." Journal of Engineering Mechanics.

Helwany, S. (2007). Applied soil mechanics with ABAQUS applications. USA, John Wiley & Sons, Inc.

Hetenyi, M. (1946). Beams on elastic foundations. USA, University of Michigan Press, Ann Arbor, MI.

Hetenyi, M. (1950). "A general solution for the bending of beams on an elastic foundation of arbitrary continuity." J. Appl. Phys. 21: 55–58.

Higgins, W., Vasquez, C., Basu, D. and Griffiths, D. V. (2013). "Elastic Solutions for Laterally Loaded Piles." Journal of Geotechnical and Geoenvironmental Engineering 139(7): 1096-1103.

Kavvadas, M., Gazetas, G. and Gazetas, G. (1993). "Kinematic seismic response and bending of free-head piles in layered soil." Geotechnique 43(2): 207-222.

Kerr, A. D. (1964). "Elastic and viscoelastic foundation models." Journal of Applied Mechanics 31(3): 491-498.

Kondner, R. L. (1963). "Hyperbolic Stress-Strain Response: Cohesive Soils." Journal of the Soil Mechanics Foundations Division 89: 115-143.

Kramer, S. L. (1996). Geotechnical Earthquake Engineering. Upper Saddle River, NJ, USA, Pearson Education (US).

Kuhlemeyer, R. L. (1979). "Static and dynamic laterally loaded floating piles." Journal of Geotechnical Geoenvironmental Engineering 105(2): 289-304.

Kuhlemeyer, R. L. (1979). "Static and dynamic laterally loaded floating piles." 105(ASCE 14394).

Makris, N. and Gazetas, G. (1992). "Dynamic pile-soil-pile interaction. Part II: Lateral and seismic response." Earthquake Engineering & Structural Dynamics 21: 145-162.

Matlock, H. (1970). Correlation for Design of Laterally Loaded Piles in Soft Clay. Offshore Technology Conference.

Matlock, H. (1970). Correlation for design of laterally loaded piles in soft clay. Offshore technology conference, OnePetro.

Matlock, H. (1970). Correlations for design of laterally loaded piles in soft clay. Offshore Technology Conference. Houston, Texas, Offshore Technology Conference: 77-94.

McClelland, B. and Focht, J. (1956). "Soil Modulus for Laterally Loaded Piles." 82(4): 1081-1081-1081-1022.

Mcclelland, B. and Focht, J. A. (1956). "Soil Modulus for Laterally Loaded Piles." Journal of the Soil Mechanics Foundations Division 123: 1-22.

Moghaddasi, M., Cubrinovski, M., Chase, J. G., Pampanin, S. and Carr, A. (2011). "Effects of soil–foundation–structure interaction on seismic structural response via robust Monte Carlo simulation." Engineering Structures 33(4): 1338-1347.

Molenkamp, F. and Smith, I. M. (1980). "Hysteretic and viscous material damping." International Journal for Numerical and Analytical Methods in Geomechanics 4(4): 293-311.

Mostafa, Y. and El Naggar, M. H. (2002). "Dynamic analysis of laterally loaded pile groups in sand and clay." Canadian Geotechnical Journal 39: 1358-1383.

Mylonakis, G. (1995). Contributions to static and seismic analysis of piles and pile-supported bridge piers PhD dissertation, State University of New York at Buffalo.

Mylonakis, G. (2001). "Elastodynamic model for large-diameter end-bearing shafts." Soils and foundations 41(3): 31-44.

Mylonakis, G., Nikolaou, S. and Gazetas, G. (2006). "Footings under seismic loading: Analysis and design issues with emphasis on bridge foundations." Soil Dynamics and Earthquake Engineering 26(9): 824-853.

Ng, C. W. W. and Zhang, L. M. (2001). "Three-Dimensional Analysis of Performance of Laterally Loaded Sleeved Piles in Sloping Ground." Journal of Geotechnical and Geoenvironmental Engineering 127(6): 499-509.

Nogami, T. and Novak, M. (1977). "Resistance of soil to a horizontally vibrating pile." Earthquake Engineering and Structural Dynamics 5(3): 249-261.

Nogami, T. and Novak, M. (1977). Resistance of soil to a horizontally vibrating pile.

Novak, M. (1974). "Dynamic stiffness and damping of piles." Canadian Geotechnical Journal 11(4): 574-598.

Novak, M. (1974). "Effect of soil on structural response to wind and earthquake." 3(1): 79-96.

Novak, M., Aboul-Ella, F. and Nogami, T. (1978). "Dynamic soil reactions for plane strain case." Journal of the Engineering Mechanics Division 104(4): 953-959.

Novak, M. and Nogami, T. (1977). "Soil-pile interaction in horizontal vibration." Earthquake Engineering & Structural Dynamics 5(3): 263-281.

O'Rourke, M. J. and Dobry, R. (1982). "Spring and dashpot coefficients for machine foundations on piles." ACI Symposium Publication 78: 177-198.

Obrzud, R. and Truty, A. (2012). "The hardening soil model-a practical guidebook z soil." PC100701 Report.

Pacheco, G., Suarez, L. and Pando, M. (2008). Dynamic lateral response of single piles considering soil inertia contributions.

Pasternak, P. L. (1954). "On a new method of an elastic foundation by means of two foundation constants." Gosudarstvoennoe Izdatelstvo Literaturi po Stroitelsuve I Arkhitekture, Moscow (in Russian).

Pender, M. J. (1993). "Aseismic pile foundation design analysis." Bulletin of the New Zealand society for Earthquake Engineering 26: 49-160.

Poulos, H. G. and Davis, E. H. (1980). Pile Foundation Analysis and Design. Canada, The University of Sydney.

Randolph, M. F. (1981). "The response of flexible piles to lateral loading." Geotechnique 31(2): 247-259.

Reese, L. C. (1977). "Laterally loaded piles: program documentation." Journal of the Geotechnical Engineering Division 103(4): 287-305.

Reese, L. C., Cox, W. R. and Koop, F. D. (1974). Analysis of Laterally Loaded Piles in Sand. Offshore Technology Conference.

Reese, L. C. and Impe, W. F. V. (2011). Single piles and pile groups under lateral loading. London,UK, Taylor & Francis Publishers.

Reese, L. C. and Matlock, H. (1960). Numerical analysis of laterally loaded piles, University of Texas, Bureau of Engineering Research.

Reese, L. C. and Sullivan, W. R. (1984). Documentation of Computer Program COM624, University of Texas at Austin. Geotechnical Engineering Center.

Reese, L. C. and Welch, R. C. (1975). "Lateral loading of deep foundations in stiff clay." Journal of the Geotechnical engineering division 101(7): 633-649.

Roesset, J. M. (1980). Stiffness and damping coefficients of foundations. Proc. ASCE Geotechnical Engineering Division National Convention.

Rovithis, E., Mylonakis, G. and Pitilakis, K. (2013). "Dynamic stiffness and kinematic response of single piles in inhomogeneous soil." Bulletin of Earthquake Engineering 11: 1949–1972.

Rovithis, E., Pitilakis, K. and Mylonakis, G. (2009). "Seismic analysis of coupled soil-pile-structure systems leading to the definition of a pseudo-natural SSI frequency." Soil Dynamics and Earthquake Engineering 29: 1005-1015.

Scott, R. F. (1981). Foundation analysis. New Jersey, USA, Prentice-Hall, Englewood Cliffs, N.J.

Shirato, M., Kohno, T. and Nakatani, S. (2009). Geotechnical criteria for serviceability limit state of horizontally loaded deep foundations. Geotechnical Risk and Safety, CRC Press: 133-140.

Skempton, A. W. (1984). The Bearing Capacity of Clays. SELECTED PAPERS ON SOIL MECHANICS: 50-59.

Sun, K. (1994). "Laterally Loaded Piles in Elastic Media." Jornal of Geotechnical Engineering 120(8): 1324-1344.

Syngros, K. (2004). Seismic response of piles and pile-supported bridge piers evaluated through case histories. PhD, City University of New York.

Vardanega, P. J. and Bolton, M. D. (2013). "Stiffness of Clays and Silts: Normalizing Shear Modulus and Shear Strain." 139(9): 1575-1589.

Velez, A., Gazetas, G. and Krishnan, R. (1983). "Lateral dynamic response of constrained head piles." Jornal of Geotechnical Engineering 109(8): 1063-1081.

Vesic, A. B. (1961). "Bending of beams resting on isotropic elastic solid." Journal of the Engineering Mechanics Division 87(2): 35-54.

Vicente, E. (1982). Equivalent spring and damping coefficients of piles subjected to horizontal dynamic loading. MSc, Rensselaer Polytechnic Institute.

Whitman, R. V. and Richart, F. E. (1967). Design procedures for dynamically loaded foundations.

Worku, A. (2010). Part I: A Generalized Formulation of Continuum Models for Elastic Foundations. GeoFlorida 2010: 1641-1650.

Worku, A. (2013). "Calibrated analytical formulas for foundation model parameters." International Journal of Geomechanics, ASCE: 340–347.

Worku, A. (2014). "Development of a calibrated Pasternak foundation model for practical use." International Journal of Geotechnical Engineering 8(1): 26-33.

Yang, Z. and Jeremić, B. (2002). "Numerical analysis of pile behaviour under lateral loads in layered elastic–plastic soils." International Journal for Numerical and Analytical Methods in Geomechanics 26(14): 1385-1406.

Yin, J.-H. (2000). "Closed-form solution for reinforced timoshenko beam on elastic foundation." Journal of Engineering Mechanics 126(8): 868-874.

APPENDIX

A. APPENDIX A

A.1 Solution for the differential equation (Equation (4.5))

The governing differential equation of a beam on a two-parameter subgrade model is derived in Section (4.2.2). In this section, a detailed solution for it is presented

The differential equation, as it can be seen in Equation (A.1), is of order four, and it is solved using the method of variation of parameters.

$$(EI)_P \frac{d^4 w(z)}{dz^4} - T\frac{d^2 w(z)}{dz^2} + k_s w(z) = 0 \tag{A.1}$$

Substituting $w(z) = e^{mz}$ into Equation (A.1), the following characteristic equation is obtained

$$(EI)_P m^4 e^{mz} - Tm^2 e^{mz} + k_s e^{mz} = 0 \tag{A.2}$$

After simple forward simplification, the characteristic equation has a form

$$m^4 - \frac{T}{(EI)_P} m^2 + \frac{k_s}{(EI)_P} = 0 \tag{A.3}$$

The characteristic equation can generally have up to four distinct roots. They are given by

$$m_1 = \sqrt{\frac{T}{2(EI)_p} + i\sqrt{\frac{k_s}{EI} - \left(\frac{T}{2EI}\right)^2}}\ ,\ m_2 = -\sqrt{\frac{T}{2(EI)_p} + i\sqrt{\frac{k_s}{EI} - \left(\frac{T}{2EI}\right)^2}}$$

$$m_3 = \sqrt{\frac{T}{2(EI)_p} - i\sqrt{\frac{k_s}{EI} - \left(\frac{T}{2EI}\right)^2}} \text{ and } m_4 = -\sqrt{\frac{T}{2(EI)_p} - i\sqrt{\frac{k_s}{EI} - \left(\frac{T}{2EI}\right)^2}}$$

With this roots, the general solution of Equation (A.1) is obtained as

$$w(z) = A_1 e^{m_1 z} + A_2 e^{m_2 z} + A_3 e^{m_3 z} + A_4 e^{m_4 z} \tag{A.4}$$

The expression under the internal square root in all the roots given above can be positive, zero, or negative. Hence, three cases arrive that are treated separately below,

Case 1 (Positive internal square root)

In order for the expression under the internal square root to be positive, the following inequality must be satisfied

$$\frac{k_s}{EI} > \left(\frac{T}{2EI}\right)^2 \text{ which implies, } T < 2\sqrt{(EI)_p\, k_s}$$

According to Hetenyi (1946), Scott (1981) and (Yin 2000), in normal conditions, pile is stronger than the surrounding soil. So, in most practical problems, the force T has a value in the region covered by this case.

In this case, four m distinct roots exists as two pairs of complex conjugate numbers. They are found as follows:

$$m_1 = \sqrt{\frac{T}{2(EI)_p} + i\sqrt{\frac{k_s}{EI} - \left(\frac{T}{2EI}\right)^2}}$$

$$= \sqrt{\frac{T}{2(EI)_p} + i\sqrt{\left(\sqrt{\frac{k_s}{EI}}\right)^2 - \left(\frac{T}{2EI}\right)^2}}$$

$$= \sqrt{\frac{T}{2(EI)_p} + i\sqrt{\left(\sqrt{\frac{k_s}{EI}} - \frac{T}{2EI}\right)\left(\sqrt{\frac{k_s}{EI}} + \frac{T}{2EI}\right)}}$$

$$= \sqrt{\frac{T}{2(EI)_p} + i2\sqrt{\left(\lambda^2 - \frac{T}{4EI}\right)}\sqrt{\left(\lambda^2 + \frac{T}{4EI}\right)}} \quad \text{; where } \lambda^2 = \sqrt{\frac{k_s}{4(EI)_p}}$$

$$= \sqrt{\frac{T}{2(EI)_p} + i2\beta\alpha} \text{ where } \alpha = \sqrt{\left(\lambda^2 + \frac{T}{4EI}\right)} \text{ and } \beta = \sqrt{\left(\lambda^2 - \frac{T}{4EI}\right)}$$

Substituting back $T/2(EI)_p = \alpha^2 - \beta^2$ into the last expression

$$m_1 = \sqrt{\alpha^2 + i2\beta\alpha - \beta^2} = \sqrt{(\alpha + i\beta)^2}$$

$$= \alpha + i\beta$$

The rest of the roots are determined using the same procedure, and the results are given as; $m_2 = -(\alpha + i\beta)$, $m_3 = \alpha - i\beta$ and $m_4 = -(\alpha - i\beta)$.

Using these roots, the general solution (Equation (A.4)) will take a form

$$w(z) = A_1 e^{(\alpha+i\beta)z} + A_2 e^{-(\alpha+i\beta)z} + A_3 e^{(\alpha-i\beta)z} + A_4 e^{-(\alpha-i\beta)z} \tag{A.5a}$$

Equation (A.5a) can further be simplified using equalities; $e^{i\beta z} = \cos(\beta z) + i\sin(\beta z)$ and $e^{-i\beta z} = \cos(\beta z) - i\sin(\beta z)$. And it is given as

$$w(z) = \begin{pmatrix} A_1 e^{\alpha z}\left(\cos(\beta z) + i\sin(\beta z)\right) \\ + A_2 e^{-\alpha z}\left(\cos(\beta z) - i\sin(\beta z)\right) \\ + A_3 e^{\alpha z}\left(\cos(\beta z) - i\sin(\beta z)\right) \\ + A_4 e^{-\alpha z}\left(\cos(\beta z) + i\sin(\beta z)\right) \end{pmatrix} \tag{A.5b}$$

After collecting terms with 'sine' and 'cosine' separately, we have

$$w(z) = \begin{pmatrix} \left((A_1 + A_3)e^{\alpha z} + (A_2 + A_4)e^{-\alpha z}\right)\cos(\beta z) \\ \left((iA_1 - iA_3)e^{\alpha z} + (-iA_2 + iA_4)e^{-\alpha z}\right)\sin(\beta z) \end{pmatrix} \tag{A.5c}$$

Introducing new coefficients into Equation (A.5c), we can have the simplified displacement equation similar to the one given in Equation (4.6).

$$w(z) = \left(C_1 e^{\alpha z} + C_2 e^{-\alpha z}\right)\cos(\beta z) + \left(C_3 e^{\alpha z} + C_4 e^{-\alpha z}\right)\sin(\beta z) \tag{A.6}$$

Case 2 (Zero)

In order, expression under the inside square root to be zero, the following equality must be satisfied

$$\frac{k_s}{EI} = \left(\frac{T}{4EI}\right)^2 \text{ which implies, } T = 2\sqrt{(EI)_p\, k_s}$$

The expression under the inside square root is zero, which implies the four m roots will converge to two real double roots, which can be expressed as; $m_1 = m_3 = \tilde{\alpha}$ and $m_2 = m_4 = -\tilde{\alpha}$ where $\tilde{\alpha} = \sqrt{T/2(EI)_p}$.

According to the variation of parameters approach, whenever there exist non-distinct double real roots, the general solution of Equation (A.1) is obtained as

$$w(z) = (C_1 + zC_2)e^{\alpha z} + (C_3 + zC_4)e^{-\alpha z} \tag{A.7}$$

Case 3 (Negative)

In order, the expression under the inside square root to be negative, the following inequality must be satisfied

$$\frac{k_s}{EI} < \left(\frac{T}{4EI}\right)^2 \text{ which implies, } T < 2\sqrt{(EI)_p\, k_s}$$

Using the same procedure used in Case 1, the values of the four distinct real roots are determined as follows.

$$m_1 = \sqrt{\frac{T}{2(EI)_p} + i\sqrt{\left(\frac{T}{2EI}\right)^2 - \frac{k_s}{EI}}}$$

$$= \sqrt{\frac{T}{2(EI)_p} + i\sqrt{\left(\frac{T}{2EI}\right)^2 - \left(\sqrt{\frac{k_s}{EI}}\right)^2}}$$

$$= \sqrt{\frac{T}{2(EI)_p} + i2\sqrt{\left(\frac{T}{4EI} - \sqrt{\frac{k_s}{4EI}}\right)\left(\sqrt{\frac{k_s}{4EI}} + \frac{T}{4EI}\right)}}$$

$$= \sqrt{\frac{T}{2(EI)_p} + i2\sqrt{\left(\frac{T}{4EI} - \lambda^2\right)\left(\lambda^2 + \frac{T}{4EI}\right)}} \quad ; \text{where } \lambda^2 = \sqrt{\frac{k_s}{4(EI)_p}}$$

$$= \sqrt{\frac{T}{2(EI)_p} + i2\tilde{\beta}\alpha} \text{ where } \tilde{\beta} = i\beta = \sqrt{\left(\frac{T}{4EI} - \lambda^2\right)}$$

Substituting back $T/2(EI)_p = \alpha^2 + \tilde{\beta}^2$ into the last expression

$$m_1 = \sqrt{\alpha^2 + 2\tilde{\beta}\alpha + \tilde{\beta}^2} = \sqrt{\left(\alpha + \tilde{\beta}\right)^2}$$

$$= \alpha + \tilde{\beta}$$

The rest of the roots are given as, $m_2 = -\left(\alpha + \bar{\beta}\right)$, $m_3 = \alpha - \bar{\beta}$ and $m_4 = -\left(\alpha - \bar{\beta}\right)$. Substituting back all the roots back to equation (A.4), the displacement equation for the third case is found to be

$$w(z) = \left(C_1 e^{\alpha z} + C_2 e^{-\alpha z}\right)\cosh\left(\bar{\beta} z\right) + \left(C_3 e^{\alpha z} + C_4 e^{-\alpha z}\right)\sinh\left(\bar{\beta} z\right) \qquad \text{(A.8)}$$

A.2 A typical solution for the deflection equation

In the previous section, the generalized deflection equation for three different cases is derived. Furthermore, in this section, the workflow used in Mathematica 12 for solving the coefficients in the generalized deflection equation for the fixed-head fixed-base pile is presented. The boundary conditions used for the formulation are given in Section 4.2.4.1.

First, by using the boundary conditions at the pile head, the expression of C_1 and C_1 are determined.

I. For fixed-head piles, the slope at the pile head equals zero ($\frac{\mathrm{d}}{\mathrm{d}z} w(z)\Big|_{z=0} = 0$).

Implementing this boundary condition, we have

$$-\alpha C_1 + \beta C_2 + \alpha C_3 + \beta C_4 = 0$$

and solving for C_1;

$$C_1 = \frac{\beta C_2 + \alpha C_3 + \beta C_4}{\alpha}$$

II. The shear at the pile head equals applied load P ($(EI)_P \frac{\mathrm{d}^3}{\mathrm{d}z^3} w(z)\Big|_{z=0} = P$)

After applying this boundary condition, we have

$$2\beta\left(EI\right)_p\left(\alpha^2+\beta^2\right)\left(C_2+C_4\right)=P$$

and solving for C_2

$$C_2=\frac{P-2\alpha^2\beta C_4 EI_p-2\beta^3 C_4 EI_p}{2\beta\left(\alpha^2+\beta^2\right)EI_p}$$

Using the boundary condition at the pile base, the remaining coefficients (C_3 and C_3) are obtained

III. The slope at the pile base equals zero ($\frac{\mathrm{d}}{\mathrm{d}z}w(z)\Big|_{z=L}=0$).

After applying this boundary condition, we have

$$\frac{1}{2\alpha\beta\left(EI\right)_p}\begin{pmatrix}\cosh\left(L\alpha\right)\\-\sinh L\alpha\end{pmatrix}\begin{pmatrix}-P\sin\left(L\beta\right)\\+2\alpha\beta\left(-2\begin{pmatrix}\cosh\left(L\alpha\right)\\+\sinh\left(L\alpha\right)\end{pmatrix}\begin{pmatrix}\beta\cosh\left(L\alpha\right)\sin\left(L\beta\right)\\-\alpha\cos\left(L\beta\right)\sinh\left(L\alpha\right)\end{pmatrix}\right)C_3\left(EI\right)_p\\+2\alpha\beta\left(2\begin{pmatrix}\cosh\left(L\alpha\right)\\+\sinh\left(L\alpha\right)\end{pmatrix}\begin{pmatrix}\alpha\cosh\left(L\alpha\right)\sin\left(L\beta\right)\\+\beta\cos\left(L\beta\right)\sinh\left(L\alpha\right)\end{pmatrix}\right)C_4\left(EI\right)_p\end{pmatrix}=0$$

and solving for C_3

$$C_3=\frac{\left(P\sin\left(L\beta\right)-4\alpha\beta\begin{pmatrix}\cosh\left(L\alpha\right)\\+\sinh\left(L\alpha\right)\end{pmatrix}\begin{pmatrix}\alpha\cosh\left(L\alpha\right)\sin\left(L\beta\right)\\+\beta\cos\left(L\beta\right)\sinh\left(L\alpha\right)\end{pmatrix}C_4\left(EI\right)_p\right)}{\left(4\alpha\beta\begin{pmatrix}\cosh\left(L\alpha\right)\\+\sinh\left(L\alpha\right)\end{pmatrix}\begin{pmatrix}-\beta\cosh\left(L\alpha\right)\sin\left(L\beta\right)\\+\alpha\cos\left(L\beta\right)\sinh\left(L\alpha\right)\end{pmatrix}\left(EI\right)_p\right)}$$

IV. Translation at the pile base equals zero ($w(z)\big|_{z=L} = 0$)

$$\frac{\left(\begin{pmatrix}\cosh(L\alpha)+\sinh(L\alpha)\end{pmatrix}\begin{pmatrix}-P\begin{pmatrix}\beta\cos(2L\beta)-\beta\cosh(2L\alpha)\\+\alpha\sin(2L\beta)+\beta\sinh(2L\alpha)\end{pmatrix}\\+4\beta\left(\alpha^2+\beta^2\right)\begin{pmatrix}\alpha\sin(2L\beta)\\+\beta\sinh(2L\alpha)\end{pmatrix}C_4\left(EI\right)_p\end{pmatrix}\right)}{4\beta\left(\alpha^2+\beta^2\right)\left(\cosh(L\alpha)+\sinh(L\alpha)\right)\begin{pmatrix}\beta\cosh(L\alpha)\sin(L\beta)\\-\alpha\cos(L\beta)\sinh(L\alpha)\end{pmatrix}EI_p}=0$$

solving for C_4

$$C_4=\frac{P\begin{pmatrix}-\beta+\cosh(2L\alpha)\left(\beta\cos(2L\beta)+\alpha\sin(2L\beta)\right)\\+\left(\beta\cos(2L\beta)+\alpha\sin(2L\beta)\right)\sinh(2L\alpha)\end{pmatrix}}{4\beta\left(\alpha^2+\beta^2\right)\left(\cosh(L\alpha)+\sinh(L\alpha)\right)^2\begin{pmatrix}\alpha\sin(2L\beta)\\+\beta\sinh(2L\alpha)\end{pmatrix}\left(EI\right)_p}$$

Substituting all the coefficients determined above into the deflection equation given in Equation (4.6) or Equation (A.4), after some simplification, we can have a deflection equation for fixed-head fixed base piles given below.

$$w(z)=\frac{P}{\left(EI\right)_p\left(2\lambda^2\alpha\beta\begin{pmatrix}\alpha\sin(2\beta L)\\+\beta\sinh(2\alpha L)\end{pmatrix}\right)}\begin{pmatrix}-\alpha^2\cosh(z\alpha)\sin(L\beta)\sin\left((L-z)\beta\right)\\+\beta\begin{pmatrix}\alpha\cosh(L\alpha)\sin(z\beta)\sinh\left((L-z)\alpha\right)\\+\beta\cos(z\beta)\sinh(L\alpha)\sinh(L-z)\alpha\\-\alpha\cos(L\beta)\sin\left((L-z)\beta\right)\sinh(z\alpha)\end{pmatrix}\end{pmatrix}$$

This expression is identical to the one given in Equation (4.16)

B. APPENDIX B

B.1 Calibration factor

In order to obtain the general calibration factor, first an Excel spreadsheet (Figure B-5) was developed for each soil-pile boundary conditions. Then, different analyses were conducted until the pile head deflection and the pile deflected shape is in agreement with the PLAXIS 3D output (with a maximum error of $\pm 3\%$). Different calibration factors were found for different soil and pile properties as shown in the semi-log plots of Figure B-1.

The effect of slenderness ratio on the value of the calibration factor is negligible for both the free-head and fixed-head piles that is why the expression of calibration factor for both free-head and fixed-head piles is only a function of pile-soil stiffness ratio and Poisson's ratio.

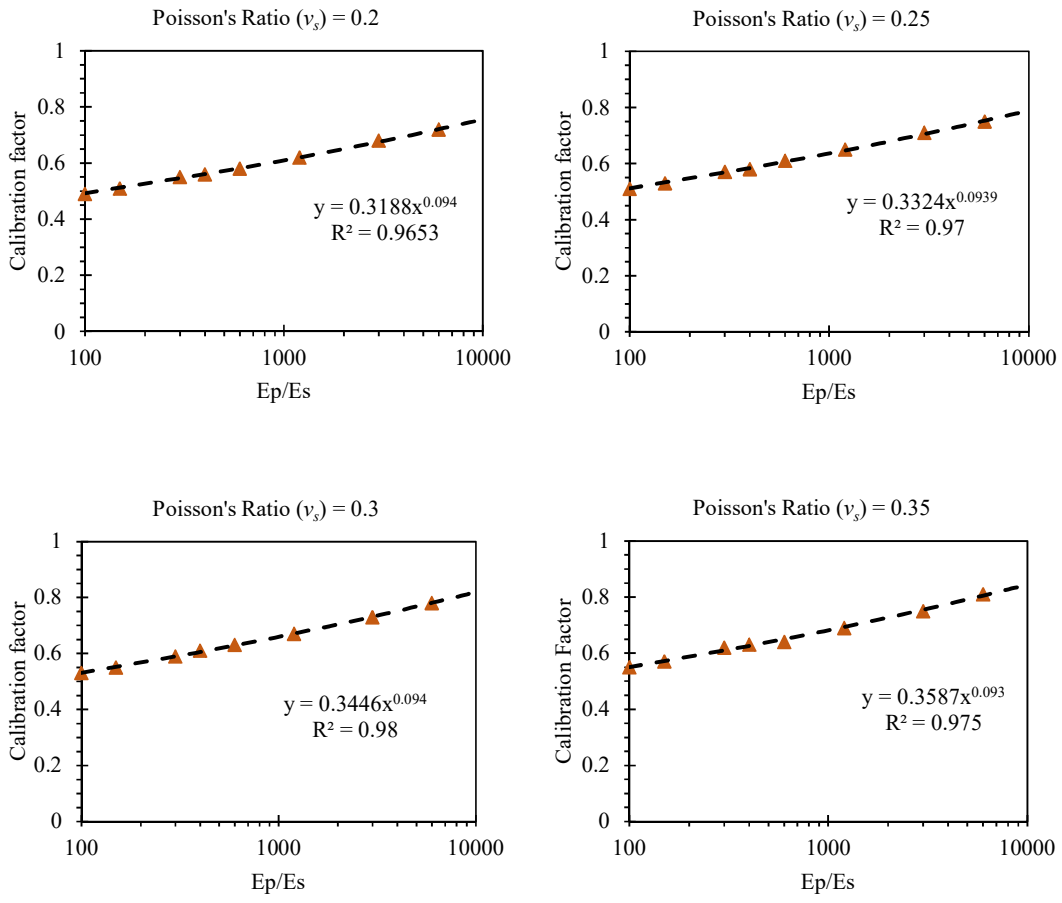

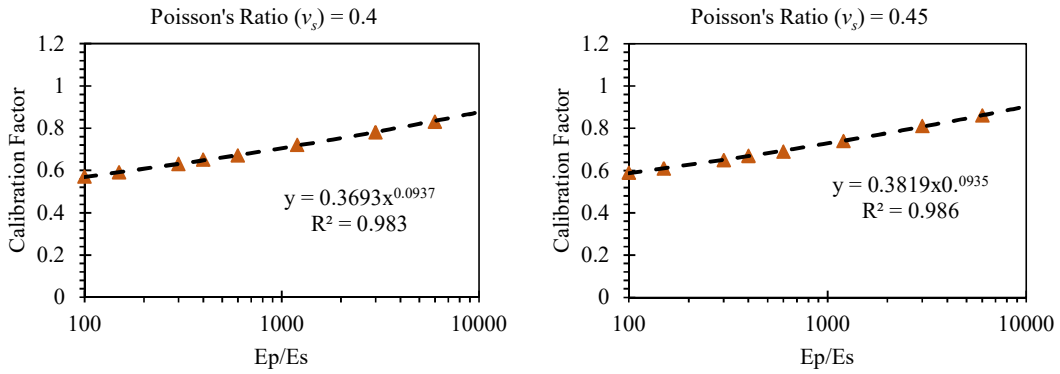

Figure B-1: Variation of calibration factor for fixed-head piles in homogeneous soil profiles: for different Poisson's ratio values

Figure B-1 portrays the variation of the calibration factor for different Poisson's ratio and pile-soil stiffness ratio. After curve fitting, it is evident that all the curves have the general form of;

$$\chi = \gamma_a \left(\frac{E_p}{E_s} \right)^{\gamma_b} \tag{B.1}$$

where both γ_a and γ_b evolve to be dependent on the soil Poisson's ratio, Table B-1 gives the variation of both parameters with v_s .

Table B-1: Variation of γ_a and γ_b with soil Poisson's ratio for a fixed-head pile

Poisson's Ratio (v_s)	γ_a	γ_b
0.2	0.3188	0.094
0.25	0.3321	0.0939
0.3	0.3446	0.094
0.35	0.3587	0.093
0.4	0.3693	0.0937
0.45	0.3819	0.0935

The exponent γ_b has a standard deviation of 0.000353, indicating that it is not much dependent on the variation of Poisson's ratio. So, the average value was taken, which gives a maximum of $\pm 0.3\%$ error when compared to the original value. Therefore, the value of $\gamma_b = 0.0937$ is obtained.

In the case of γ_a, the values are sensitive to v_s and are thus plotted in Figure B-2 which resulted in the best-fitting relation shown.

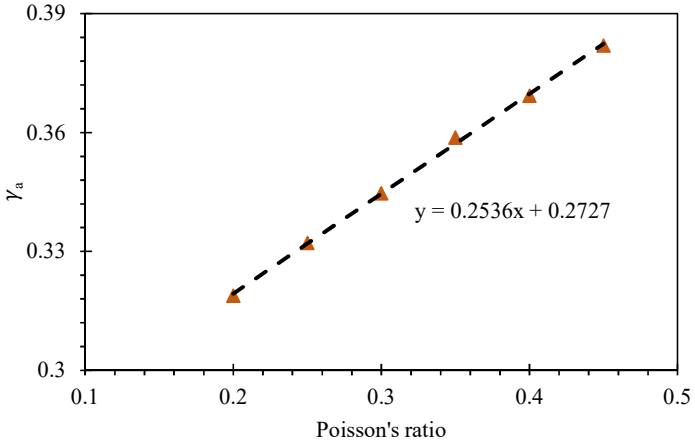

Figure B-2: Variation of γ_a for fixed-head piles in homogeneous soil profiles.

Based on the above results the calibration factor for fixed head piles is determined as given in Equation (B.2). This is given in Equation (4.17) in the main text.

$$\chi = (0.2536\nu_s + 0.2727)\left(\frac{E_p}{E_s}\right)^{0.0936} \tag{B.2}$$

Similarly, variation of the calibration factor for free-head piles are given in Figure A-3

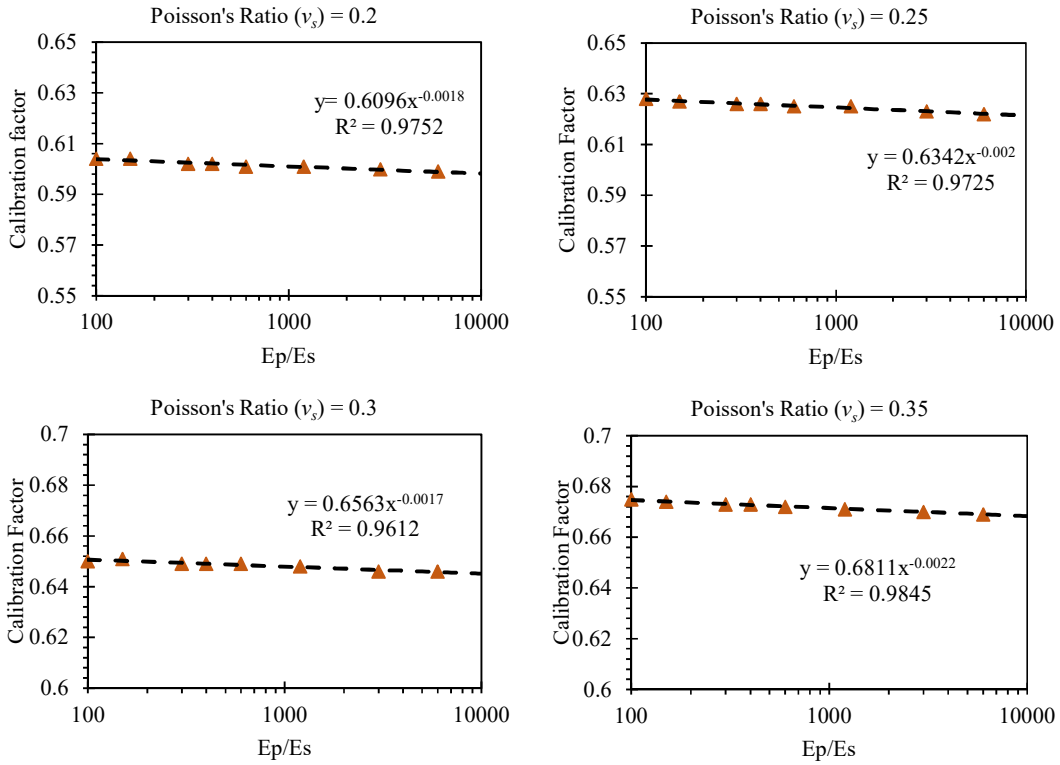

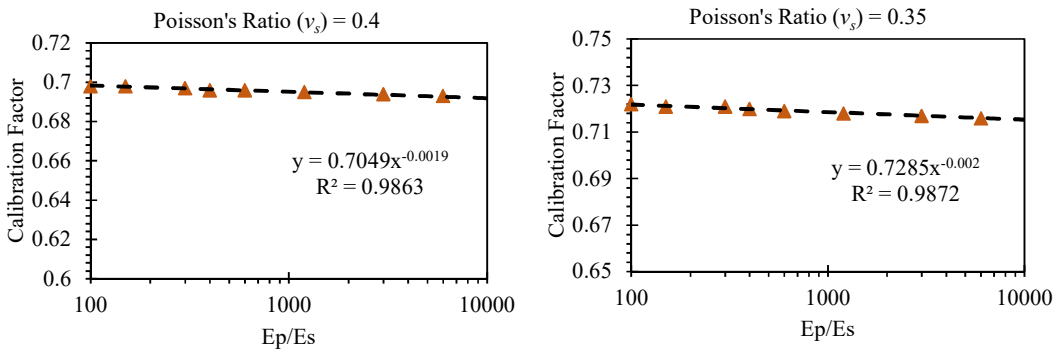

Figure B-3: Variation of calibration factor for free-head piles in homogeneous soil profiles. for different Poisson's ratio values

A similar trend exists as in the fixed-head pile. The expression given in Equation (B.3) is determined.

$$\chi = \gamma_a \left(\frac{E_p}{E_s} \right)^{\gamma_b} \tag{B.3}$$

Where both γ_a and γ_b are both generally dependent on the Poisson's ratio. Table B-2 gives the summary of the variation of both parameters.

Table B-2: Variation of γ_a and γ_b with soil Poisson's ratio for a free-head pile

Poisson's Ratio (ν)	γ_a	γ_b
0.2	0.6096	-0.0018
0.25	0.6342	-0.002
0.3	0.6563	-0.0017
0.35	0.6811	-0.0022
0.4	0.7049	-0.0019
0.45	0.7285	-0.002

The exponent γ_b shows a standard deviation of 0.00016. Suggesting that it is not much dependent on the variation of Poisson's ratio. For the case of γ_b all the values were approximated to the nearest three decimal number ($\gamma_b = -0.002$). In the Case of, γ_a, which is sensitive to Poisson' ratio, curve fitting is conducted.

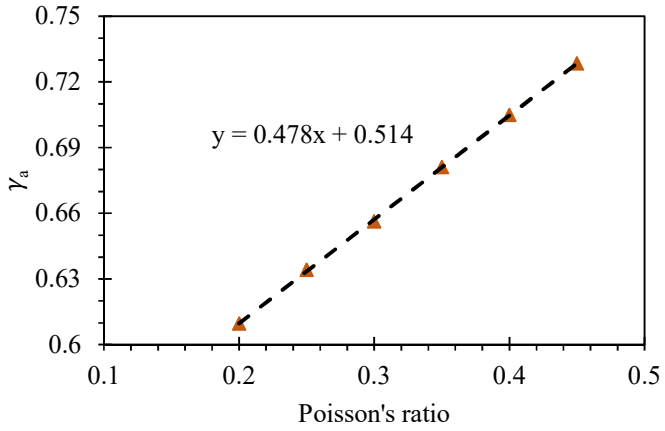

Figure B-4: Variation of γ_a for free-head piles in homogeneous soil profiles.

Based on the above results the calibration factor for free-head piles has been determined and is given by Equation (B.4) which is given in Equation (4.18) of the main text.

$$\chi = \left(0.478 v_s + 0.514\right)\left(\frac{E_p}{E_s}\right)^{-0.002} \tag{B.4}$$

B.2 Excel template for lateral response of piles under static loading

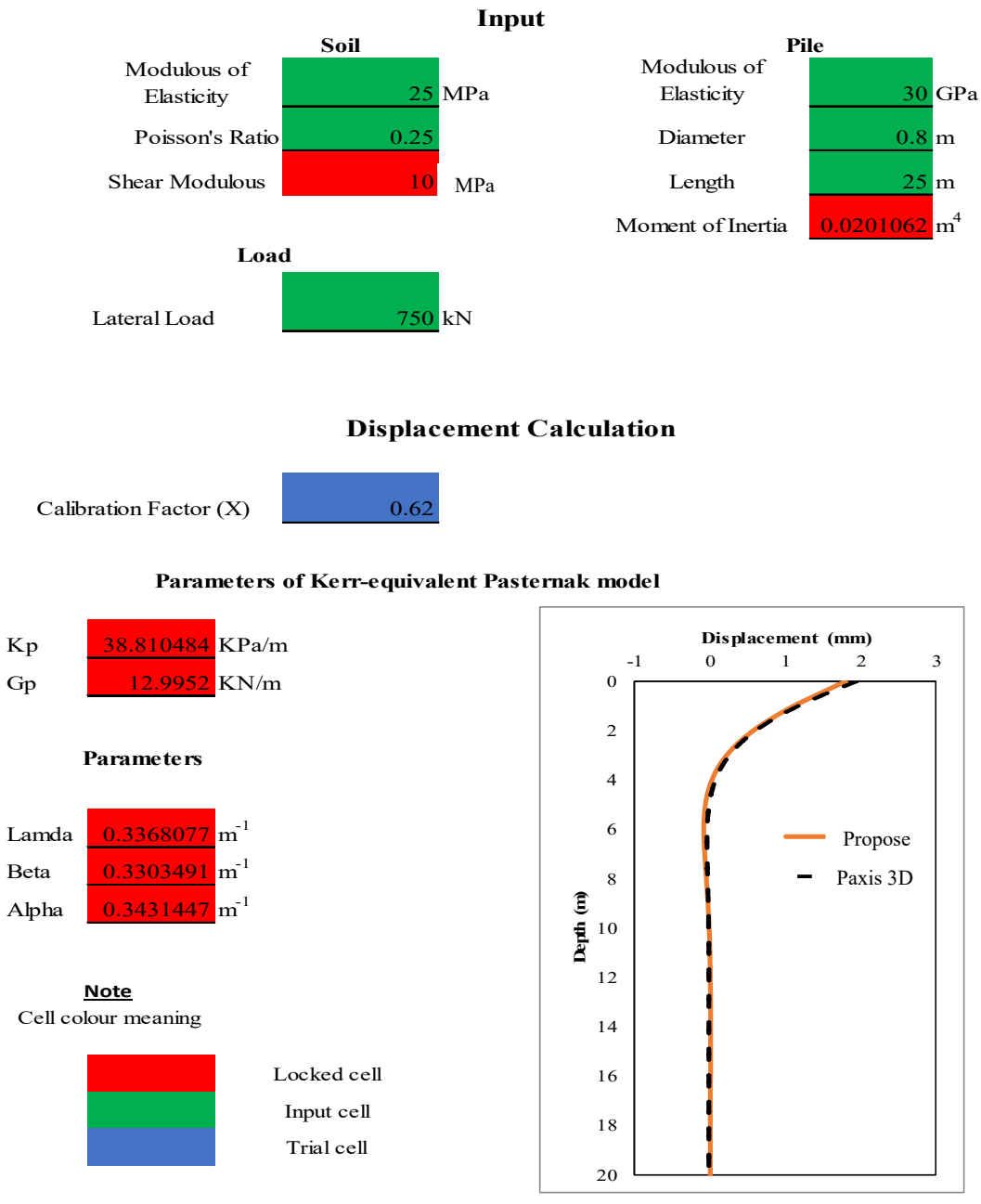

Figure B-5: Excel template for lateral response of single piles.

C. APPENDIX C

C.1 Critical pile length

In Section 4.4 of the main text, an introduction to critical pile length with derived expressions for all soil-pile boundary condition is presented. In this section the detailed procedure used in deriving the expressions of critical pile length for all soil-pile boundary conditions is presented.

As it is discussed in Section 4.4, different researchers used different approach in deriving the critical pile length, L_c. In this study a new approach is used. And in it the critical pile length is defined as *a pile length corresponding to a point beyond which increasing the pile length has no effect on the pile head stiffness.* In order to express the above principle using mathematical formulation, a new parameter called variation factor, Φ, is introduced. The variation factor is a ratio between the generalized pile head stiffness (which is a function of, E_P, E_s, v_s, d and L) and the pile head stiffness of long pile (which is a function of, E_P, E_s, v_s and d). Both pile head stiffnesses are derived in Section 4.4 of the main text. Hence, in this section only the derivation of the critical pile length for all soil-pile boundary condition is presented.

As discussed above, the variation factor is a ratio between two pile head stiffnesses (one a function of length and the other not). So, for none zero pile length, one can expect the value of the variation factor to be different from one. But according to the definition of the critical pile length, for piles with $L > L_c$ the pile head stiffness remains the same. As a result, the variation factor become one; this can be seen in Figure 4-22 through 4-25 of the main text.

The critical pile length, as discussed above, is a point at which the variation factor become one. From our earlier discussion, the variation factor is dependent on E_P, E_s, v_s, d and L. For the sake of simplicity, the above four dimensional parameters (E_P, E_s, d and L) and one dimensionless parameter (v_s) are reduced to two dimensionless parameters (L/d and E_p/G_s).

After this, different values of L/d are tired until the point at which the variation factor become one is found (which is the critical slenderness ratio, L_c/d). This method is implemented for different values of E_p/G_s and also for all soil-pile boundary conditions. The results are given in Table C-1

Table C-1: Variation critical pile length for all soil-pile boundary conditions.

E_p/G_s	L_c/d			
	FxHFxB	FxHFB	FrHFxB	FrHFB
200	4.7	6.0	5.6	5.8
400	5.8	7.5	6.9	6.9
600	6.4	8.3	7.8	8.0
800	7.0	9.2	8.5	8.5
1000	7.3	10	9.2	8.9
1200	7.9	10.4	9.5	9.5
1400	8.1	10.8	10.1	10.0
1600	8.4	11.0	10.5	10.6
1800	8.9	11.4	10.7	11.0
2000	9.0	12.0	11.2	11.1
2200	9.4	12.2	11.4	11.5
2400	9.6	12.6	11.7	11.8
2600	9.8	12.9	12.0	12.0
2800	10.0	13.0	12.3	12.4
3000	10.1	13.4	12.7	12.5
3200	10.2	13.7	13.0	12.7
3400	10.4	13.8	13.2	13.1
3600	10.5	14.0	13.5	13.4
3800	10.7	14.2	13.7	13.6
4000	11.1	14.4	13.6	13.8
4200	11.2	14.6	13.9	14.0
4400	11.3	14.8	14.1	14.2
4600	11.5	15.0	14.3	14.4
4800	11.6	15.3	14.5	14.4
5000	11.7	15.6	14.7	14.5

With the aim of finding an expression for the critical pile length, the values given in Table C-1 are plotted in Figure C-1. And from the figure it is evident that, the discrete data given in table C-1 are best fitted using a power function. The expression found from fitting the curves are given in Equation (C.1), (C.2), (C.3) and (C.4), which are critical pile length for FxHFxBP, FxHFBP, FrHFxBP and FrHFBP, respectively.

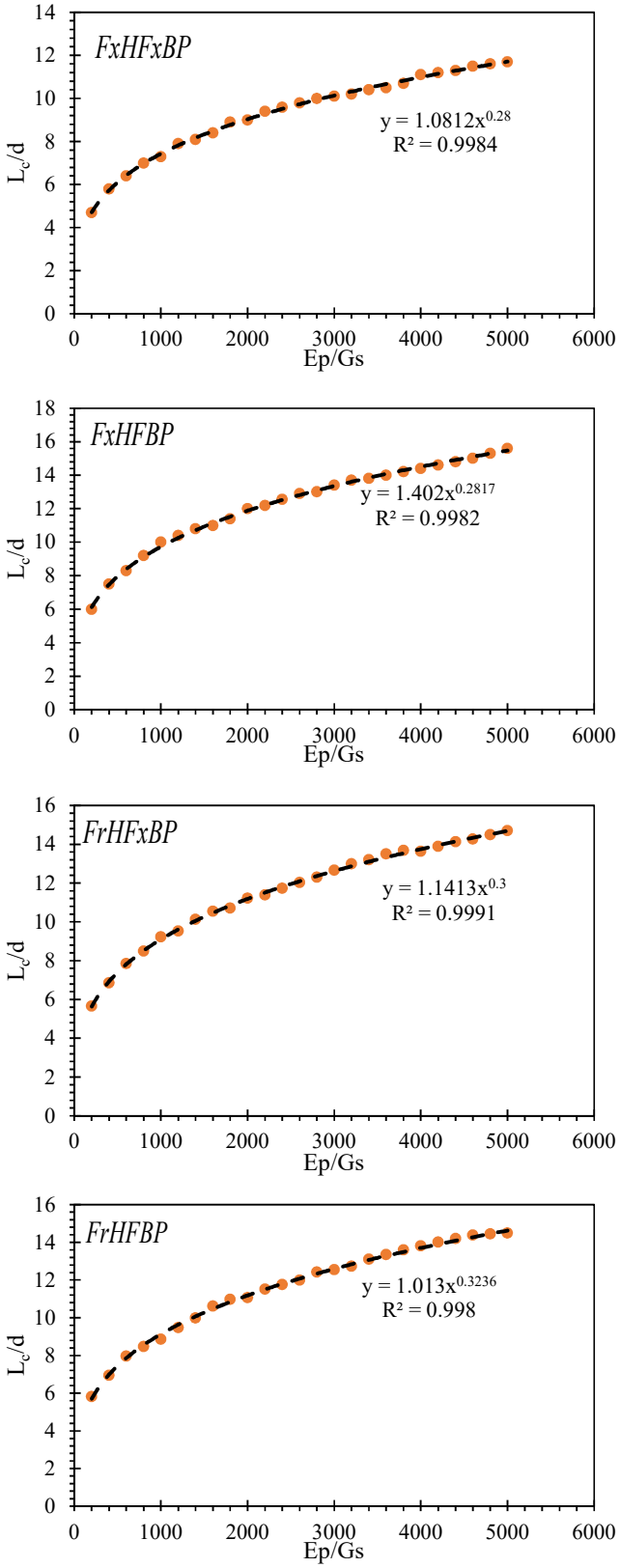

Figure C-1: Variation of critical pile slenderness ratio

The fitted equation shown in the figures are presented below and all the expressions are similar to the once given in the main text.

Fixed-head fixed-base pile

$$\frac{L_c}{d} = 1.08\left(\frac{E_p}{G_s}\right)^{0.28} \tag{C.1}$$

Fixed-head floating-base pile

$$\frac{L_c}{d} = 1.4\left(\frac{E_p}{G_s}\right)^{0.2817} \tag{C.2}$$

Free-head fixed-base pile

$$\frac{L_c}{d} = 1.14\left(\frac{E_p}{G_s}\right)^{0.3} \tag{C.3}$$

Fixed-head floating-base pile

$$\frac{L_c}{d} = \left(\frac{E_p}{G_s}\right)^{0.3236} \tag{C.4}$$

D. APPENDIX D

D.1 Equivalent damping at the pile head

In Section 6.2 of the main text, distributed dashpot coefficients (c_m and c_{rad}) where determined. But if one wants to study the dynamic pile response manually, the distributed dashpot coefficients has to be converted to an equivalent overall dashpot coefficient at the pile head. In order to do this the approach proposed by Gazetas and Dobry (1984) is used.

Gazetas and Dobry (1984) using principle of conservation of energy, proposed an expression (Equation (D.1)) for computing the overall dashpot coefficient C_x. Which is computed from c_m and c_{rad} distributed along the pile.

$$C_x = c_x \int_0^L Y^2(z)\,dz \tag{D.1}$$

where

c_x distributed dashpot coefficient in the horizontal direction

$Y(z) = w(z)/w(0)$ is static deflection profile normalized to a unit top amplitude.

The value of $\gamma = \int_0^L Y^2(z)\,dz$, for all soil-pile boundary conditions, is solved using Mathematica 12 and the steps followed, for fixed-head fixed-base pile, are presented below.

First, the value of $Y(z)$ is solved simply using the ratio between $w(z)$ and $w(z)\big|_{z=0}$. The result is given as

$$Y(z) = \frac{\left(\begin{array}{l}\beta\left(\begin{array}{l}\alpha\cosh(L\alpha)\sin(z\beta)\\ +\beta\cos(z\beta)\sinh(L\alpha)\end{array}\right)\sinh\left((L-z)\alpha\right)\\ -\alpha\left(\begin{array}{l}\alpha\cosh(z\alpha)\sin(L\beta)\\ +\beta\cos(L\beta)\sinh(z\alpha)\end{array}\right)\sin\left((L-z)\beta\right)\end{array}\right)}{-\alpha^2\sin^2(L\beta)+\beta^2\sinh^2(L\alpha)} \tag{D.2}$$

Next, the value of $\gamma = \int_0^L Y^2(z)\,dz$ is solved and the result is given as

$$\gamma = \frac{\begin{pmatrix} -4L\alpha\beta\left(\alpha^2+\beta^2\right)\begin{pmatrix}-\alpha^4-\beta^4+\alpha^2\left(\alpha^2+\beta^2\right)\cos\left(2L\beta\right)\\ +\beta^2\left(\alpha^2+\beta^2\right)\cosh\left(2L\alpha\right)\end{pmatrix} \\ -2L\alpha^2\left(\alpha+\mathrm{i}\beta\right)\beta^2\left(\mathrm{i}\alpha+\beta\right)^3\cosh\left(2L\left(\alpha-\mathrm{i}\beta\right)\right) \\ +2L\alpha^2\left(\mathrm{i}\alpha-\beta\right)^3\left(\alpha-\mathrm{i}\beta\right)\beta^2\cosh\left(2L\left(\alpha+\mathrm{i}\beta\right)\right) \\ -2\alpha\left(\alpha^2+\beta^2\right)^2\left(\alpha^2+2\beta^2\right)\sin\left(2L\beta\right)+\alpha^5\left(\alpha^2+5\beta^2\right)\sin\left(4L\beta\right) \\ -2\beta\left(\alpha^2+\beta^2\right)^2\left(2\alpha^2+\beta^2\right)\sinh\left(2L\alpha\right)+\beta^5\left(5\alpha^2+\beta^2\right)\sinh\left(4L\alpha\right) \\ +\alpha\beta\left(\left(\alpha+\mathrm{i}\beta\right)\begin{pmatrix}2\alpha^4-3\mathrm{i}\alpha^3\beta\\ +2\alpha^2\beta^2+3\mathrm{i}\alpha\beta^3+2\beta^4\end{pmatrix}\right)\sinh\left(2L\left(\alpha-\mathrm{i}\beta\right)\right) \\ +\alpha\beta\left(\left(\alpha-\mathrm{i}\beta\right)\begin{pmatrix}2\alpha^4+3\mathrm{i}\alpha^3\beta\\ +2\alpha^2\beta^2-3\mathrm{i}\alpha\beta^3+2\beta^4\end{pmatrix}\right)\sinh\left(2L\left(\alpha+\mathrm{i}\beta\right)\right) \end{pmatrix}}{8\alpha\beta\left(\alpha^2+\beta^2\right)\left(\alpha^2+\beta^2-\alpha^2\cos\left(2L\beta\right)-\beta^2\cosh\left(2L\alpha\right)\right)^2} \tag{D.3}$$

Finally, as it can be seen from Equation (D.3), the expression of γ is very tedious for hand calculation. So, the expression is plotted and fitted using power function (as it can be seen in Figure 6-7 of the main text). the fitted expression is given in Equation (6.28) of the main text.

Using the same procedure, the value of γ for free-head piles is determined and it is given in Equation (6.27).